Water model investigation of the influence of submerged entry nozzle on the turbulent flow in thin slab casting

A thesis submitted to the Montanuniversität Leoben
for the degree of Master of Science (MSc.)

presented by
Nunner Georg
Leoben, October 2016

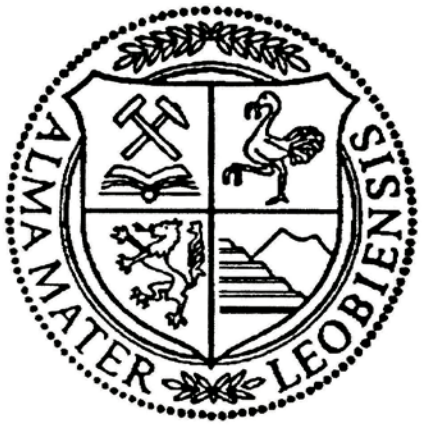

Examiner: Assoz. Prof. Dr.-Ing. Menghuai Wu
Chair for Simulation and Modelling of Metallurgical Processes
Department of Metallurgy

The financial support by RHI AG, the Austrian Federal Ministry of Economy, Family and Youth and the National Foundation for Research, Technology and Development within the framework of the Christian Doppler Laboratory for Advanced Process Simulation of Solidification and Melting is gratefully acknowledged.

Kurzfassung

Es wurde ein Wassermodell-Experiment für Dünnbrammengießen durchgeführt. Die Größe des Versuchsaufbaus wurde im Vergleich mit operierenden Anlagen, im Verhältnis 1:2 verkleinert. Das Ziel dieses Experimentes war es, das Design der Eintauchrohre (SEN) zu optimieren. Um dies zu erreichen wurden verschiedene Portöffnungen (6, 8, 10, 12, 15 und 18 mm) und unterschiedliche Wandbreiten (1150, 1400 und 1700 mm) der Kokille verwendet. Andere Parameter wie z.B.: Kokillentiefe (112.5 mm) und Eintauchtiefe mit 210 mm waren bei allen Versuchen konstant. Während der Versuche wurde rote Tinte eingespritzt und mit einer hochauflösenden Kamera das Strömungsmuster aufgezeichnet.

Die Ergebnisse dieser Wassermodell-Experimente zeigten drei verschiedene Strömungsmuster: stabil, transient und instabil. Dabei fiel auf dass die Portöffnung der Eintauchrohre eine kritische Einflussgröße darstellt. Ein instabiles Strömungsmuster wurde teilweise ab einer Portöffnung von mehr als 10 mm beobachtet. Die Ergebnisse zeigen aber eindeutig an, dass bei der Verwendung einer 18 mm Portöffnung konstant ein instabiles Strömungsmuster entsteht.

Um die Dynamik der Strömungen in der Kokille zu verstehen wurde ein ausgewählter Fall mit einer Kokillengröße von 1400*112.5 mm² und einer Gießgeschwindigkeit von 3.4 m/s simuliert. Die Simulation wurde mit drei verschiedenen Vernetzungen evaluiert. Das Ergebnis war, dass ein ausreichend feine Vernetzung benötigt wird um das Strömungsmuster, welches während der Experimente beobachtet wurde, zu reproduzieren.

Abstract

A water model experiment for thin slab casting was performed. The geometry of the water model was 1:2 under scaled in comparison to the size as operated in plant. The final goal of this experiment was to optimize the design of the submerged entry nozzles (SEN). Therefore, the SEN varied in the port gap from 6, 8, 10, 12, 15 to 18 mm. The mold width varied from 1150, 1400 to 1700 mm. Some other parameters were fixed constant, e.g. the mold depth was 112.5 mm, and the immersion depth of SEN in the mold was 210 mm. During experiment dye was injected, and a high resolution camera was used to record the flow pattern.

The results of the water model experiment showed three different flow patterns: stable, transient and unstable flow. The gap size of the SEN was critical. It was evident that the results by using the SEN with the large gap, e.g. 18 mm, were always unstable. It was observed from the current experiment that unstable flow occurred when the SEN gap was larger than 10 mm.

In order to understand the dynamics of the flow in the mold, a chosen case with the mold section of 1400*112.5 mm^2 and a casting speed of 3.4 m/s was simulated. The simulation results were compared with the results of the water model experiment. Simulations with three different mesh sizes were evaluated. It was found that sufficient mesh refinement is required to reproduce the flow patterns as observed from the experiments.

Eidesstattliche Erklärung

Ich erkläre an Eides statt, dass ich die vorliegende Masterarbeit selbstständig und ohne fremde Hilfe verfasst, andere als die angegebenen Quellen und Hilfsmittel nicht benutzt und die den verwendeten Quellen wörtlich und inhaltlich entnommenen Stellen als solche erkenntlich gemacht habe.

.....

Nunner Georg

Acknowledgement (Danksagung)

Mit Dank möchte ich all die Hilfe und Unterstützung wertschätzen, die mir während der Erstellung meiner Diplomarbeit von meiner Familie, meinen Betreuern und ehemaligen Arbeitskollegen zuteilwurde. Besonders möchte ich mich bei meinen Eltern für die langjährige Unterstützung bedanken, ohne die dieses Studium nicht möglich gewesen wäre. Ebenfalls möchte ich meiner Frau Mariella danken, die mir immer mit ihrer Unterstützung und vor allem auch mit Ihrer Geduld zur Seite stand.
Speziell möchte ich mich bei Herrn Assoz. Prof. Dr.-Ing Menghuai Wu, dem Hauptbetreuer meiner Diplomarbeit und Leiter des Christian Doppler Labors für Prozesssimulation von Erstarrungs- und Umschmelzvorgängen bedanken. Seine fachliche Kompetenz, konstruktive Kritik aber auch Motivation haben in vielen Gesprächen sehr zum Gelingen dieser Diplomarbeit beigetragen. Vielen Dank auch Herrn Dr. Alexander Vakhrushev, als Zweitbetreuer der Diplomarbeit und seine Unterstützung im experimentellen und numerischen Teil dieser Arbeit.

Ebenfalls möchte ich mich auch bei DI Gernot Hackl und Wolfgang Fellner, RHI AG, bedanken die mich bei der Durchführung der Versuche sehr unterstützt haben.
Ich möchte aber auch meinen ehemaligen Arbeitskollegen für die gute und freundschaftliche Zusammenarbeit danken. Speziell sei hier auch das Sekretariat mit Sabine Strassegger und Jennifer Dorner erwähnt sowie auch die EDV – Abteilung.

Content (Inhaltsverzeichnis)

Acronyms (Akronyme)

TSC	Thin slab casting
CSP	Compact strip production
ISP	Inline strip production
ESP	Endless strip production
SEN	Sub entry nozzle

Figure Caption (Abbildungsverzeichnis)

Table Caption (Tabellenverzeichnis)

1 Metallurgical Fundamentals of Thin Slab Casting (TSC)

1.1 Thin Slab Casting (TSC)

Thin slab casting (TSC) in direct combination with hot rolling is nowadays an established technology. TSC with end dimensions of 50 mm is possible thanks to the development of a funnel type mold. Liquid steel is provided into the mold by a submerged entry nozzle (SEN). A general map of TSC process can be seen in Figure 1. [1]

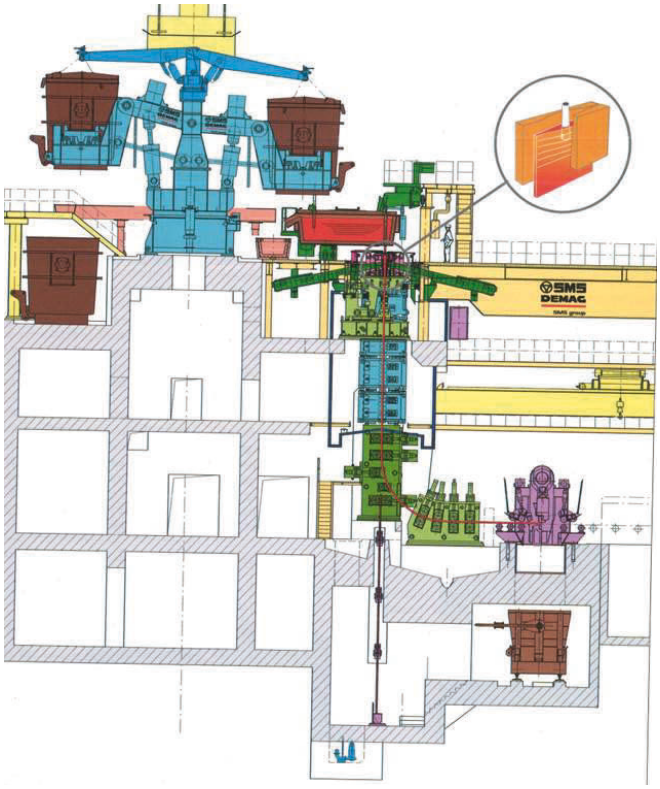

Figure 1. Schematic of a thin slab casting plant. [1]

Steel which comes from the secondary metallurgy at a steel plant is cast into molds of different shapes, sizes and weights. Until the 1970s this casting process was marked as ingot casting with permanent molds. Nowadays this process route is replaced by continuous casting. Ingot casting is used today for the production of heavy forged parts. [1]

Because of the continuous casting process the output of liquid steel could be raised for 10% which lead to savings in energy and materials. Due to the faster solidification of the casting process the material has lower segregation and a more homogeneous structure. Also the opportunity of automatization of the process leads to a better control and an even process. [1]

Typical problems which have to be controlled during continuous casting processes are:

- Clogging,
- Sticker,
- Break through,

- Bulging,
- Periodical fluctuations of the meniscus,
- Oscillation marks at the surface of the string,
- Surface defects as inclusions,
- Cracks at the surface or the development of cavities,
- Segregations.[1]

Important parameters for the quality of the slab are:

- Temperature of the liquid steel in the tundish,
- Casting powder (composition and properties),
- Cooling of the mold,
- Conicity and coating of the mold,
- Mold oscillation,
- Casting speed,
- Secondary cooling,
- Distance of supporting rollers.[1]

The adjustment of steel temperature, out pull velocity, amount of steel in the mold and slab cooling is very sensitive to the steel quality and that's why the control of the process is very important. In Figure 2 a schematical overview of the process control can be seen.[1]

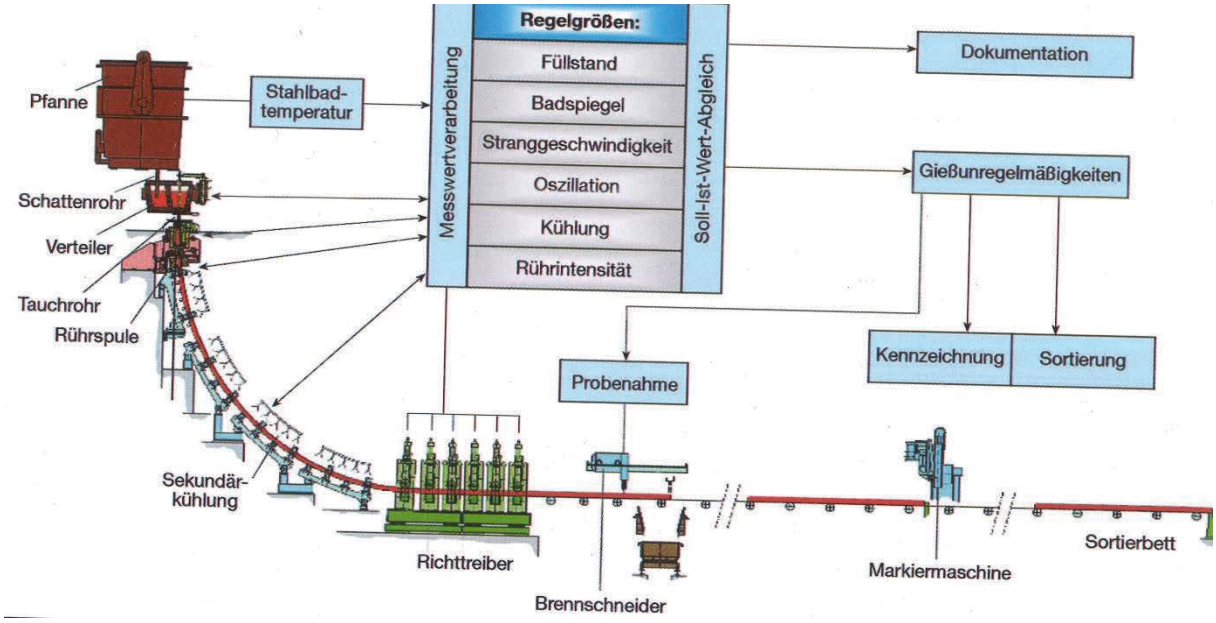

Figure 2. Overview of the continuous casting process control.[1]

Three main production routes for flat products are developed which are called direct strand reduction or final gauge casting.

- Thin slab casting (Casting thickness 50 – 90 mm).
- Direct strip casting (Casting thickness 10 – 15 mm).
- Twin roll casting (Casting thickness 1- 5 mm).[1]

In Figure 3 a comparison of the traditional continuous casting to the production routes of the flat products can be seen.

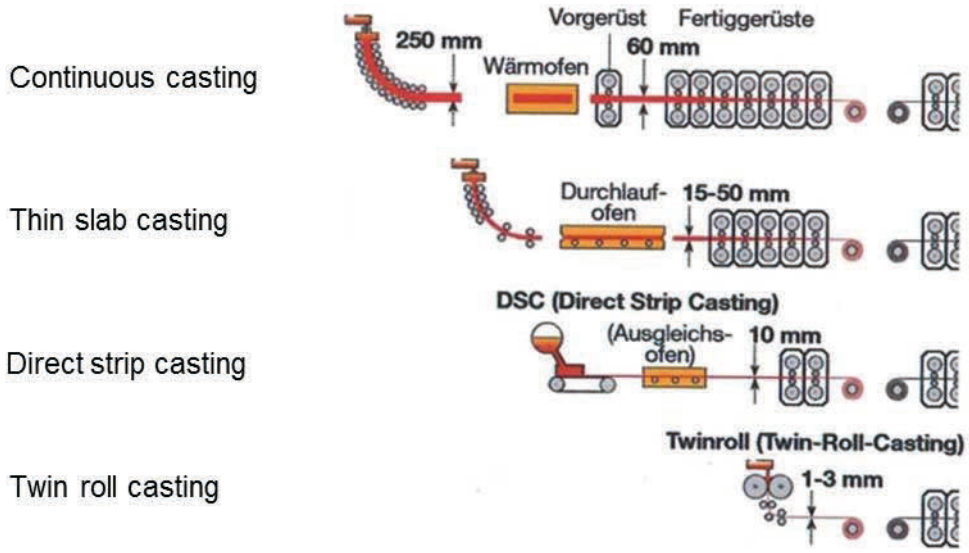

Figure 3. Comparison of the production routes.[1]

From this general overview it is clearly seen that the process chain gets smaller by reaching almost the end dimension of the flat product during the casting process.[1]

In Figure 4 the whole process chain of a TSC which is between 250 – 280 m long can be seen.

Three main production routes for flat products are developed which are called direct strand reduction or final gauge casting.

- Thin slab casting (Casting thickness 50 – 90 mm).
- Direct strip casting (Casting thickness 10 – 15 mm).
- Twin roll casting (Casting thickness 1- 5 mm).[1]

In Figure 3 a comparison of the traditional continuous casting to the production routes of the flat products can be seen.

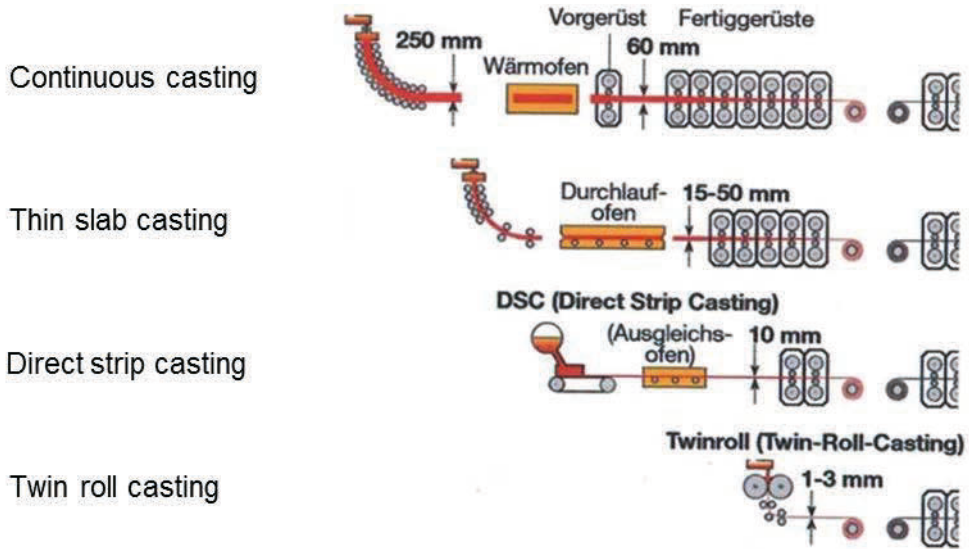

Figure 3. Comparison of the production routes.[1]

From this general overview it is clearly seen that the process chain gets smaller by reaching almost the end dimension of the flat product during the casting process.[1]

In Figure 4 the whole process chain of a TSC which is between 250 – 280 m long can be seen.

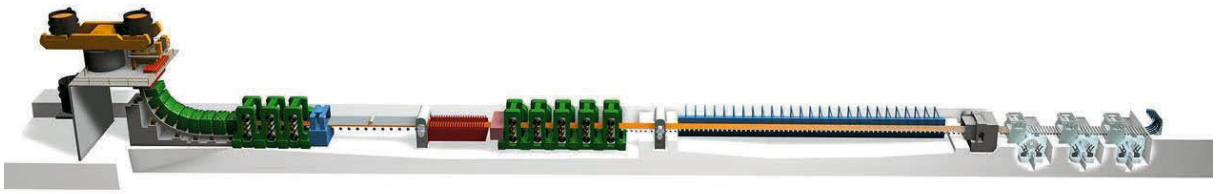

Figure 4. Process route of a TSC plant.[2]

Advantages of TSC in comparison to the conventional continuous casting:

- Small variation of mechanical properties because of constant velocity of the rolling process and temperature balance in the roller hearth furnace,
- Lower costs,
- Small segregation sensitivity because of smaller grain size,
- Good surface quality,
- Lower energy consumption and environment pollution.[3,4]

1.1.1 Compact Strip Production (CSP)

In a CSP the liquid steel is cast into thin slabs which after temperature equalisation in a tunnel furnace are rolled directly in the rolling mill without roughing.

CSP is a technology for producing hot rolled strip at low production costs in combination with high productivity and product quality.[5]

In Figure 5 a layout of the CSP process can be seen.

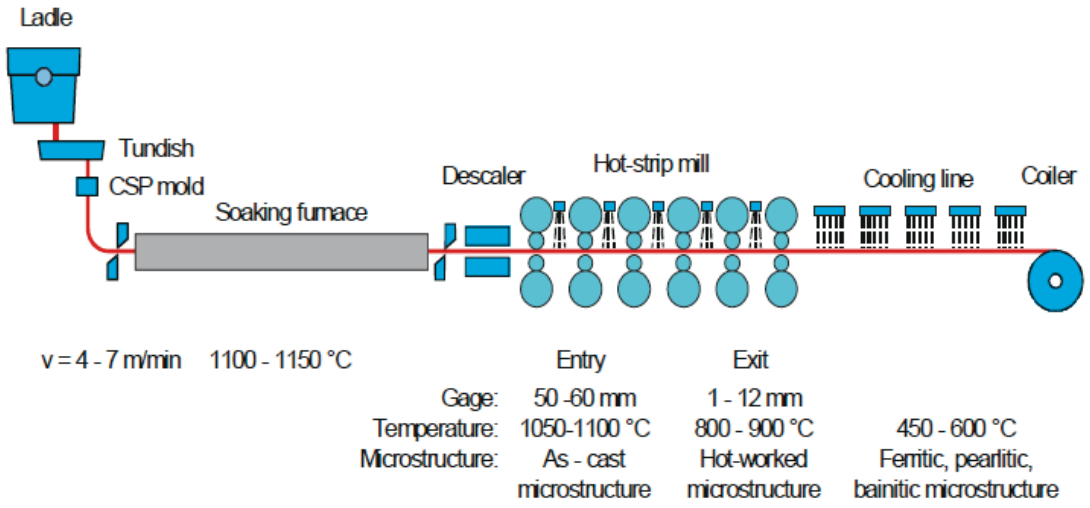

Figure 5. Schematic representation of a compact strip production plant.[6]

The characteristic of the CSP technology is the integration of three factors:

- Equipment design and automation,
- Technological practices,
- Material characteristics (composition and microstructure).[5]

Significant differences are inherent in the engineering design and material processing of CSP plants, in contrast to conventional hot rolled strip production. It is these differences that provide considerable potential advantages for the future manufacture of high performance hot rolled strip. [5]

The principal features of CSP technology that have a major effect on the metallurgical properties of hot rolled finished product are:

- Thin slab casting,
- Direct charging and rolling of a thin slab,
- Laminar cooling and coiling.[5]

One of the important characteristics of thin slab casting is the higher solidification rate in comparison with conventional slab casting. The faster solidification rate results in smaller secondary dendritic arm spacing and considerably less macro segregation. This feature is a major factor contributing to the superior constitutional homogeneity of CSP hot rolled strip.[5]

The direct charging and rolling of a hot thin slab without a roughing mill has a significant effect on the microstructure. The thin slab enters the CSP rolling mill with an as-cast structure where as in a conventional rolling operation the transfer bar has a recrystallized

structure. This dissimilar thermomechanical history leads to differences in precipitate formation (micro-alloying elements, MnS, etc.). During the deformation process in the CSP rolling mill, two objectives must be met in addition to establishing the necessary geometry for the hot rolled strip (width, thickness, flatness and profile). First, the dendritic as-cast microstructure has to be compacted and transformed into a homogenous recrystallized microstructure. Second, the austenite has to be conditioned so that the subsequent polymorphic transformation results in an extremely fine grained ferritic phase. Plastic deformation is deliberately used in CSP rolling to control the subsequent solid state reactions during laminar flow cooling and at the coiler.[5]

A high nucleation density for the subsequent austenite transformation can be achieved by finish rolling below the recrystallization stop temperature. This transformation takes place on the runout table to the coilers. Thus, the laminar cooling section can be employed as an efficient instrument for heat treatment and consequently the desired final structure can be adjusted. The cooling section is kept as short as possible for coiling at high temperature and ensuring annealing with substantial softening inside the coil.[5]

In Figure 6 the CSP plants around the world can be seen which are built and planned to the year 2006.

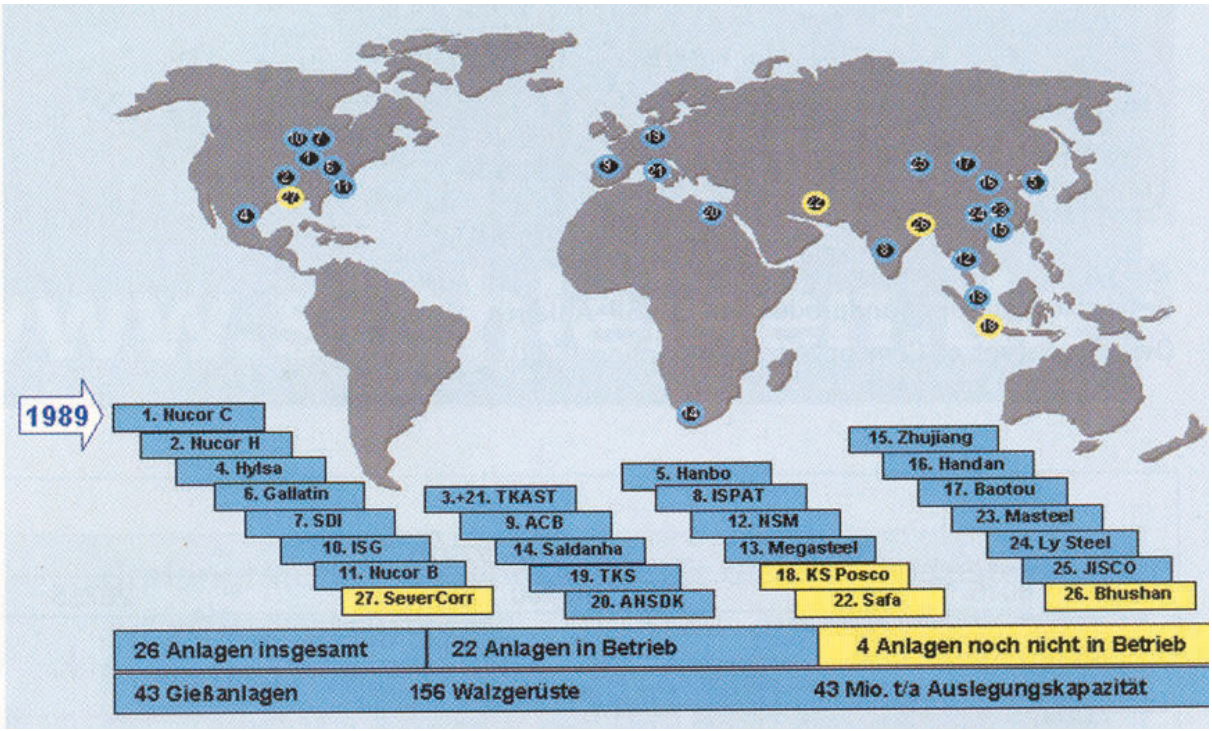

Figure 6. The world wide distribution of the CSP until the year 2006.[7]

In the year 2012 28 CSP plants are operating worldwide and producing 50 Mt of hot strips, which represents 10% of the world wide hot strips production.[8]

1.1.2 Inline Strip Production (ISP)

ISP technology is a unique technology for processing high quality, thin gauge and hot rolled strip. [9] It allows a tenfold reduction in times and a space compared with traditional processes and obtains a new process and high-quality product with extraordinary performance at decidedly lower costs starting from a shape closer to the final gauge.[10]

The principles are to exploit the heat of the liquid steel coming from the ladle furnace in an inline process and to continuously roll the thinnest possible slab to obtain very thin strip with properties and a quality such as to allow it to replace cold rolled strip for certain applications.[10]

The development of the In-line Strip Production process (Arvedi ISP) became an important milestone on the way to an endless thin slab casting and rolling process. It was characterised by the direct connection of continuous casting with the roughing mill, the tunnel furnace replaced by a very short induction heater with the roughing mill linked to the finishing mill by a compact coil furnace (Cremona furnace).[11]

In Figure 7 the layout of an ISP process can be seen.

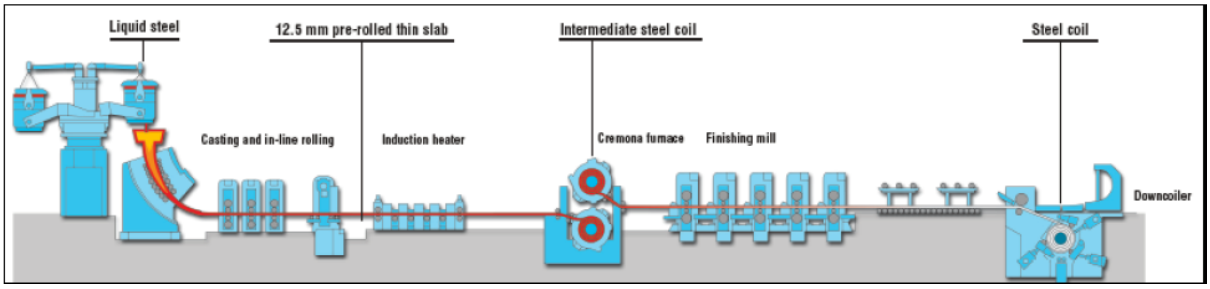

Figure 7. Overview of an Inline Strip Production plant.[10]

In 2006, sales of ISP steel, mainly for the automotive, tube and construction industries, were divided among the following areas of application (see Figure 8).[12]

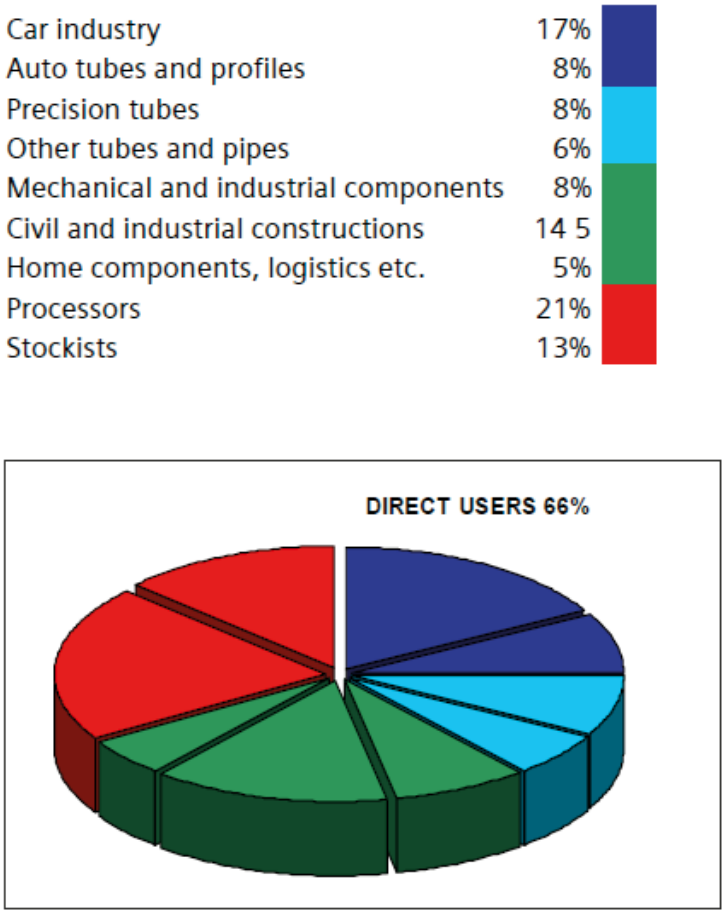

Figure 8. ISP production fields.[12]

Special attention has been paid to caster design features such as casting speeds, slab thickness, dynamic soft reduction strategy and secondary cooling design in order to cope with the demanding product mix.[12]

The main metallurgical challenges can be summarised as follows:

- Good surface quality is essential because API (American Petroleum Institute) grades are crack sensitive;
- In the thin slab casting process no slab conditioning is allowed. This implies that slab surface cracks or depressions must be avoided in the casting practice otherwise slabs will be downgraded;
- No trace of oscillation marks must remain on the surface of the rolled product
- Internal quality must be at highest level;
- Grain size must be minimised for control of toughness;

- Centerline segregation must be minimum.[13]

The ISP has many advantages compared to the conventional casting process from a process, product and investment point of view:

- Low rolling forces due to reduction in high temperature region using liquid core reduction and high reduction mill (HRM) with consequent reduction in rolling energy consumption,
- Stable and highly flexible process due to the setting of the casting and rolling process parameters,
- A wide choice of process parameters which can be adjusted to each strip,
- A wide range of medium – high quality products,
- Excellent homogeneity of microstructure and properties over the whole strip,
- Low investment costs due to the compact line and lean rolling stand layout,
- Low processing costs because of excellent heat exploition and stable processing.[9]

1.1.3 Endless Strip Production (ESP)

The Endless Strip Production is a direct Evolution of the ISP which is patented by the steel producer Acciaieria Arverdi SpA in Italy.[12] The ESP was introduced as the hot strip production by thin slab casting and direct rolling was a complete controlled process. Both steps are directly linked but can be operated in a decoupled process. The basic requirement to implement the coupled ESP process is a high mass flow which balances the different individual process steps. With this high production values, ultra-thin strip gauges having extraordinary product quality and uniform material properties can be achieved.[14]

The equipment in an ESP plant has the task of solidifying, reducing, reheating, transporting, cutting descaling, measuring, cooling and coiling the product as it journeys from liquid steel to finished coil.[14]

The layout of a ESP line can be seen in Figure 9.[10]

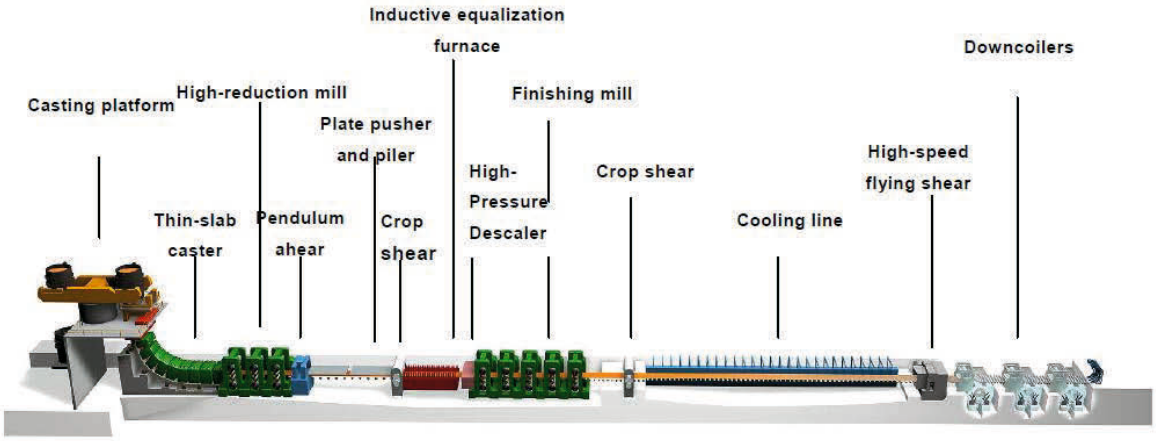

Figure 9. Overview of the endless strip production route.[9]

The ESP line is characterized by

- Fully continuous strip production,
- Outstanding production capacity with a single casting line,
- High volume production of ultra-thin strip,
- High volume production of high quality strip,
- The lowest costs from liquid steel to hot rolled coil,
- The most compact line layout.[12]

ESP allows production of thinner gauges and an expansion of the range of thermos-mechanical steels. Energy consumption is calculated to be about 75% less than that of a conventional process, due to a more complete exploitation of the energy in the liquid steel and less recourse to cold rolling.[12]

The evolution of continuous casting heads for thin slab castings or rather to close to end dimension castings.

The avoidance of cooling to room temperature between casting and starting of reheating before rolling significantly reduced the specific energy consumption. The ESP process has demonstrated stability, high production capacity and has proved to be suitable for producing a wide range of steel grades from low carbon to sour gas resistant line pipe steels.[11]

To achieve these goals developments in the production process were necessary, e.g. the funnel shape mold and the SEN are one of them.

1.2 Submerged Entry Nozzles (SEN)

The primary function of the nozzle is to protect the liquid metal from reoxidation during transfer between metallurgical vessels. The SEN has an important influence on steel quality through its effect on the flow pattern in the mold.[15]

A schematic of the continuous casting process is depicted in Figure 10. Steel flows from the tundish and then it exits down through a Submerged Entry Nozzle (SEN) and into the mold. Here, the steel freezes against the water cooled copper walls to form a solid shell, which is continuously withdrawn from the bottom of the mold at a casting speed that matches the flow of the incoming metal.[16]

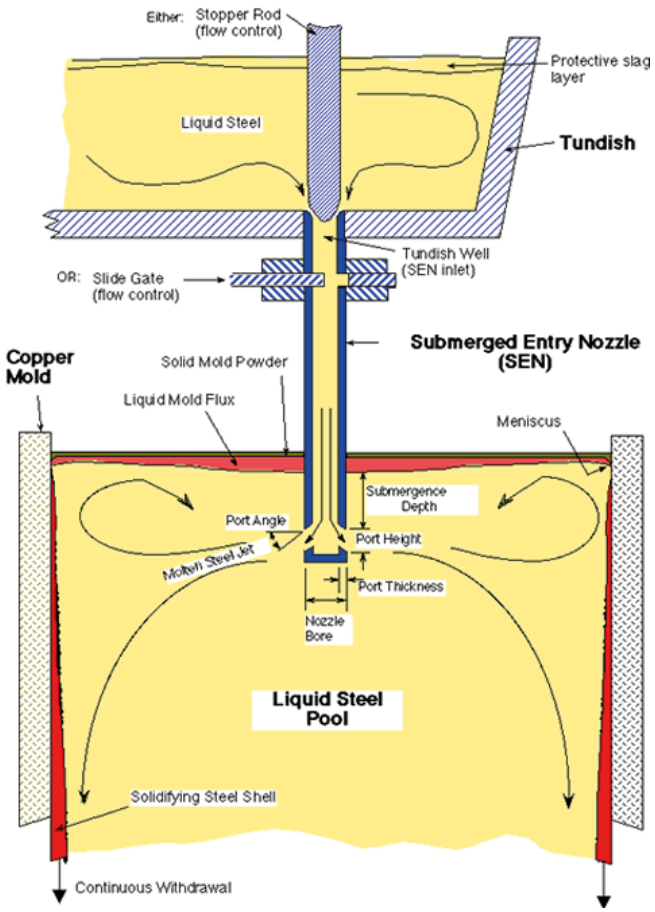

Figure 10. Schematic of continuous casting, tundish and SEN.[16]

The design of submerged entry nozzles (SEN) is critical for controlling steel flow turbulence in continuous casting molds. This is most important in thin slab funnel type molds, which operate at high casting speeds in relatively confined volumes.[17,18]

The SEN should deliver steel uniformly into the mold while preventing problems such as surface waves, meniscus freezing and crack formation. Impingement of hot liquid metal with high momentum against the solidifying shell can contribute to shell thinning and even costly breakouts, where liquid steel bursts from the shell.[19,20] Flotation of inclusions into the protective molten slag layer can be enhanced by an appropriate flow pattern inside the mold. Plant experience has found that many serious quality problems are directly associated with SEN operation and the flow pattern in the mold. For example, surface waves and turbulence near the top free surface can entrain some of the slag or gas bubbles into the steel, causing dangerous large inclusions and surface slivers.[21]

Finally, clogging due to inclusion build up on the SEN walls redirects the flow through the SEN, and hence, affects the jet characteristics exiting from the SEN ports. As a result, the ports are usually oversized to accommodate some clogging before the flow becomes constricted.[22]

Another key factor for SEN design is to avoid free shear strain rates induced by long discharging jets, especially when the casting speed increases as Torres-Alonso et al. indicated.[23]

The shape of the nozzle is one of the few casting design variables that has an important impact on quality and yet can be easily changed at low cost over a wide spectrum of design. The most influencing design variables are: bore size, port angle, port opening size , nozzle wall thickness, port shape (round, oval, square), number of ports (bifurcated or multiport), and nozzle bottom design.[22]

In the following sections different designs of the SEN with different port numbers and their influence on flow pattern in the mold are explained.

1.2.1 2 - Port SEN

For conventional slab casting, usually bifurcated SEN is used. The port design is characterized by an upward angle, a horizontal angle or a downward angle. The choice of the SEN port angle is generally determined in accordance with types of steels to be cast and casting conditions.[24]

Downward port angles are preferred over upward port angles because the later promote larger turbulence on the melt meniscus. Moreover, large port dimensions lead to recirculating flows just in the upper edge of the port, leading to backflow conditions and aggravating clogging problems. Most of the SEN designs available in the market observe this characteristic under the reasoning that large ports help to compensate the clogging effects of alumina. Smoothing the angle of the interior upper port edge decreases the clogging and the backflow issues.[25]

Many researchers have observed that the lack of turbulence in the SEN outlet leads to a "straight" jet, and, thereby, lower top-surface velocities. This result shows how important to achieve a precise description of the SEN outlet dynamic behaviour is.[26]

1.2.1.1 2 – Port SEN Rectangular Ports

Calderon – Ramos I. claims that the flow pattern in the mold is determined by the flow dynamics of liquid steel through the nozzle ports and consequently from their specific geometries.[21]

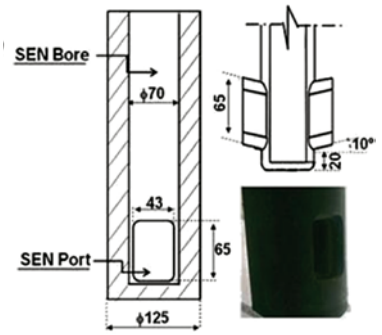

Figure 11. Geometry and size of a 2 - port SEN with rectangular ports.[25]

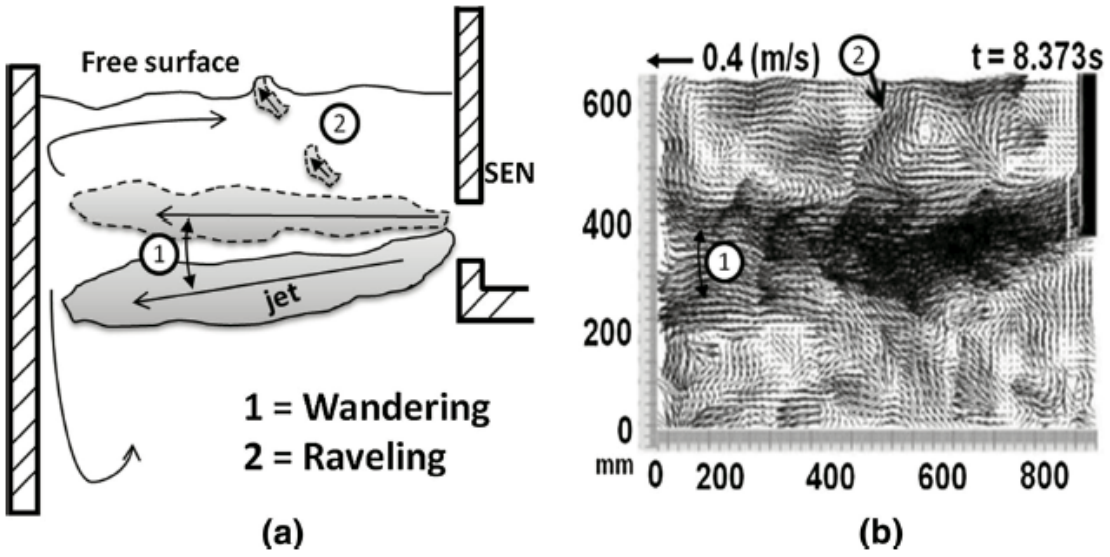

Figure 12. Wandering and raveling phenomena.[25]

The jet is wandering accompanied by its partial disintegration through raveling effects that means, the intermittent separation of fluid streams from the main jet that is directed toward the meniscus. The raveling effects (Figure 12) are indicated by the arrows in Figure 13 (b) through (d). It is also proven by Calderon – Ramos I. that the ravelling effects become more frequent at deeper immersion depth. At some other instants, the jet impacts the narrow wall of the mold with relatively high velocities as is pointed out by the arrow in Figure 13 (a). By using SEN with rectangular ports the flow pattern can described mostly as double roll flow although the meniscus level undergoes large variations. The surface velocities are quite large even when the immersion depth is varying.[25]

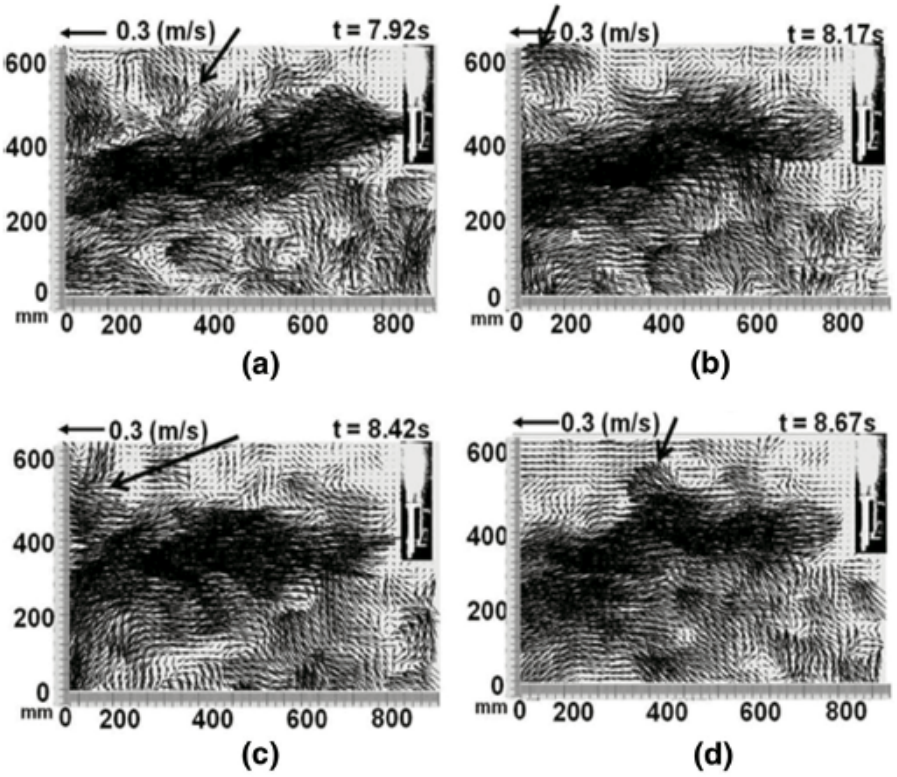

Figure 13. Velocity field using SEN with rectangular ports.[25]

Summarize this facts it is obvious that this SEN causes more turbulent flow in meniscus and submeniscus region.

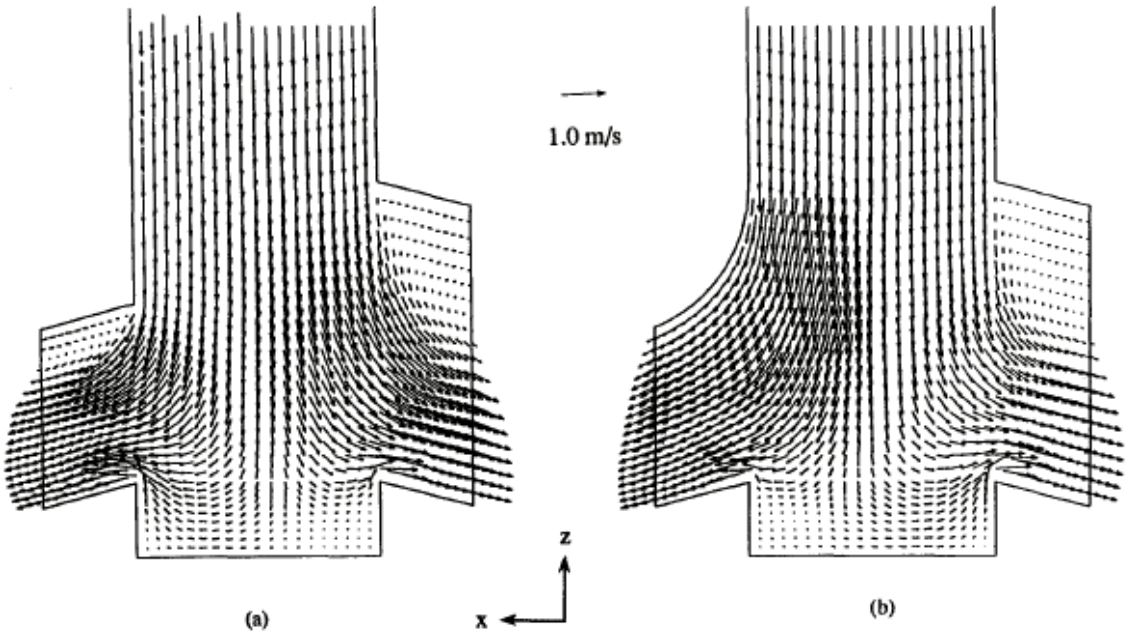

Figure 14. Calculated flow field in the port area with non-uniform port openings: (a) sharp upper corner and (b) curved upper corner.[27]

The angle of the bottom of the port is the most influential variable-controlling jet angle entering the mold, although the jet always leaves at a steeper downward angle than the SEN port angle. The mean jet angle conforms more closely to the port angle when the effective area fraction is large, making the recirculation region at the top of the port smaller. Shorter, thicker, and narrower ports (relative to the nozzle bore area) force the flow to conform more closely to the shape of the port walls. This increases the influence of the port angle, producing shallower jet angles, higher velocities, smaller spread angles, increased turbulence intensity, less swirling flow, and higher effective area fractions. Port curvature promotes a smoother transition from the nozzle tube to the port regions, which consequently increases the effective area fraction and reduces both the peak velocities and the detrimental recirculation zone. A recirculation zone appears at the top of the port (effective area fraction less than 1), unless the combined area of both ports is smaller than the bore area or the port edges are curved. Casting speed increases only the jet speed and the turbulence levels; it does not affect the jet angle or any other characteristic of the jet.[27]

The standard 2 port SEN made by RHI AG can be seen in Figure 15 (a).Depending on the operation conditions, significant mold level fluctuations can be induced by the mold fluid flow behaviour (Figure 15 (b) and (c)).There is no exact color scale but the red color indicates

highest casting speed and the blue color the lowest. These instabilities, in conjunction with the related high shear stresses developed at the liquid steel/mold powder interface, are the main reason for mold flux entrainment into the solidified shell.[24]

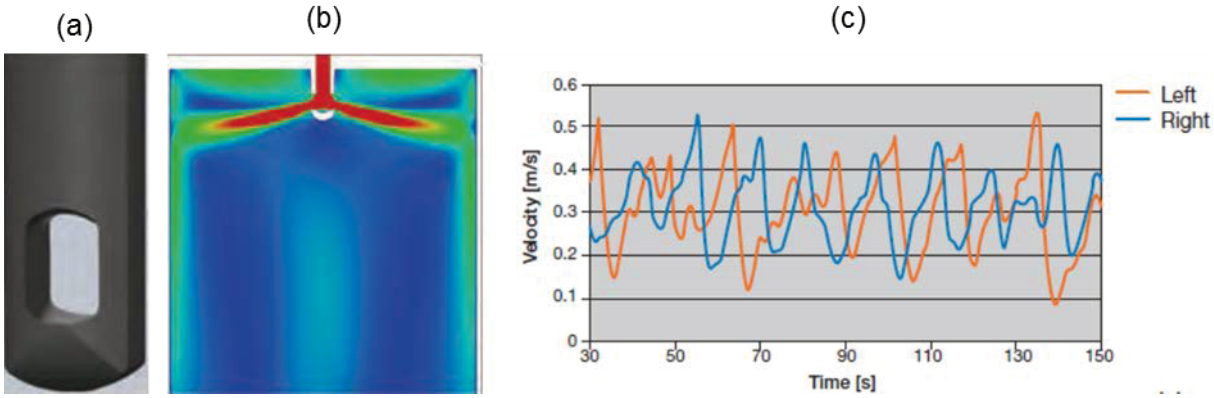

Figure 15. Sketch of the standard 2 port SEN made by RHI and a snapshot of the velocity distribution and the history of the submeniscus velocity for the standard design.[24]

In order to decrease the surface velocity, a modification was implemented at the port area of a standard SEN design as shown in Figure 15 (a). The modified SEN (Figure 16 (a)) comprises a groove in the SEN port bottom. This groove has a remarkable effect on the behaviour of the jet, leading to a far stable mold flow (Figure 16 (b) and (c)). This measure is recommended for a high throughput to keep the meniscus level stable.[24]

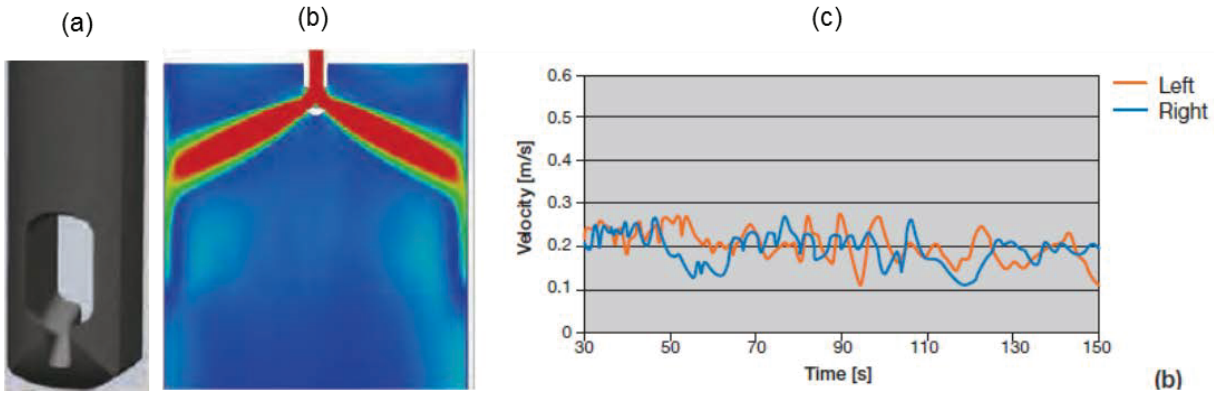

Figure 16. Sketch of the modified 2 port SEN made by RHI and a snapshot of the velocity distribution and the history of the submeniscus velocity for the modified design.[24]

Another modification of the standard 2 Port SEN design was investigated by Yuichi Tsukaguchi et al. (Figure 17). The generation of swirling flow in a submerged entry nozzle is a fundamental way to stabilize flow in a continuous casting mold. The swirling-flow submerged entry nozzle can improve the surface quality of slabs and steel coils and increase the casting speed by increasing flow stability in the mold.[28]

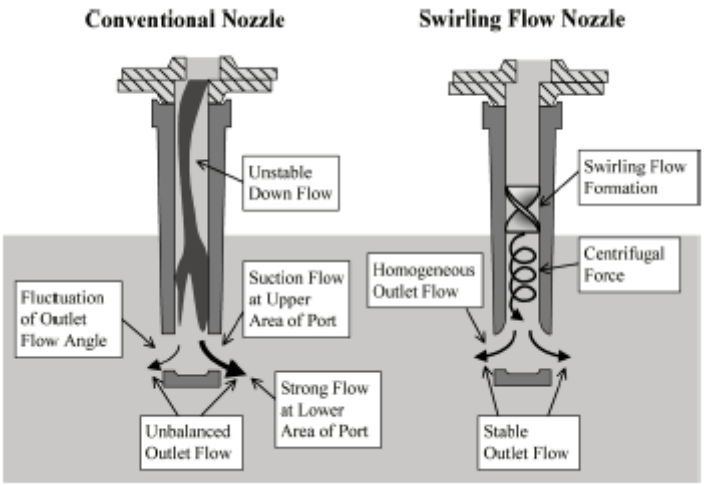

Figure 17. Schematic view of flow formation in nozzle.[28]

A third modification was investigated by Brunnmayer et al. Previous simulation work described a stabilisation effect of an additional hole with non-satisfying single roll flow at enormous wave heights. An improvement of the side port flow condition could be attained by eliminating the recirculation zone near these ports (Figure 18).[29]

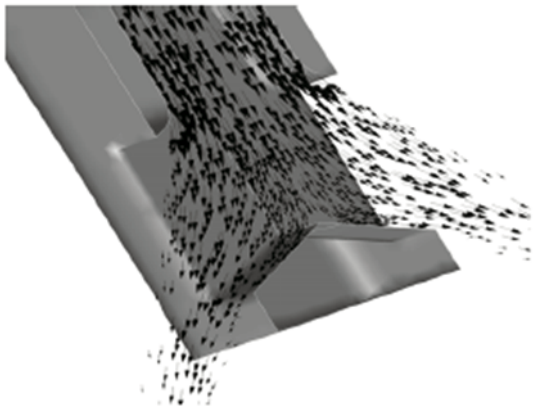

Figure 18. Optimized bifurcated SEN.[30]

Contours of velocity magnitudes and temperature (Figure 19 (a) and (b)) show a quasi-steady side port jet moving towards the narrow side of the mold and generating double roll flow pattern with a large upper recirculation.[29]

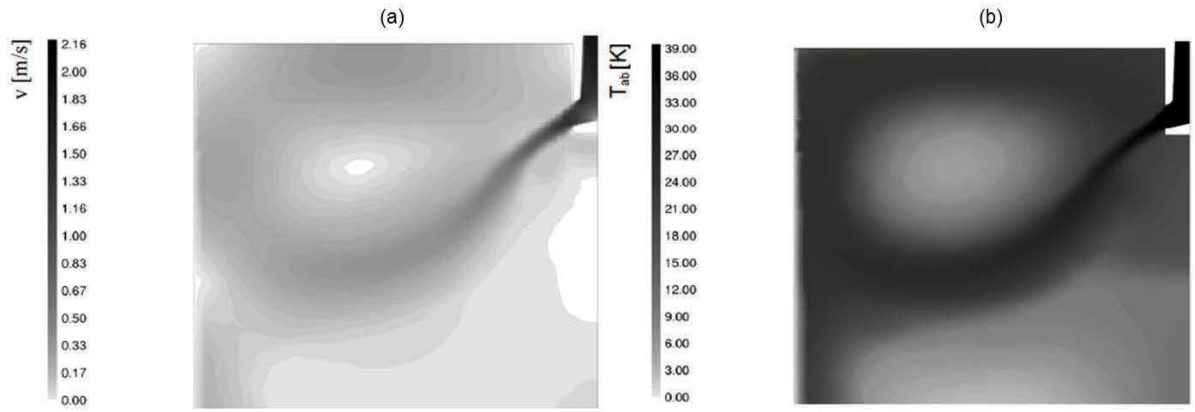

Figure 19. Velocity and temperature contours of the optimized SEN.[29]

A higher and more homogenous temperature distribution at the meniscus and a reduction of the wave heights to approximately a third compared to other 2- or 3- port SEN can be achieved. This seems to be good operation conditions for high quality slabs.[29]

1.2.1.2 2 – Port SEN Square Ports

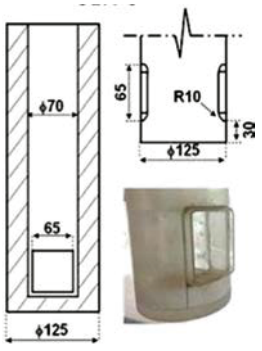

Figure 20. Geometry and size of a 2 - port SEN with square ports.[25]

By using the SEN with square ports at a shallow position (e.g.: 115 mm) the flow pattern can be described as single roll flow. The raveling effects using SEN with square ports are also more frequent compared to SEN with rectangular ports as is shown by the arrows in Figure 21 if it is used at deeper position (e.g.: 185 mm).[25]

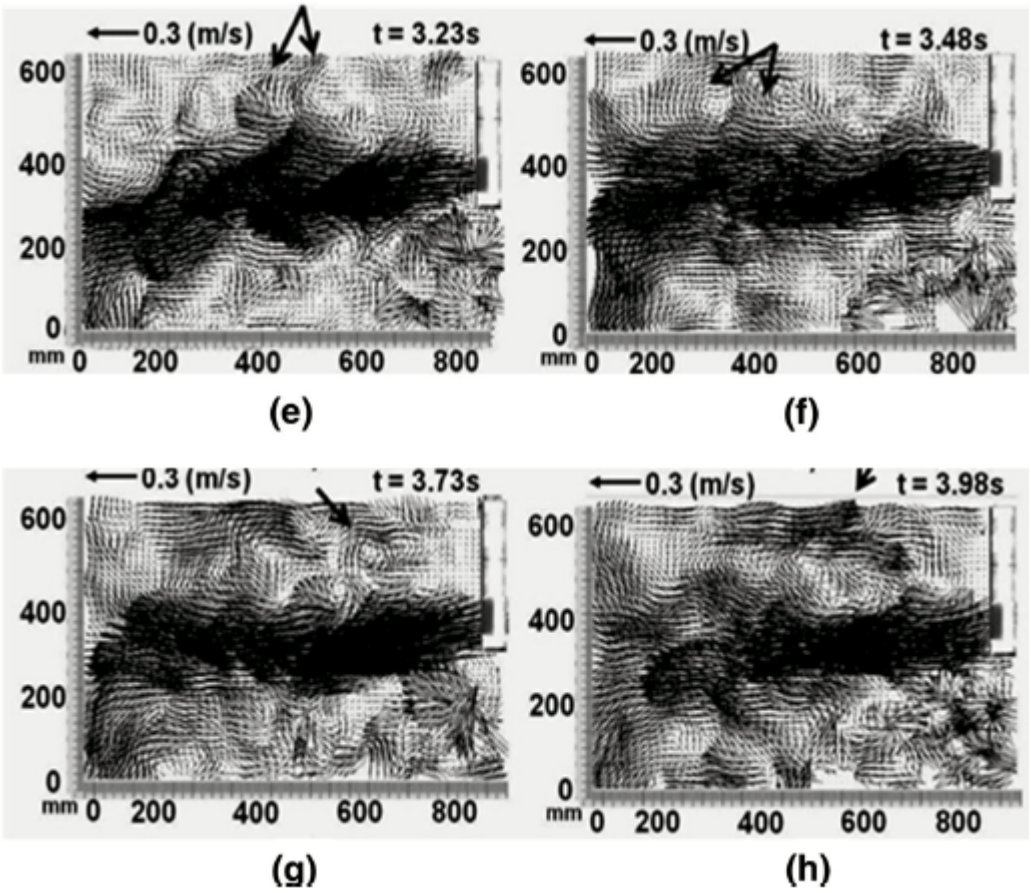

Figure 21. Velocity fields by using SEN with square ports.[25]

The SEN with rectangular ports yields larger meniscus velocities in the deep position than in the shallow position. SEN with square ports yields opposite effects. The discharging jets using either nozzle suffer effects of strong wandering and raveling effects with detached streams that enhance turbulence in the meniscus and submeniscus regions. When a detaching flow from the jet meets another originated by the impact with the mold, narrow wall turbulence is particularly intensified. These effects are more severe using SEN with rectangular ports. It is also shown that independent from immersion depth the SEN with square port show smaller velocity peaks. That is why SEN with square ports is recommended over SEN with rectangular ports for casting operations.[25]

1.2.1.3 2 – Port SEN Round Ports

It was found that rectangular port geometry works better than the typical cylindrical port.[30] SEN with round ports (Figure 22) generate more swirls and have a larger spread angle than rectangular ones having the same cross-section area.[25]

The delivered liquid presents less dispersion comparing to the SEN with cylindrical port designs which reduces the appearance of a backflow.[30]

Real C. did some numerical simulations with a bifurcated SEN with 2 round ports with a downwards angle of 15 degrees because this kind of SEN is in industry widespread. The black dots in Figure 22 indicate measuring points for the velocity inside the SEN. It was proved that using the LES (large eddy simulation) turbulence model it is possible to reproduce periodic behaviors observed in plant. It was observed that the periodic behaviour is a consequence of the dynamic interaction between the fluid at the SEN pool and the fluid immediately above it. Additionally, it was found that the characteristics of the periodic behavior depend at least on the casting speed.[26]

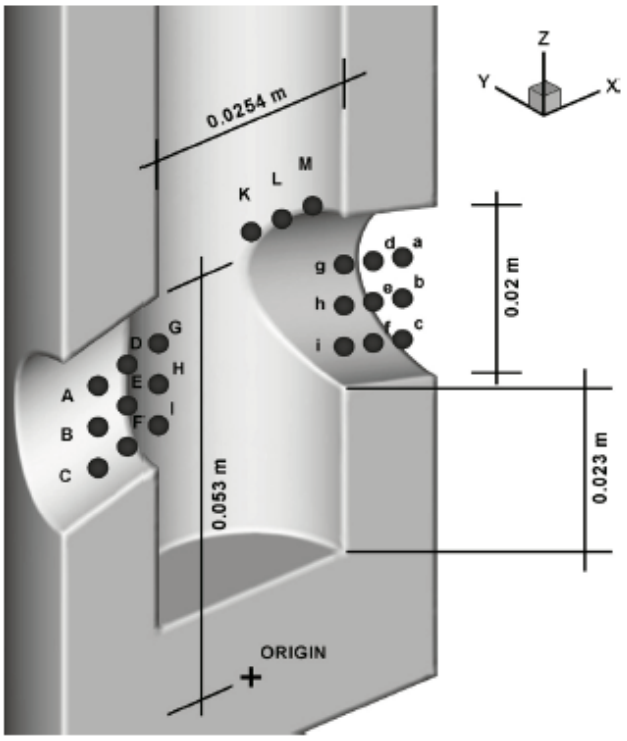

Figure 22. 2 Port SEN design with round ports and a recessed bottom.[26]

Asymmetry with respect to XZ plane was obtained and two main vortexes with opposite rotational motions on the plane YZ were observed (Figure 23). A change in the vortex number, size, and rotational direction at the SEN exit ports observed at different casting speeds and appears to be the result of a very complex dynamic behavior inside the SEN. This behaviour can be explained by analysing the dynamic interaction between the fluid in the pool and the fluid above it. The relationship between the velocity variation range and the casting speed is non-linear and further research must be carried out in order to understand this relationship fully.[26]

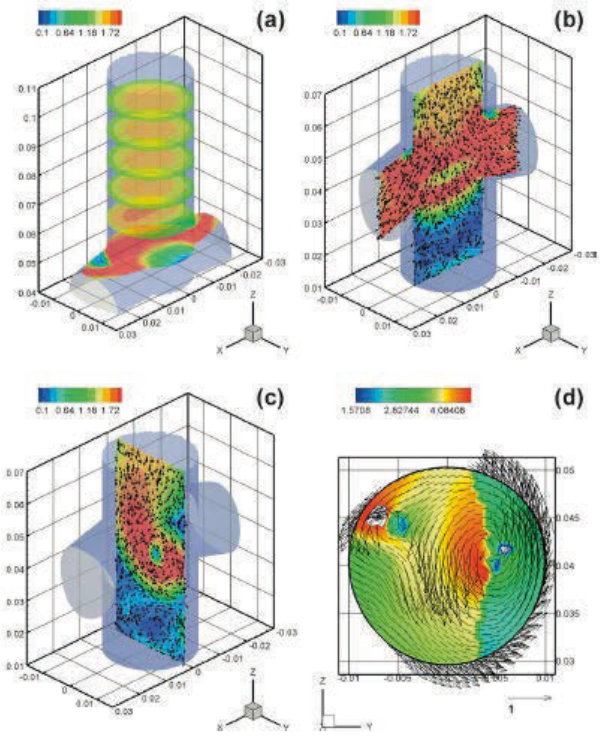

Figure 23. Flow behaviour inside the 2 round ports and a recessed bottom SEN using the LES.[26]

1.2.1.4 2 – Port SEN Design 1

The 2 - port SEN Design 1 has two lateral ports separated by a short divider. Main dimensions of this nozzle can be seen in Figure 24.

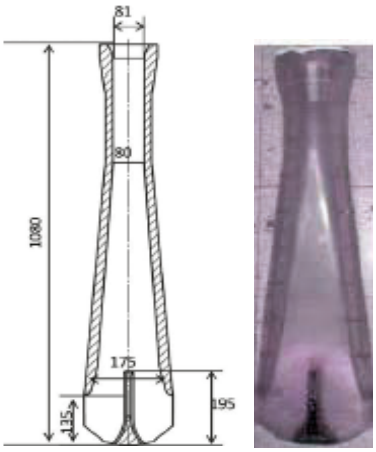

Figure 24. 2 - Port SEN Design 1.[17,18]

With the design shown in Figure 24 an upper flow without generating an active lower roll flow can be achieved and creates a stagnant large zone below the nozzle, which has a negative effect according to the casting operation (Figure 25). A change in immersion depth influences the flow pattern easily. The stagnant zone below the nozzle is decreasing. The shown results represent a casting speed of 7.5 m/min and two different immersion depths (220 mm and 350 mm).[17]

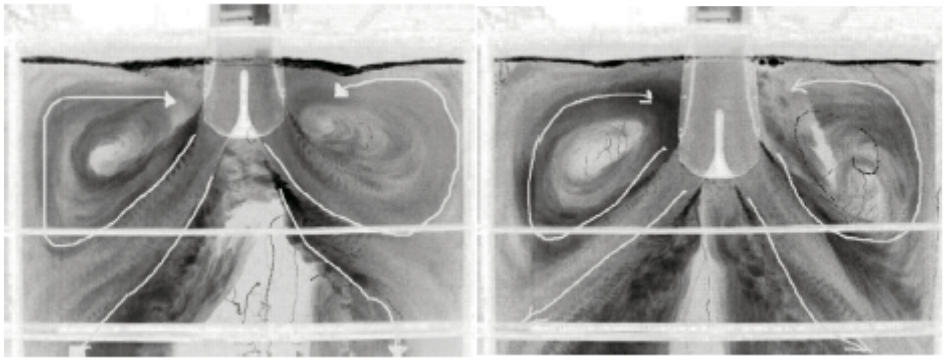

Figure 25. Flow pattern in the mold at immersion depth 220 mm and 350 mm at a casting speed of 7.5 m/min.[18]

The meniscus analysis shows heavy depressions at the positon of the funnel, including the formation of vortices (Figure 26 (a)). Figure 26 (b) shows the history of instantaneous velocity of the submeniscus velocity. The positon of the monitoring spot can be seen in Figure 27.

This positon was chosen because it is just the transition zone between the straight parallel wide molds and the funnel where the flow is more instable.[18]

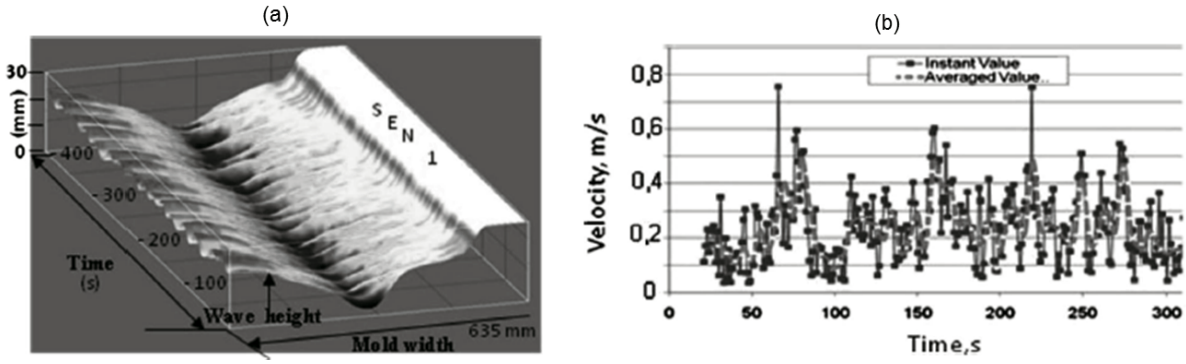

Figure 26. Wave fluctuation topography from water modelling at an immersion depth of 220 mm with analysis of the submeniscus velocity.[18]

This 2 – port SEN creates very high instantaneous velocities. This conveys a high probability for flux entrainment under these casting conditions.[18]

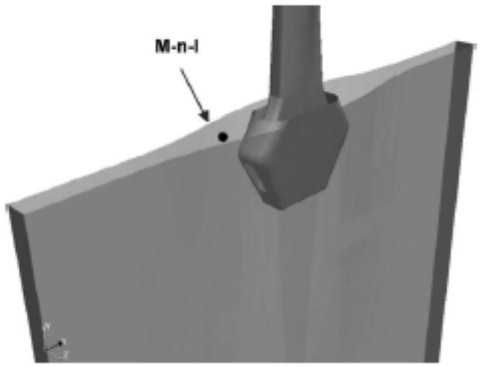

Figure 27. Position of the monitoring spot.[18]

1.2.1.5 2 – Port SEN Design 2

Compared to the nozzle design shown in Figure 24 similar results can be achieved with the 2 – Port SEN Design 2 (Figure 28).

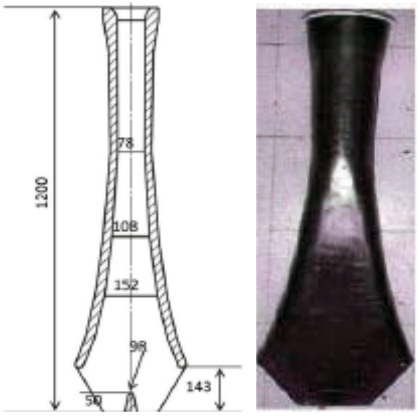

Figure 28. 2 - Port SEN Design 2. [17,18]

It also induces a strong single upper roll flow but without a stagnant zone below the nozzle bottom (Figure 29). The presence of severe meniscus depressions remains, thus indicating instability at the position of the funnel. By changing the immersion depth the flow pattern is changing complete. Stagnant zones exist in the corner of the mold due to non-symmetric mixing behaviour.[18]

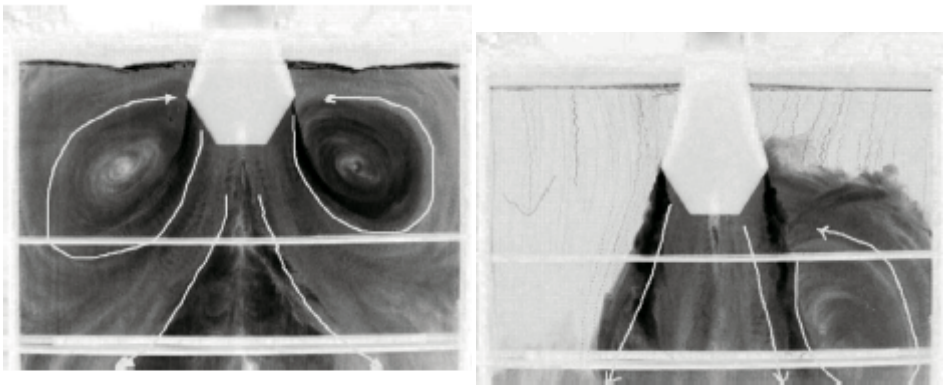

Figure 29. Flow pattern in the mold at immeriosn depth 220 mm and 350 mm at a casting speed of 7.5 m/min.[18]

The position of the monitoring spot can be seen in Figure 27. As Figure 30 shows similar results to the other 2 – port SEN with lower variations in velocity can be achieved.

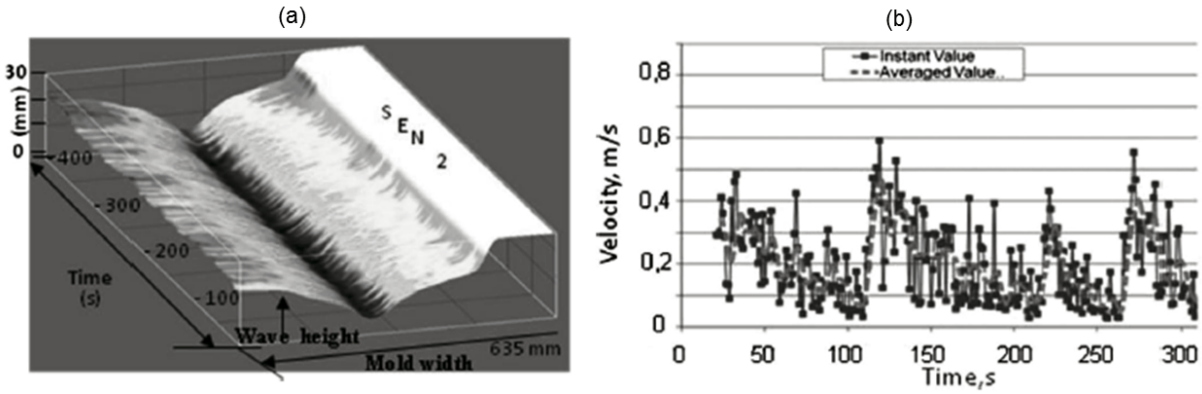

Figure 30.Wave fluctuation topography from water modelling at an immersion depth of 220 mm with analysis of the submeniscus velocity.[18]

1.2.2 4 - Port SEN

A four-port, funnel-shaped SEN produces shallower jet angles, lower peak velocities, and a greater effective area fraction, as compared with the standard bifurcated nozzle.[27]

1.2.2.1 4 - Port SEN Design 1

The 4 – port SEN shown in Figure 31 is designed to achieve turbulence control and meniscus stability by highly symmetric flow and a vortex free bath surface. This design is based on the theoretical aspects of boundary layer and aerodynamics principles applied to steel flow through the SEN.[17]

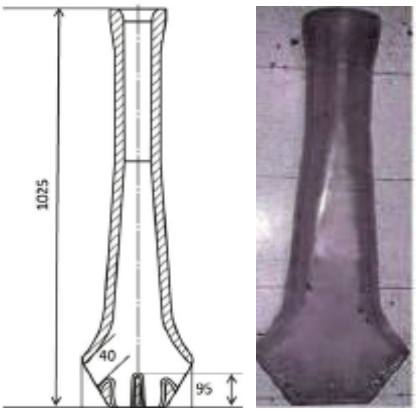

Figure 31. 4 Port SEN. [17,18]

In water model experiments done by Morales et al. can be seen that by using this 4 port SEN designs no stagnant zones and a double roll flow pattern can be achieved (Figure 32). This flow pattern is independent from the immersion depth. This 4 - port SEN maintains a stable meniscus without the formation of strong vortices or depressions.[17,18]

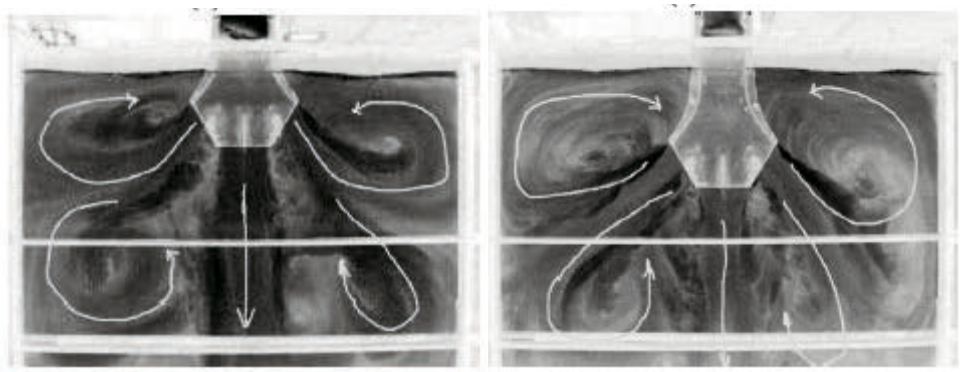

Figure 32. Average flow pattern at different immersion depth.[18]

This 4 – port design shows more stable meniscus Figure 33 (a) and creates compared to the two 2 – port SEN lower and constant velocities (Figure 33 (b)).[18] This results in stable bath topography.

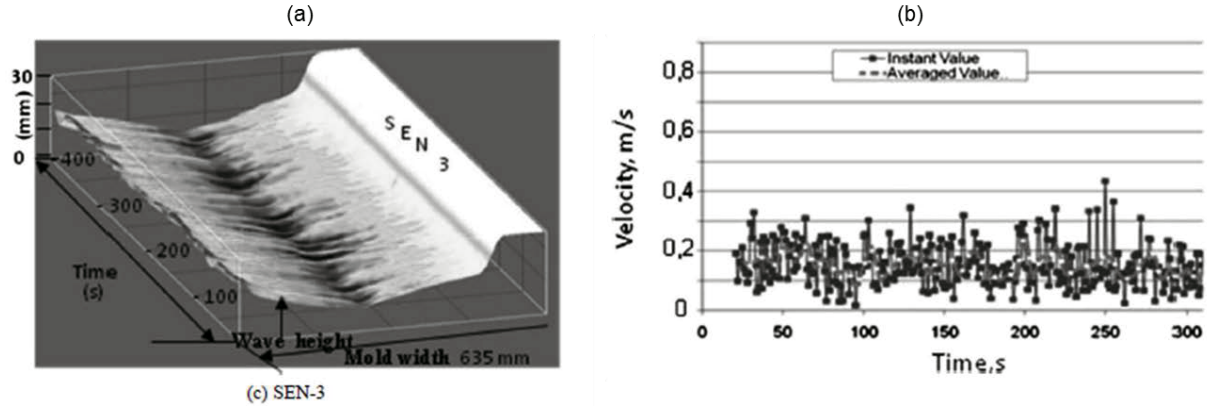

Figure 33.Wave fluctuation topography from water modelling at a immersion depth of 220 mm with analysis of the submeniscus velocity.[18]

1.2.2.2 4 - Port SEN Design 2

Simulations work with the 4 Port SEN design (Figure 34) was done by M.H. Zarea in cooperation with Saba Steel Iran.[31]

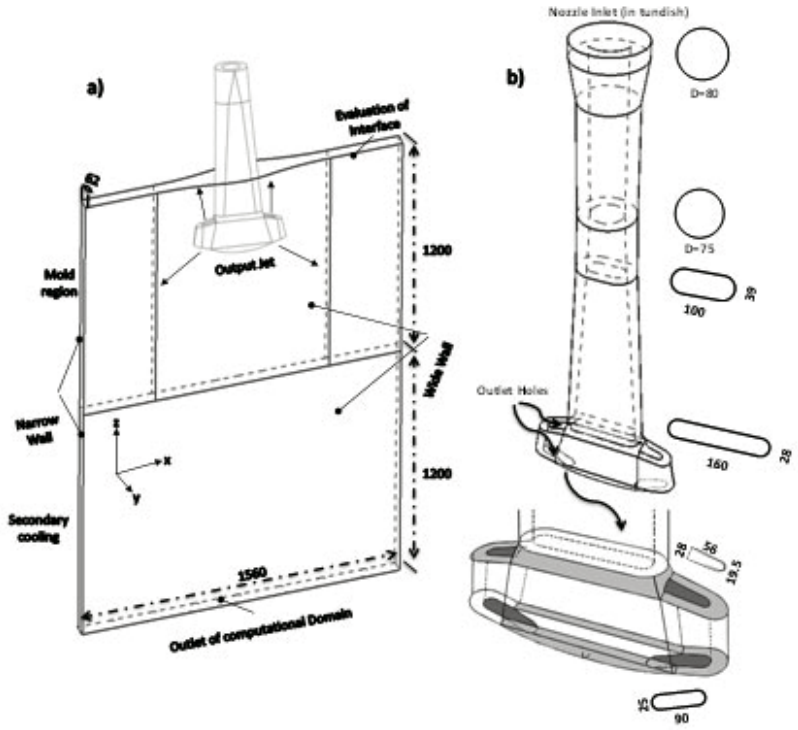

Figure 34. 4 - Port SEN designed by Saba steel company.[32]

In Figure 35 a 3D flow field at a casting speed of 3.4 m/min and an immersion depth of 300 mm can be seen. Based on the simulations about 14-17% of the input melt goes out from the upper ports which is preventing solidification of the steel on the top surface especially at the peripheral parts of the nozzles and moving part of the impurities to the free surface.[31]

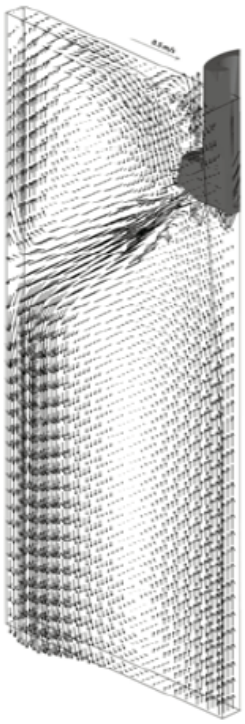

Figure 35. 3D liquid flow field pattern.[29]

The top recirculation zone is formed by the steel that reaches the narrow wall of the mold and then flows towards the steel/slag interface. The outlet flow from the lower port of nozzles touches the mold walls while it still intends to go down the mold and creates the lower recirculation zone.[31]

The results of the heat distribution of the liquid in the mold can be seen in Figure 36. The flow from the lower holes hits to the thin walls and forms lower and upper rings. In the centre of the mold the liquid temperature is lower because of low fluid flow velocity and lower super heat dissipation in this region. The melt flow at the top surface of the mold has enough super heat for avoiding freezing.[31]

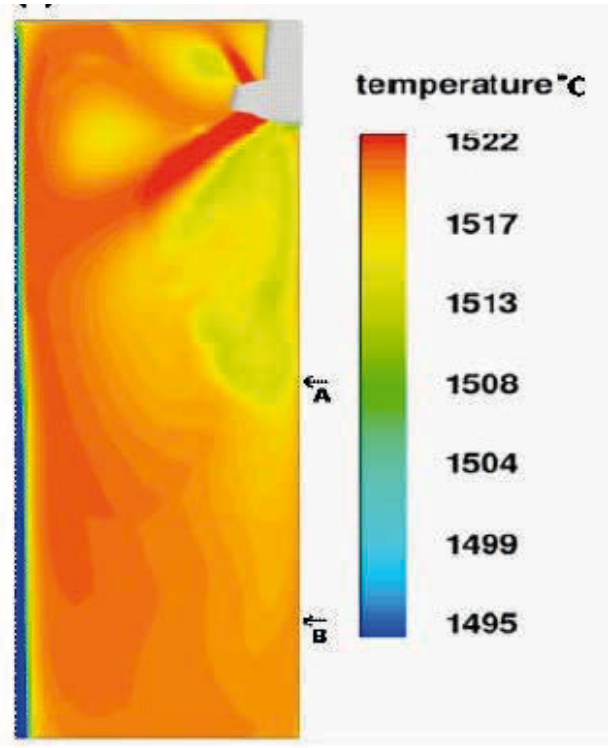

Figure 36. Heat distribution inside the mold (casting speed 3.5 m/min, immersion depth 300 mm).[31]

1.2.3 5 – Port SEN

Experiments and analysis with a 5 Port SEN design (Figure 37) was performed by Young Jin Jeon et al.[29]

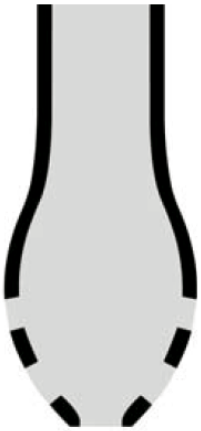

Figure 37. Sketch of a 5 Port SEN.[33]

For this investigation a casting speed of 6.17 m/min and the maximum flow rate U = 50 m³/h are selected. High flow rates generate recirculation flows with high velocity gradients. In Figure 38 the velocity distribution of three different flow rates can be seen. This 5 – port nozzle shows a complex flow pattern because of the five exits. The flow pattern seems to be similar independent from the flow rates. The lower vortex flow may be generated by the periodic meniscus flows. The vortex pairs appear between the SEN and the funnel and are generated by the crush and the rolling of the cross-flow. The formation of these vortices is affected by the meniscus velocity as well as the velocity in the vicinity of the meniscus. As the number of recirculation regions increases, the quantity of the flow that influences the meniscus is reduced. As a result, the inner and meniscus flows are stabilized.[33]

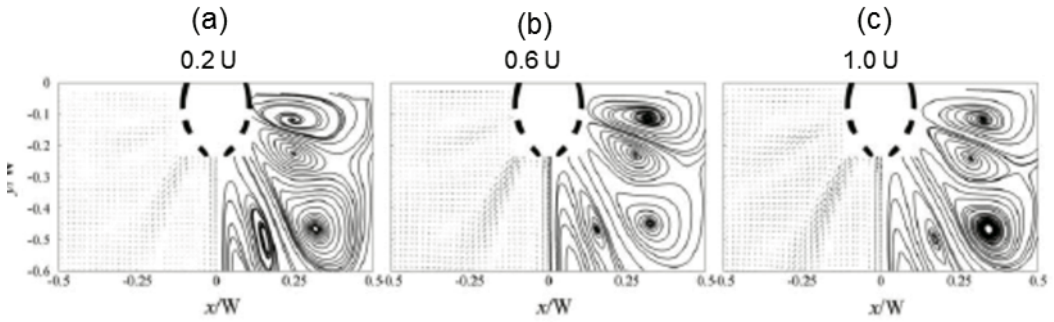

Figure 38. Mean velocity vectors and streamlines.[33]

Only a few publications have validated their mathematical simulations with experimental measurements of speed and flow pattern/behaviour in the mold and unfortunately this situation leaves the unanswered question: what characteristics of a SEN should be considered as the right ones for a specific task. As mentioned before there are many factors which influences the flow pattern and behaviour and that is why further studies have to be done for a better understanding of the whole process inside the mold. The latest development of the 4 – port and 5 – port SEN show good results during the casting process in thin slab castings to achieve goals like higher casting speed, good mixing behaviour, sufficient heat distribution and a stable meniscus topography.

2 Water Model Experiments

The flow pattern in a given continuous casting mold can be determined in several different ways. Water is often used as model medium to mimic the molten steel. A transparent plastic mold with a under scaled size is constructed as casting mold.

Water models have been proven to be accurate for single phase flows regardless of the model scale factor, so long as the flow is fully turbulent. Obtaining accurate flow patterns is very difficult when gas injection is significant, and some phenomena, such as slag layer behaviour, cannot be modelled quantitatively, owing to the inherent differences in fluid properties, such as density and surface tension.[23]

2.1 Water Model Setup

The idea or the meaning of water model experiments in the steel metallurgy is very simple. Some properties especially the flow behaviour of water is similar to liquid steel. That makes practical research at that scientific field much easier and helps to develop new products.

The water model apparatus is built up at the training centre of the RHI in Leoben. The walls of the apparatus are made of Plexiglas. The plate with the submerged entry nozzle

(SEN) can be moved to any position to simulate any immersion depth (E) of the SEN. (see Figure 39). The immersion depth is defined from the meniscus to the upper edge of the port. The scale of the model is 1:2 to real size of thin slab casting.

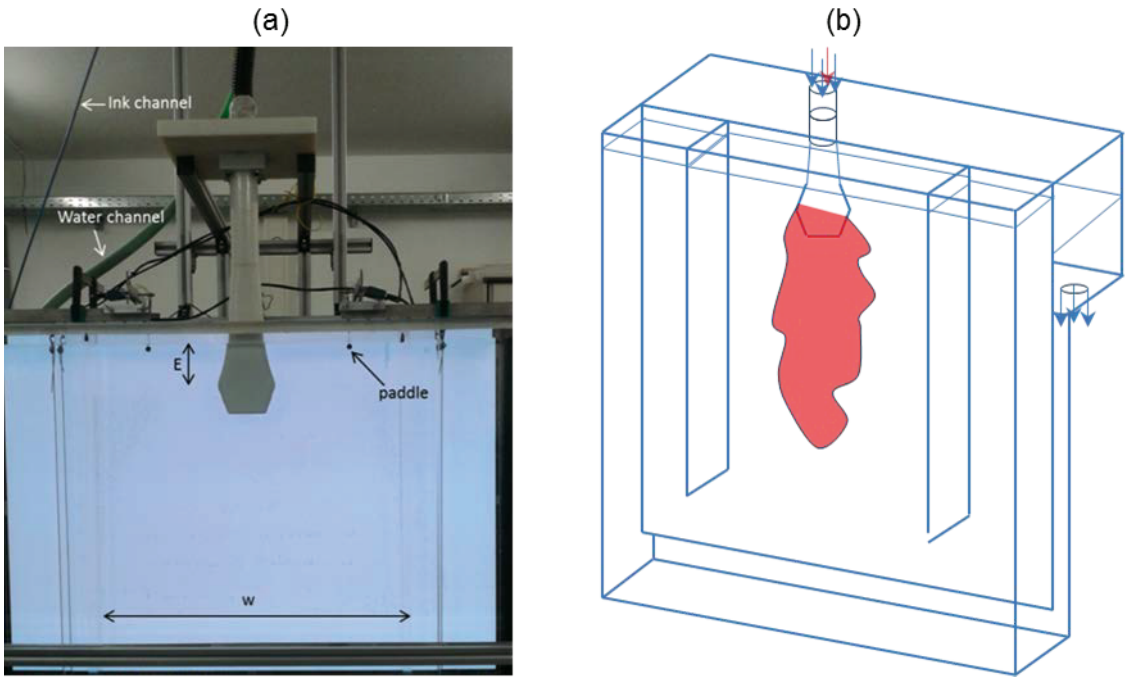

Figure 39. (a) water model set up (b) water model sketch.

Different UFM - single port SEN designs were produced by a 3D – printer at the RHI which should produce the flow pattern of a multi-port SEN design. The designs of the SEN with 6 mm gap and 18 mm can be seen in Figure 40.

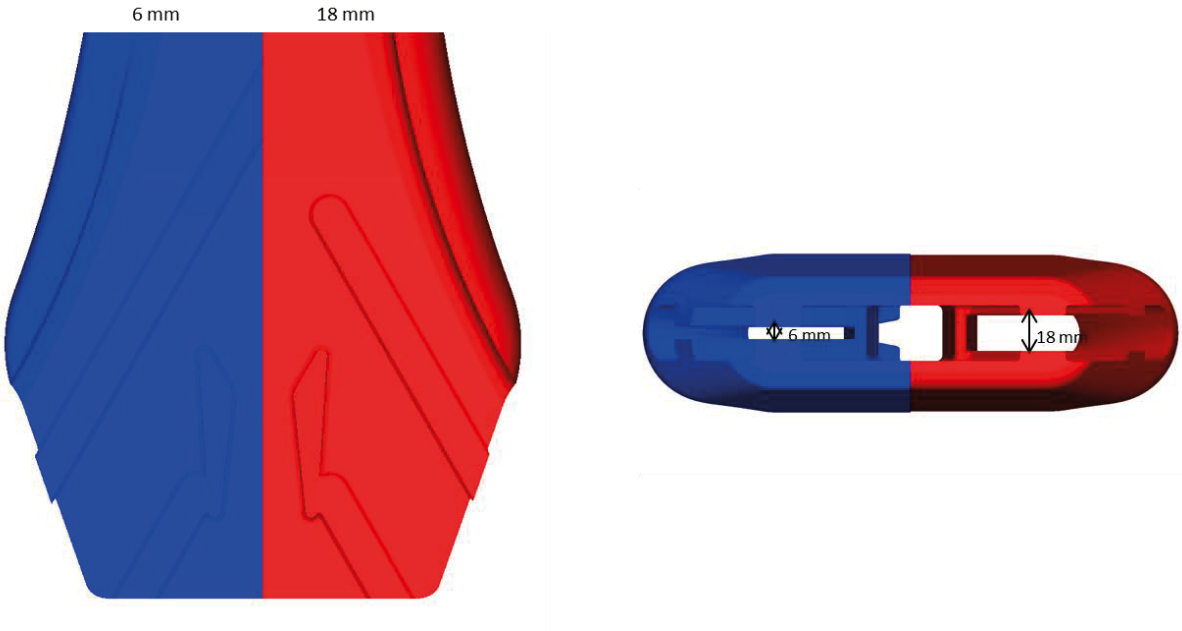

Figure 40. The UFM - single port SEN design with 6 mm (blue) and 18 mm (red) gap.

The water flow rate can be controlled automatically or by hand. To keep the water level constant there is an outlet on the back of the apparatus.

A separate dye or ink channel which is connected to the water channel is also present. The dye injection gives a good representation of the mixing behaviour. The experimental team of the RHI decided to use dye to make the jet flow visible instead of using particles. By using particles a few problems occur. First of all it is difficult to find a material which has almost the same density as water because if the particles are lighter than water the particles are trying to flow upwards or decrease the jet velocity. By using heavier particles the opposite effect appears. Another disadvantage of using small spherical particles is getting a sufficient amount of the particles into the channel to make the jet visible for a qualitative analysis possible. Using dye injection is the easiest way to make the jet and the flow pattern during the experiment visible.

The paddles on the left and right sight of the SEN which are positioned about 10 mm under the water surface measure the submeniscus velocity of the flow. This velocity is measured for duration of 30 min with a time step of 0.1 seconds. This is done to have enough data to analyse the submeniscus velocity and to be sure that the flow is stable before starting dye injection.

All data which are recorded during the trials are recorded and visualized by an in-house software package.

2.2 Plan of Experiments

Three different main cases are defined. The trials vary in mold width, casting speed (i.e. flow rate) and SEN gap size. The plan of experiments can be seen in Table 1. The mold thickness is kept constant (112.5 mm) during the whole experiment.

			SEN gap size [mm]					
	Mold width [mm]	Casting speed [m/min]	6	8	10	12	15	18
Case 1	1150	2.4	x	x	x	x		x
Case 2a	1400	2.0						x
Case 2b	1400	2.4						x
Case 2c	1400	3.4	x	x	x	x	x	x
Case 3	1700	2	x	x	x	x		x

Table 1. Plan of experiment.

All cases are repeated five times to ensure the repeatability of the experiment and to make a statistical overview of the results possible.

2.3 Experiment procedure

Every case with the certain SEN gap size was set up by the technician, Mr Fellner (RHI). The whole apparatus was filled up with water. The certain flow rate corresponding to the

casting speed was calculated and programmed. Because it is a 1:2 model the casting speed or the water flow rate is adapted by Froude.

$$Q_m = \left(\frac{1}{x}\right)^{2.5} \times Q_r \quad (1)$$

In equation (1) Q_m $[\frac{m^3}{h}]$ is the water flow rate, Q_r $[\frac{m^3}{h}]$ is the melt flow rate for the real dimensions. x defines the scaling factor. In our case x is always 2.

Q_r is calculated as:

$$Q_r = \left(\frac{Width\ [mm] \times Thickness\ [mm] \times Casting\ Speed[\frac{m}{min}]}{1000000}\right) \times 60 \quad (2)$$

In Table 2 all the used and calculated values can be seen.

Width [mm]	Thickness [mm]	Casting speed [m/min]	Melt flow rate Q_r [m³/h]	Scale 1:x	Water flow rate Q_m [m³/h]
1150	112.5	2.4	18.63	2	3.29
1400	112.5	2.0	18.90	2	3.34
1400	112.5	2.4	22.68	2	4.01
1400	112.5	3.4	32.13	2	5.68
1700	112.5	2.0	22.95	2	4.06

Table 2. Calculated water flow rates.

At the beginning of every trial Q_m is calculated for each case. To get a stable flow pattern and make a qualitative analysis possible the submeniscus velocity is measured after 10 minutes the apparatus was completely filled with fresh water. It is recorded for 30 minutes with a measuring time step of 0.1 seconds.

Next step is the injection of the dye. These trials take about 30 seconds each. During that time dye was injected for about six seconds. A high resolution camera took about 15-18 pictures per seconds. Should the dye injection be repeated, duration of 5 minutes has to be waited until the water in the system becomes clean again.

3 Results of Water Model Experiments

The camera takes about 15-18 pictures per second and every run is recorded for 30 seconds. Five runs with the same settings are made. The pictures are processed with the open source software ImageJ. ImageJ is an open source Java image processing program inspired by NIH Image.

Snapshots in Figure 41, as recorded by the camera, show the typical flow pattern in the TSC mold. The dimensions of the mold are 1150*112 mm². The casting speed is 2.4 m/min and the SEN gap size is 12 mm. As mentioned before these dimensions are real operating dimensions in steel plants. The water model is scaled down by 1:2 because of the available space at the laboratory. Also the casting speed is adapted to the model.

In the beginning of the dye injection a symmetric flow can be seen and also the beam is divided into three parts which spread out in different directions. The double vortex generation starts at an early time. It can be seen that the dye is transported very even all over the whole domain. Even after the dye injection it is clearly to see that the fresh water streams continuously into the mold.

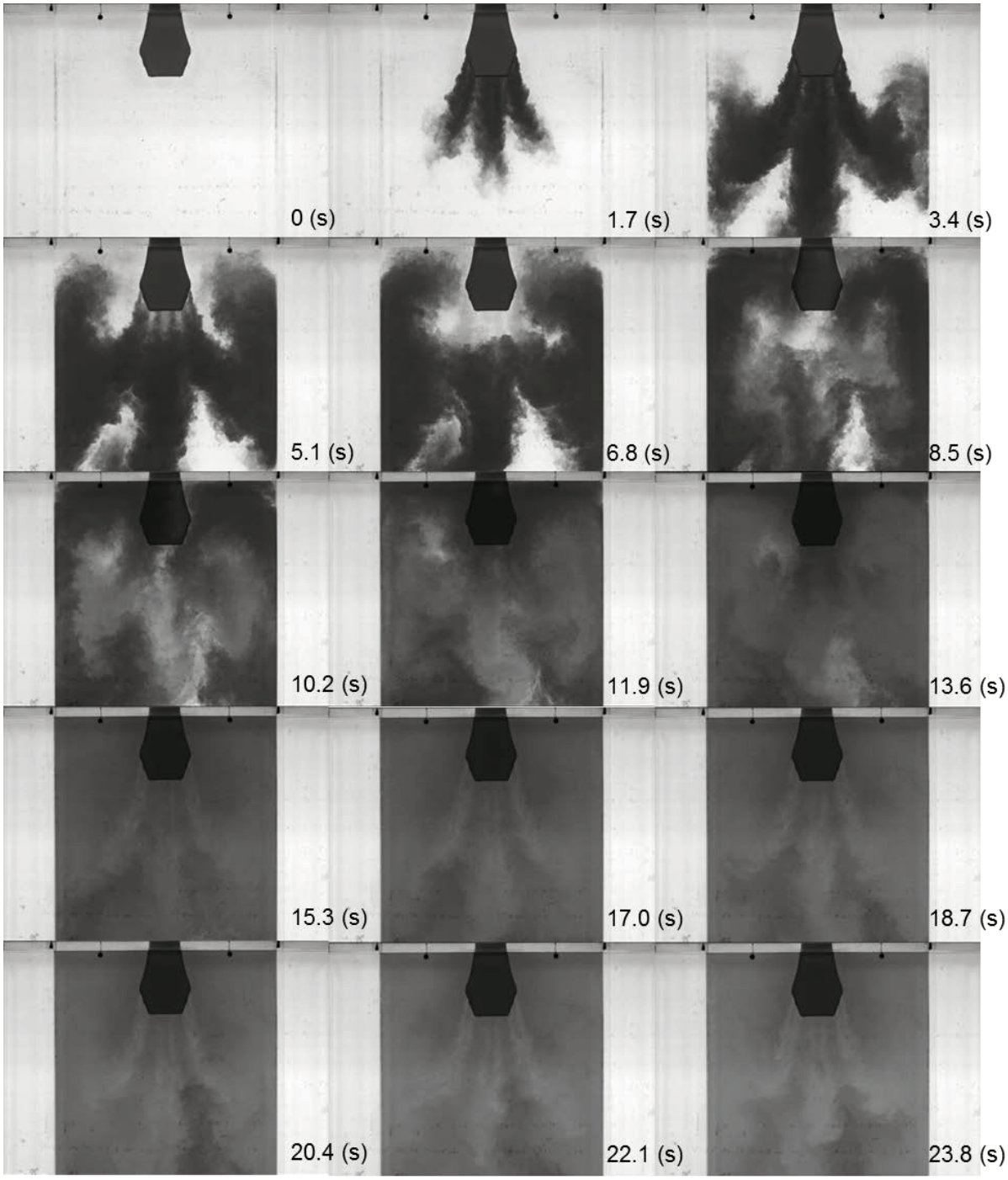

Figure 41. Example of flow pattern in the mold of case 1 (Table 1) with the SEN gap 12 mm. These snapshots are taken in a constant time interval of 1.7 (s).

In Figure 42 another example of an unstable and unsymmetrical flow for the case 2c (Table 1) can be seen. The dimensions for the mold are 1400*112 mm². The casing speed is 3.4 m/min and the SEN – gap is 18 mm. As written before the dimensions refer to real equipment size and not to the model.

In the beginning of the dye injection three separated beams can be seen. Here the beams have the same direction. Just one single vortex on the left side of the model is build. Because of the vortex the beam changes its direction from left side to straight downwards. After some time the direction of the beam changes again and flows in right direction.

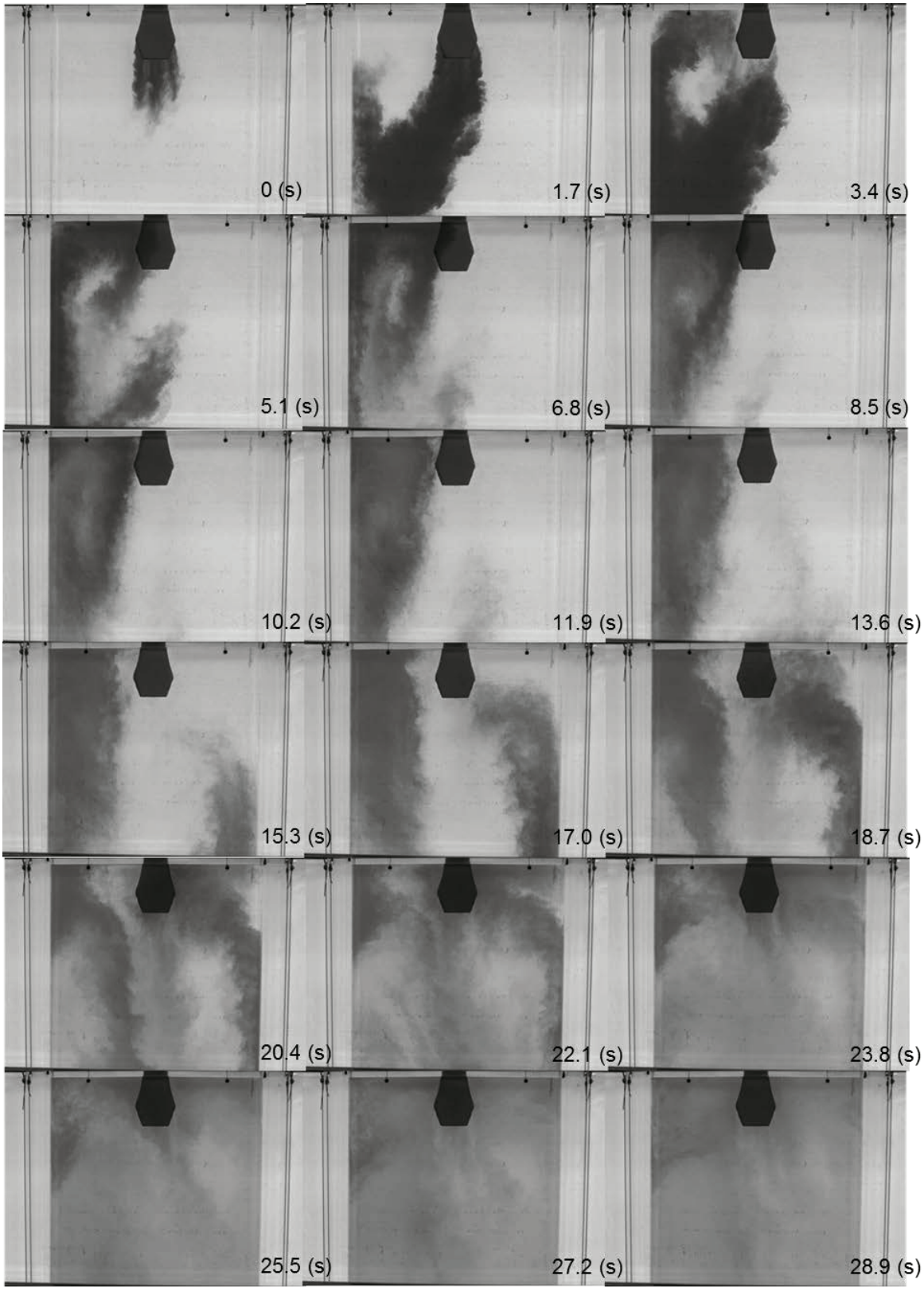

Figure 42. Example of the flow pattern in the mold of case 2c (Table 1) with the SEN gap 18 mm. These snapshots are taken in a constant time interval of 1.7 (s).

During the experiments a change in direction of the flow can be observed. For analysis the pictures with same flow direction are overlapped. Darker areas show higher concentration of the dye. At the end of recording time lighter areas indicate higher concentration of new incoming water. It is assumed that the direction of the beam before dye injection is the same as in the beginning of the injection. Without any dye in the model it is impossible to give an qualitative analysis of the flow.

In order to assist the analysis of the flow pattern, the flow direction is marked by arrows. Yellow arrows indicate the incoming flow and the red arrows show the backflow.

Typically three different flow patterns are observed: stable, unstable and transient. The transient means the flow pattern changes for different runs with the same settings.

3.1 Stable Flow

In this chapter results of all three cases will be seen. Case 1 is defined with a mold width of 1150 mm and a depth of 112.5 mm. The casting speed is determined with 2.4 m/min. With this settings and gap sizes of 6, 8, 10 and 12 mm stable flow is achieved. Every trial is repeated five times to demonstrate the repeatability of the experiment results. Stable flow is determined with almost constant flow pattern during all repeats.

3.1.1 Case 1 SEN Gap Size 6 mm:

In Figure 43 all 5 runs can be seen. It is clearly seen that between these 5 different runs no difference in the flow pattern appear. 5 different flow directions (yellow arrows) are clearly seen. The jets on the top are creating a vortex on the left and on the right side which makes a material transportation to the top of the mold possible. The dye is transported to the bottom by the side currents and the jet which goes straight down.

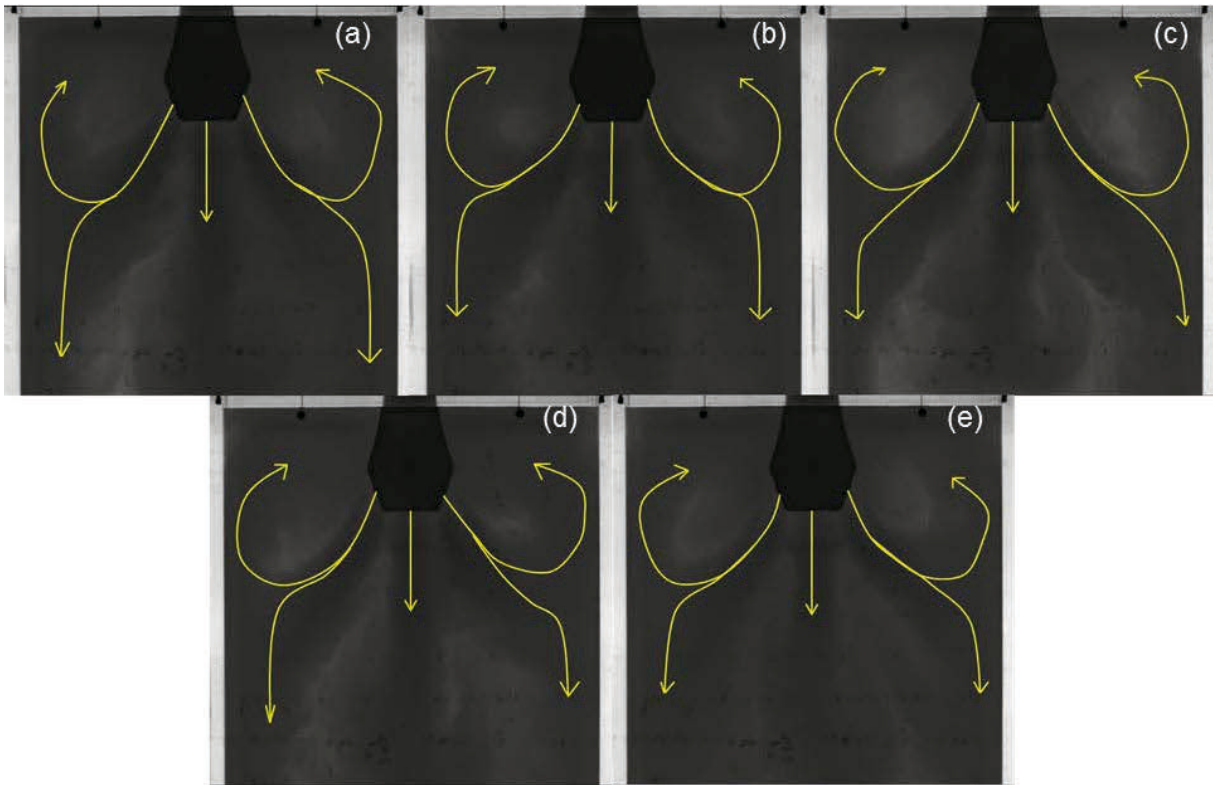

Figure 43. Results of case 1 for the SEN gap size 6 mm (a) – (e) (Run 1-5).

Insignificant differences may be seen in the size or shape of the vortexes on the left and right side. During the experiment the water was lead to every section in the mold which is also one aim during the casting process in the plant.

3.1.2 Case 1 SEN Gap Size 8 mm:

In Figure 44 all five runs of case 1 for the SEN gap size of 8 mm can be seen. The flow pattern is stable. There is a vortex development on the top of the mold. The dye is transported to ground. Slightly differences can be seen in the shape and size of the upstreaming vortexes on the left and right side of the SEN. The size and shape of the upper vortexes influences also the jets which stream in the direction of the wall and downwards. That is the reason why small differences in the flow pattern can be seen.

The metallurgical function of this SEN design to transport new material in all sections of the mold is fulfilled

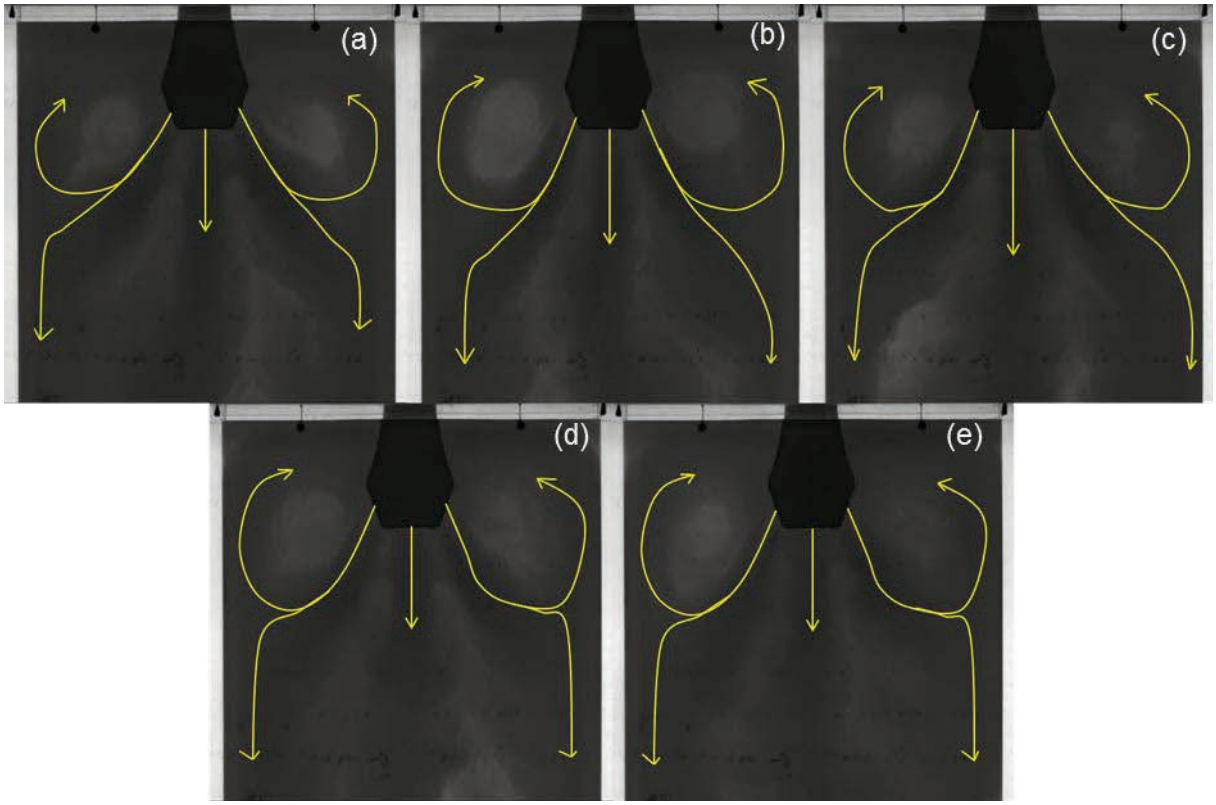

Figure 44. Results of case 1 for the SEN gap size 8 mm (a) – (e) (Run 1-5).

3.1.3 Case 1 SEN Gap Size 10 mm:

In Figure 45 all five runs of case 1 for the SEN gap size of 10 mm can be seen. This scenario describes a stable flow situation. As seen in the trials before there are small differences in the size and shape of the jets and vortexes. In Figure 45 (e), the fifth run, it is evident that during the experiment less dye was transported to the upper left corner than to the right one. In that case the down streaming jet starts oscillating compare to the different runs. A reason for the change of direction of the down streaming jet can be caused by the backflow from the bottom of the mold.

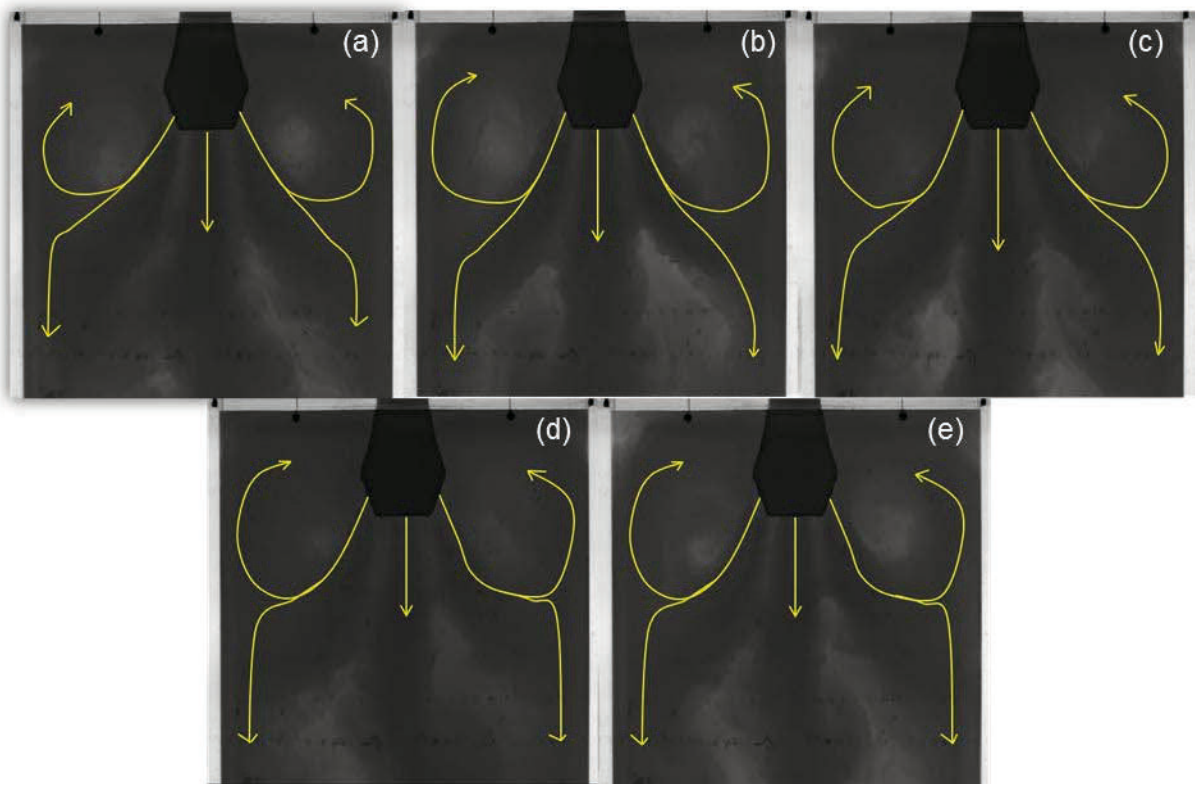

Figure 45. Results of case 1 for the SEN gap size 10 mm (a) – (e) (Run 1-5).

3.1.4 Case 1 SEN Gap Size 12 mm:

In Figure 46 the results of all 5 runs of the case 1 for the SEN with the 12 mm gap can be seen. The results shows similar flow pattern compared to the previous ones. The dye is transported to all sections of the mold. Some differences in the shape and size of the vortexes and jets between the several runs can be seen.

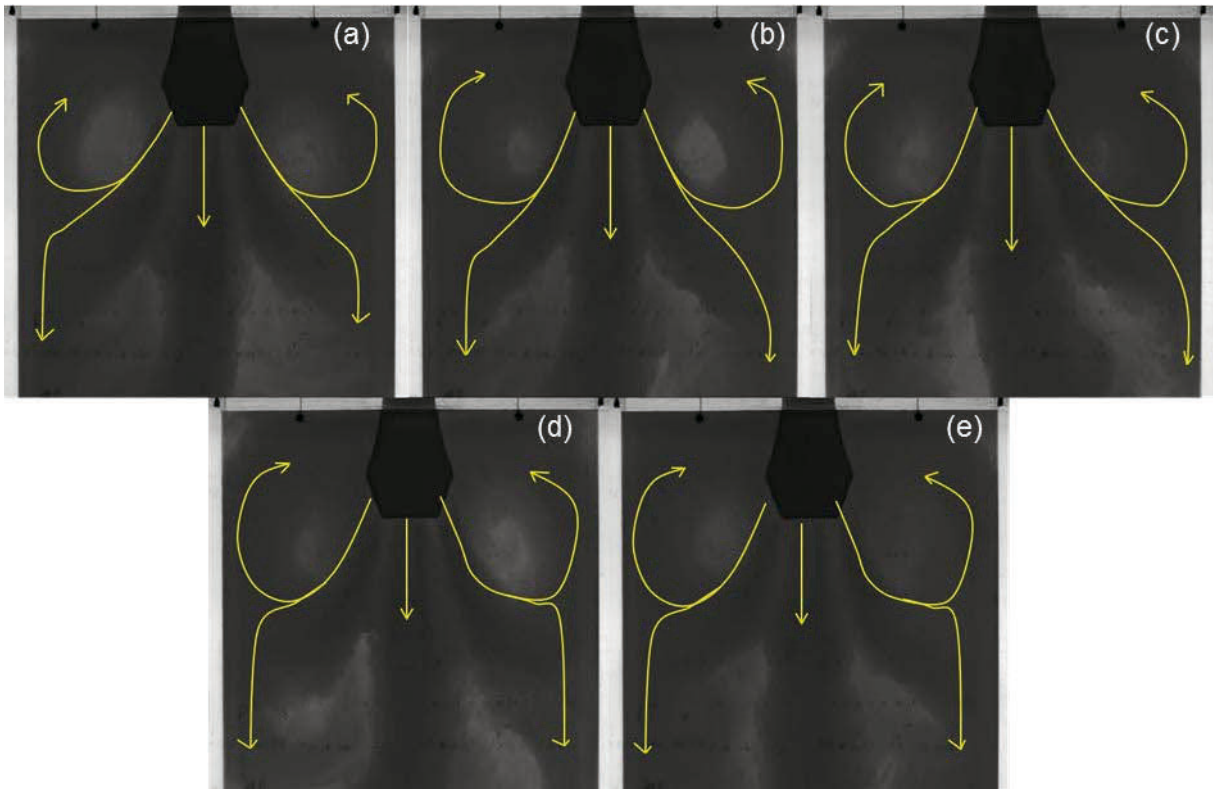

Figure 46. Results of case 1 for the SEN gap size 12 mm (a) – (e) (Run 1-5).

3.1.5 Case 2c SEN Gap Size 6 mm:

Case 2 is divided into three different parts/settings. The mold design and the SEN gap (18 mm) are always the same. The casting speed was varied. The different casting speeds are 2 m/min (Case 2a), 2.4 m/min (Case 2b) and 3.4 m/min (Case 2c). Case 2c is also done with all other SEN gap sizes. For case 2c a new SEN model with 15 mm gap size was produced.

Case 2c is defined by a mold width of 1400 mm times 112.5 mm and a casting speed of 3.4 m/min. In that case the SEN with the gaps of 6, 8, 10, 12, 15 and 18 mm are used. Every trial was is repeated five times.

In Figure 47 all five runs for case 2c with the same settings can be seen. The flow pattern in all five runs is same over the whole recording time of 30 seconds. In every image the jet which goes straight downwards can be recognized. Also the development of the vortex on the left and right top corner is clearly seen. From both side ports a current which flows diagonal downwards can be observed. In every part of the observed area dye is transported.

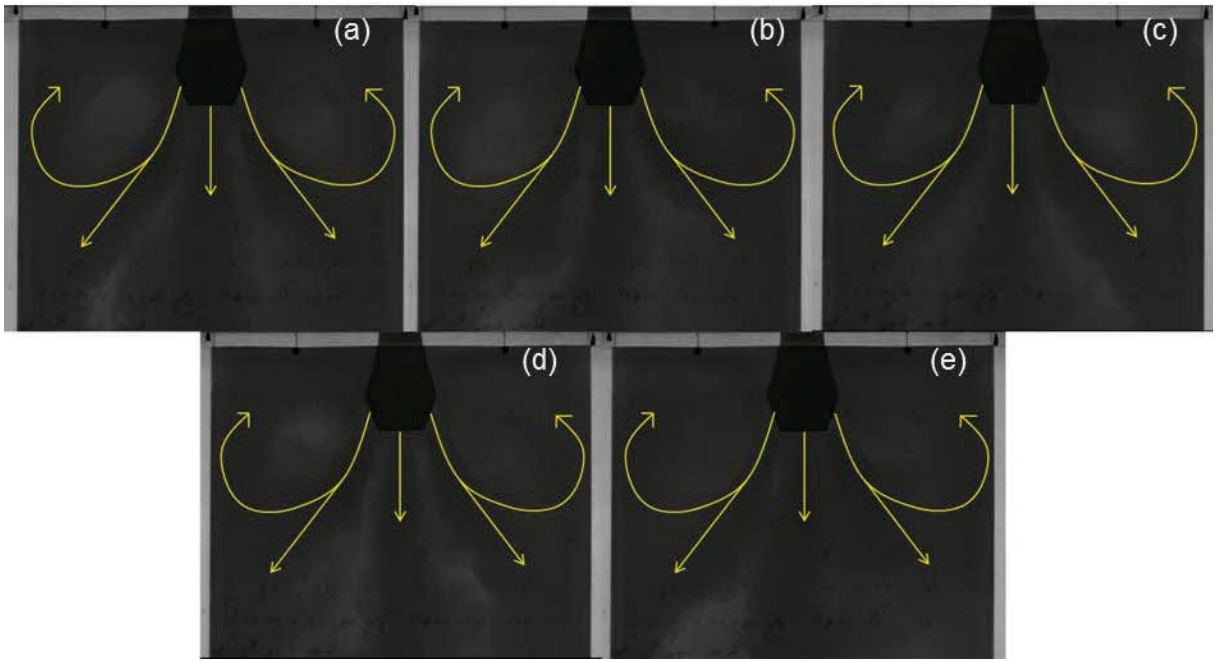

Figure 47. Results of case 2c for the SEN gap size 6 mm (a) – (e) (Run 1-5).

3.1.6 Case 2c SEN Gap Size 8 mm:

The results of case 2c for the SEN with the 8mm gap are similar to the results of gap size of 6 mm (Figure 47). In all 5 runs the flow pattern is same over the whole recording time. The side ports on the left and right side are creating a vortex at the top corner. Also currents out coming from the side ports which flow diagonal downwards are present. The beam which goes straight downwards is also clearly seen on all five images.

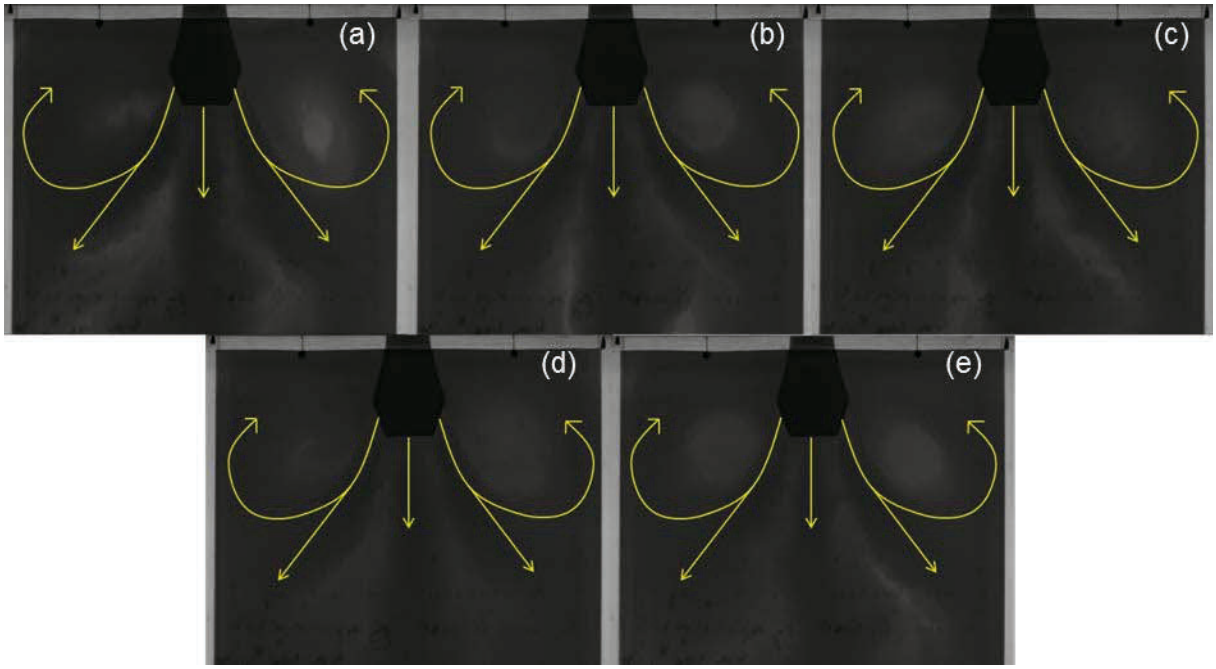

Figure 48. Results of case 2c for the SEN gap size 8 mm (a) – (e) (Run 1-5).

3.1.7 Case 3 SEN Gap Size 6 mm:

Case 3 is defined by a 1700 * 112.5 mm mold with a casting speed of 2 m/min. The SEN gaps used are 6, 8, 10, 12 and 18 mm. As in the other cases every trial was repeated five times to get a good overview of the flow pattern.

In Figure 49 all five runs with the same settings can be seen. There is no change in flow direction or behaviour observed. In all five runs a vortex creation on the left and right side with in the mold can be seen. In the first run (Figure 49 (a)) no dye is transported to the right corner in the bottom of the mold. In all five runs a current which goes straight down can be clearly seen.

Compared to the other results with the stable flow there are huge differences. In that cases there are just three instead of five single jets. In the first image no dye is transported to the right corner in the bottom which is not wished for the real plant. The size of the right vortex in the last image is a little bit different compared to the other four.

The creating of three currents instead of five, lead to a degradation of the mass and heat transport during the casting process.

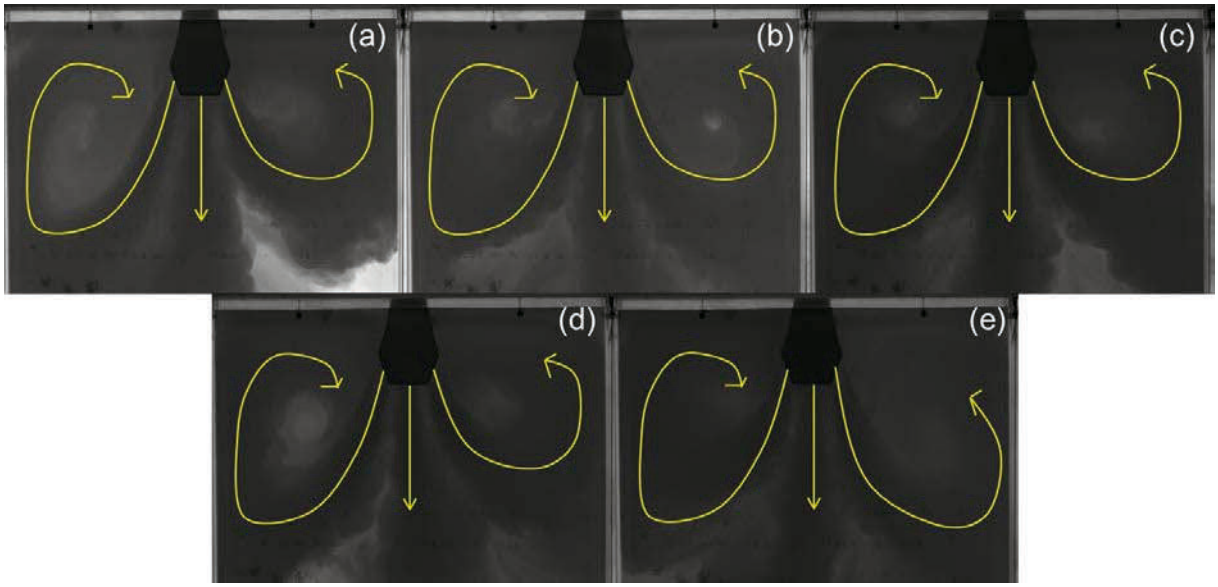

Figure 49. Results of case 3 for the SEN gap size 6 mm (a) – (e) (Run 1-5).

Stable flow pattern is one of the aims of the production of thin slab castings. It is important for constant mass and temperature distribution.

3.2 Transient Flow

Transient flow pattern is characterised by not repeating the exact same flow schemes during all five runs for the same settings.

3.2.1 Case 2c SEN Gap Size 10 mm:

The results of case 2c for the gap size of 10 mm can be seen in Figure 50. In the first four images the results are quite the same. Two vortexes are created and a single jet is going downwards. The vortices distinguish in size and shape. That is why there are lighter areas at the corners of the images because there is not as much dye being transported to these areas. In Figure 50 (d) dye is transported to the bottom because the vortices develop in a deeper section as in the Figure 50 (a)-(c). In Figure 50 (e), the fifth run, differences to the other four runs can be recognized. There are two upstreaming vortices, one going straight

downwards and two streaming diagonal to both mold walls. In that case the dye transport is more constant than in the other four runs.

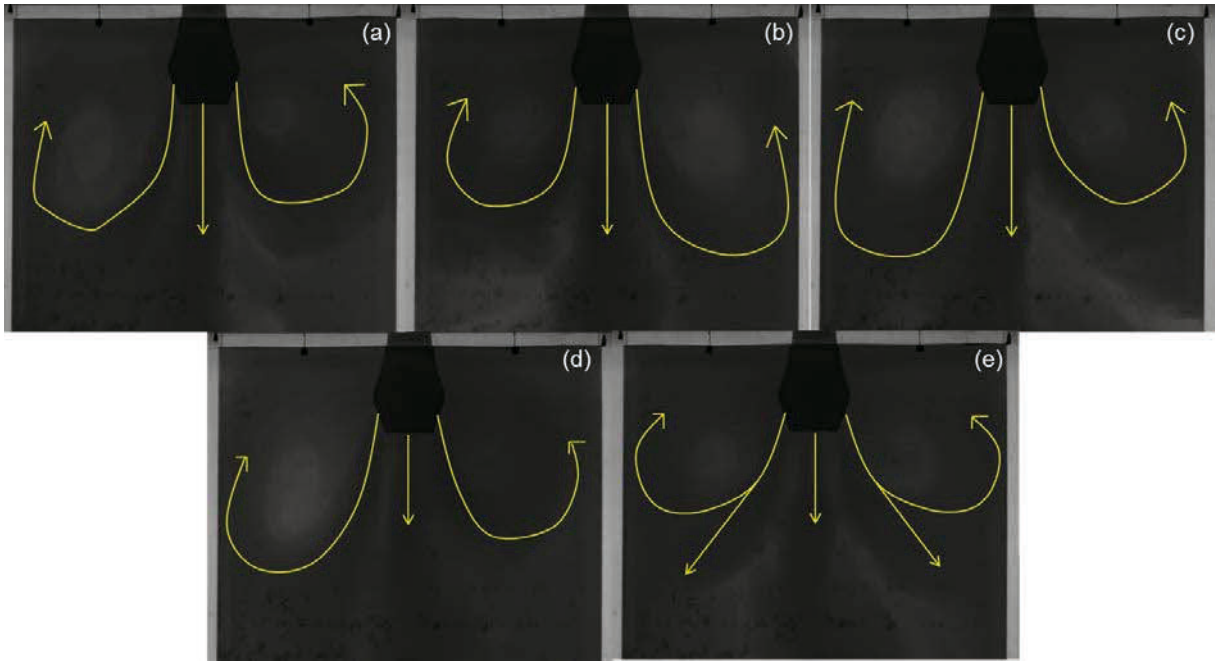

Figure 50. Results of case 2c for the SEN gap size 10 mm (a) – (e) (Run 1-5).

3.2.2 Case 3 SEN Gap Size 8 mm:

In Figure 51 (a) – (d) the first four runs can be seen. The flow pattern doesn't change during the recording time. In Figure 51 (a) two vortexes can be seen. The jet which flows straight downwards is present. There are some lighter sections which correspond to less dye concentration. In real plant casting this would be a huge disadvantage for producing slabs.

In the second run (Figure 51 (b)) the flow pattern is different to the first one. On the left side a vortex is seen which transports the dye to the left section at the top. The vortex on the right is larger than the left one. Also the jet which flows straight downwards is present. This flow behaviour is not preferable for real casting situations.

The third run (Figure 51 (c)) is also different compared to the previous runs. A straight downwards jet and a vortex on the right side can be observed. A backflow stream is upcoming from the left.

The fourth run shows just one beam which flows to the right side Figure 51 (d). One huge vortex is developed during the whole recording time. At the left side of the mold no dye is transported. In real thin slab casting processes this would be very dangerous because this can lead to an abort of the casting process.

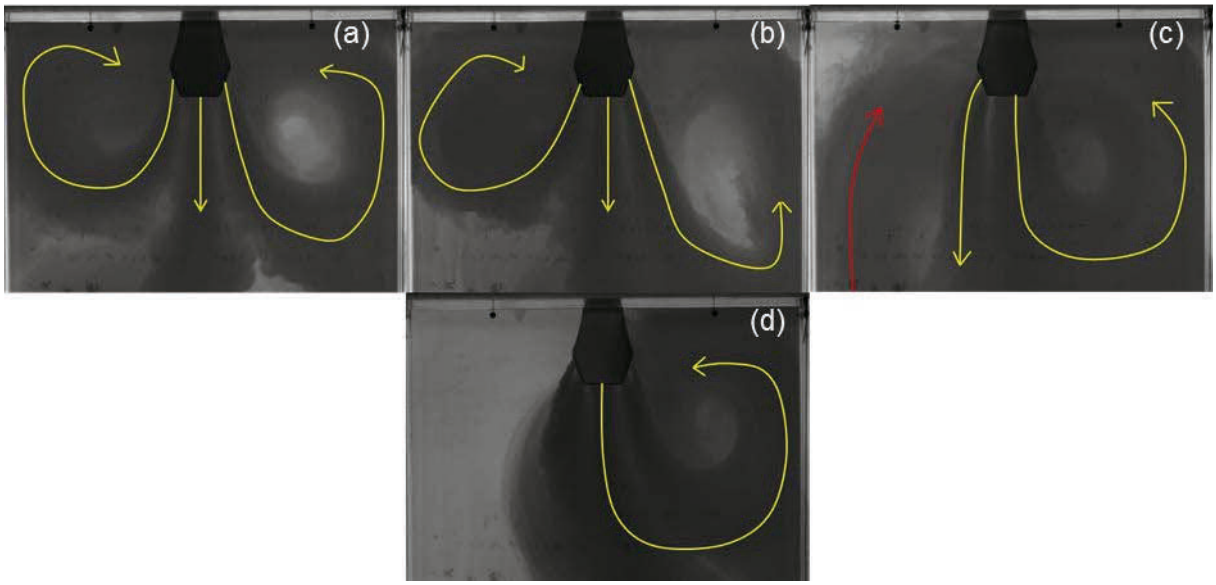

Figure 51. Results of case 3 for the SEN gap size 8 mm (a) – (d) (Run 1-4).

In the fifth run with of case 3 with the SEN gap size of 8 mm a change of the flow pattern can be observed. In Figure 52 (a) the first 21.25 seconds of this run can be seen. It looks like one beam is present which flows straight down and creates a vortex at the left side of the mold. At the right side a very strong backflow can be observed which reaches the surface and streams from the right to the left side. In Figure 52 (b) the last 10 seconds of recording time are shown. One jet is creating a vortex at the right side of the mold. At the left side there is a backflow upstreaming.

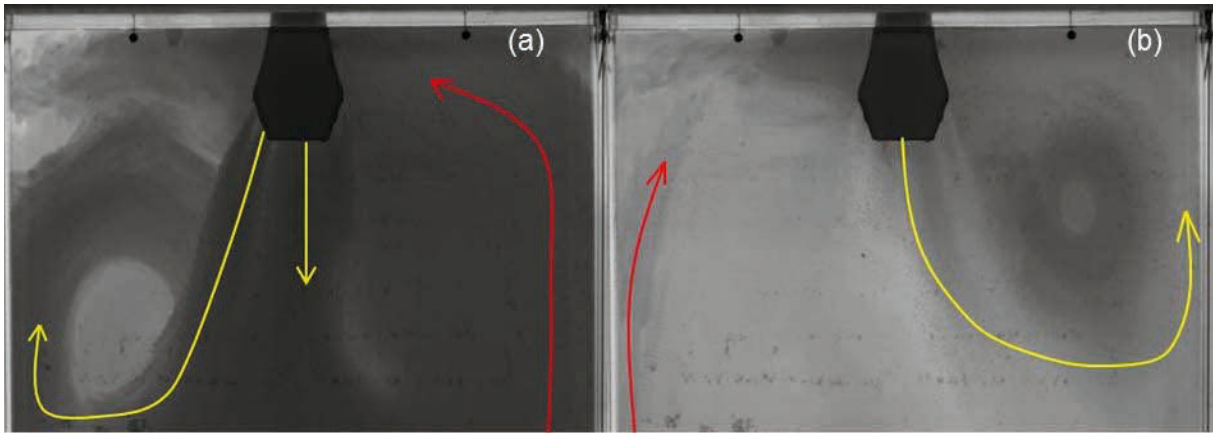

Figure 52. Results of case 3 of SEN for the gap size 8 mm (a) – (b) (Run5).

3.2.3 Case 3 SEN Gap Size 10 mm:

In Figure 53 (a) the first 21.06 seconds can be seen. A large vortex is created on the left side. The dye is transported to the left side because of the backflow at the right section. During the last 10.19 seconds one down streaming jet is present. In that last stage of the trial at both side of the wall a backflow is present (Figure 53 (b)).

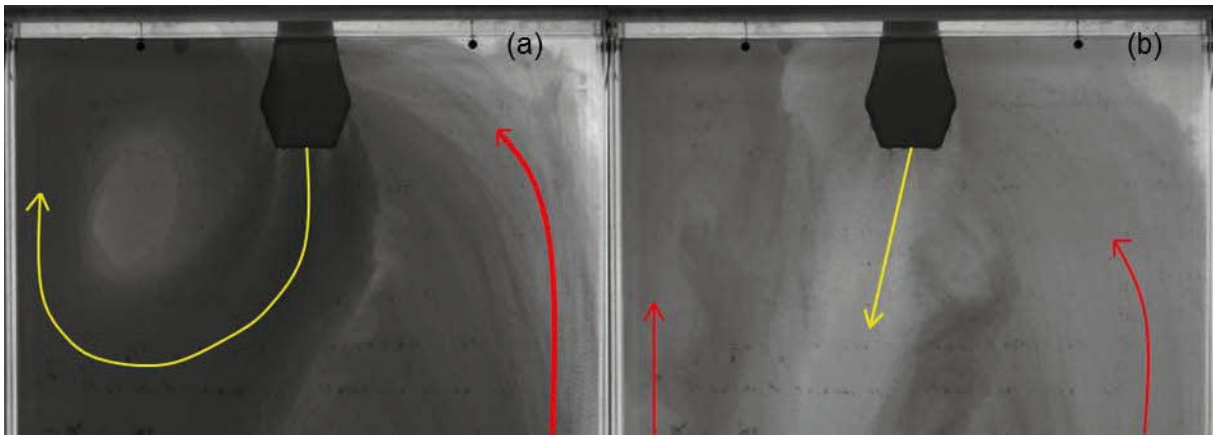

Figure 53. Results of case 3 for the SEN gap size 10 mm (a) – (b) (Run1).

In Figure 54(a) the first 16.25 seconds are seen. The jet is streaming straight downwards and a strong backflow on the right section is present. At the left section there is also an upstreaming backflow visible In Figure 54 (b) the jet changes its direction to the right section.

The backflows on both sides of the walls are still present for the last 15 seconds. It is recognizable that on the top left corner almost no dye was transported during the recording time.

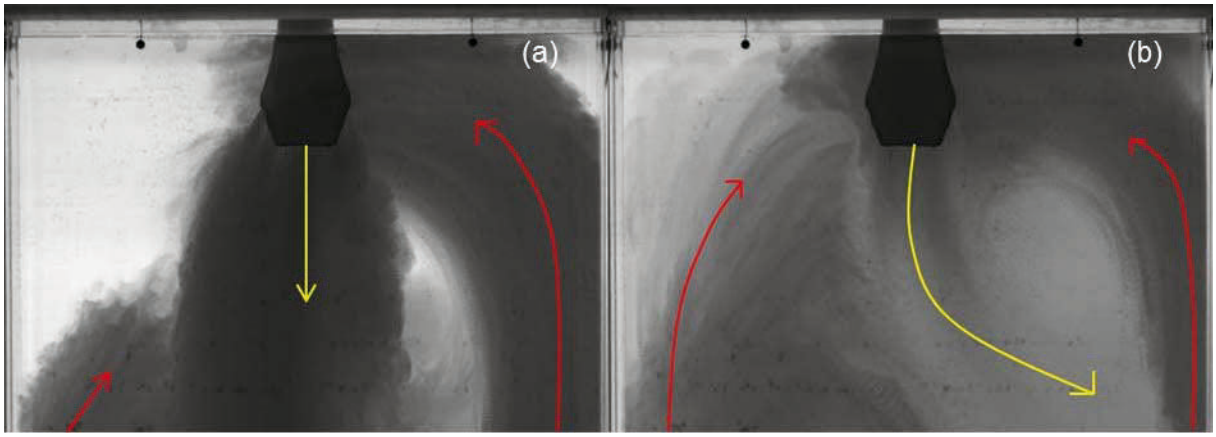

Figure 54. Results of case 3 for the SEN gap size 10 mm (a) – (b) (Run2).

In Figure 55 (a-c) the last three runs of case 3 for the SEN gap 10 mm can be seen. In Figure 55 (a)-(b) the two vortices at the left and right section can be seen. A beam which flows straight downwards is present at both runs. In the fourth run (Figure 55 (b)) it is observed that at the lower section at the left side almost no dye is transported.

During the fifth run (Figure 55 (c)) a beam which goes straight downwards and to the right can be seen. That is the reason for an upcoming backflow which creates a vortex at this section. At the upper part of the left section a vortex is present. At the lower left section less dye is transported.

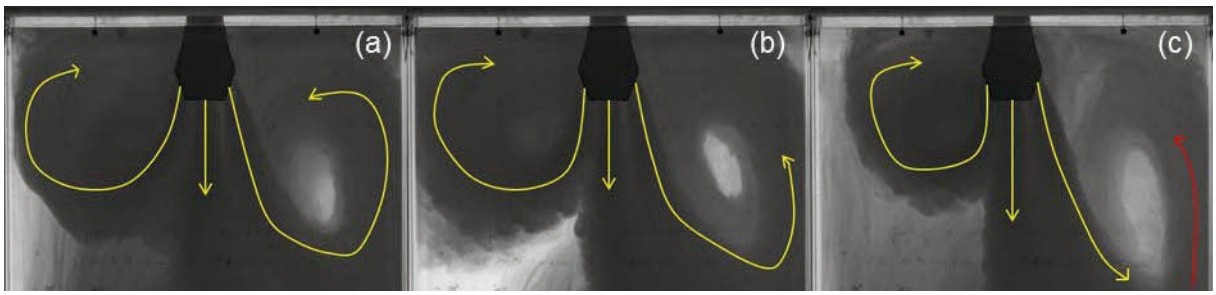

Figure 55. Results of case 3 for the SEN gap size 10 mm (a) Run3, (b) Run4, (c) Run5.

Transient flow can be very risky for the process of thin slab casting. There is a possibility of breakdown of the production because of this flow behaviour inside the mold. The heat and mass transportation is not constant which can lead to freezing inside the mold.

3.3 Unstable Flow

Unstable flow behaviour is characterised by an unpredictable flow pattern during the runs with same settings. Industries are interested in the cases with unstable flow, because the casting casting speed, i.e. mass flow rate, is much higher than other cases with a stable flow.

3.3.1 Case 1 SEN Gap Size 18 mm:

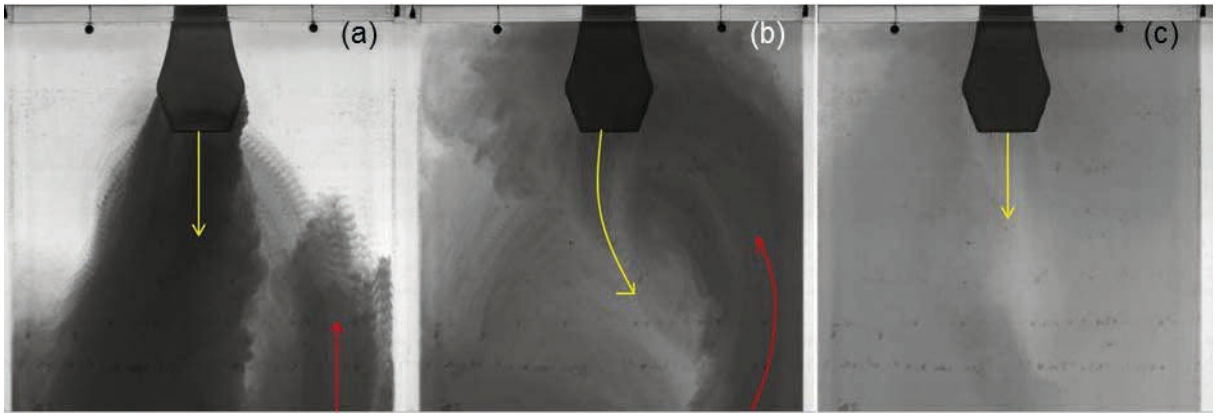

Figure 56. Results of case 1 for the SEN gap size18 mm (a) time interval 10.73 (s), (b) time interval 14.8 (s), (c) time interval 7.47 (s) (Run 1).

Using the SEN with 18 mm gap huge differences appear. In Figure 56 (a) one huge current which goes straight downwards can be seen. This lasts for 10.73 seconds. There is no separation in different jets as seen by the other cases before. At the right section of the mold a backflow from the bottom part of the mold can be recognized. A change of flow direction to the right side can be seen (Figure 56 (b)). The backflow reaches the surface. After a time interval of 14.8 seconds the beam flows straight downwards again Figure 56 (c).

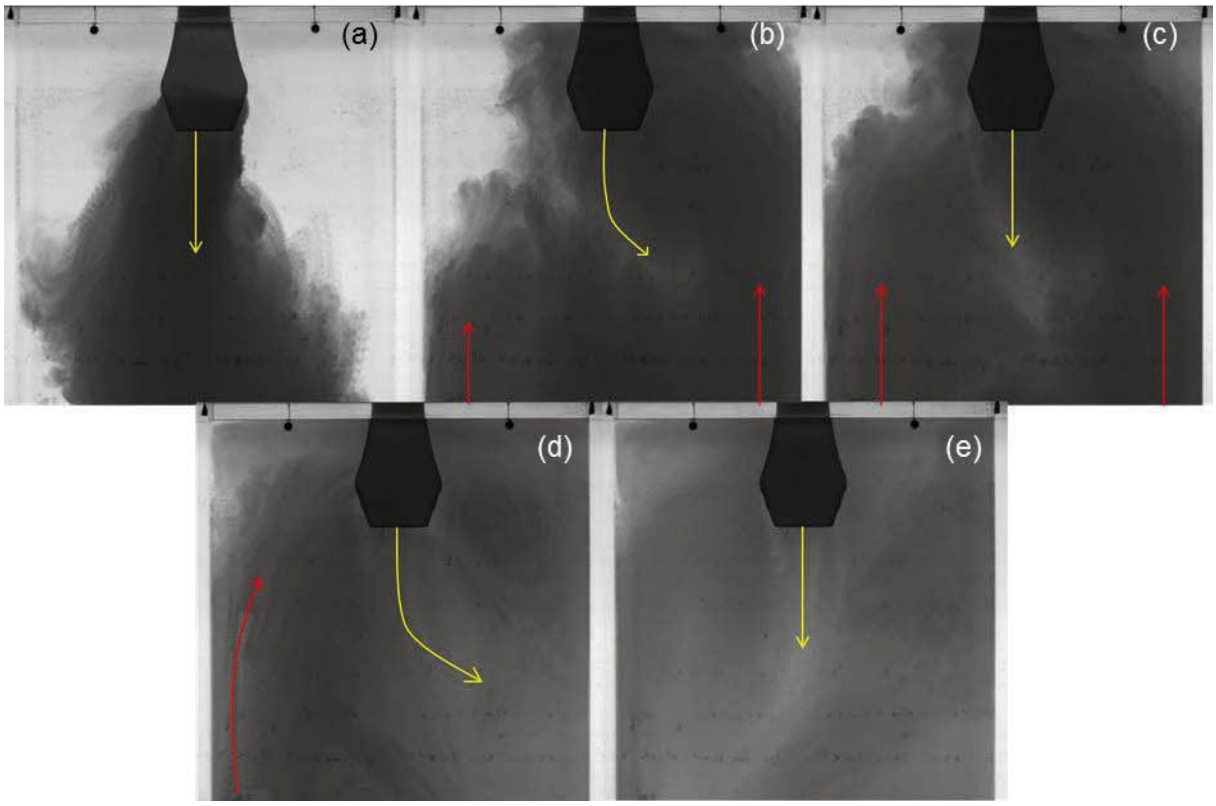

Figure 57. Results of case 1 for the SEN gap size 18 mm (a) time interval 6.66 (s), (b) timer interval 0.73 (s), (c) time interval 11.87 (s), (d) time interval 10.6 (s), (e) time interval 3.14 (s) (Run2).

The second run of the SEN with 18 mm shows differences in the flow pattern compared to the first run. A single jet goes downwards for 6.66 seconds which can be seen in Figure 57 (a). In Figure 57 (b) a short change in direction (0.73 seconds) to the right can be observed. Backflows at the right and left section at the mold walls are present. The next change of flow direction can be seen in Figure 57 (c) This flow pattern has a duration of 11.87 seconds. There the backflow on both sides of the mold walls is still present. Another change in direction can be seen in Figure 57 (d). Backflow of the water is just at the left section of the mold wall visible. This can be observed for another 10.6 seconds. A last change of flow direction can be seen in Figure 57 (e). At the end of recording time the current goes straight downwards.

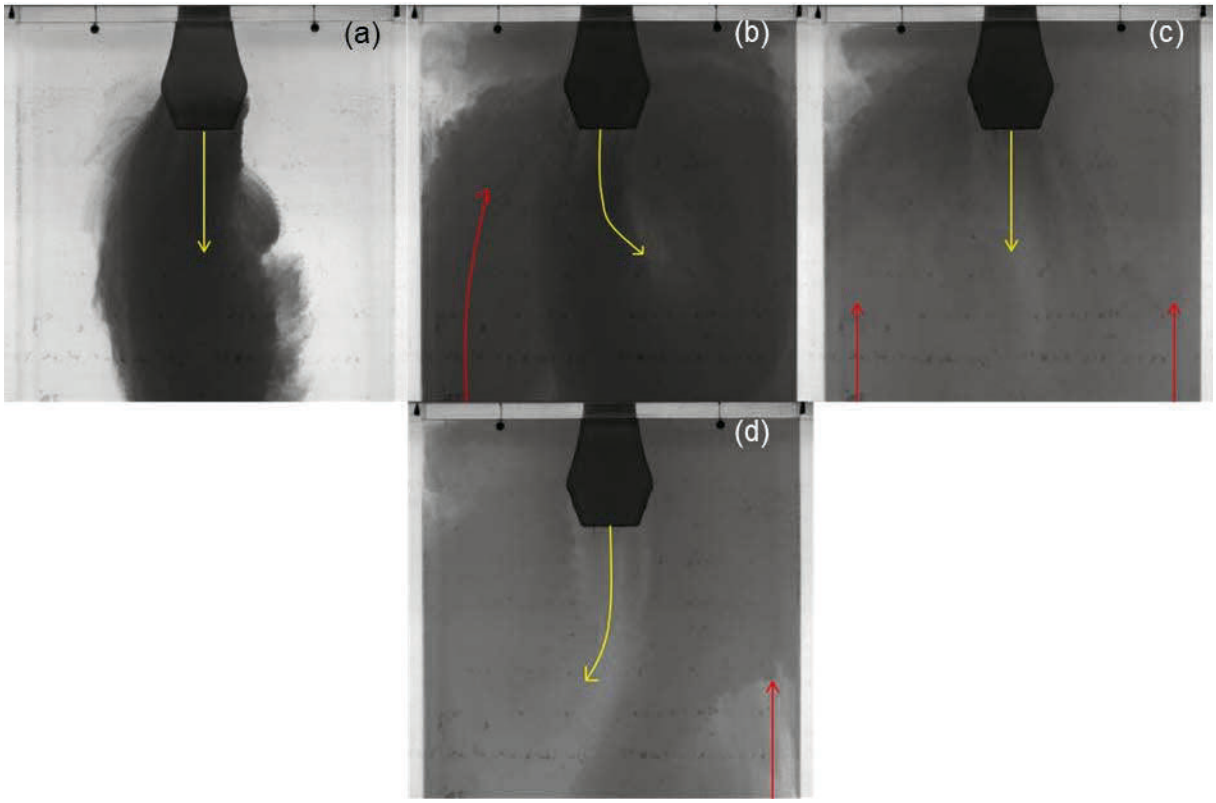

Figure 58. Results of case 1 for the SEN gap size 18 mm (a) time interval 5.6 (s), (b) time interval 16.67 (s), (c) time interval 8.2 (s), (d) time interval 2.6 (s) (Run3)

The third run of case 1 for the SEN gap size 18 mm also shows instability in flow behaviour. The first recorded jet is going straight downwards for 5.6 seconds (Figure 58 (a)). The next direction of the current is to the right and from the left bottom a huge amount of dye is coming back upwards. This flow behaviour takes place for about 16.67 seconds (Figure 58 (b)). The next 8.2 seconds the jet streams straight downwards again and backflow at both sections of the mold wall is streaming upwards (Figure 58 (c)). The last 2.6 seconds the single jet flows to the left section of the mold which is may caused by the backflow at the right section (Figure 58 (d)).

The beginning of the fourth run starts with a single jet to right section of the mold section. The backflow comes up from the left side of the wall. This takes 15.6 seconds and can be seen in Figure 59 (a). In Figure 59 (b) a change in direction can be observed. Also the backflow keeps coming up from the left section and is creating a small vortex. It can be seen that there is almost no dye transported to the top left corner of the mold. A small amount of backflow is coming up from the right corner at the bottom of the recording window. After 9.67

seconds the jet changes its direction to the right side. Figure 59 (c) summarizes the last 7.93 seconds of recording time. A backflow at the right corner is still present (Figure 59(c)).

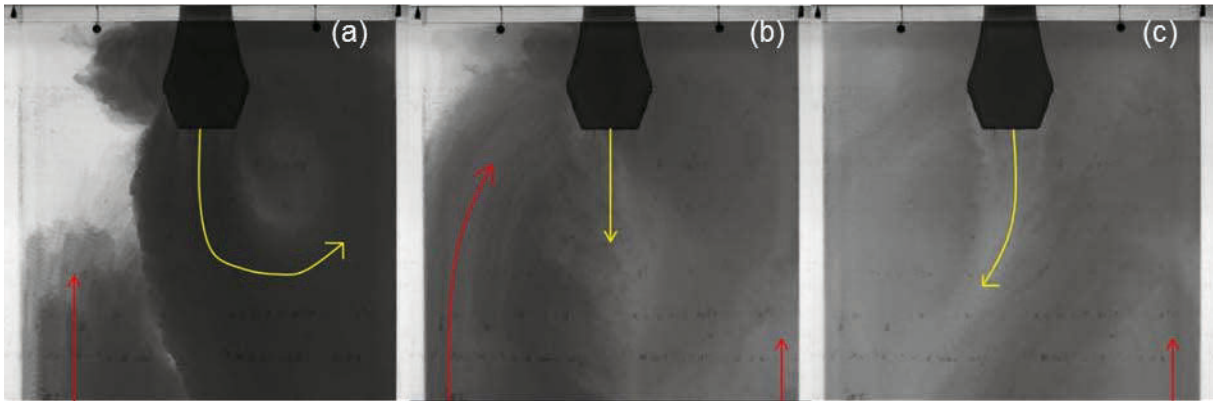

Figure 59. Results of case 1 for the SEN gap size 18 mm (a) time interval 15.6 (s), time interval 9.67 (s), (c) time interval 7.93 (s) (Run4)

The fifth run of case 1 for the SEN gap 18 mm starts with a left flow of the jet. A vortex creation at the right top corner can be seen in Figure 60 (a). This is recorded for 9.6 seconds. In Figure 60 (b) a change to a straight downwards flow can be seen. Also a strong backflow at both sides of the mold wall is present. This lasts for 4.4 seconds. It is clearly to see that until that time no dye is transported to the left top corner. There are also some sections at the right top corner with less dye concentration compared to others. In Figure 60 (c) a change of flow direction to the left side can be seen. The backflow is still present and visible. This is recorded for 15.2 seconds. In Figure 60 (d) the jet flows straight downwards again. The backflow is coming up from the right section of the wall.

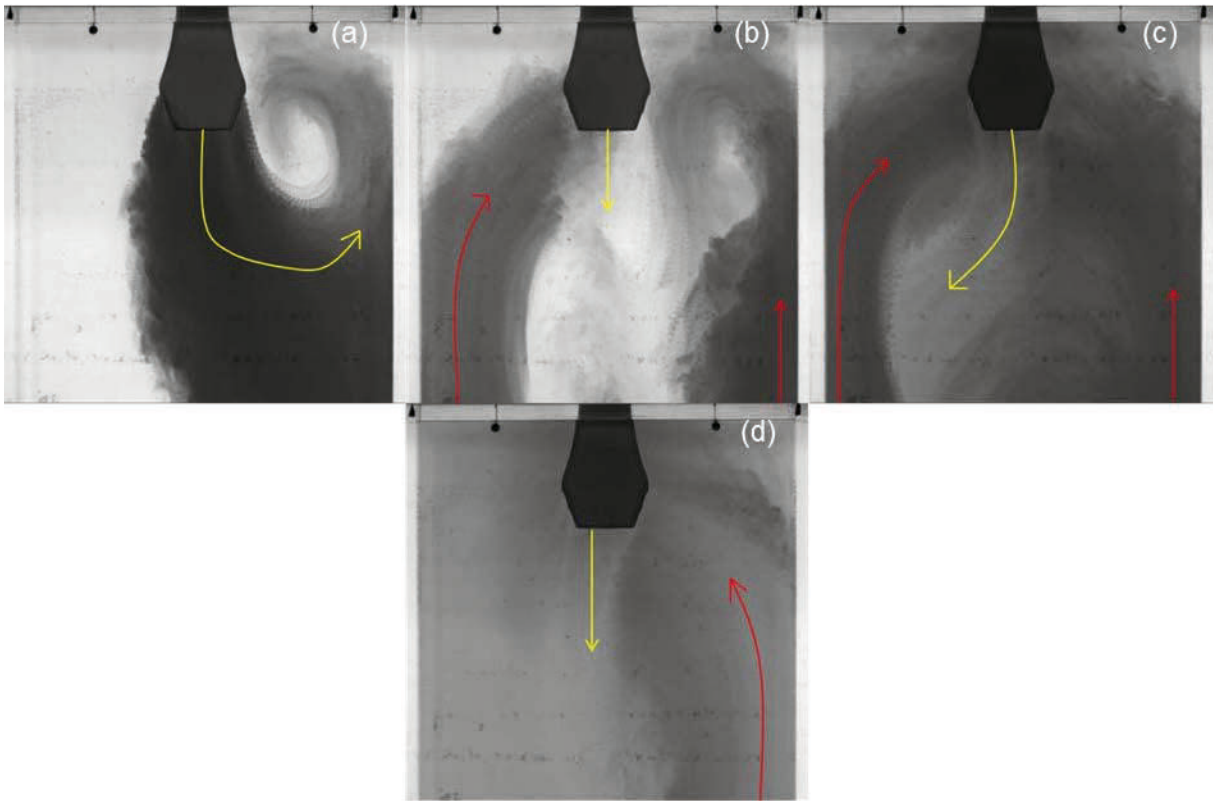

Figure 60. Results of case 1 for the SEN gap size 18 mm (a) time interval 9.6 (s), time interval 4.4 (s), time interval 15.2 (s), (d) time interval 3.8 (s) (Run5).

3.3.2 Case 2a SEN Gap Size 18 mm:

The first run for case 2a for SEN gap size 18 mm shows stable flow behaviour. One single vortex at the left section can be seen. From the right bottom a straight upcoming backflow is present. No dye is transported to the top right corner (see Figure 61).

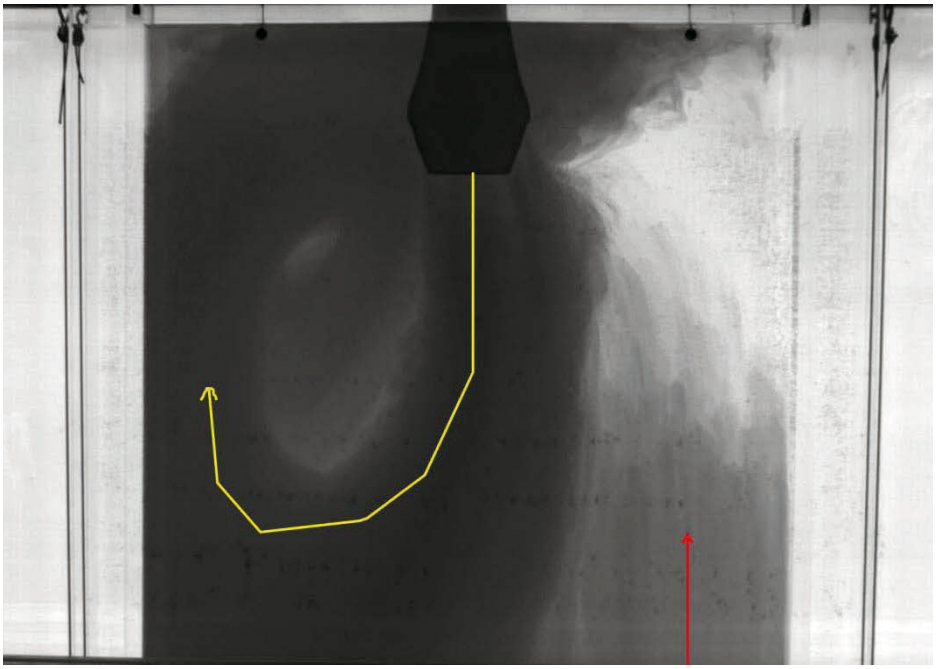

Figure 61. Results of case 2a for the SEN gap size 18 mm (Run1).

The second run shows huge differences in the flow pattern compared to the first one (Figure 61). In the beginning the beam flows to the right section of the mold and also a backflow from the bottom at the left side of the mold is seen (Figure 62 (a)). After 16.1 seconds the jet changes its direction to straight downwards and the backflow is still present. This happens for about 7.1 seconds. For the last seconds of recording time the down streaming jet is dividing into two jets. The backflow on the left side of the wall is still present (Figure 62 (c)).

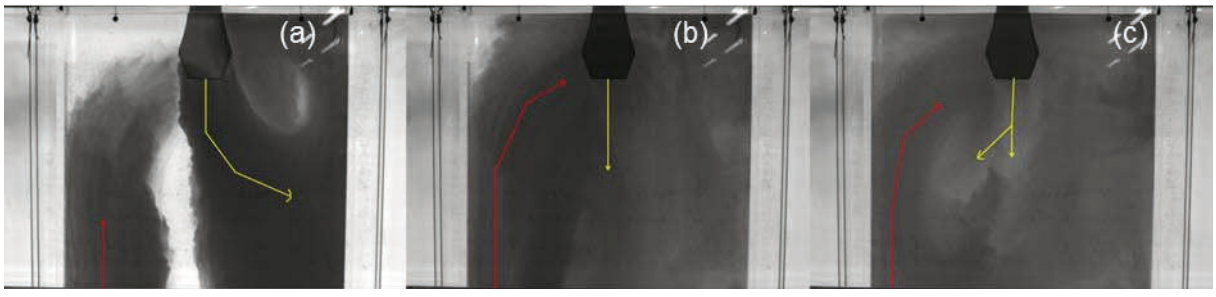

Figure 62. Results of case 2a for the SEN gap size 18 mm (a) time interval 16.1 (s), (b) time interval 7.1 (s), (c) time interval 9.8 (s) (Run2).

The jet at the third run creates a vortex at the left section of the mold. This flow pattern is visible for 21.27 seconds. During that time no dye is transported to the right section of the mold. Afterwards the jet changes the direction to straight downwards (Figure 63 (b)). In Figure 63 (b) the backflow at the right side of the wall is clearly to see.

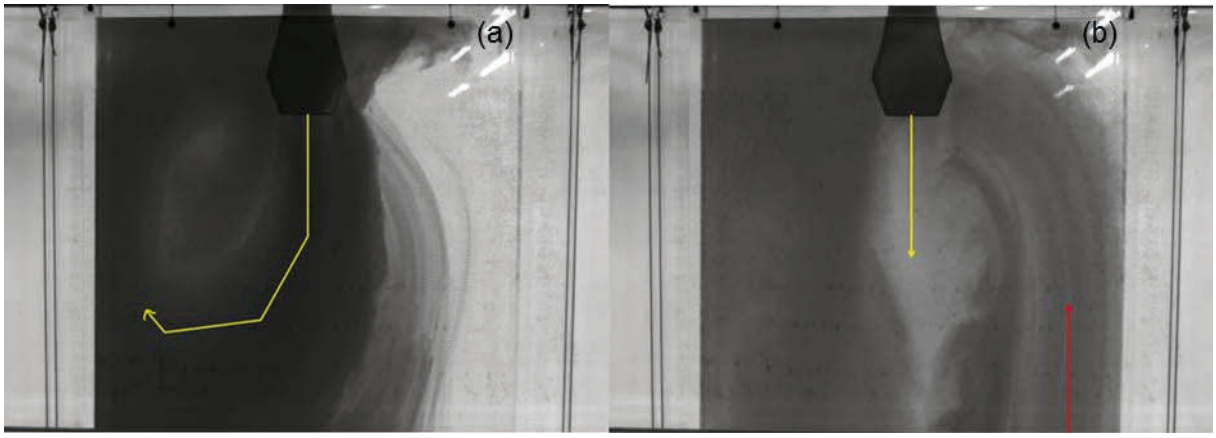

Figure 63. Results of case 2a for the SEN gap size 18 mm (a) time interval 21.27 (s), (b) time interval 11.73 (s) (Run3)

The fourth run starts with a large vortex development at the right section of the mold. At the left wall side of the mold a backflow is coming up (Figure 64 (a)). After 21.4 seconds the directions changes to straight downwards for 3.93 seconds (Figure 64 (b)). In the end the jet flows to the left side for 7.67 seconds (Figure 64 (c)). An upcoming backflow from the left side is also visible.

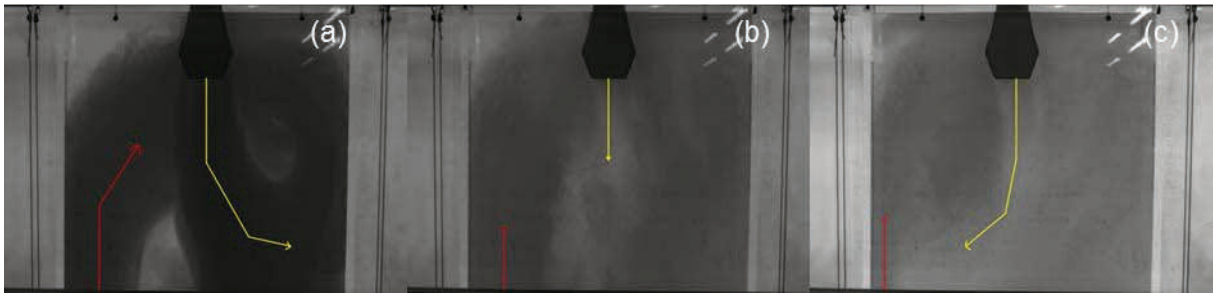

Figure 64. Results of case 2a for the SEN gap size 18 mm (a) time interval 21.4 (s), (b) time interval 3.93 (s), (c) time interval 7.67 (s) (Run4)

The fifth run of case 2a for the SEN gap size 18 mm starts with a creation of a huge vortex at the left section of the mold. This flow pattern is present for 10.13 seconds (Figure 65 (a)). Afterwards the jet changes to a straight downward flow for 9.73 seconds. An upcoming backflow is also present and producing a vortex which flows straight into the down streaming jet (Figure 65 (b)). This can be the reason why the jet changes its flow direction to the right section of the mold for the last 13.13 seconds (Figure 65 (c)).

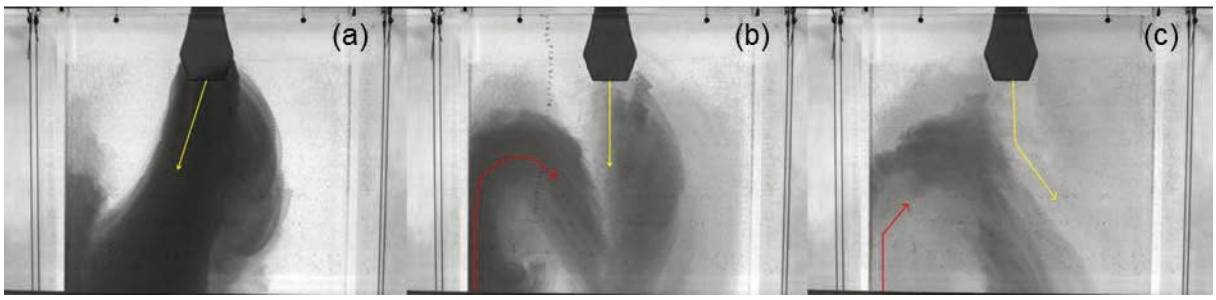

Figure 65. Results of case 2a for the SEN gap size 18 mm (Run5).

3.3.3 Case 2b SEN Gap Size 18 mm:

The first run with the settings of case 2b for the SEN gap size 18 mm starts with a straight down streaming flow. At both mold wall sides a backflow is coming up. The backflow at the left side is faster than at the right side. The backflow on the left side reaches the meniscus level and circulate to the right area of the apparatus. This takes place within 17 seconds (Figure 66 (a)). Afterwards the jet changes its direction to the left side for 13.27 seconds (Figure 66 (b)). The backflow at the right section of the mold still exists. For the last 2.73 seconds the jet changes its direction to straight downwards again. The whole area gets lighter because the dye solutes and distributes in the fresh incoming water (Figure 66 (c)).

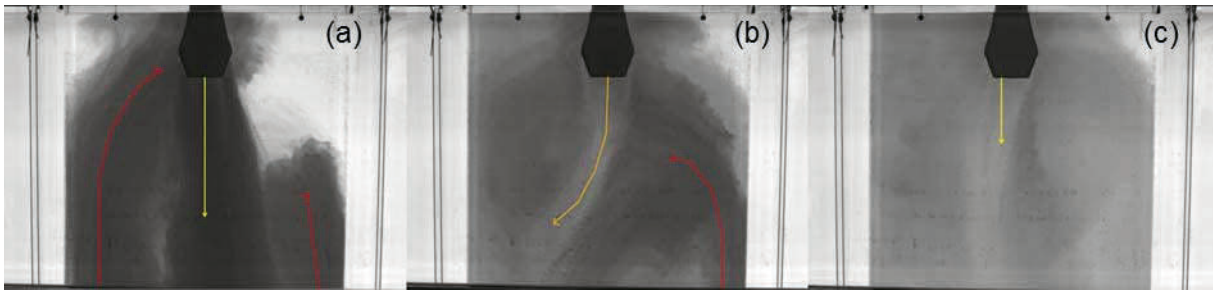

Figure 66. Results of case 2b for the SEN gap size 18 mm (a) time interval 17 (s), (b) time interval 13.27 (s9, (c) time interval 2.73 (s) (Run1).

The second run starts with a huge vortex development at the right section of the mold. This flow pattern takes 15.2 seconds (Figure 67 (a)). Afterwards the jet changes its flow direction to straight downwards for 15.47 seconds. Also a backflow on the left side can be seen (Figure 67 (b)). The last 2.3 seconds the jet flows to the left section of the mold. A backflow at the left and right mold wall can be observed (Figure 67 (c)).

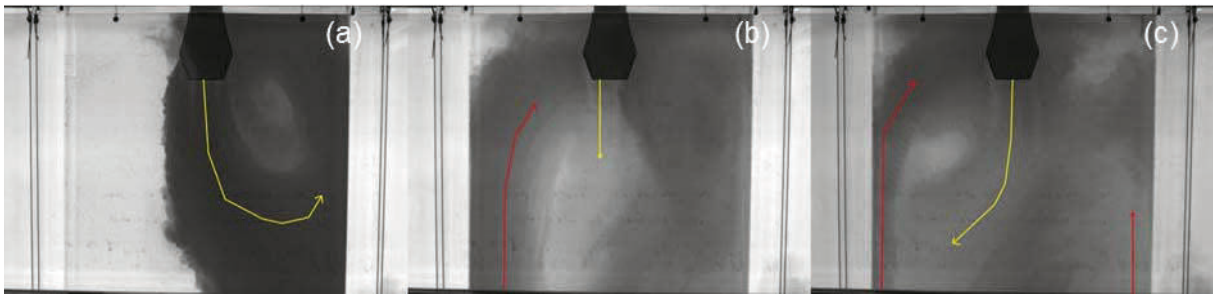

Figure 67. Results of case 2b for the SEN gap 18 mm (a) time interval 15.2 (s), (b) time interval 15.47 (s), (c) time interval 2.3 (s) (Run2)

The third run of case 2b for the SEN gap 18 mm starts with a left sided jet. This flow behaviour is present for 10.2 seconds. During that time no dye is transported to the left section of the mold (Figure 68 (a)). The next 5.73 seconds the jet flows straight downwards and at the right mold wall a strong backflow is streaming up. The last 17.07 seconds the jet changes its direction to right section of the mold. At the left side of the mold a backflow is coming up (Figure 68 (c)).

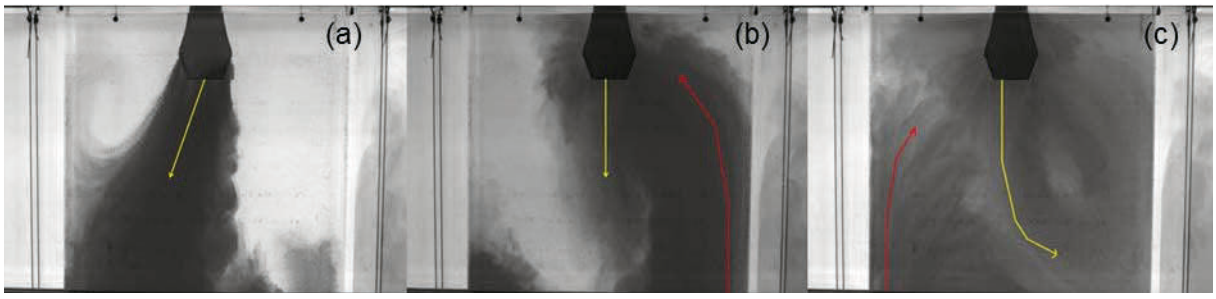

Figure 68. Results of case 2b for the SEN gap 18 mm (a) time interval 10.2 (s), (b) time interval 5.73 (s), (c) time interval 17.07 (s) (Run3).

The fourth run of case 2b for the 18 mm SEN gap size starts with a left flow of the jet. This flow pattern is present for 10.13 seconds (Figure 69(a)). At the right corner a backflow straight coming up from the bottom part of the mold can be seen. The next 2.06 seconds the jet goes straight downwards and the backflow is proceeding (Figure 69 (b)). The last 20.8 of recording time a jet flows to the right section of the mold. Also a new backflow at the left bottom corner of the mold is present (Figure 69 (c)).

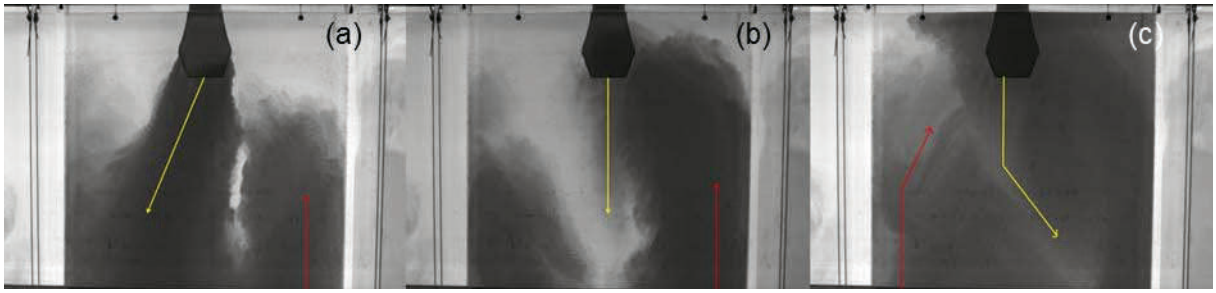

Figure 69. Results of case 2b for the SEN gap 18 mm (a) time interval 10.13 (s), (b) time interval 2.06 (s), (c) time interval 20.8 (s) (Run4).

The fifth run with the same setting starts with a left flow of the jet which is creating a huge vortex at the top of the left section of the mold (Figure 70 (a)). After 18.07 seconds the jet changes its direction to straight downwards for the next 5.27 seconds (Figure 70 (b)). For the last 9.67 seconds the out coming flow goes to the right side of the mold. At the left wall a backflow from the bottom part can be seen (Figure 70 (c)).

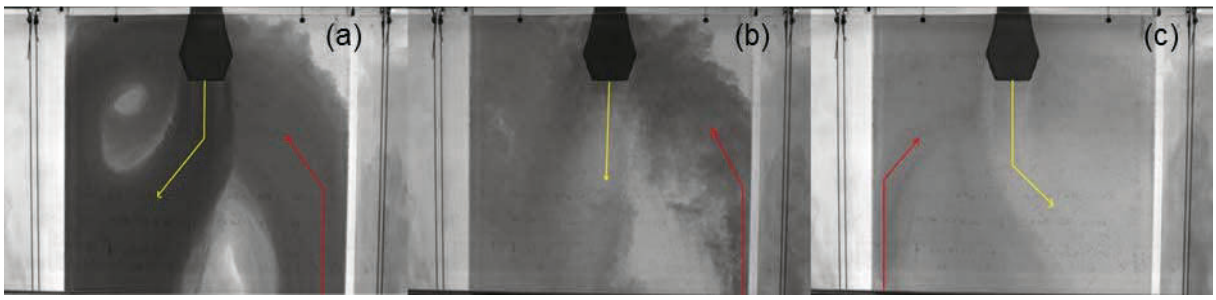

Figure 70. Results of case 2b for the SEN gap 18 mm (a) time interval 18.07 (s), (b) time interval 5.27 (s), (c) time interval 9.67 (s) (Run5).

3.3.4 Case 2c SEN Gap Size 12 mm:

The first run of case 2c with the SEN gap size 12 mm can be seen in Figure 71. Figure 71 (a) represents the first 6.6 seconds of this run. A large vortex development at the right section of the mold can be seen. A strong backflow at the left section can be seen as well. Figure 71 (b) the next 10 seconds can be seen. The jet flows straight downwards and at both side of the mold walls a backflow is present. For the next 2.75 seconds the jet changes its direction to the left section of the mold. A large vortex develops. The backflow is present at the right mold side at that stage of the trial (Figure 71 (c)). The last 9 seconds of this run can be seen in Figure 71 (d). The jet flows straight downwards again and the backflow at the right section of the mold is still present.

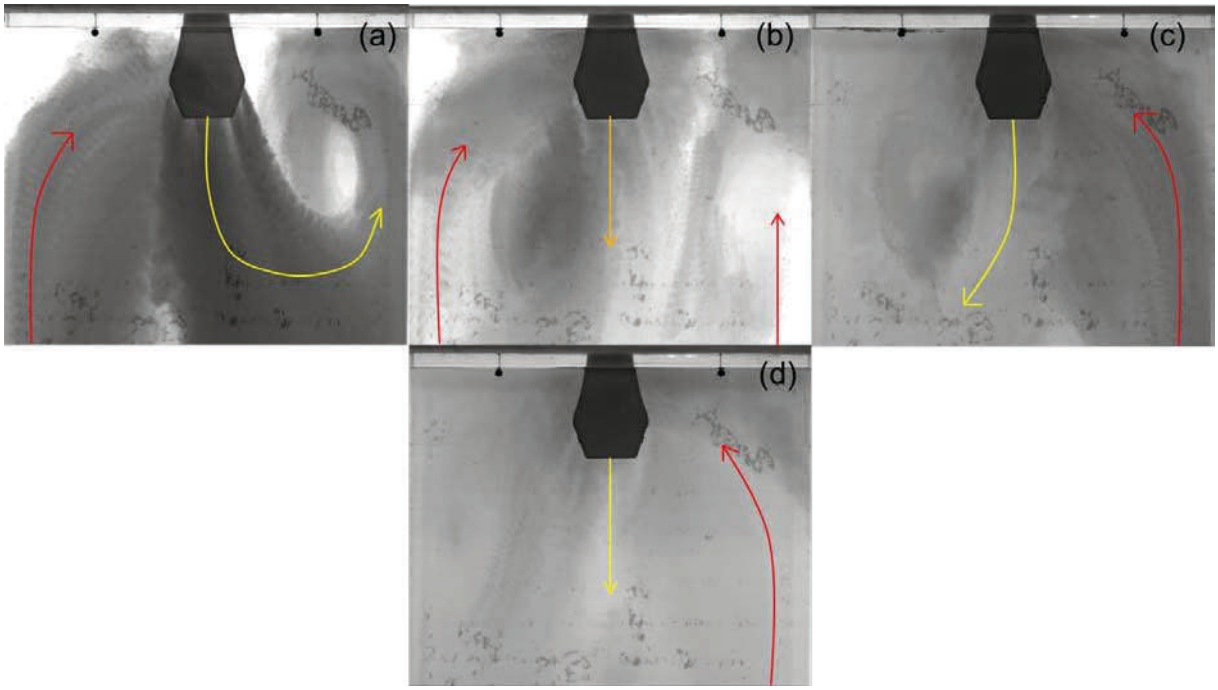

Figure 71. Results of case 2c for the SEN gap size 12 mm(a) time interval 6.6 (s), (b) time interval 10.0 (s), (c) time interval 2.75 (s), (d) time interval 9.0 (s) (Run1).

In Figure 72 (a) the first 18.4 seconds of the second run can be seen. The jet flows to the left section of the mold and creates a large vortex. At the right section of the mold a backflow is coming up from the bottom part of the mold. The jet changes its direction to straight downwards for 1.56 seconds (Figure 72 (b)). The backflow at the right section of the mold is still present. It can be seen that no dye is transported to top right corner until that time. The

last 11.25 seconds the jet changes its direction to the right section of the mold. At that period the backflow is at the left section (Figure 72 (c)).

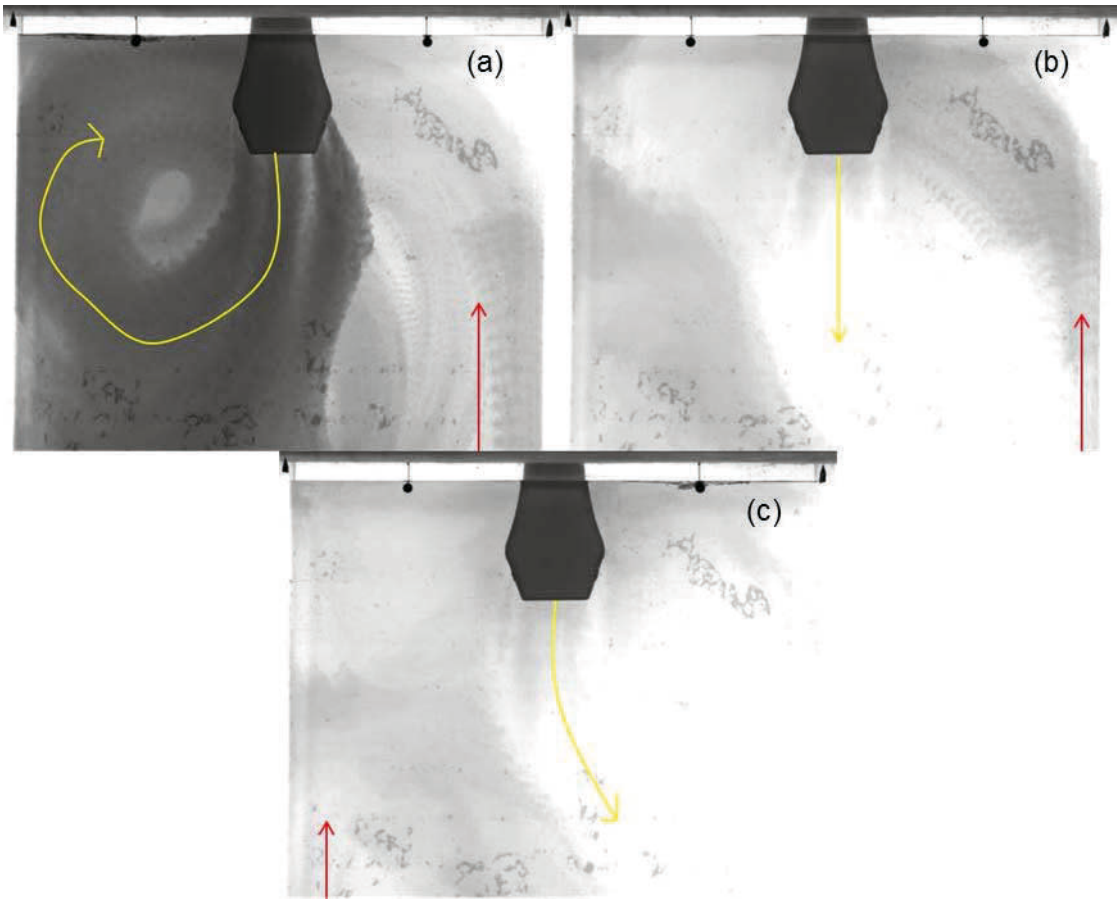

Figure 72. Results of case 2c for the SEN gap size 12 mm (a) time interval 18.4 (s), (b) time interval 1.56 (s), (c) time interval 11.25 (s) (Run2).

The first 9.38 seconds of the third run can be seen in Figure 73 (a). A jet creating a vortex at the left section of the mold can be seen. The jet changes its direction to straight downwards for the next 6.25 seconds (Figure 73 (b)). An upcoming backflow can be observed at both sides. The jet flows to the right section of the mold for the last 15.63 seconds. The backflow is present at the right section of the mold (Figure 73 (c)).

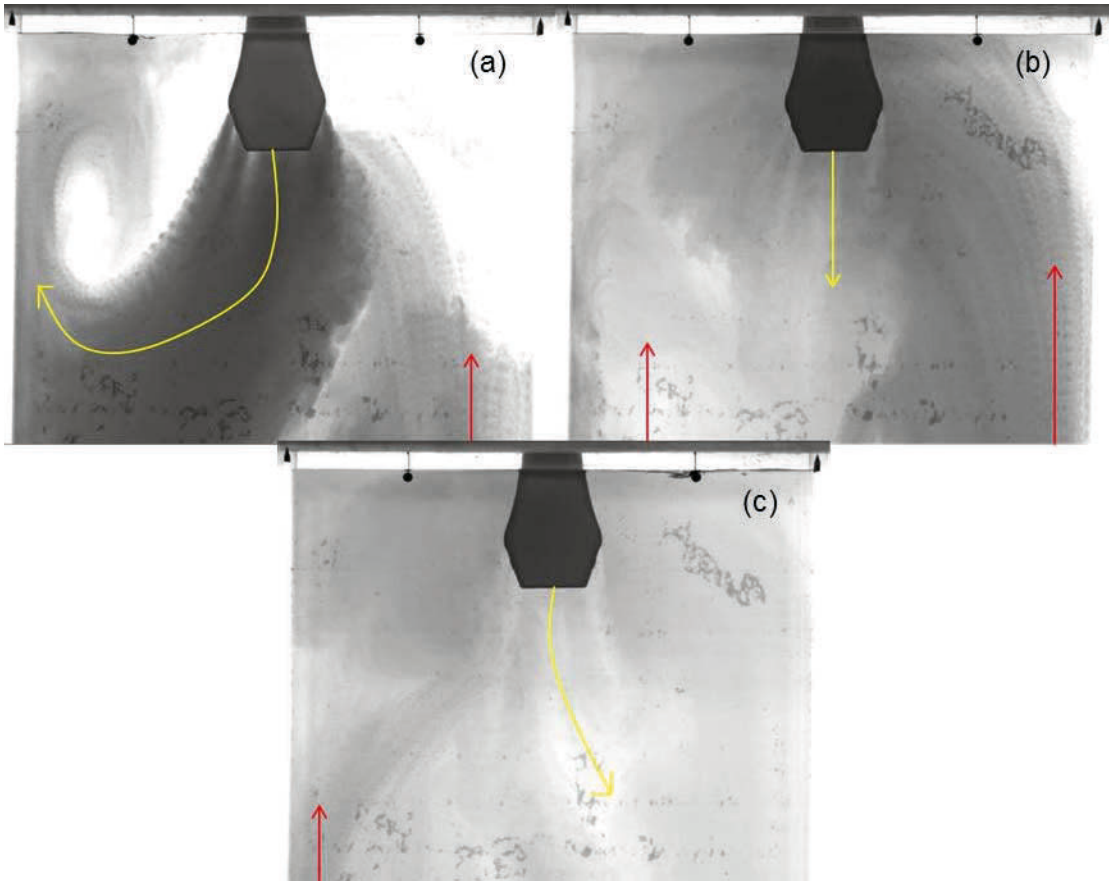

Figure 73. Results of case 2c for the SEN gap size 12 mm (a) time interval 9.38 (s), (b) time interval 6.25 (s), (c) time interval 15.63 (s) (Run3).

The first 5.8 seconds of the fourth run of case 2c with SEN gap size 12 mm can be seen in Figure 74 (a). The jet is down streaming to the lower area of the mold spreads out to the left section of the mold. During the next 2.3 seconds the jet flows in two directions (Figure 74 (b)). One flows to the left section and the other one straight downwards. An upcoming backflow at the right section of the mold can be observed. Afterward the jet flows to right section. During that time (15.25 seconds) a backflows at both sides is present (Figure 74 (c)). During the last 7.99 second the jet goes straight downwards again. A backflow at the right section of the mold can be observed Figure 74 (d).

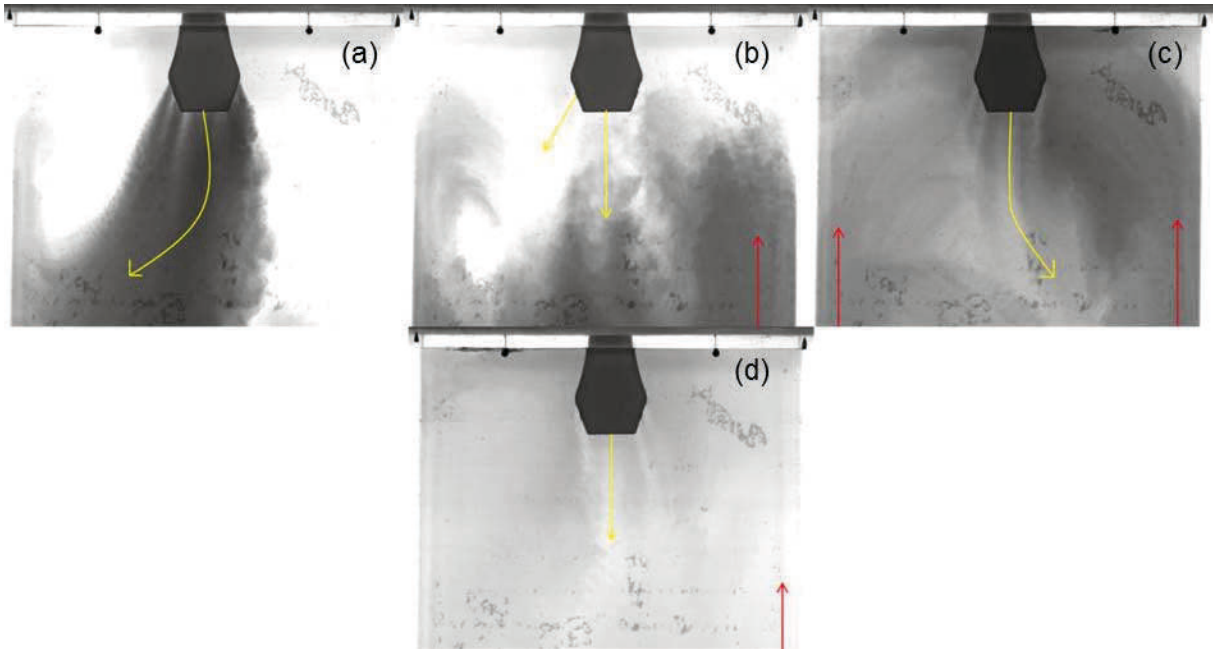

Figure 74. Results of case 3c for the SEN gap size 12 mm (a) time interval 5.8, (b) time interval 2.3 (s), (c) time interval 15.25 (s), (d) time interval 7.94 (s) (Run4).

The fifth run of case 2c for the SEN gap size 12 mm results in a stable flow pattern (Figure 75). A single jet during the whole recording time can be observed. The jet flows to the left section of the mold and creates a large vortex. A backflow is streaming up from the right bottom part of the mold. During the whole recording time no dye was transported at the right upper part of the mold.

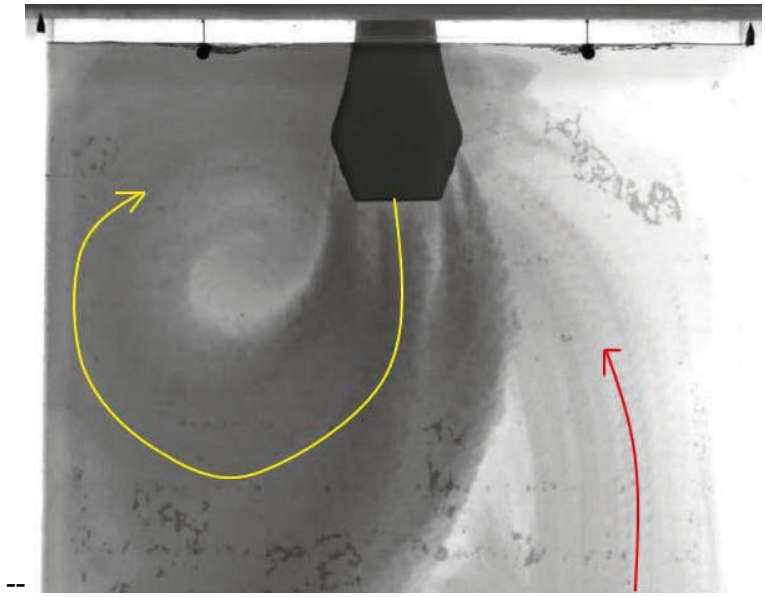

Figure 75. Results of case 2c for the SEN gap size 12 mm (Run5).

3.3.5 Case 2c SEN Gap Size 15 mm:

The first run of case 2c for the SEN gap size 15 mm starts with a single jet which flows straight downwards but its tip tend to the right section of the mold (Figure 76 (a)). A backflow from the left section from the bottom is streaming up. This period takes 12.2 seconds afterwards the jets changes to straight downwards flow. At both sides of the wall a backflow is present (Figure 76 (b). The last 2.43 seconds the jet flows to the left section of the wall where the backflow is still present (Figure 76 (c)).

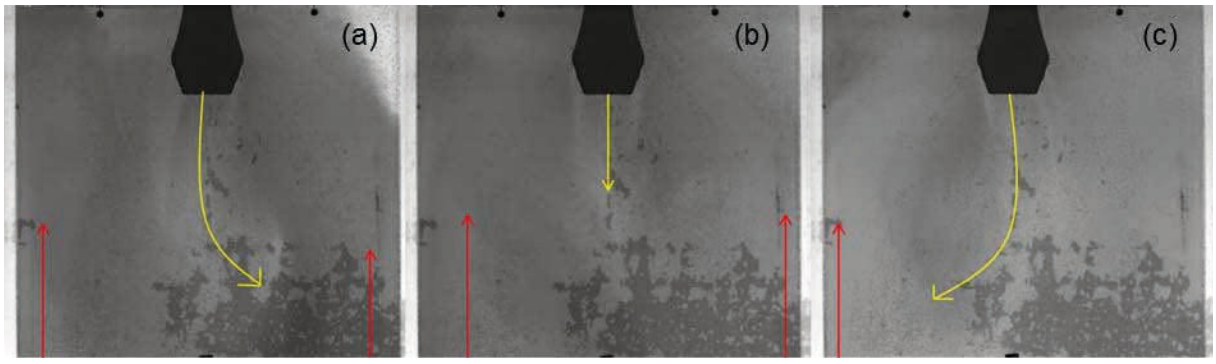

Figure 76. Results of case 2c for the SEN gap size 15 mm (a) time interval 12.2 (s), (b) time interval 18.37 (s), (c) time interval 2.43 (s) (Run1)

The first 9.28 seconds of the second run of case 2c for the SEN gap size 15 mm starts with a left streaming jet (Figure 77 (a)). A backflow is coming up from the left bottom part of the mold. The next 6.15 second the current flows straight downwards. The backflow on the left side can still be observed (Figure 77 (b)). The last 15.63 seconds the jet changes its direction to the left section of the mold. The backflow at the left section is still present (Figure 77 (c)).

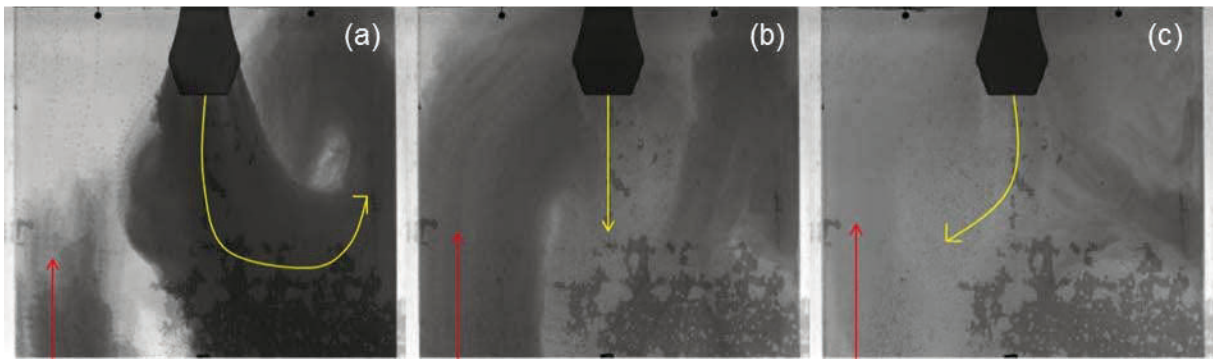

Figure 77. Results of case 2c for the SEN gap size 15 mm (a) time interval 9.28 (s), (b) time interval 6.15 (s), (c) time interval 15.63 (s) (Run2)

In Figure 78 (a) a vortex development at the right section of the mold is seen. A backflow is streaming up at the left side of the wall. This takes about 15.63 seconds. The jet changes its direction from flowing to the right side to straight downwards. The backflow at the left side is still present which can be seen in Figure 78 (b). This takes 5 seconds until the jet changes its direction again. For the last 10.63 seconds the jet flows to the left section of the mold. The backflow at the left section still can be observed. The last stage can be seen in Figure 78 (c).

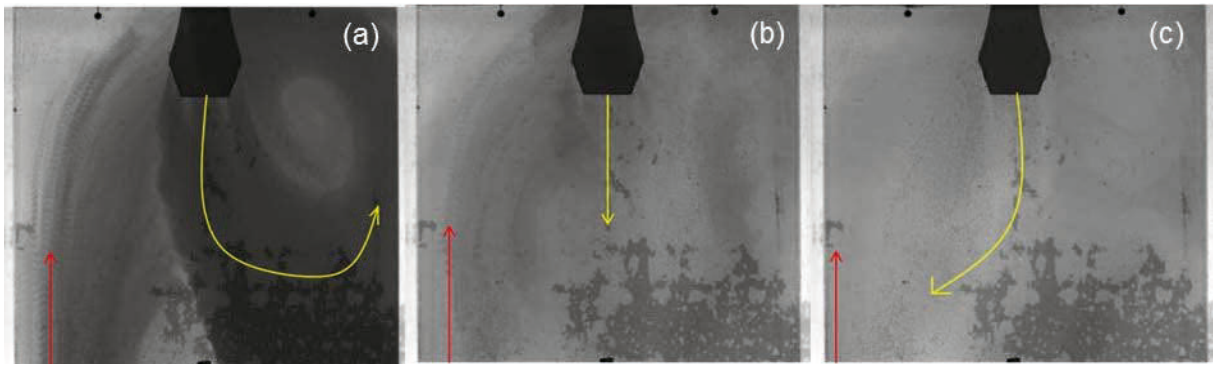

Figure 78. Results of case 2c for the SEN gap size 15 mm (a) time interval 15.63 (s), (b) time interval 5 (s), (c) time interval 10.63 (s) (Run3).

The fourth run of case 2c for the SEN gap size 15 mm can be seen in Figure 79. In Figure 79(a) a vortex development at the right section of the mold is seen. A backflow is streaming up at the left side of the mold. This flow pattern is visible for 12.5 seconds. In Figure 79 (b) a change in direction of the flow can be observed. The jet flows straight downwards and the backflow at the left side of the mold is still present. After a period of 8.13 seconds the flow pattern is changing again. In Figure 79 (c) the jet flows to the left section of the mold. A backflow is streaming upwards at the right mold wall. This is visible for 11.88 seconds.

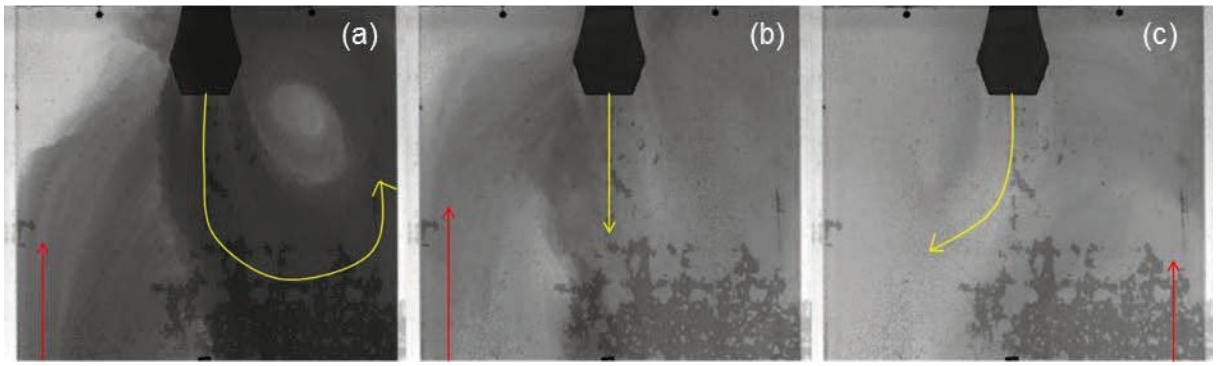

Figure 79. Results of case 2c for the SEN gap size 15 mm(a) time interval 12.5 (s), (b) time interval 8.13 (s), (c) time interval 11.88 (s) (Run4).

In Figure 80 the fifth run of case 2c for the SEN gap size 15mm can be seen. The jet flows to the left section of the mold and creates a vortex. A backflow at the right side of the mold is also present. This flow pattern is visible for 13.75 seconds and can be seen in Figure 80 (a). After 5.63 seconds the flow direction changes to straight downwards which can be seen in Figure 80 (b). A backflow at the left section of the mold can be observed. In Figure 80 (c) the jet changes its direction to the right section of the mold. The backflow at the left side of the mold is still present. This lasts for 11.88 seconds.

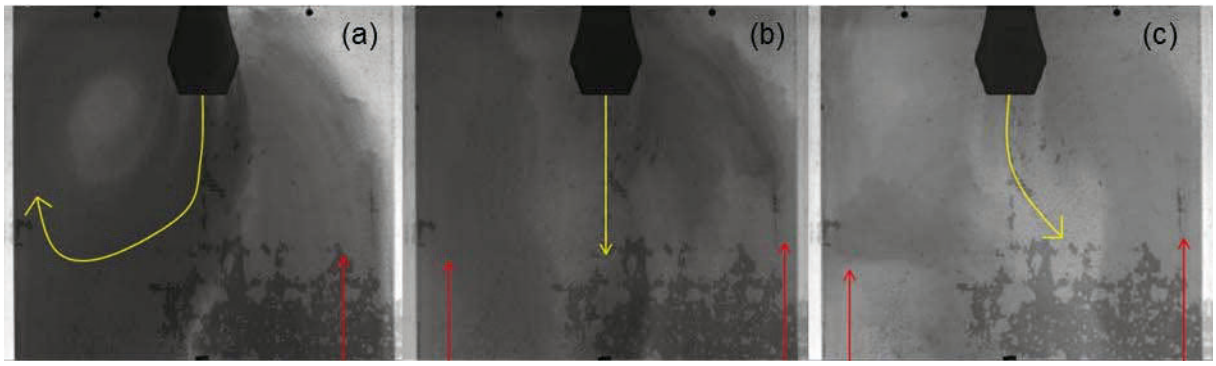

Figure 80. Results of case 2c for the SEN gap size 15 mm (a) time interval 13.75 (s), (b) time interval 5.63 (s), (c) time interval 11.88 (s) (Run5).

3.3.6 Case 2c SEN Gap Size 18 mm:

In Figure 81 results of the first run of case 2c for the SEN gap size 18 mm is seen. That case has the highest mass flow rate because of the SEN gap size of 18 mm and the casting speed of 3.4 m/min. Figure 81 (a) represents the first 15.33 seconds of this run. The jet flows to the left section of the mold and creates a vortex. During that time no dye is transported to the right section of the mold. In Figure 81 (b) the jet changes its direction to straight downwards and a backflow can be seen. The backflow creates a vortex which reaches the SEN and reaches the meniscus. This flow pattern is present for 11.47 seconds. The last 6.2 seconds of this run can be seen in Figure 81 (c). The jet flows to the right section of the mold. From the left bottom part of the mold a backflow is streaming upwards which influences the direction of the jet.

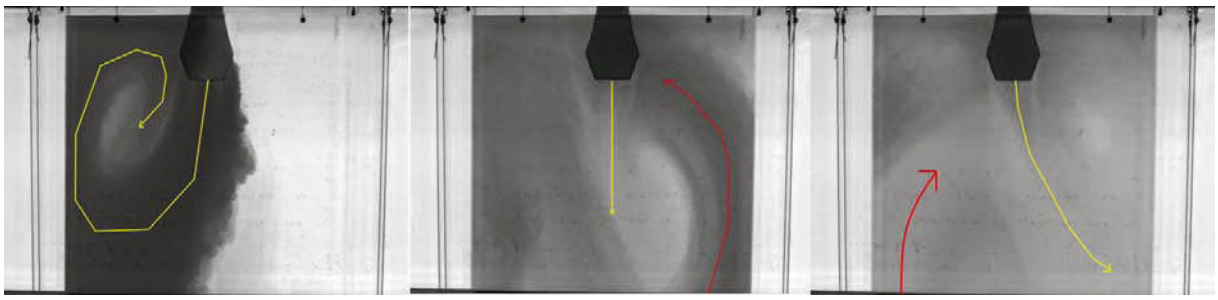

Figure 81. Results of case 2c for the SEN gap size 18 mm (a) time interval 15.33 (s), (b) time interval 11.47 (s), (c) time interval 6.2 (s) (Run1).

The jet of the second run flows slightly to the left section of the mold for 6.33 seconds (Figure 82 (a)). Afterwards the beam changes to a straight downwards flow which also generates a backflow at the left and right side of the jet (Figure 82 (b)). This flow pattern is present for 3.93 seconds. In Figure 82 (c) the beam changes its direction to the right which may is caused by the backflow streaming up from the bottom part of the mold. This flow behaviour is visible for 15.6 seconds. Another flow pattern can be seen for 5.2 seconds (Figure 82 (d). The jet flows straight downwards and causes also a backflow streaming up from the bottom of the mold. The last 1.93 seconds the direction is changing again to left section of the mold (Figure 82 (e)).

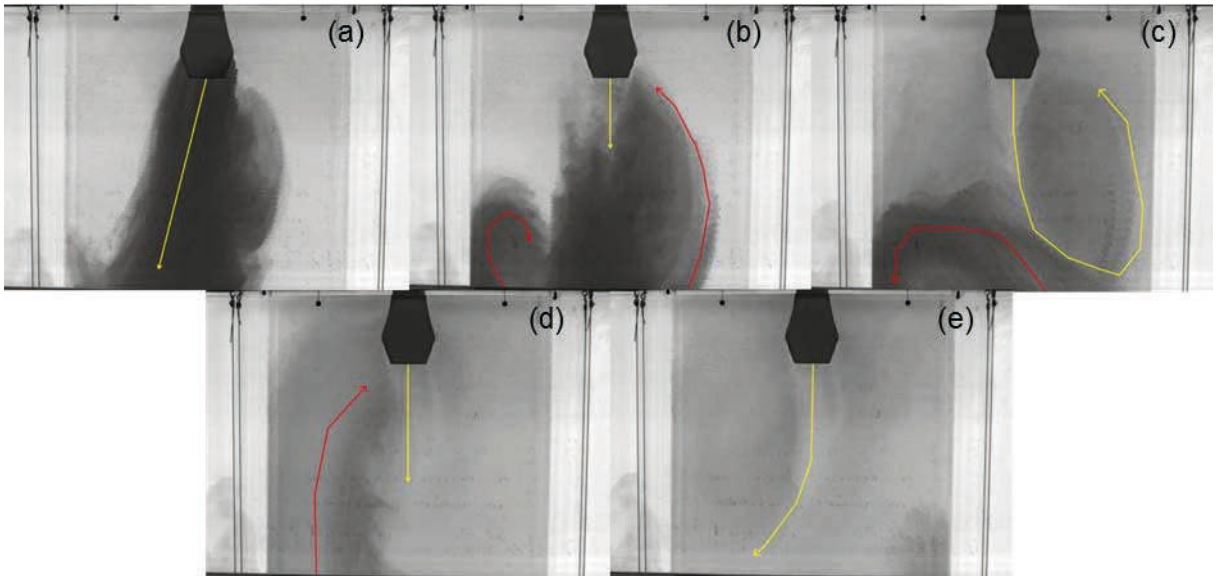

Figure 82. Results of case 2c for the SEN gap size 18 mm (a) time interval 6.33 (s), (b) time interval 3.93 (s), (c) time interval 15.6 (s), (d) time interval 5.2 (s), € time interval 1.93 (s) (Run2).

The third run of case 2c for the SEN gap size 18 mm can be seen in Figure 83. The jet flows to the right section of the mold. A backflow is streaming up from the right bottom part of the mold. This flow pattern can be seen for 10.93 seconds (Figure 83 (a)). Afterwards the jet is streaming straight downwards for 4.46 seconds (Figure 83 (b)). A backflow at both sides at the mold walls can be seen. The backflow from the left bottom part influences the jet and that is why the jet changes its direction to the right section of the mold (Figure 83 (c)). This flow

behaviour is present for 14.33 seconds. The last recording 3.27 seconds the jet flows straight downwards (Figure 83 (d)).

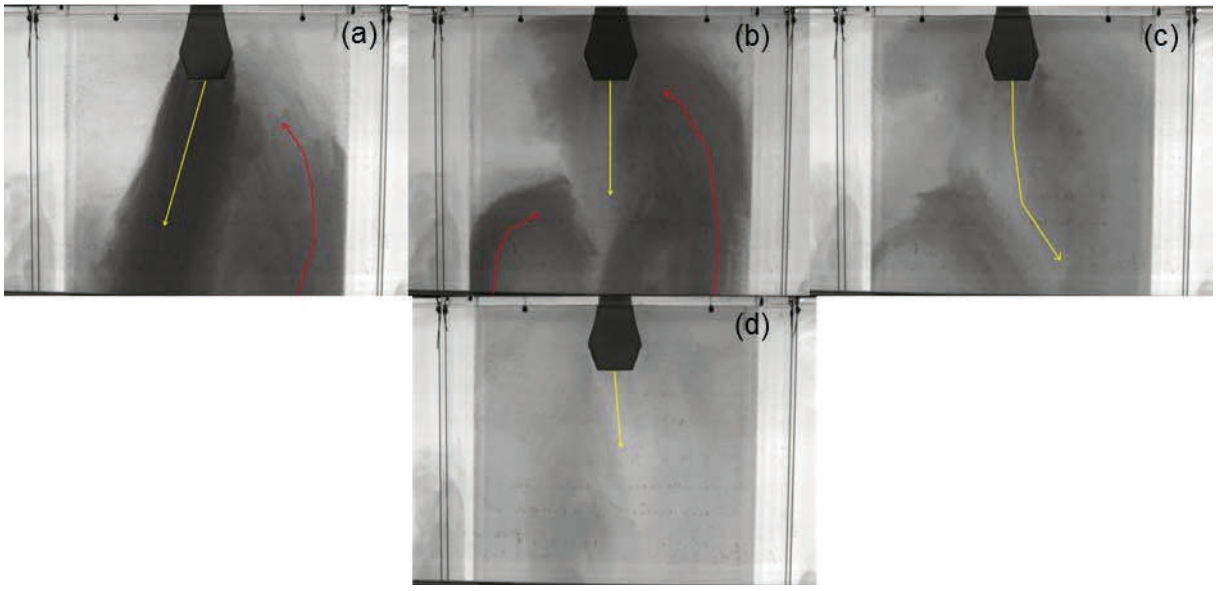

Figure 83. Results of case 2c for the SEN gap size 18 mm (a) time interval 10.93 (s), (b) time interval 4.46 (s), (c) time interval 14.33 (s), (d) time interval 3.27 (s) (Run3).

The fourth run of case 3c for the SEN gap 18 mm can be seen in Figure 84. The jet flows to the right section of the mold and creates a vortex. This flow behaviour is visible for 10.87 seconds (Figure 84 (a)). Afterwards the jet flows straight downwards again and from the left bottom of the mold a backflow is streaming upwards. This flow pattern is present for 6.87 seconds (Figure 84 (b)). The last 15.27 seconds the beam changes its direction again. The right upstreaming backflow influences the jet. That is the reason why the jet changes its flow direction to the left section of the mold (Figure 84 (c)).

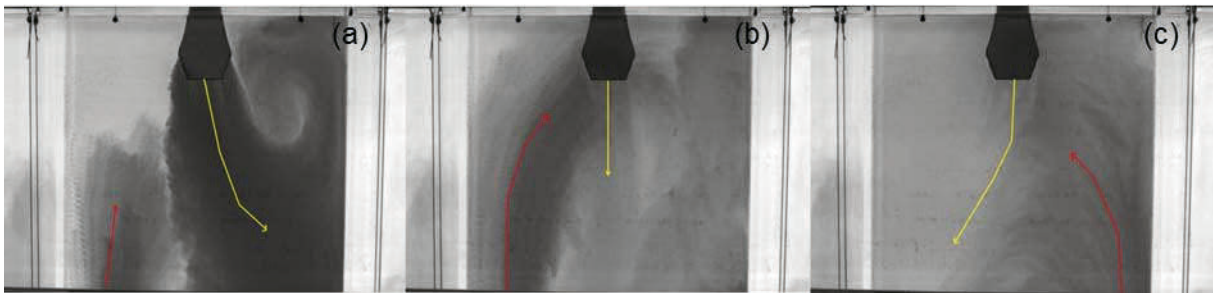

Figure 84. Results of case 2c for the SEN gap size 18 mm (a) time interval 10.87 (s), (b) time interval 6.87 (s), (c) time interval 15.27 (s) (Run4).

The fifth run with the same setting can be seen in Figure 85. The jet flows for 15.8 seconds to the left section of the mold (Figure 85 (a)). At the left mold wall a vortex is developed. Also a backflow from the right bottom part of the mold is streaming up. Afterward the jet flows straight downwards for another 2.2 seconds. The backflow from the right bottom part of the mold is still present (Figure 85 (b)). The jet flows to the right section of the mold for the last 15 seconds of recording time. At this period no significant backflow can be seen Figure 85 (c).

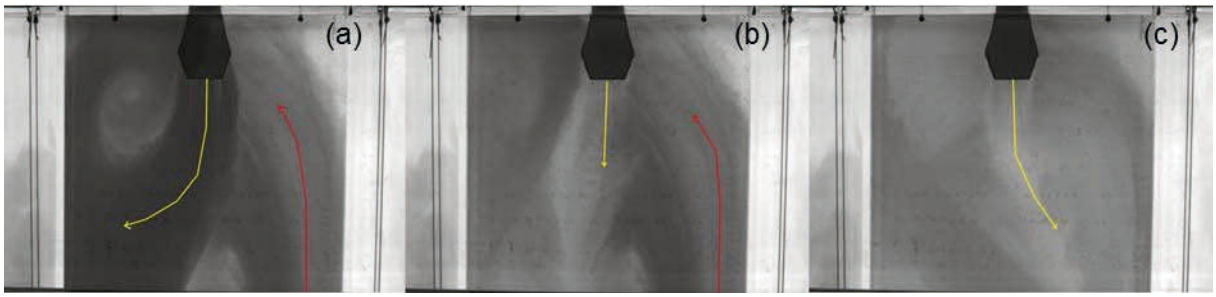

Figure 85. Results of case 2c for the SEN gap size 18 mm (a) time interval 15.8 (s), (b) time interval 2.2 (s), (c) time interval 15.0 (s) (Run5).

3.3.7 Case 3 SEN Gap Size 12 mm:

In Figure 86 the results of case 2 for the SEN gap size 12 mm can be seen. The jet flows to the right section of the mold as seen in Figure 86 (a). The development of the vortex at the right mold wall is influenced by the backflow and the jet. Another backflow at the left mold

wall is also present. This period takes 20.63 seconds until it changes its direction to straight downwards for the last 10.63 seconds. The two backflows at both mold walls are still present at this period (Figure 86 (b)).

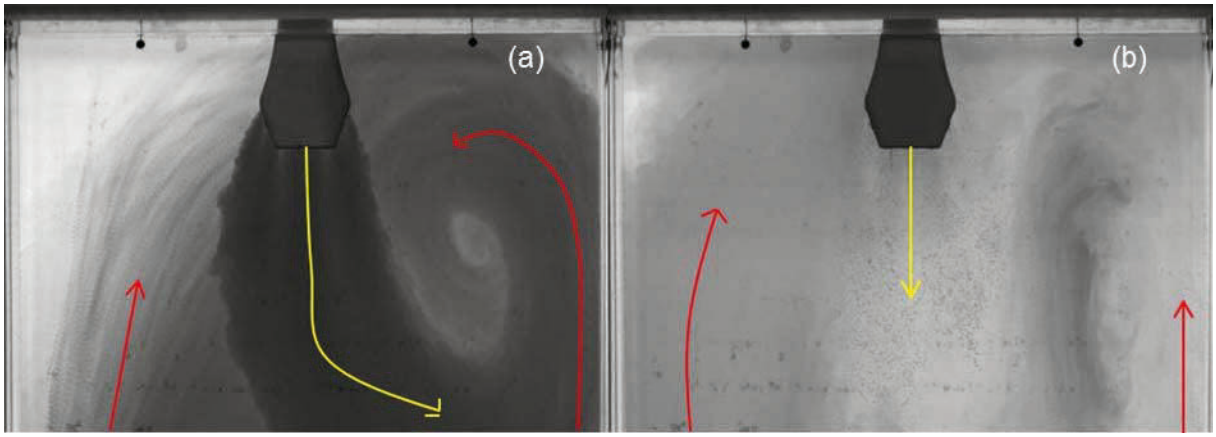

Figure 86. Results of case 3 for the SEN gap size 12 mm ((a) time interval 20.63 (s), (b) time interval 10.63 (s) (Run1).

The second run starts the same way as the first run with the same settings. The jet flows to the right section of the mold. At this area a vortex is created. A backflow is streaming up from the bottom part of the mold (Figure 87 (a)). This flow pattern can be observed for 15 seconds. Figure 87 (b) represents the last 16.25 seconds of recording time. During that period two backflows are present. At the whole recording time no dye was transported to the top left corner.

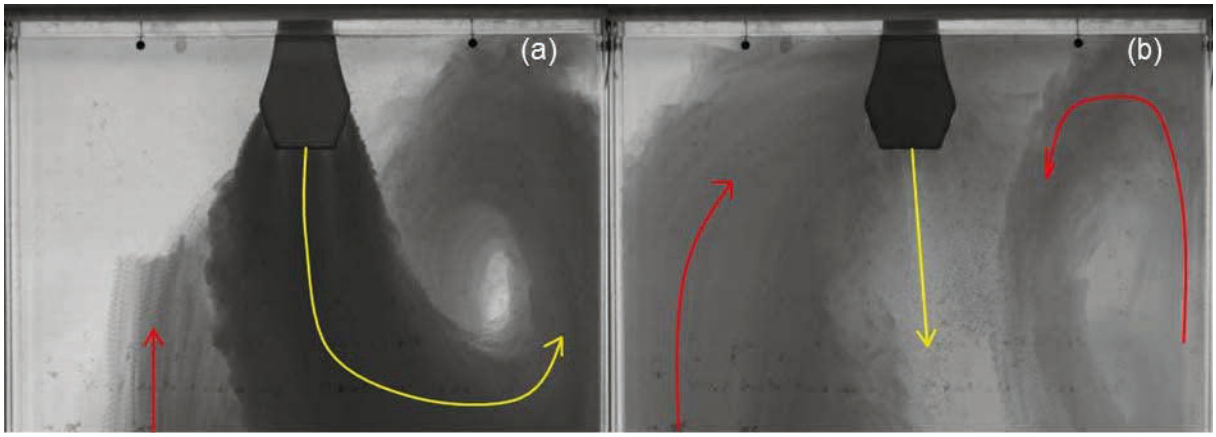

Figure 87. Results of case 3 for the SEN gap size 12 mm (a) time interval 15.0 (s), (b) time interval 16.25 (s) (Run2).

In Figure 88 the results of the third run of case 3 for the SEN gap size 12 mm can be seen. The jet flows to the left section of the mold and creates a large vortex. Almost the whole left area is mixed with the dye (Figure 88 (a)). At the right section of the mold a backflow is coming up. This flow pattern is present for 21.45 seconds. After that time the jet changes its flow direction to straight downwards. A backflow at the right side of the mold is still present and at the top right corner the concentration of dye is very low. The last period takes 10 seconds (Figure 88 (b)).

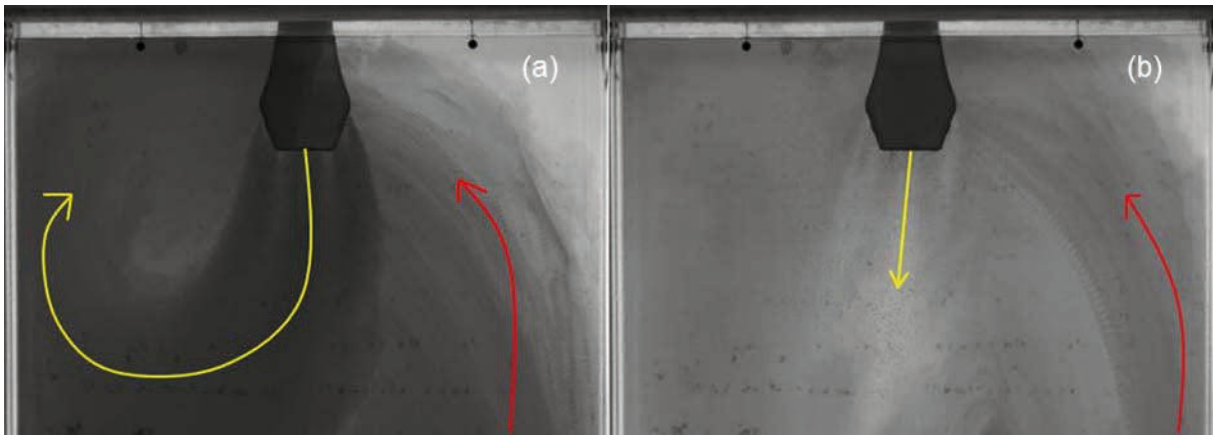

Figure 88. Results of case 3 for the SEN gap size 12 mm (a) time interval 21.45 (s), (b) time interval 10.0 (s) (Run3).

At the beginning of the fourth run a jet flowing to the right section of the mold can be seen (Figure 89 (a)). A backflow from the right bottom part of the mold is streaming up This flow

period takes 12 seconds. Afterwards the jet is streaming straight downwards. Backflows at both sides at the mold walls are visible. This flow pattern is seen 19.25 seconds (Figure 89 (b)).

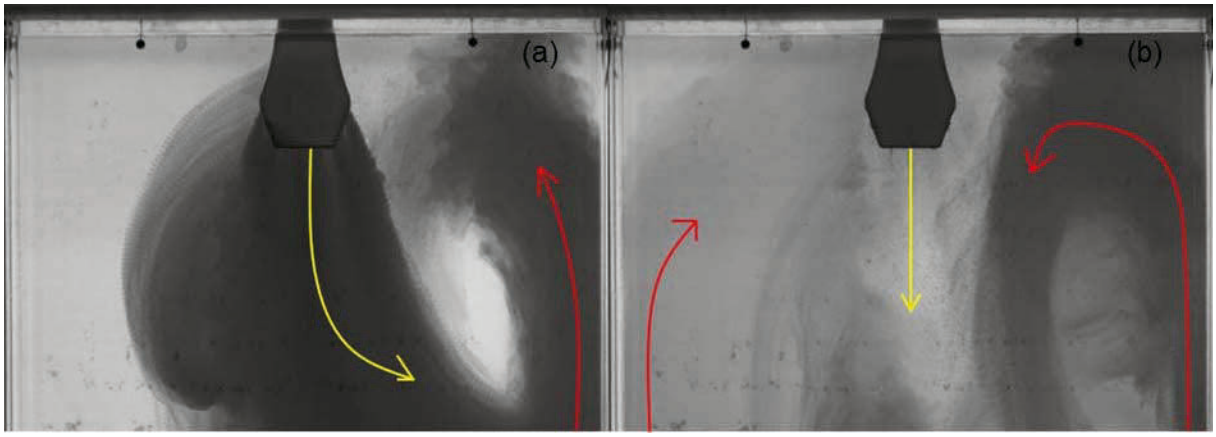

Figure 89. Results of case 3 for the SEN gap size 12 mm (a) time interval 12.0 (s), (b) time interval 19.25 (s) (Run4).

The fifth run of case 3 for the SEN gap size 12 mm shows compared to the other runs differences in the flow pattern. The flow behaviour is stable during the whole recording time (Figure 90). The jet flows to the right section of the mold and creates a vortex. At the left side of the mold a backflow is streaming up from the bottom part of the mold. No dye is transported to the top left corner of the mold.

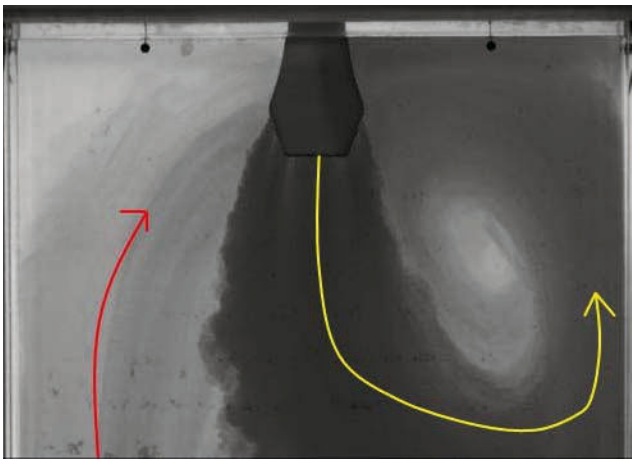

Figure 90. Results of case 3 for the SEN gap size 12 mm (Run5).

3.3.8 Case 3 SEN Gap Size 18 mm:

The first run of case 3 for the SEN gap size 18 mm can be seen in Figure 91. The jet streams straight downwards. A backflow from the right bottom part of the mold is coming up (Figure 91 (a)). At the left side of the jet some dye is recognizable which may come from some backflow at this section of the mold. This flow pattern is visible for 19.44 seconds. Afterwards the jet changes its direction to the left section of the mold (Figure 91 (b)). At the right area of the mold the backflow spread out further. During the whole recording time no dye is transported to the right top corner.

Figure 91. Results of case 3 for the SEN gap size 18 mm (a) time interval 19.44 (s), (b) time interval 13.56 (s) (Run1).

The second with the same setting starts with a straight downward flow which takes 10.19 seconds and can be seen in Figure 92 (a). The backflow is coming up from the left bottom part of the mold.

In Figure 92 (b) the change of the flow direction to the left section of the mold can be seen. It last for 21.06 seconds. Backflows at both sides of the walls are recognizable. During recording time no backflow is transported to the right corner of the mold.

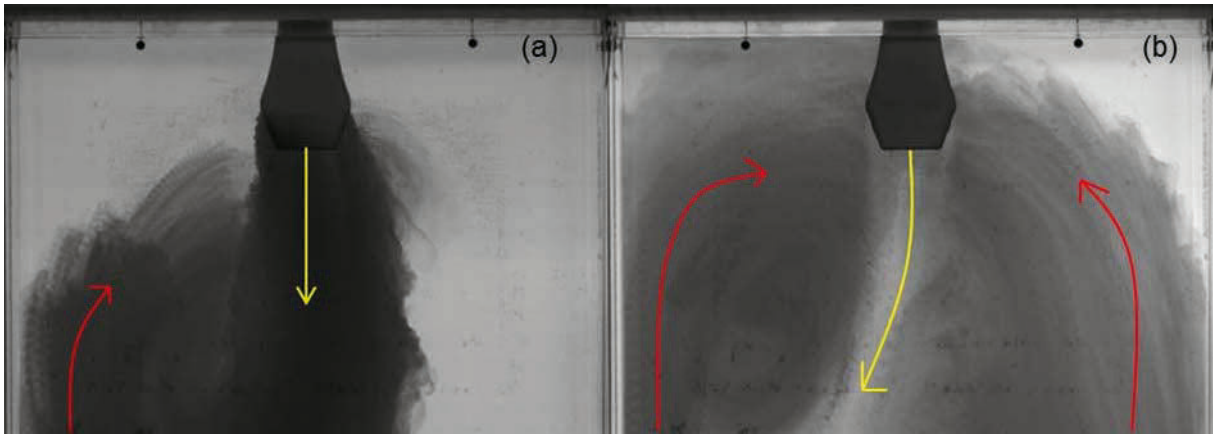

Figure 92. Results of case 3 for the SEN gap size 18 mm (a) time interval 10.19 (s), (b) time interval 21.06 (s) (Run2).

The results of run 3 of case 3 for the SEN gap size 18 mm show stable flow behaviour of the jet. A backflow at the right section of the mold is built by the down streaming jet and the upstreaming backflow at the right side at the mold wall. A backflow at the left section of the mold is also present and can be seen in Figure 93. After recording time it is recognizable that the dye was not transported to the whole area of the mold.

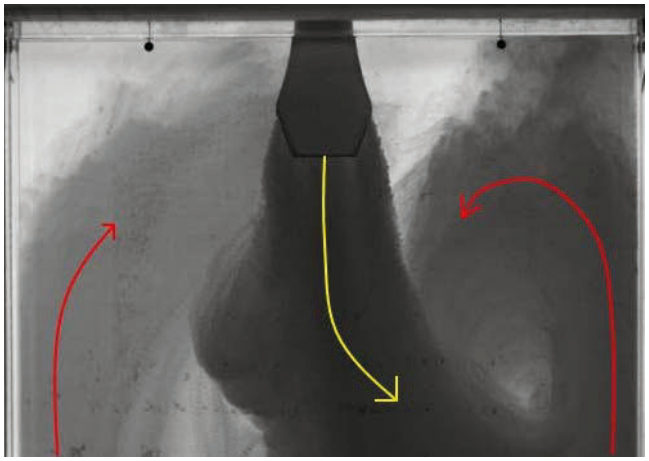

Figure 93. Results of case 3 for the SEN gap size 18 mm (Run3).

The jet of the fourth run streams to the right section of the mold. Also a backflow is streaming up at this area. This flow pattern is present for 9.56 seconds and shown in Figure 94 (a). During that period no dye is transported to the left section of the mold.

The jet flows straight downwards for the last 21.69 seconds of recording time (Figure 94 (b)). Backflow at the left and at the right mold walls appears. Almost no dye is transported to the top left corner during the whole recording time.

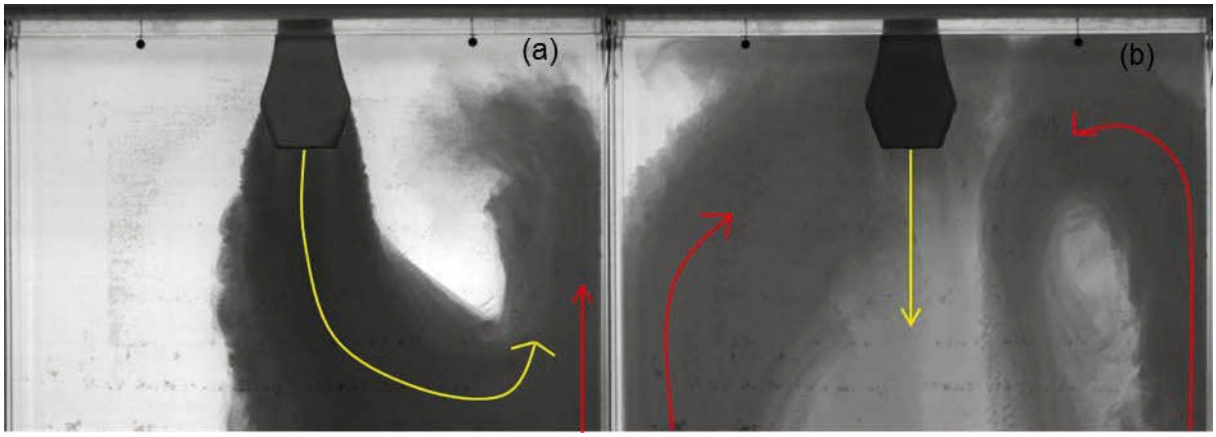

Figure 94. Results of case 3 for the SEN gap size 18 mm (a) time interval 9.56 (s), (b) time interval 21.69 (s) (Run4).

Figure 95 represents the last run of case 3 for the SEN gap size 18 mm. The flow pattern is stable during recording time. The jet streams straight downwards. Backflow at the right and the left sections of the mold are visible. During recording time no dye was transported to the top left corner of the mold.

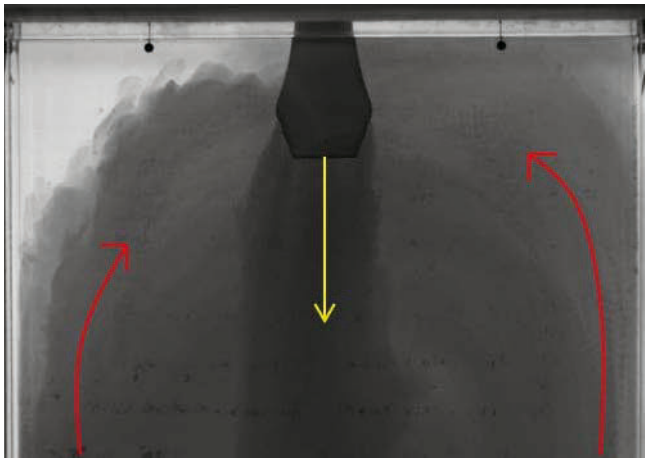

Figure 95. Results of case 3 for the SEN gap size 18 mm (Run5)

Unstable flow should be avoided during the process in real plants. Because of this flow pattern at only one section of the mold new melt, water is transported, which can lead to an undercooled zone inside the mold because of inappropriate heat/ mass transportation. Also the quality of the finished products cannot be guarantee at a certain level.

3.4 Comparison of the Submeniscus Velocity

The submeniscus velocity is measured for all cases and SEN gap sizes. The measurement was done before dye injection. Two paddles underneath the surface were fixed at the left and right sight of the SEN (Figure 96).

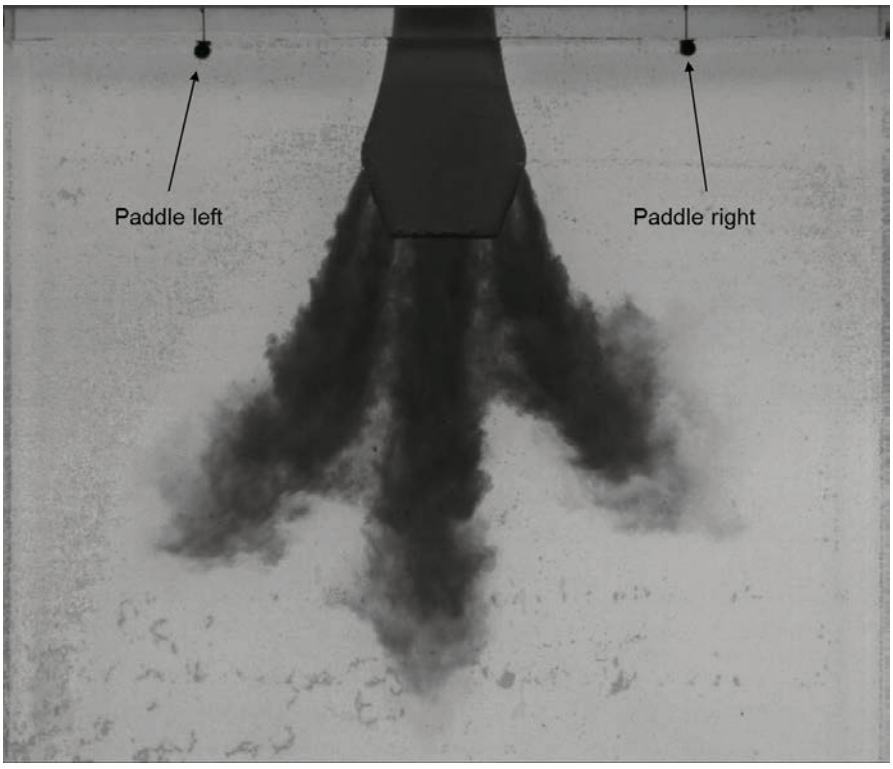

Figure 96. Schematic of submeniscus velocoty measurement.

The paddles measure the velocity for 30 minutes with a time step of 0.1 seconds. The software used is programed by RHI. The collected data are copied to Microsoft Excel.

High meniscus velocities indicate high wave fluctuations, which increase the probability of slag entrapments. A very low submeniscus velocity can be explained for example by a single down streaming jet which does not create an upstreaming vortex.

First step was to transform all data into absolute values and to calculate the average of the data of the left and right paddles by using equation 3 and 4.

$$u_{avg}^{L,R} = \frac{\Sigma |u_i|}{n} \tag{3}$$

$$u_{avg} = \frac{u_{avg}^{L} + u_{avg}^{R}}{2} \tag{4}$$

3.4.1 Case 1:

In Figure 97 the average of the measured velocities of the left and right paddles of case 1 for all gap sizes can be seen. It is recognizable that there is a difference in velocities between the left and the right section of the mold. Except by using the SEN with the gap size of 8 mm. For that case the submeniscus velocity seems to be equal.

An obviously significant decreasing of the submeniscus velocity by using the SEN with the 18 mm gap can be seen.

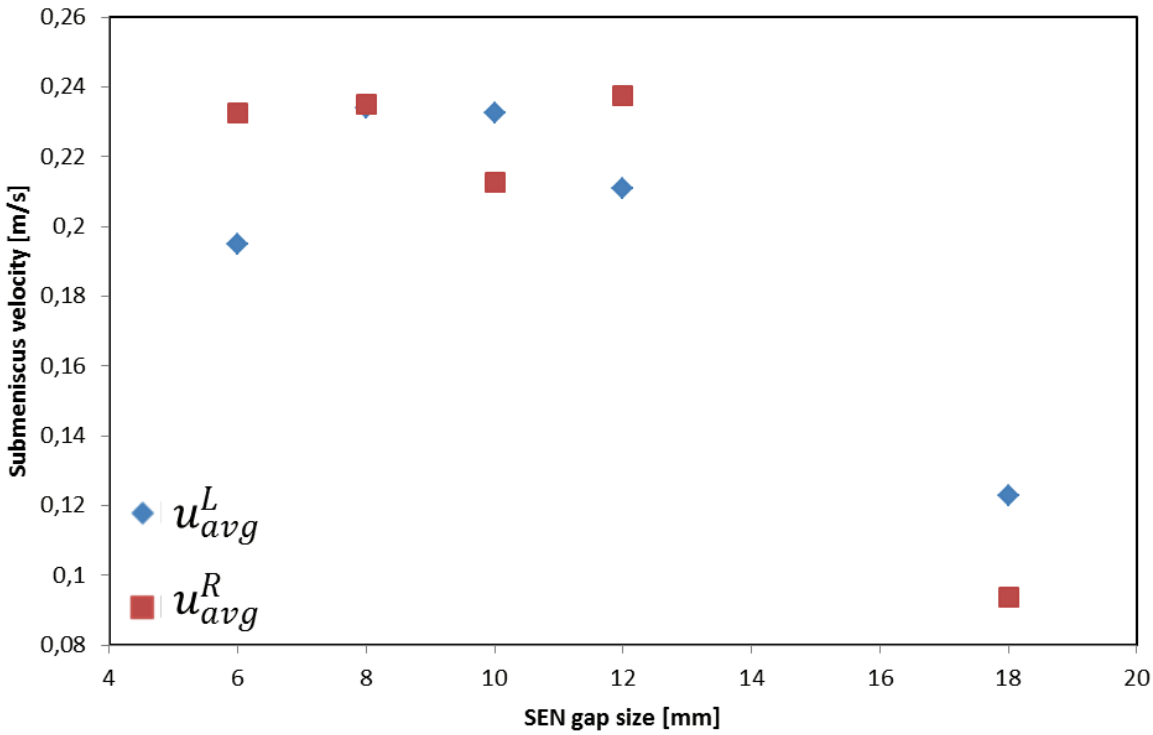

Figure 97. Average submeniscus velocity of case 1.

In Figure 98 the total average of the velocities for all gap sizes of case 1 is seen. In this diagram it is clearly seen that by using the SEN with 18mm gap size the submeniscus velocity is decreased by almost 50%.

For SEN gap sizes 6 to 12 stable flow is achieved which industry is trying to obtain during production. Unstable flow is not reliable for the production process.

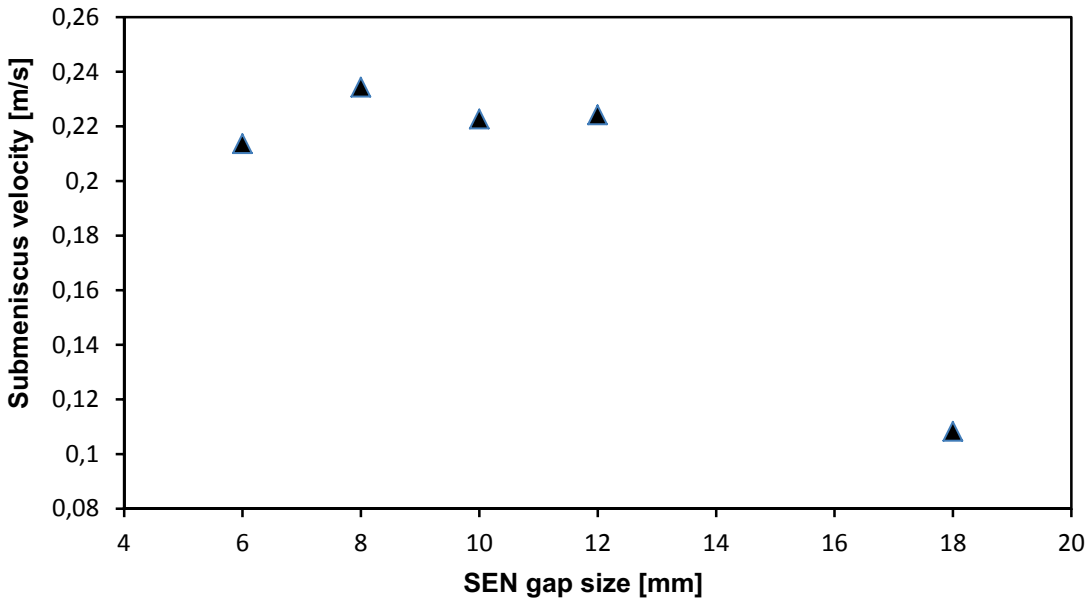

Figure 98. Total average submeniscus velocity (u_{avg}) of case 1.

Between the SEN gaps 6 to 12 the submeniscus velocity is almost constant and varies in a small range. The flow pattern of case 1 for the SEN gap size 6-12 is stable and that's the reason for almost the same submeniscus velocity. The results of the SEN gap size 18 mm show significant differences of the submeniscus velocities compared to the others. The average of the value is almost decreased by 50%. As described in chapter 3.3.1 the flow pattern is unstable

For these mold size and casting speed the results lead to the conclusion that the SEN gap size 18 mm is inappropriate because of creating a single jet and an unstable flow pattern.

3.4.2 Case 2c

In Figure 99 the absolute average values of the submeniscus velocities of the left and right paddles can be seen. The values of the velocities are decreasing by increasing the SEN gap sizes. The measured values of the SEN gap size for 6 and 8 mm varies during the record time. The highest submeniscus velocity range can be seen for the SEN gap size of 8 mm. As described before the flow pattern of case 2c for the SEN gap sizes 6 and 8 mm are stable. The submeniscus velocity for the SEN gap size 10 mm is almost equal for the left and right paddle during the recording time of 30 minutes. For that case the flow pattern is transient.

The flow pattern for the SEN gap sizes 12, 15 and 18 mm are unstable. For these gap sizes the velocities are lower compared to the other ones. Otherwise the measured velocities are very similar for the left and right paddles.

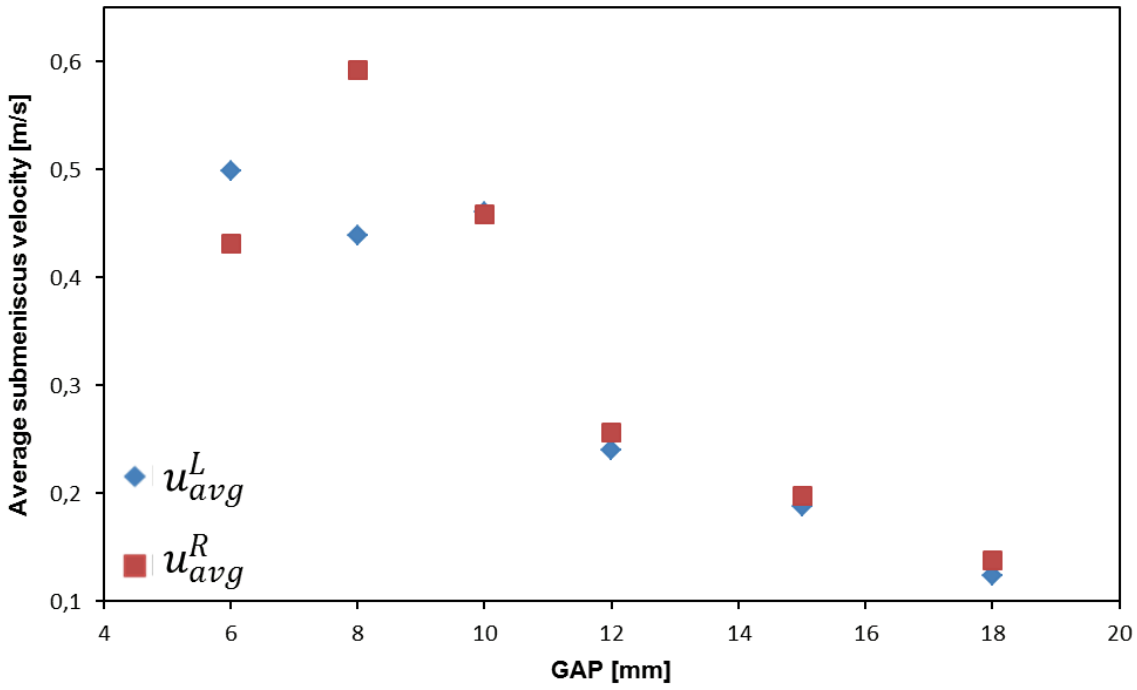

Figure 99. Average submeniscus velocity of case 2c.

In Figure 100 the total average submeniscus velocities can be seen. As described before the submeniscus velocities are decreasing by increasing the gap sizes. The velocities for the SEN gap size 6 and 10 are almost at the same level. The highest value can be seen for the SEN gap size of 8 mm. It seems that the velocities for the SEN gap 12 decreases linear to the velocity for the SEN gap size 18 mm.

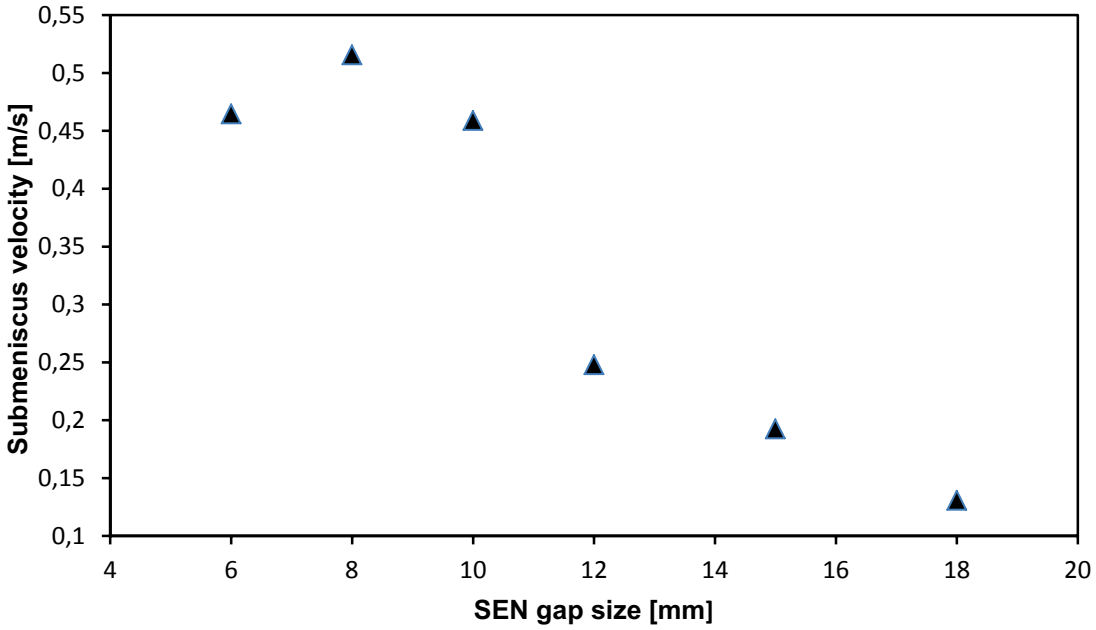

Figure 100. Total average submeniscus velocity (u_{avg}) of case 2c.

The submeniscus velocities decreases almost 70% compared to the values of the SEN for the gap size 6 and 18 mm.

The settings of case 2c showed that stable flow is achieved with for SEN gap size of 6 and 8 mm. For the SEN with gap size of 10 mm a transient flow pattern is observed which may be usable for industry because of that. The other SEN cause unstable flow which makes an use in real plants impossible.

3.4.3 Case 3

In Figure 101 the average values of the left and right paddles of case 3 can be seen. The measured values of the left and right paddle for the SEN gap size 6, 12 and 18 mm are varying in a small range during measuring time. The differences of the measured velocities are very high for the used SEN gap size 10 mm.

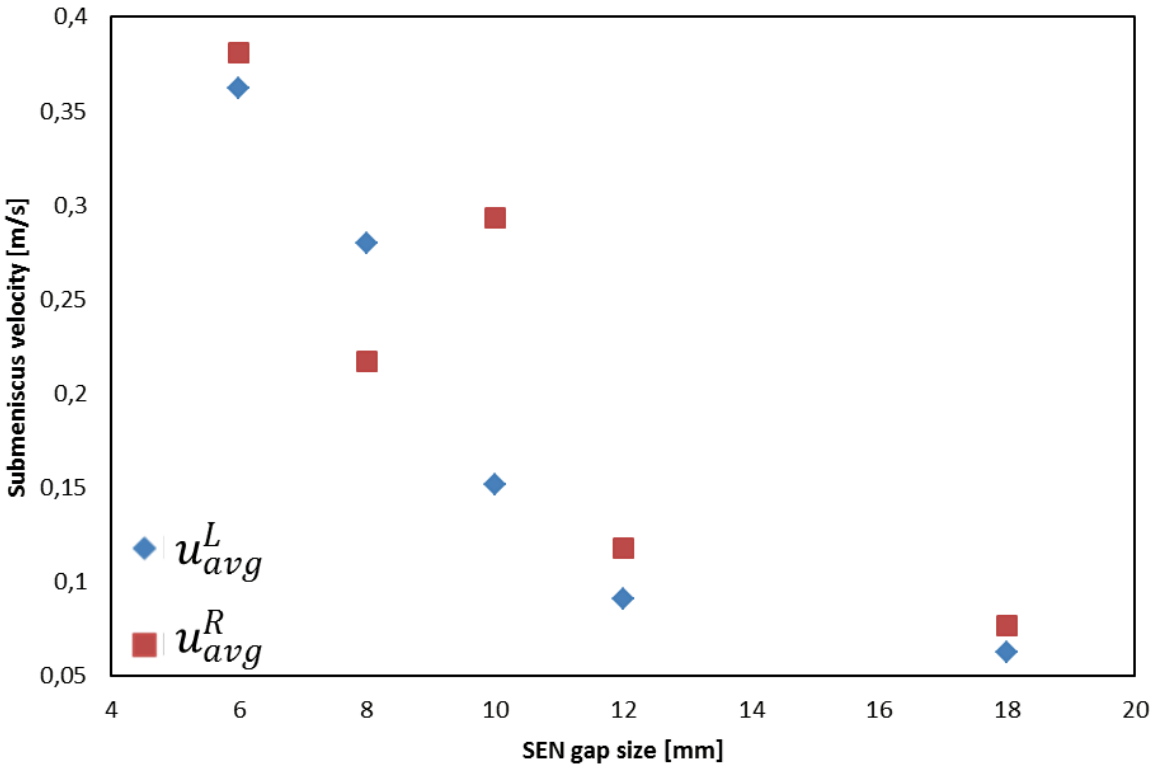

Figure 101. Average submeniscus velocity of case 3.

In Figure 102 the total average of the submeniscus velocity can be seen. Compared to the other cases the velocities decreases faster by using SEN with larger gaps. The highest value is measured for the SEN gap size 6 mm and the lowest for SEN gap size 18 mm. The flow pattern for 6 mm is stable and transient for the SEN gap sizes 8 and 10 mm. Unstable flow behaviour can be recognized for the gap size 12 and 18 mm.

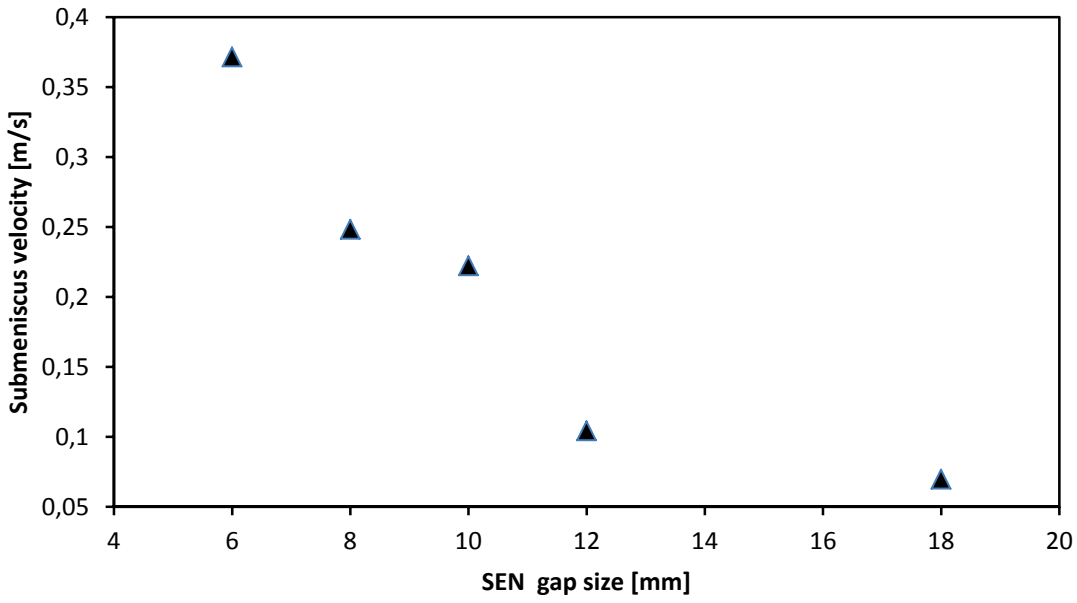

Figure 102.Total average submeniscus velocity (u_{avg}) of case 3.

For case 3 only one time a stable flow was observed (SEN gap size 6 mm). The other SEN design lead to transient or unstable flow behaviour. That is why the SEN gap size 6 mm can be suggested for thin slab casting under these conditions.

The highest submeniscus velocities are always stable flows in each case. This flow pattern is one of the aims of the thin slab casting process. By decreasing the velocity the flow pattern changes from stable to transient and finally to unstable flow.

The difficulty of transient flow is that no qualitative prediction of the flow behaviour can be made. Stable or unstable flow can appear.

The lowest velocity always indicates a single jet flow during the water model experiments.

3.5 Summary

Table 3 summarizes the results of the water model experiments. The trials in which stable flow is achieved is marked with “s”. The trials in which transient flow is achieved is marked with “t” and unstable flow with “u”.

			SEN gap size [mm]					
	Mold width [mm]	Casting speed [m/min]	6	8	10	12	15	18
Case 1	1150	2.4	s	s	s	s		u
Case 2a	1400	2.0						u
Case 2b	1400	2.4						u
Case 2c	1400	3.4	s	s	t	u	u	u
Case 3	1700	2	s	t	t	u		u

Table 3 Summary of results of the experiments

Stable flow is important for constant mass and heat transport. This is an important criterion for producing slabs in constant quality. Unstable flow may lead to partial freezing in the mold because of insufficient heat flux. No conclusion statement can be made for cases with transient flow based on the current experiment.

In industry a submeniscus velocity between 0.2 to 0.5 m/s is expected under most conditions. If the velocity is lower than 0.2 m/s the mold flux cannot be properly melted. On the other hand a submeniscus velocity above 0.5 m/s can create high surface fluctuations and vortices on the mold level can appear which can lead to entrapments.

4 Simulation Results and Comparison

One huge difference of TSC from conventional slab casting is the use of the funnel – type mold, which provides the necessary space for the SEN to conduct liquid melt into the thin slab mold. Another important feature is the shell thickness which solidifies in the mold region: 40 – 50% of slab thickness for TSC. In comparison, there is only 20- 30% of slab thickness which solidifies in the mold region for the conventional slab. Therefore, the evolution of solid shell under the influence of turbulent flow and subject to the continuous shell deformation in TSC becomes a critical issue for the modelling approach.[34]

Different models were used to calculate solidification of TSC. One of these is the "equivalent heat capacity model", as proposed by Hsiao. This model was originally proposed for the solidification without solid motion, as the transport of latent heat in the mushy zone due to the motion of the solid phase is not considered. According to recent investigations, the transport of latent heat in the moving (deforming) mushy zone plays an important part in continuously cast and solidified objects, e.g. continuous casting. In order to consider the advection of latent heat under the condition of deforming and moving mushy zone, an enthalpy – based mixture solidification model is favoured. A feature of the enthalpy based model is to provide a possibility to consider the flow solidification interaction in the mushy zone by introducing a volume-average parameter, i.e. permeability.[34]

In Figure 103 the schematic of the solidifying mushy zone can be seen.

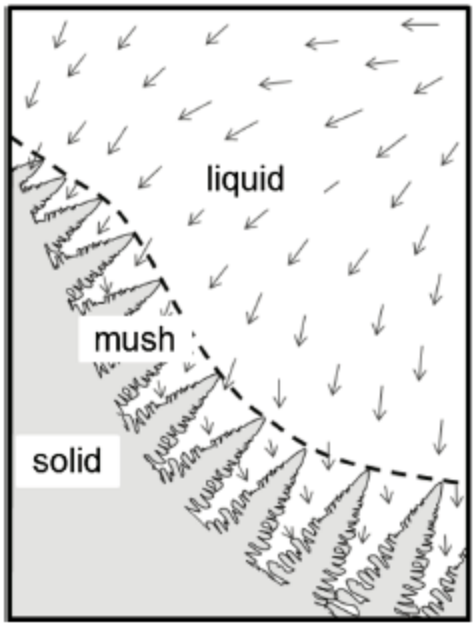

Figure 103. Schematic of the solidifying mushy zone. [34]

This model was later extended by including the turbulence model and applied to study the solidification and formation of macrosegregation under the influence of forced convection. [34]

The motion of the solid shell was assumed to be parallel and the moving velocity is constant everywhere and equal to the casting velocity by conventional continuous casting. These assumptions do not apply to TSC, where the strand shell is subject to continuous deformation due to the funnel type mold. Despite the same consideration of the experimentally determined heat flux, the use of the funnel – type mold must be treated properly, because it guides the motion of the solid shell of the strand and influences the melt flow inside the strand. [34]

4.1 Simulation Model

For simulating solidification and turbulence flow an enthalpy – based mixture solidification model has to be applied, done by Vakrushev A.[34] This mixture combines a liquid and solid phase. They are quantified by their volume fractions, f_l and f_s and $f_f + f_s = 1$.The morphology of the solid phase is usually dendritic but in that case the dendritic solid phase is

considered as a part of the mixture continuum. The flow in the mushy zone is determined according to permeability, while the motion of the solid phase has to be estimated. Free motion of crystals (equiaxed) is ignored. The mixture continuum changes continuously from pure liquid region, through the mushy zone (two-phase region), to complete solid. The evolution of the solid phase is determined by the temperature according to a $f_s - T$ relation.

To verify the simulation results by the water model experiments only the simulation of flow without solidification is needed. That is why only one phase (liquid) model is used.

4.2 Simulation Settings

The software package used is ANSYS Fluent 14 which runs on the SGI Cluster EVA 2.9/3.5 GHz with 288 Cores. The model viscous – laminar is turned on and the turbulence model is deactivated. The material used for simulation is water – liquid.

4.2.1 Simulation Geometry

In Figure 104 the geometry of the TSC model can be seen. The original mold width is 1400 mm and the thickness is 112.5 mm. The immersion depth is 210 mm the same as at the water model experiments. The total length is 2800 mm. The size of the geometry is also scaled down to 1:2 as the water model experiment.

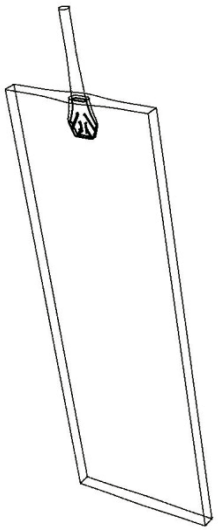

Figure 104. Geometry of the TSC model

The creation and enmeshment of the model was done by Vakrushev A. The used SEN gap size is 18 mm (Figure 105).

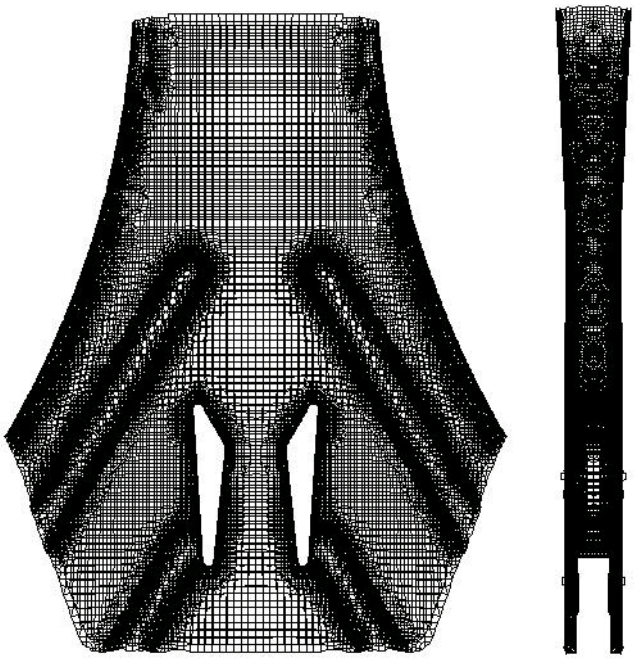

Figure 105. Scheme of the enmeshed for the SEN gap size 18 mm.

Three different enmeshment models exist, see Table 4.

Simulation Nr.	Number of node points (Million)
1	0.7
2	1.8
3	4.8

Table 4. 3 cases of mesh side.

This benchmark was done to investigate the quality of results considering the influence of mesh size. The results of simulation number 3 are not presented because there are no significant differences to simulation number 2.

The general settings are:

- Pressure based
- Absolute velocity formulation
- Gravity activated (-9.81 m/s²)

4.2.2 Boundary Conditions

The inlet velocity is calculated with velocity specification method: components. The reference frame is absolute. The velocities for the chosen y- velocities are listed in Table 5.

Casting speed steel plant [m/min]	**Inlet flow velocity [m/s]**
2	0.776
2.4	0.935
3.4	1.32

Table 5. Velocities values at the steel plant and in simulation.

The outlet velocity is fixed as pressure outlet. The top-wall is a stationary wall with specified shear. All other walls are stationary walls with no slip condition.

4.2.3 Thermal Physical Properties

The density of the liquid is 1.225 kg/m³, the temperature is fixed 288.16 K and the viscosity is 1.7894 * 10^{-5} kg/(m s). These are the standard values which ANSYS Fluent 14 suggests.

The solution methods are pressure velocity coupling with simple scheme and first order implicit. Solution controls standard values and also standard initialization is used for this calculation.

The time step is 0.001 seconds.

4.3 Results

4.3.1 0.7 Million Node Points with 3.4 m/min Casting Speed

In Figure 106 an overview of the results of the simulation can be seen. The pictures show the velocity magnitude. It is clearly seen that there are separate jets and not one single jet as seen in the results of the water model experiment (Figure 42).

After 8 seconds the down streaming jet connects with the left jet. In the middle of the mold a vortex develops and causes a backflow which also can be seen in the experiments.

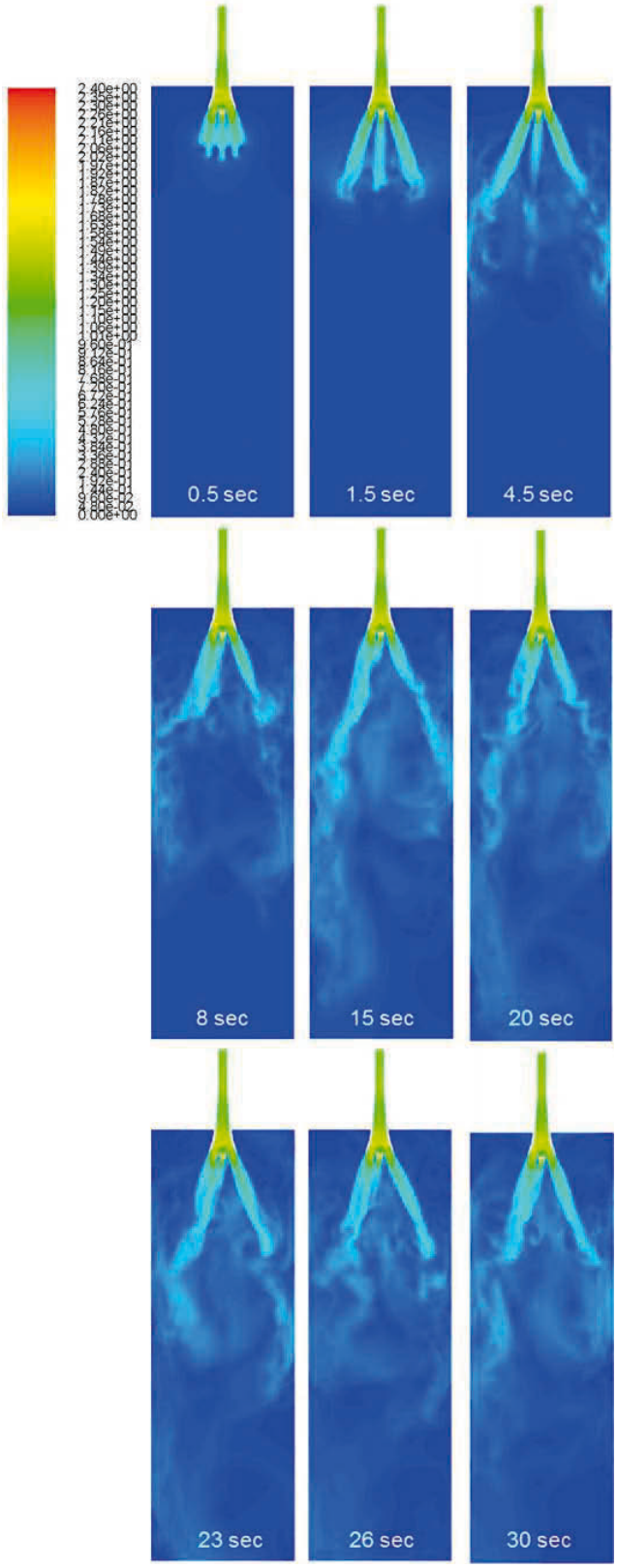

Figure 106. Evolution of the flow with simulated with 0.7 million node points (casting speed 3.4 m/min).

4.3.2 1.8 Million Node Points with 2.4 m/min Casting Speed

The results for this simulation can be seen in Figure 107. This simulation results shows huge differences to the results for the simulation with 0.7 million node points. The casting speed is reduced to 2.4 m/min and the mesh is refined to 1.8 million node points.

The results are similar to the results of the water model experiment with the same settings (Figure 42).

With beginning of the flow one huge current is visible which flows straight downwards. The jet is stable until 15 seconds: Vortexes influences the jet in a strong way and also backflows are present. Because of that the current gets unstable the deeper it is and creates a turbulent situation. That's why some small eddies are seen.

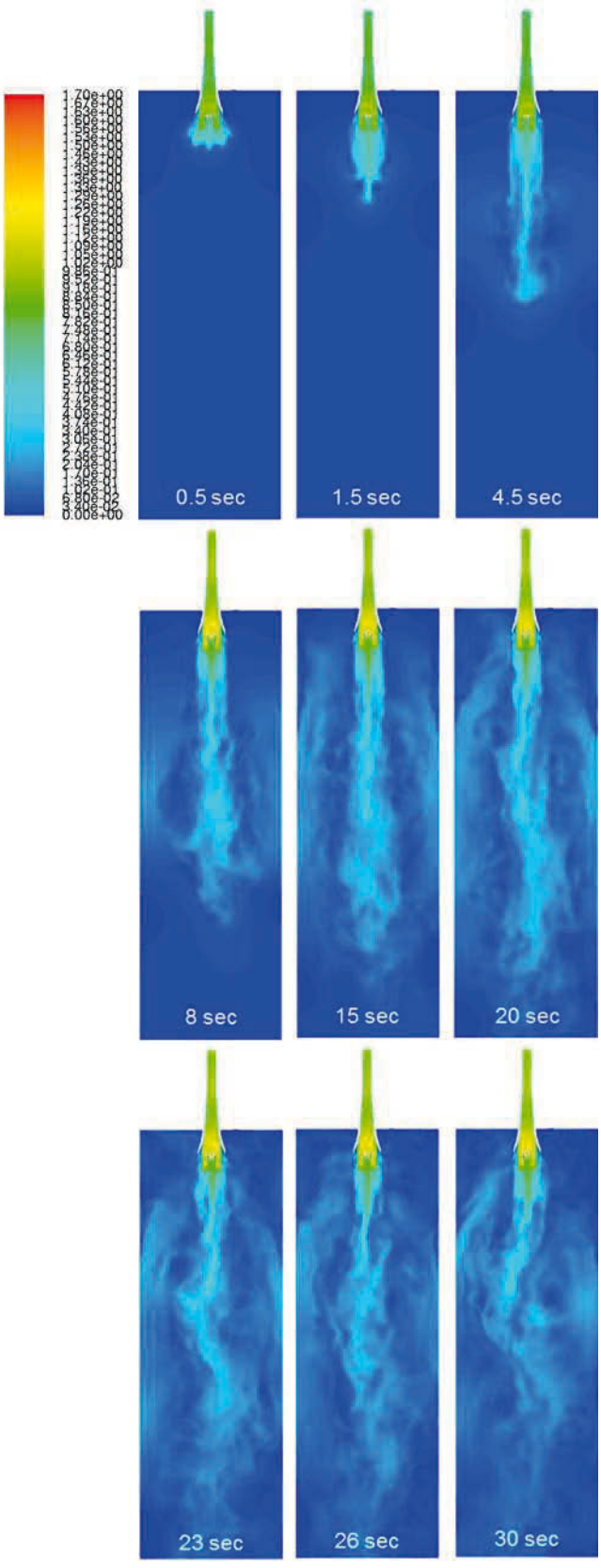

Figure 107. Evolution of the flow with simulated with 1.8 million nodes (casting speed 2.4 m/min).

4.3.3 1.8 Million Node Points with 3.4 m/min Casting Speed

In that case the casting speed was raised from 2.4 to 3.4 m/min (Figure 108). The results are different to the previous one. On the first sight an oscillating jet is recognisable. The vortexes are built at an earlier stage.

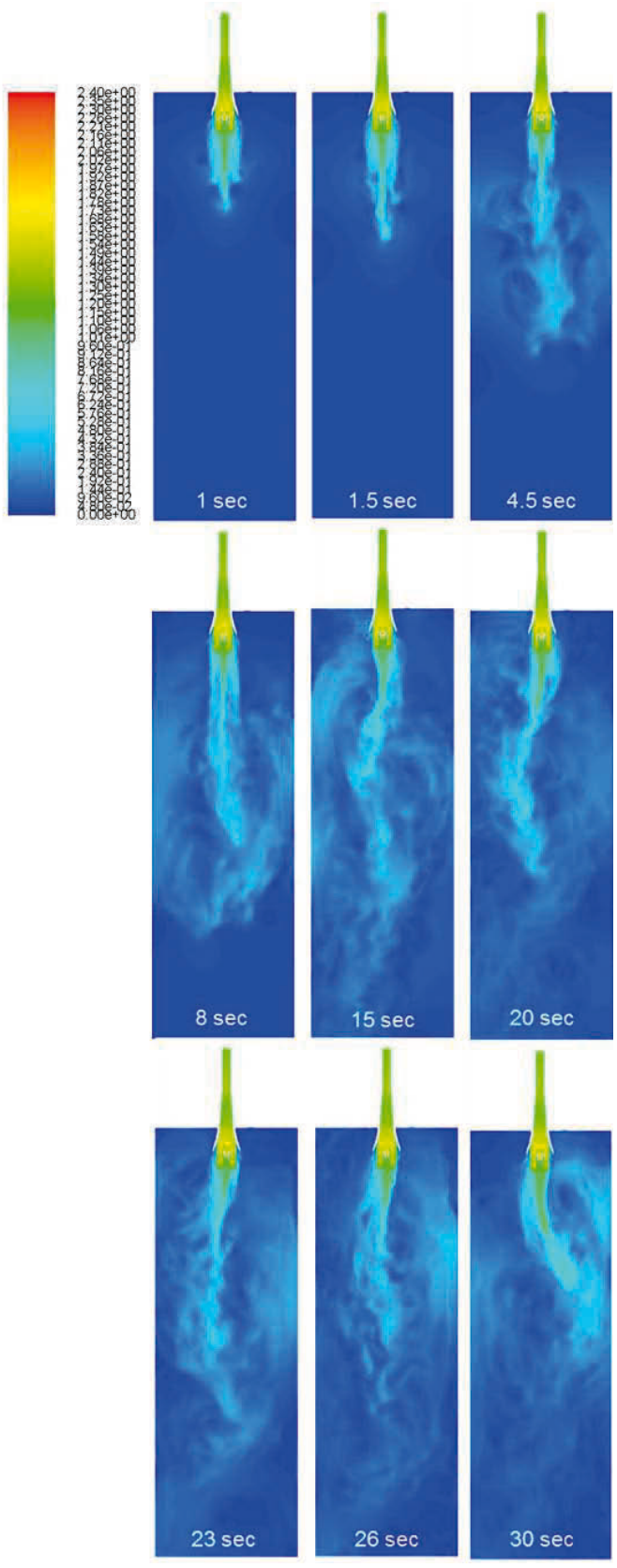

Figure 108. Evolution of the flow with simulated with 1.8 million nodes (casting speed 3.4 m/min).

4.4 Comparison with Experiment

To make a comparison between the results of water model experiment and the simulation a unify time scale has to be fixed. The moment of the dye injection is the starting point because before injection it is impossible to make any flow pattern at the water model experiment visible.

4.5 0.7 Million Node Points with 3.4 m/min Casting Speed

At the beginning of the experiment and simulation the results seems to be very similar. In Figure 109 (a) the out streaming dye is visible. Figure 109 (b) represents the results of the simulation at the same moment. At this moment it seems to be that one down streaming jet will be developed.

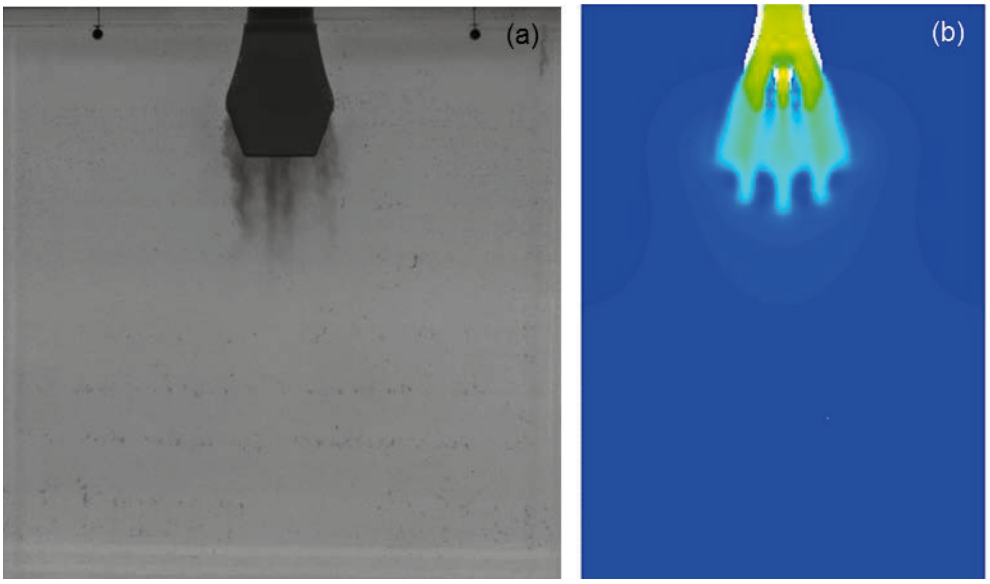

Figure 109. Comparison of experiment (case 2c) and simulation after 0.5 seconds of dye injection.

The results after 3 seconds can be seen in Figure 110. In Figure 110 (a) the down streaming single jet of the water model experiment can be seen. It is recognisable that the jet flows to the left section of the mold and is creating a vortex. The backflow reaches the meniscus level. Figure 110 (b) represents the results of the simulation. The differences in results are obvious. Compared to the results of the water model experiments are in the

simulation results three jets present at this time point. The right jet reaches deeper section of the mold at the left one. Vortices are built at the end of all three jets and create a backflow.

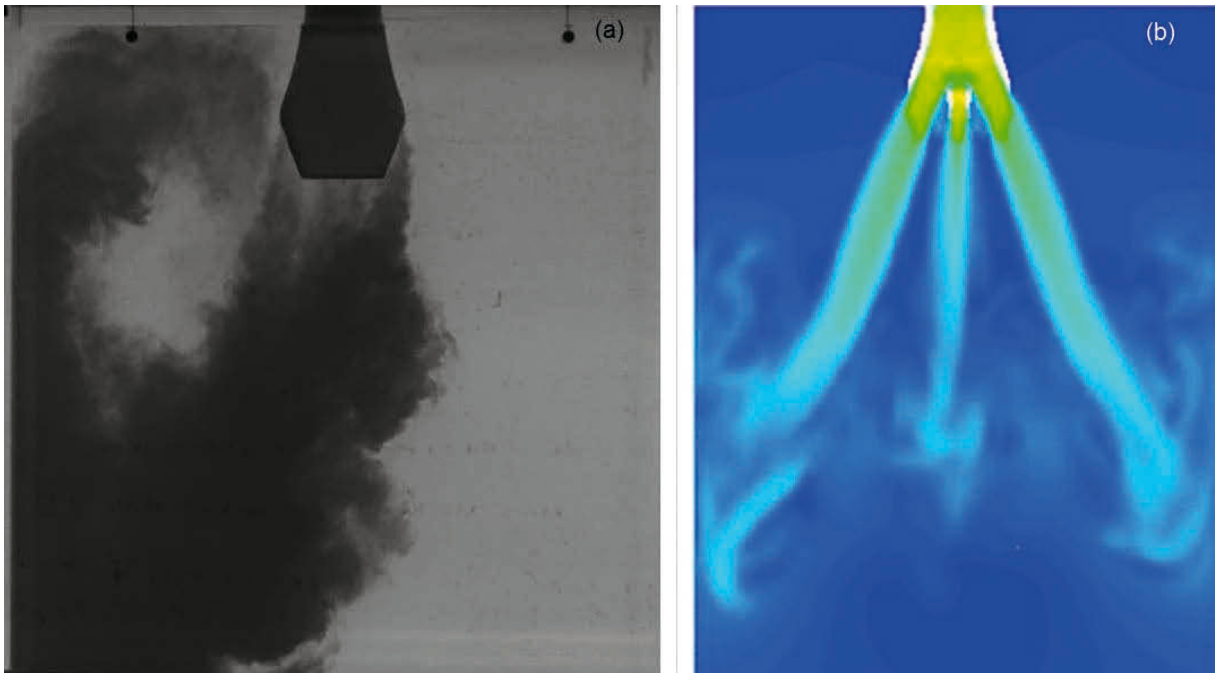

Figure 110. Comparison of experiment (case 2c) and simulation after 3 seconds of dye injection.

Figure 111 summarizes the results after 15 seconds of dye injection. The results of the water model experiment Figure 111 (a) demonstrate a single straight down streaming jet. Backflows at the left and right mold walls are present. The backflow at the left section of the mold wall reaches the meniscus level while the right one seems to flow in direction of the SEN.

The simulation result Figure 111 (b) shows that just 2 jets are present. The middle jet gets connected with the jet which stream out of the two left ports. Backflows are at both mold walls present.

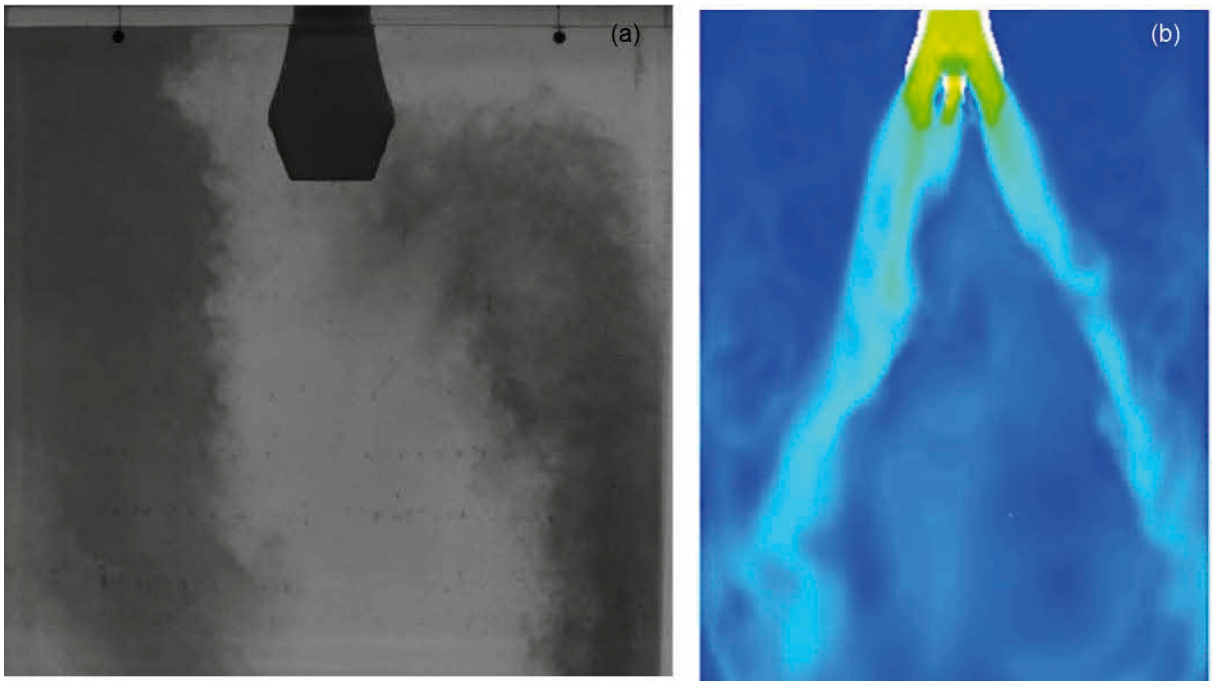

Figure 111. Comparison of experiment (case 2c) and simulation after 15 seconds of dye injection.

Figure 112 represent the results of water model experiment and the simulation after 25 seconds of dye injection, which is almost the end of recording time of the experiment. The photograph of the water model still shows a single jet flow pattern and backflows at the left and right side of the walls (Figure 112(a)).

The result of the simulation still shows two out coming jets (Figure 112 (b)). The middle jet is still connected with the jet out coming of the left ports. The areas below the jet seems to be very turbulent and backflows and vortices are developed. At that moment no flow reaches the top left corner of the mold.

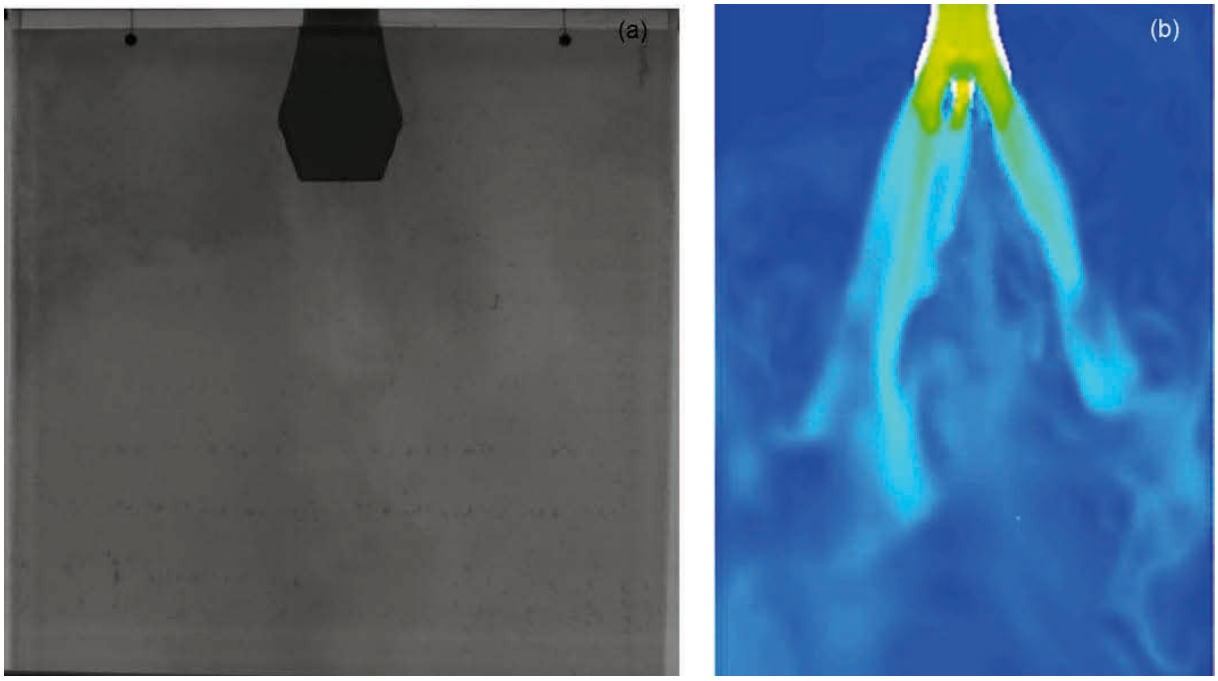

Figure 112. Comparison of experiment (case 2c) and simulation after 25 seconds of dye injection.

The results of the simulation with 0.7 million node points deliver different results compared to the experiment. It leads to the conclusion that the enmeshment has to be refined. The results from the simulation are not usable to make a qualitative statement of the flow behaviour.

4.6 1.8 Million Node Points with Casting Speed 2.4 m/min

In that case the enmeshment is finer and the casting speed is reduced to 2.4 m/s. The number of nodes increases from 0.7 to 1.8 million.

In the early stage the results look quite similar (Figure 113). In that period it seems that one straight down streaming jet will develop.

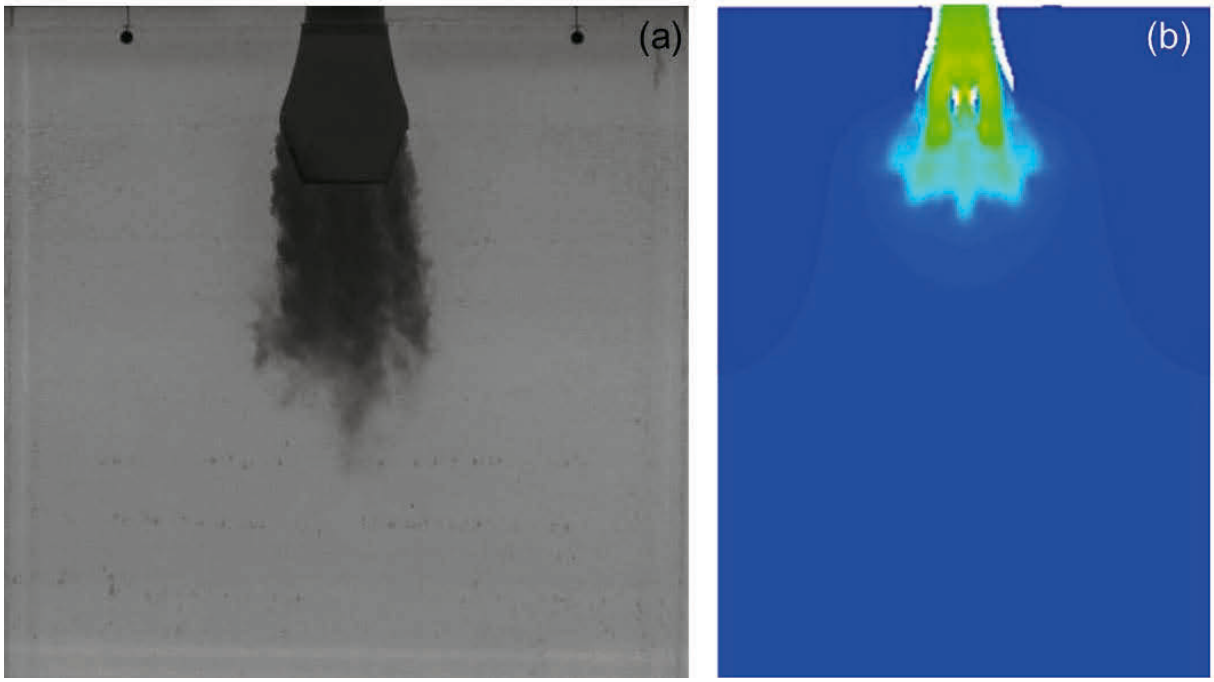

Figure 113. Comparison of experiment (case 2b) and simulation after 0.5 seconds of dye injection.

Figure 114 represents the results for the dye injection after 3 seconds. In the results of the water model experiment Figure 114 (a) and the simulation Figure 114 (b) one down streaming jet is visible. At that moment no backflow or vortices are created.

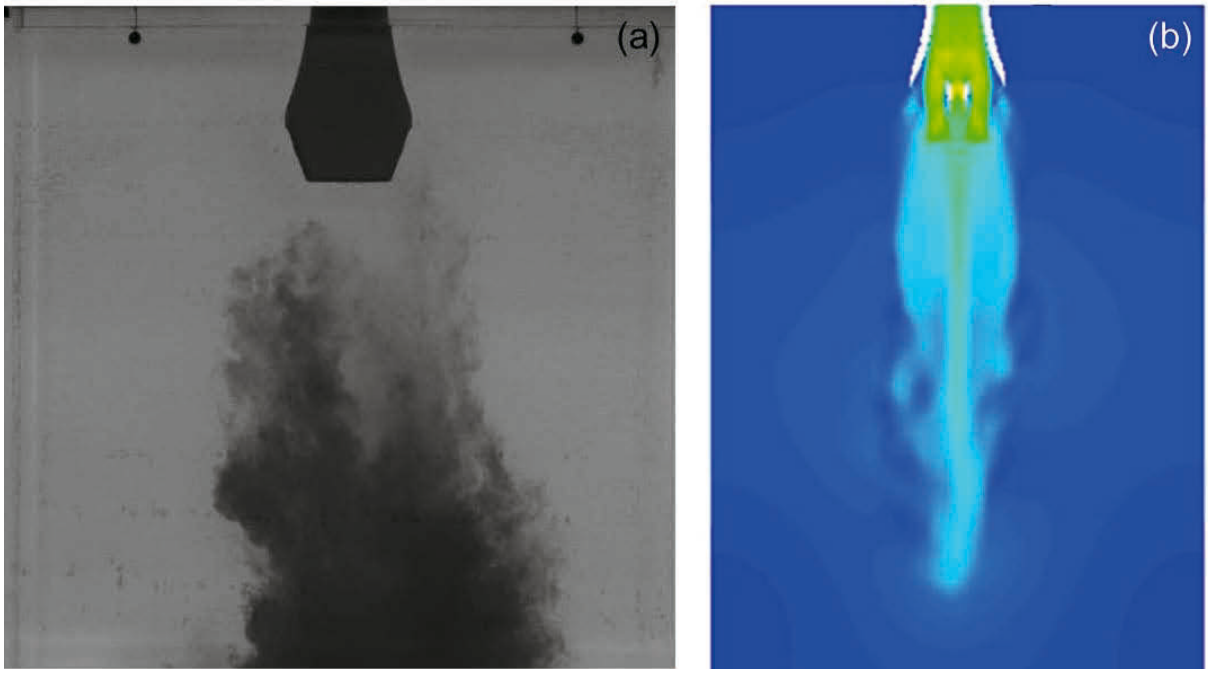

Figure 114. Comparison of experiment (case 2b) and simulation after 3 seconds of dye injection.

Differences are recognizable at 13 seconds after dye injection (Figure 115). The flow pattern of the water model experiment shows a jet which flows to the left section of the mold (Figure 115 (a)). A backflow from the right bottom part of the mold is streaming up and may influence the jet. At the left side of the mold a backflow from a previous period is still present.

The simulation result still shows a straight down streaming jet (Figure 115 (b)). Backflows are present at both sides of the mold walls. Small vortices are created at almost the whole section.

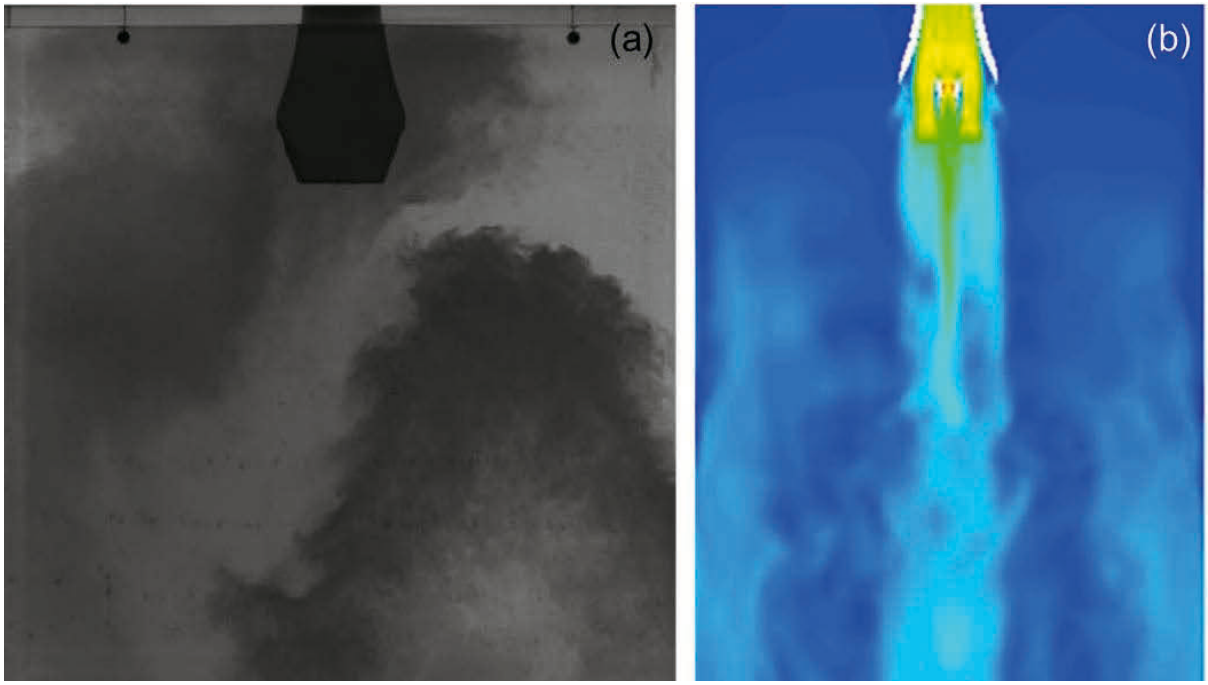

Figure 115. Comparison of experiment (case 2b) and simulation after 13 seconds of dye injection.

The results at the end of the recording time are quite similar again (Figure 116). The jet in the experiment has the same direction as the beam in the simulation result. Both are going straight downwards and the backflows which can be seen reaches the surface. The jets at both figures are sinuous. The backflow in the water model experiment is stronger at the left section of the mold. The same situation is found in the results of the simulation.

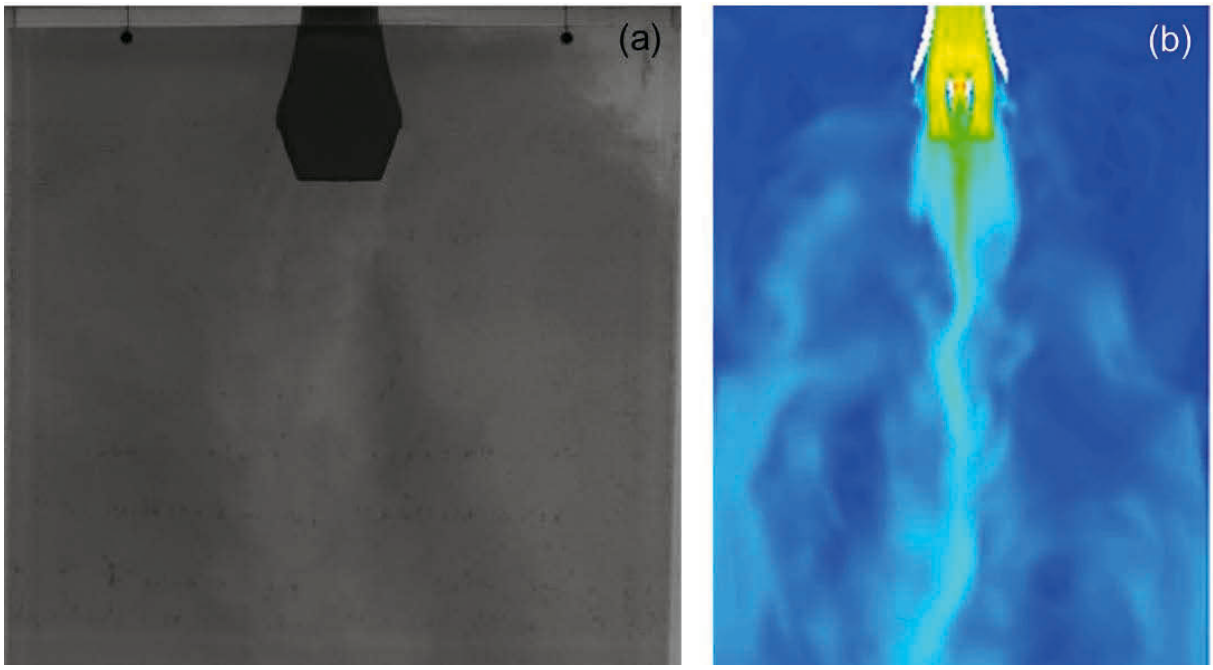

Figure 116. Comparison of experiment (case 2b) and simulation after 25 seconds of dye injection.

The results of the water model experiment and simulation are similar and comparable. The enmeshment is sufficient to deliver qualitative results.

4.7 1.8 Million Node Points Casting Speed 3.4 m/min

The enmeshment is the same as in the simulation case described in chapter 4.6. The casting speed is increased from 2.4 to 3.4 m/min. In Figure 117 the first second after dye injection can be seen. Both results show one single jet which goes straight downwards.

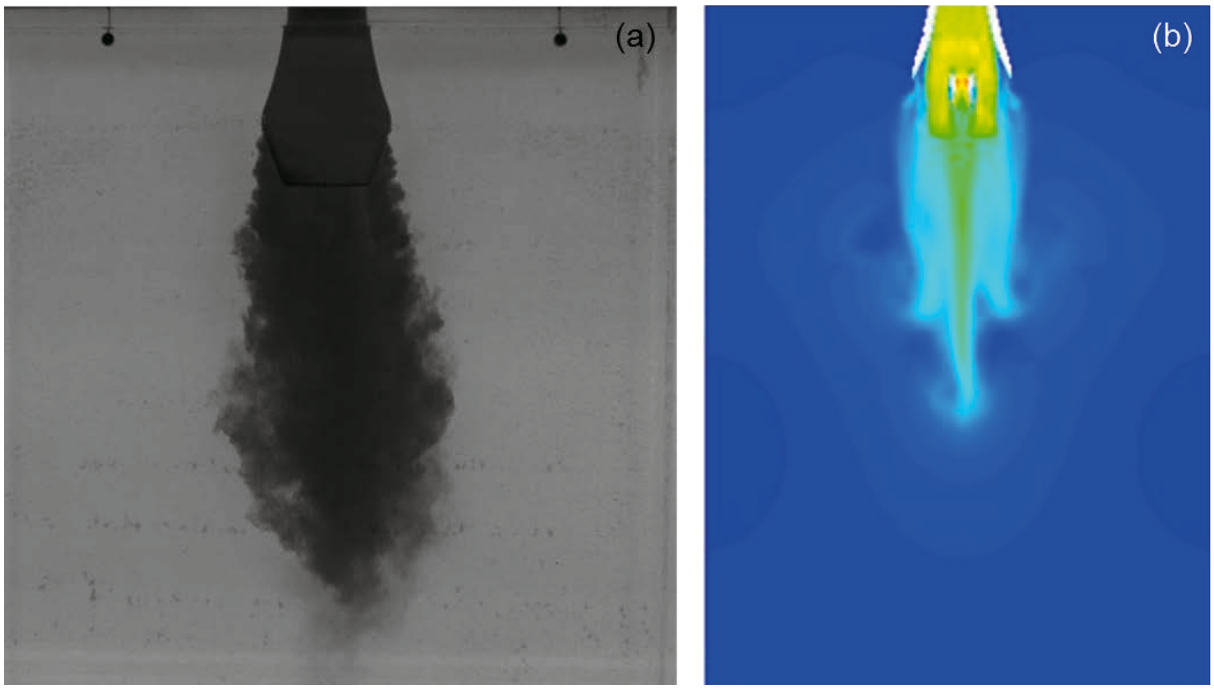

Figure 117. Comparison of experiment (case 2c) and simulation after 1 seconds of dye injection.

Figure 118 represents the results of dye injection after 5 seconds. The result of the water model experiment shows a single straight down streaming jet. At the bottom part creation of backflow and vortices can be seen (Figure 118 (a)). The simulation result for the same point shows similar results (Figure 118 (b)). One single down streaming jet is recognizable and in the middle of the visible mold small vortices are developing.

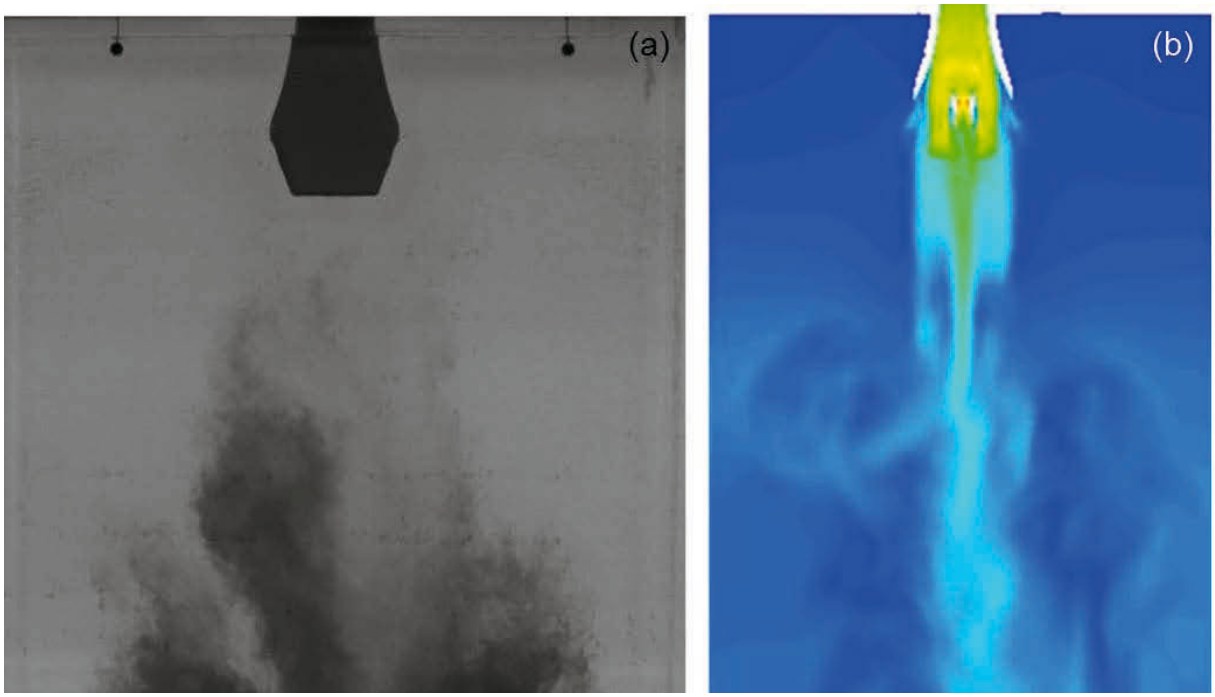

Figure 118. Comparison of experiment (case 2c) and simulation after 5 seconds of dye injection.

The flow pattern after 15 seconds of dye injection can be seen in Figure 119. It is recognizable that the result of the water model experiment and the simulation are quite similar. Figure 119 (a) shows a single jet which streams to the left section of the mold and creates a large vortex and backflow. At the right section of the mold a backflow is also present. At the right top corner less dye is transported until that moment.

In Figure 119 (b) the result of the simulation can be seen. As mentioned before the flow pattern is similar to the water experiment. A single jet is visible which tend to flow to the left section of the mold. A vortex and backflow is visible at the left section of the mold. A smaller vortex can be seen at the lower right section. Also the top right corner is less influenced by the flow behaviour inside the mold.

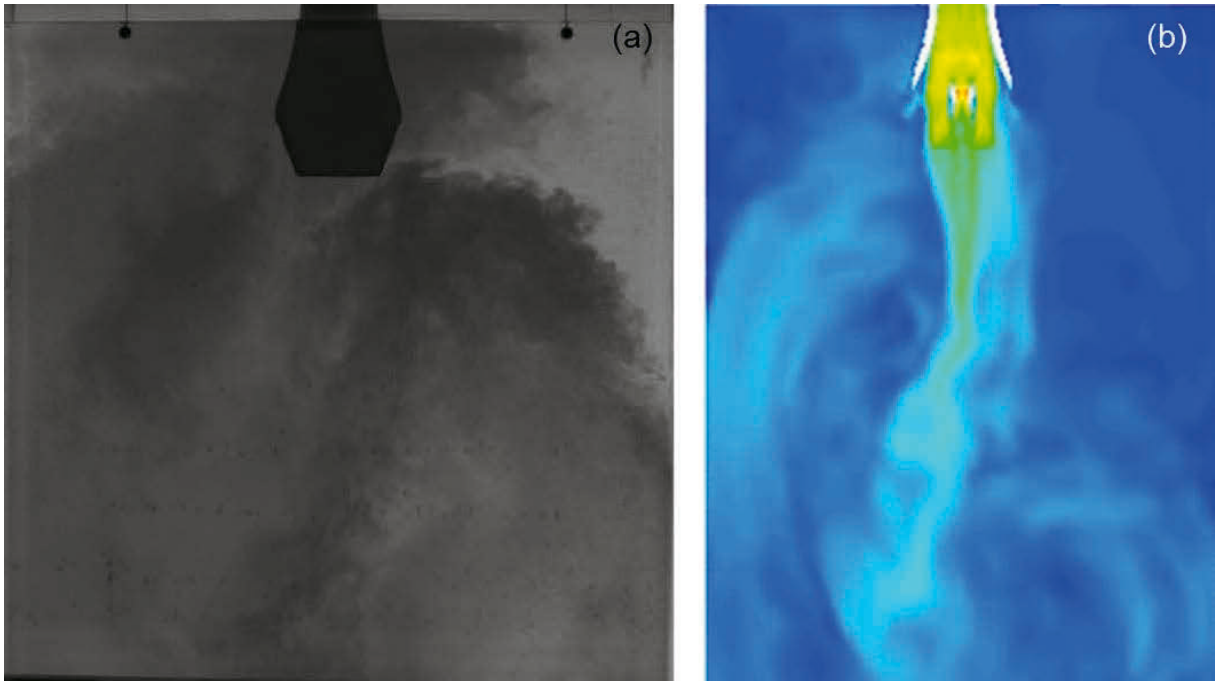

Figure 119. Comparison of experiment (case 2c) and simulation after 15 seconds of dye injection.

Figure 120 illustrate the results of dye injection after 20 seconds. The results are quite similar as at the previous time points.

The experiment shows that the jet streams straight downwards but tends to go to the left section of the mold (Figure 120 (a)). A reason therefore may be the backflow at the right side of the mold which streams up to the region of the SEN and influences the jet.

The result of the simulation also shows a single down streaming jet (Figure 120 (b)). It is recognizable that a part of the jet creates a vortex at the left section of the mold. The backflow at the right section seems to be less turbulent than the backflow at the left section.

The result of the water model experiment shows that no dye was transported to the top right corner: The simulation also shows that this part of the mold is less influenced by the flow behaviour inside the mold.

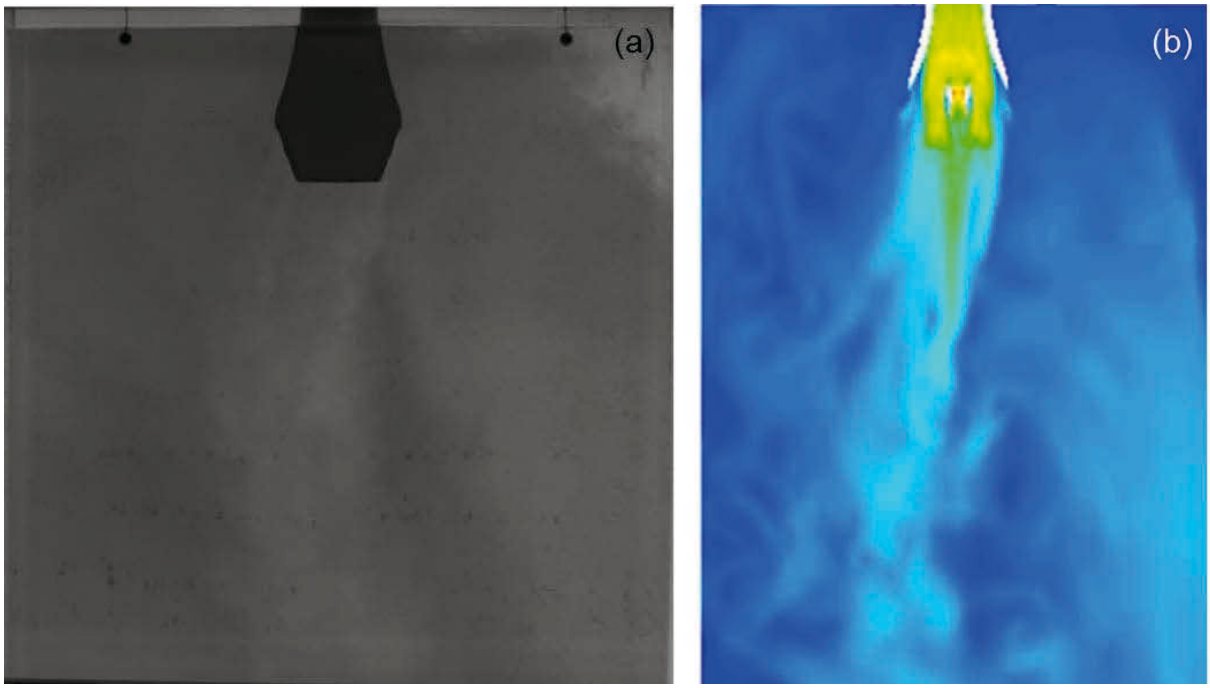

Figure 120. Comparison of experiment (case 2c) and simulation after 20 seconds of dye injection.

The comparison of the water model experiment and the simulation leads to the conclusion that both results are comparable if sufficient mesh refinement is done. As seen in chapter 4.5 the results of the simulation with 0.7 million nodes is completely different as the results of the water model experiment with the same setting.

There are advantages if the results of the experiments and simulation can be compared. More information of the process or flow behaviour can be carried out by simulation. This can lead to an improvement of the product or process.

5 Conclusion

State-of-the-art of the thin slab casting (TSC) technique is reviewed. There are different modifications of the production route for TSC, like CSP, ISP and ESP. The design of the submerged entry nozzle (SEN) is one of the key components for the TSC process. Different designs/development of SEN are made through the years. By increasing casting speed and mass flow the SEN should provide the mold with melt in a constant and controllable manner. Therefore, new designs of SEN are necessarily tested in water model experiments and with simulations before they are recommended for plant implementation.

RHI AG invented a new single port SEN design, namely UFM-SEN. In this master thesis the new SEN was investigated in a water model experiment and with numerical simulations. Different settings were made, as shown in Table 6. During water model experiment 3 different flow patterns were found: stable, transient and unstable flow. The summary of the results can be seen in Table 6. Symbols of “s”, “t” and “u” indicate flow patterns of “stable”, “transient” and “unstable”.

			SEN gap size [mm]					
	Mold width [mm]	Casting speed [m/min]	6	8	10	12	15	18
Case 1	1150	2.4	s	s	s	s		u
Case 2a	1400	2.0						u
Case 2b	1400	2.4						u
Case 2c	1400	3.4	s	s	t	u	u	u
Case 3	1700	2	s	t	t	u		u

Table 6. Summary of results of the experiments

The pattern of stable flow guarantees a constant heat and mass distribution inside the mold. Therefore, it is expected that the controllable quality of TSC can be achieved by the stable flow. Transient and unstable flow patterns are not recommended for industry, because the flow and the heat transfer inside the mold seems not controllable.

Simulations were made to reproduce the water model experiment numerically. The comparison between experimental results and numerical simulations shows that the experimental result is numerically reproducible, but the mesh quality for the simulation is crucial. Mesh sizes with 0.7 million node points are too rough to reproduce the experiment by simulation. The calculated flow pattern by the coarse mesh is different from the one of the experiment. Simulation results with 1.8 million node points are very close to the results of the experiments. The numerical results with a further fine mesh, i.e. 4.8 million node points, does not improve the calculation accuracy significantly, in comparison with the results with 1.8 million node points. Therefore, for the reason of computational efficiency the simulation with the mesh of 1.8 million node points is sufficient.

Advantages of simulations are that further different settings or design options can be made more efficiently regarding to both cost and lead time. All details of the flow can be made visible numerically; hence understanding to the process can be improved.

6 References (Literaturverzeichnis)

[1] Stahlinstitut VDEh, Stahlfibel, Verlag Stahleisen GmbH, Düsseldorf, 2007, pp. 80-86.

[2] C. Bernhard, Kapitel 3 Gießtechnik III – Anlagentechnik des Stranggießens, Skriptum Eisen und Stahlmetallurgie Modul 2, WS 2009/10, p.4.

[3] G. Flemming, F. Hofmann, W. Rohde, D. Rosenthal, Die CSP – Anlagentechnik und ihre Anpassung an erweiterte Produktionsprogramme, Stahl und Eisen, 113 (1993) Nr.2, pp. 37-46.

[4] F.-P. Pleschiutschnigg, H.-D. Hoppmann, I. Hagen, G. Gosio, Die ISP – Technologie, ihre Möglichkeit und erste Produktionserfahrungen, Stahl und Eisen, 113 (1993), Nr.3 pp. 53-67.

[5] G. Flemming, K.-E. Hengser, Present and future CSP technology expands product range, AISE Tecnology, January 2000, pp 53-57.

[6] K.-E. Hengser, Processing of advanced structural steels on CSP plants, Metalurgija, 41 (2002) (3), pp. 183-190.

[7] C.-P. Reip, W. Hennig, J. Kempken, S. Kramer, Challenges and solutions of compact strip production, Stahl und Eisen, 126 (2006), Nr.7, pp. 41-42, 44-47.

[8] C. Bilgen, C. Klein, C. Klinkenberg, J. Müller, From CSP to CSP flex: the new concept for thin slab casting, Millennium Steel, 2012, pp 90-96.

[9] G. Arverdi, F. Mazzolari, J. Siegl, G. Holleis, Arverdi ESP first thin slab endless casting and rolling results, Ironmaking & Steelmaking, 37 (2010), Issue 4, pp. 271-275.

[10] F. Mazzolari, G. Arvedi, M. Calinoi, ISP and ESP technology in integrated mills and mini mills – new potentials for steel producers, Rolling & Processing Conference 08, Paper No. 5.2.

[11] S. Bragin, A. Rimnac, B. Linzer, A. Bianchi, A. Mantova, A. Rizzi, C. Bernhard, Arvedi ESP process – an ultimate technology connecting casting and rolling in endless mode, Rolling 2013, S. 1-13.

[12] G. Arverdi, F. Mazzolari, J. Siegl, G. Holleis, A. Angerbauer, Acciairia Arverdi, Cremona Works – From ISP to ESP ultimate casting and direct rolling technology, Rolling & Processing Conference 08, Paper No. 5.1.

[13] O. Known, Thin slab hot rolling process in Asia: installations, core technology and competitiveness, La Revue de Metallurgie, January 2003, pp. 25 – 33.

[14] R. Shore, Casting technology and machine design solution for ESP plants, Rolling & Processing Conference 08, Paper No. 5.3.

[15] F.-M. Najjar, B. G. Thomas, D.- E. Hershey, Turbulent flow simulations in bifurcated nozzles: Effects of design and casting operation, Metallurgical Transactions, 26B (4), 1995, pp. 749-765.

[16] B. G. Thomas, P. Vanka, Study of Transient Flow Structures in the Continuous Casting of Steel, 2000 NSF Design & Manufacturing Grantees Conference, Vancouver, Canada, Jan. 5-8. 2000, p.14.

[17] Y. Tang, M. Krobath, G. Nitzl, SEN Design optimation using transient flow simulation and modelling at high-speed thin slab casting, Proceedings of the 2009 international symposium of thin slab casting and rolling, pp. 173-180.

[18] R.D. Morales, Y. Tang. G. Nitzl, Design of a submerged entry nozzle for thin slab molds operating at high casting speeds, ISIJ International, 52 (2012), No 9, pp. 1607-1615.

[19] X. Huang, B.G. Thomas B.G, F.M. Najjar, Modeling Superheat Removal during Continuous Casting of Steel Slabs, Metallurgical Transactions, 23B(1993), pp. 339-356,

[20] H. Nakato, M. Ozawa, K. Kinoshita, Y. Habu, T. Emi, Factors Affecting the Formation of Shell and Longitudinal Cracks in Mold during High Speed Continuous Casting of Slabs, Trans. Iron Steel Inst. Japan, 24 (11), (1984), pp. 957-965.

[21] J. Herbertson, Q.L. He, P.J. Flint, R.B. Mahapatra, Modelling of Metal Delivery to Continuous Casting Molds, 74th Steelmaking Conference, Washington, D.C., (1991), 74, pp. 171-185.

[22] B.G. Thomas B.G., Chapter 4.3 Continuous casting operation fluid flow, Making, Shaping, and Treating of Steel, 11th Ed. (2000), A. Cramb, ed., AISE Steel Found.

[23] E. Torres-Alonso, R.D. Morales, Cyclic turbulent instabilities in a Thin slab mold. Part I: Physical Model, Metallurgical and Materials Transactions, 41B(2010), pp. 583- 597.

[24] G. Hackl, Y. Tang, G. Nitzl, D. Chalmers, J.D. Dorricot, L.J. Heaslip, Flow control refractory design optimization of submerged entry nozzles by simulation technology, AIST.org, (2014), pp. 47 – 54,

[25] I. Caldero, N. Ramos, R.D. Morales, The Role of Submerged Entry Nozzle Port Shape on Fluid Flow Turbulence in a Slab Mold, Metallurgical and Materials Transactions, 46B(2015), pp. 1314 – 1325.

[26] C. Real, R. Miranda, M. Barron, L. Hoyos, J. Gonzales, Transient Internal Flow Characterization of a Bifurcated Submerged Entry Nozzle, ISIJ International, 46(2006), No.8, pp 1183-1191.

[27] F.D. Naijar, B.G. Thomas, D.E. Hershey, Numerical Study of Steady Turbulent Flow through Bifurcated Nozzles in Continuous Casting, Metallurgical and materials Transaction, 26B(1995), pp 750-765.

[28] Y. Tsukaguchi, H. Hayashi, H. Kurimoto, S. Yokoya, K. Marukawa, T Tanaka, Development of Swirling – flow Submerged Entry Nozzles for Slab Casting, ISIJ International, Vol. 50 (2010), No. 5, pp. 721-729,

[29] M. Brunnmayer, P. Gittler, J. Watzinger, Stabilization of Unsteady Flow in the Mold Region of a Wide Slab Caster by Submerged Entry Nozzles Design Optimization with CFD, Second International Conference on CFD in the Mineral and Process Industries, Csiro, Melbourne, Australia, December 1999, pp. 217-222.

[30] S. Garcia-Hernandez, R.D. Morales, J. Barreto, K. Morles-Higa, Numerical Optimization of Nozzle Ports to Improve the Fluidynamics by Controlling Back flow in a Continuous Casting Slab Mold, ISIJ International, 53 (2013), No. 10, pp. 1794–1802.

[31] M.H. Zarea, A.H. Meysami, SH. Mahmoudi, M. Hajisafari, M.Mazaratabaki, Simulation of Fluid Flow and Solidification in the Funnel Type Crystallizer of Thin Slab Continuous Cast, Oriental Journal of Chemistry, 29(2013), pp 1325 – 1337.

[32] H. Liu, C. Yang, H. Zhang, Q. Zhai, Y. Gan, Numerical Simulation of Fluid Flow and Thermal Characteristics of Thin Slab in the Funnel-Tape Molds of Two Casters, ISIJ International, 51 (2011), No.3, pp 392 – 401.

[33] J.Y. Jeon, H.J.S. Young, S. Lee, Flow Oscillations and Meniscus Fluctuations in a Funnel – Type Water Model, Metallurgical and Materials Transaction, 41B(2010), pp 121 – 130.

[34] A. Vakrushev, M. Wu, A. Ludwig, Y. Tang, G. Hackl, G. Nitzl, Numerical Investigation of Shell Formation in Thin Slab Casting of Funnel – Type Mold, Metallurgical and Materials Transaction, 45B,(2014), pp 1024 – 1037.

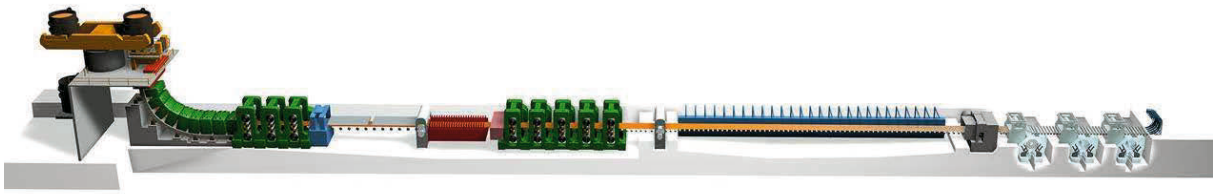

Figure 4. Process route of a TSC plant.[2]

Advantages of TSC in comparison to the conventional continuous casting:

- Small variation of mechanical properties because of constant velocity of the rolling process and temperature balance in the roller hearth furnace,
- Lower costs,
- Small segregation sensitivity because of smaller grain size,
- Good surface quality,
- Lower energy consumption and environment pollution.[3,4]

1.1.1 Compact Strip Production (CSP)

In a CSP the liquid steel is cast into thin slabs which after temperature equalisation in a tunnel furnace are rolled directly in the rolling mill without roughing.

CSP is a technology for producing hot rolled strip at low production costs in combination with high productivity and product quality.[5]

In Figure 5 a layout of the CSP process can be seen.

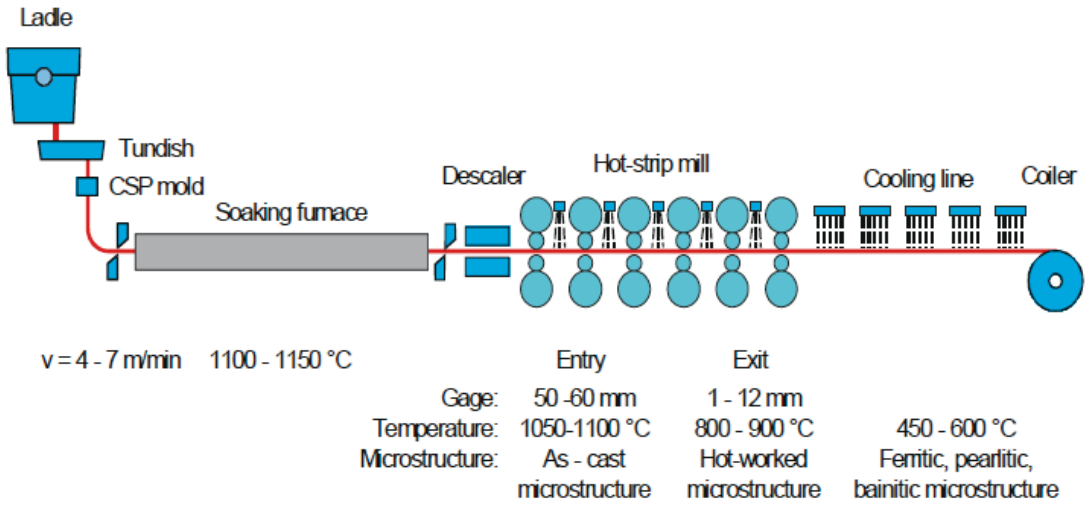

Figure 5. Schematic representation of a compact strip production plant.[6]

The characteristic of the CSP technology is the integration of three factors:

- Equipment design and automation,
- Technological practices,
- Material characteristics (composition and microstructure).[5]

Significant differences are inherent in the engineering design and material processing of CSP plants, in contrast to conventional hot rolled strip production. It is these differences that provide considerable potential advantages for the future manufacture of high performance hot rolled strip. [5]

The principal features of CSP technology that have a major effect on the metallurgical properties of hot rolled finished product are:

- Thin slab casting,
- Direct charging and rolling of a thin slab,
- Laminar cooling and coiling.[5]

One of the important characteristics of thin slab casting is the higher solidification rate in comparison with conventional slab casting. The faster solidification rate results in smaller secondary dendritic arm spacing and considerably less macro segregation. This feature is a major factor contributing to the superior constitutional homogeneity of CSP hot rolled strip.[5]

The direct charging and rolling of a hot thin slab without a roughing mill has a significant effect on the microstructure. The thin slab enters the CSP rolling mill with an as-cast structure where as in a conventional rolling operation the transfer bar has a recrystallized

In the year 2012 28 CSP plants are operating worldwide and producing 50 Mt of hot strips, which represents 10% of the world wide hot strips production.[8]

1.1.2 Inline Strip Production (ISP)

ISP technology is a unique technology for processing high quality, thin gauge and hot rolled strip. [9] It allows a tenfold reduction in times and a space compared with traditional processes and obtains a new process and high-quality product with extraordinary performance at decidedly lower costs starting from a shape closer to the final gauge.[10]

The principles are to exploit the heat of the liquid steel coming from the ladle furnace in an inline process and to continuously roll the thinnest possible slab to obtain very thin strip with properties and a quality such as to allow it to replace cold rolled strip for certain applications.[10]

The development of the In-line Strip Production process (Arvedi ISP) became an important milestone on the way to an endless thin slab casting and rolling process. It was characterised by the direct connection of continuous casting with the roughing mill, the tunnel furnace replaced by a very short induction heater with the roughing mill linked to the finishing mill by a compact coil furnace (Cremona furnace).[11]

In Figure 7 the layout of an ISP process can be seen.

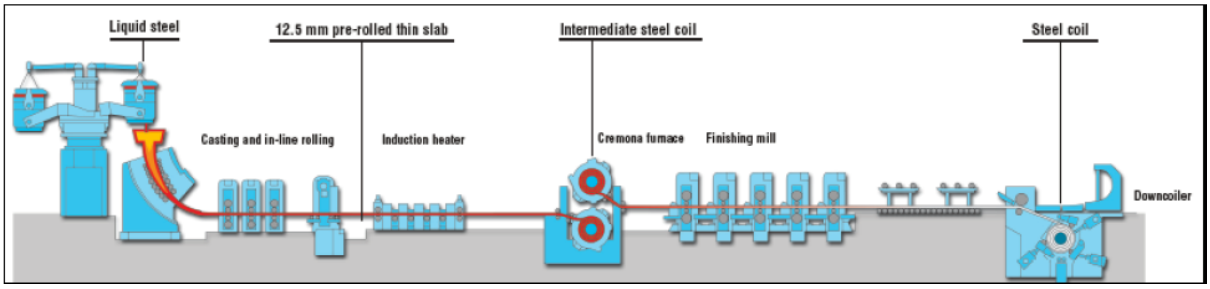

Figure 7. Overview of an Inline Strip Production plant.[10]

In 2006, sales of ISP steel, mainly for the automotive, tube and construction industries, were divided among the following areas of application (see Figure 8).[12]

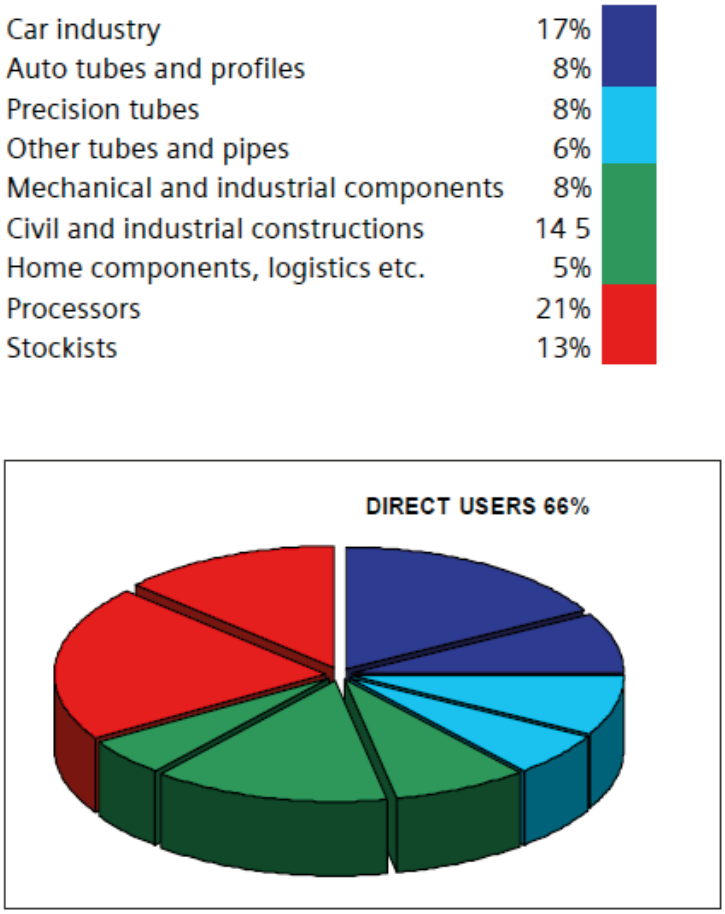

Figure 8. ISP production fields.[12]

Special attention has been paid to caster design features such as casting speeds, slab thickness, dynamic soft reduction strategy and secondary cooling design in order to cope with the demanding product mix.[12]

The main metallurgical challenges can be summarised as follows:

- Good surface quality is essential because API (American Petroleum Institute) grades are crack sensitive;
- In the thin slab casting process no slab conditioning is allowed. This implies that slab surface cracks or depressions must be avoided in the casting practice otherwise slabs will be downgraded;
- No trace of oscillation marks must remain on the surface of the rolled product
- Internal quality must be at highest level;
- Grain size must be minimised for control of toughness;

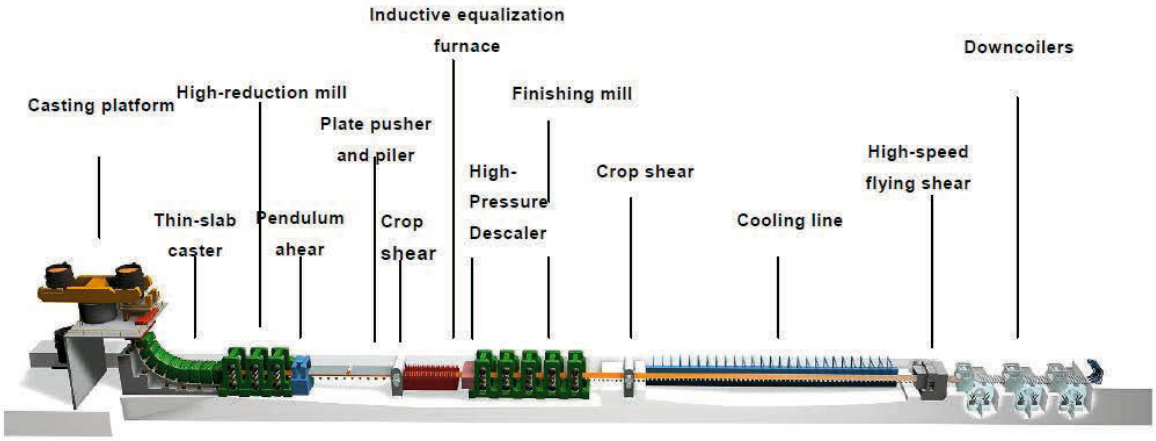

Figure 9. Overview of the endless strip production route.[9]

The ESP line is characterized by

- Fully continuous strip production,
- Outstanding production capacity with a single casting line,
- High volume production of ultra-thin strip,
- High volume production of high quality strip,
- The lowest costs from liquid steel to hot rolled coil,
- The most compact line layout.[12]

ESP allows production of thinner gauges and an expansion of the range of thermos-mechanical steels. Energy consumption is calculated to be about 75% less than that of a conventional process, due to a more complete exploitation of the energy in the liquid steel and less recourse to cold rolling.[12]

The evolution of continuous casting heads for thin slab castings or rather to close to end dimension castings.

The avoidance of cooling to room temperature between casting and starting of reheating before rolling significantly reduced the specific energy consumption. The ESP process has demonstrated stability, high production capacity and has proved to be suitable for producing a wide range of steel grades from low carbon to sour gas resistant line pipe steels.[11]

1.2.1 2 - Port SEN

For conventional slab casting, usually bifurcated SEN is used. The port design is characterized by an upward angle, a horizontal angle or a downward angle. The choice of the SEN port angle is generally determined in accordance with types of steels to be cast and casting conditions.[24]

Downward port angles are preferred over upward port angles because the later promote larger turbulence on the melt meniscus. Moreover, large port dimensions lead to recirculating flows just in the upper edge of the port, leading to backflow conditions and aggravating clogging problems. Most of the SEN designs available in the market observe this characteristic under the reasoning that large ports help to compensate the clogging effects of alumina. Smoothing the angle of the interior upper port edge decreases the clogging and the backflow issues.[25]

Many researchers have observed that the lack of turbulence in the SEN outlet leads to a "straight" jet, and, thereby, lower top-surface velocities. This result shows how important to achieve a precise description of the SEN outlet dynamic behaviour is.[26]

1.2.1.1 2 – Port SEN Rectangular Ports

Calderon – Ramos I. claims that the flow pattern in the mold is determined by the flow dynamics of liquid steel through the nozzle ports and consequently from their specific geometries.[21]

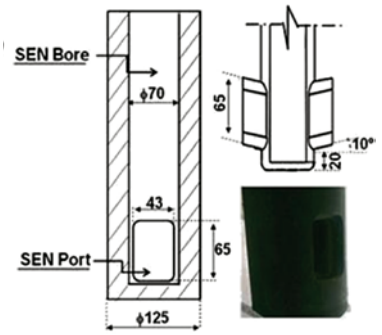

Figure 11. Geometry and size of a 2 - port SEN with rectangular ports.[25]

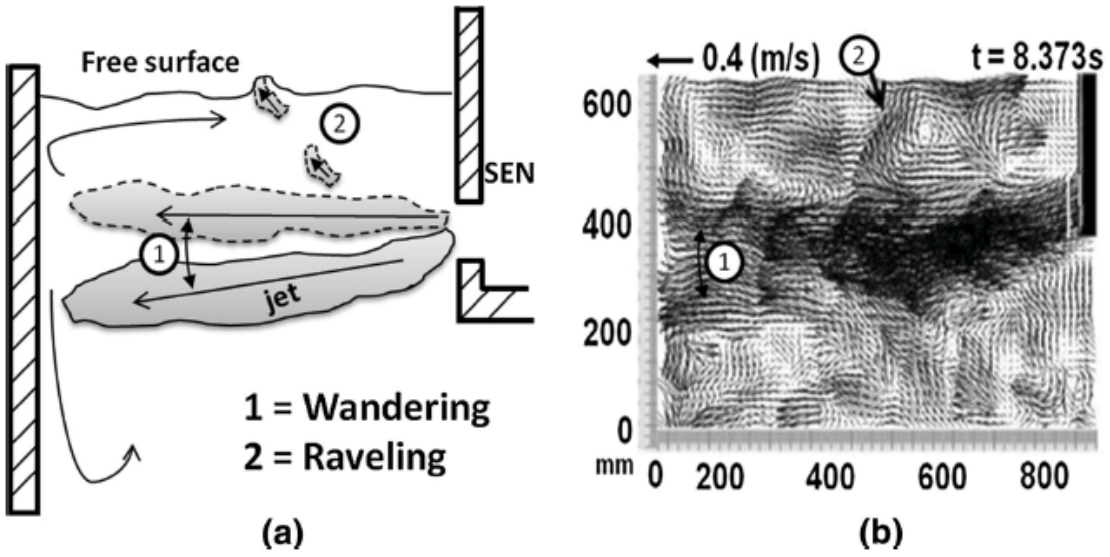

Figure 12. Wandering and raveling phenomena.[25]

The jet is wandering accompanied by its partial disintegration through raveling effects that means, the intermittent separation of fluid streams from the main jet that is directed toward the meniscus. The raveling effects (Figure 12) are indicated by the arrows in Figure 13 (b) through (d). It is also proven by Calderon – Ramos I. that the ravelling effects become more frequent at deeper immersion depth. At some other instants, the jet impacts the narrow wall of the mold with relatively high velocities as is pointed out by the arrow in Figure 13 (a). By using SEN with rectangular ports the flow pattern can described mostly as double roll flow although the meniscus level undergoes large variations. The surface velocities are quite large even when the immersion depth is varying.[25]

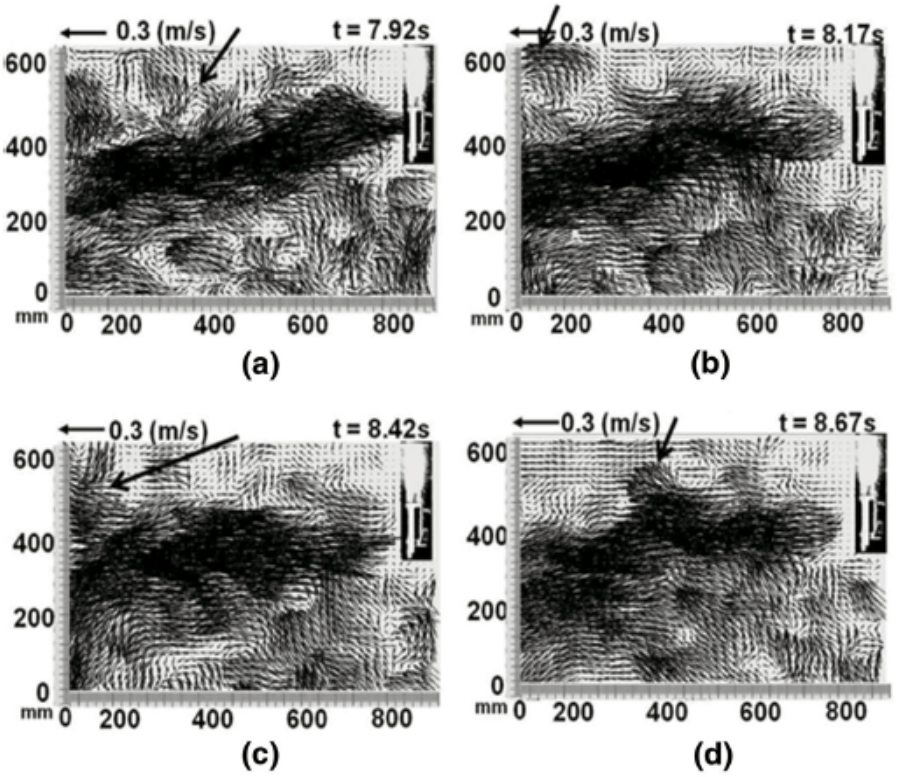

Figure 13. Velocity field using SEN with rectangular ports.[25]

Summarize this facts it is obvious that this SEN causes more turbulent flow in meniscus and submeniscus region.

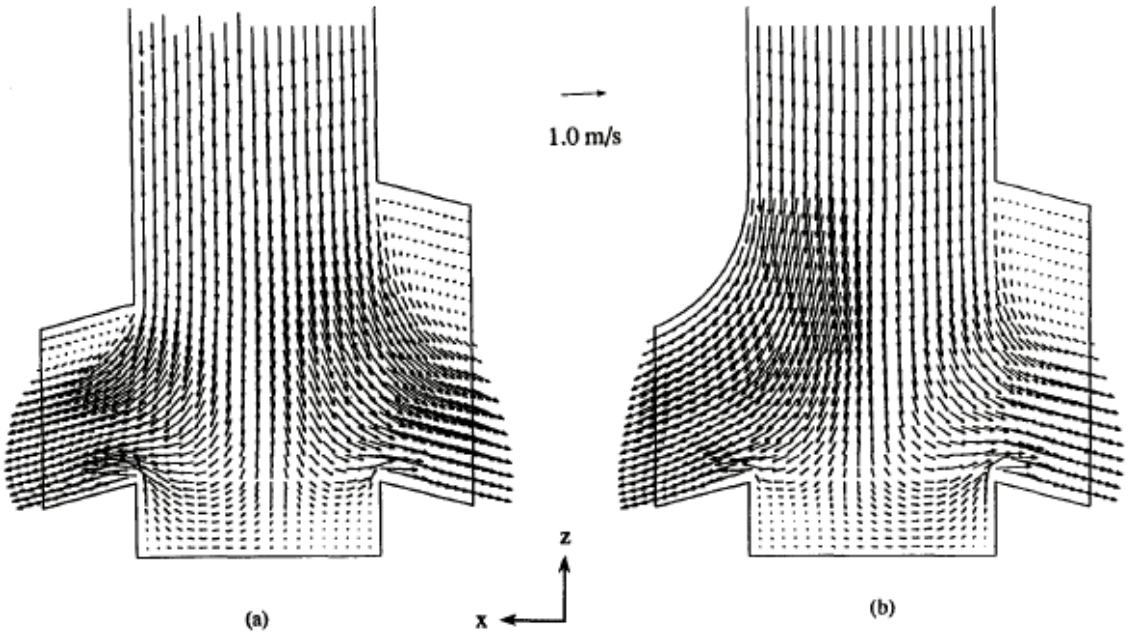

Figure 14. Calculated flow field in the port area with non-uniform port openings: (a) sharp upper corner and (b) curved upper corner.[27]

The angle of the bottom of the port is the most influential variable-controlling jet angle entering the mold, although the jet always leaves at a steeper downward angle than the SEN port angle. The mean jet angle conforms more closely to the port angle when the effective area fraction is large, making the recirculation region at the top of the port smaller. Shorter, thicker, and narrower ports (relative to the nozzle bore area) force the flow to conform more closely to the shape of the port walls. This increases the influence of the port angle, producing shallower jet angles, higher velocities, smaller spread angles, increased turbulence intensity, less swirling flow, and higher effective area fractions. Port curvature promotes a smoother transition from the nozzle tube to the port regions, which consequently increases the effective area fraction and reduces both the peak velocities and the detrimental recirculation zone. A recirculation zone appears at the top of the port (effective area fraction less than 1), unless the combined area of both ports is smaller than the bore area or the port edges are curved. Casting speed increases only the jet speed and the turbulence levels; it does not affect the jet angle or any other characteristic of the jet.[27]

The standard 2 port SEN made by RHI AG can be seen in Figure 15 (a).Depending on the operation conditions, significant mold level fluctuations can be induced by the mold fluid flow behaviour (Figure 15 (b) and (c)).There is no exact color scale but the red color indicates

highest casting speed and the blue color the lowest. These instabilities, in conjunction with the related high shear stresses developed at the liquid steel/mold powder interface, are the main reason for mold flux entrainment into the solidified shell.[24]

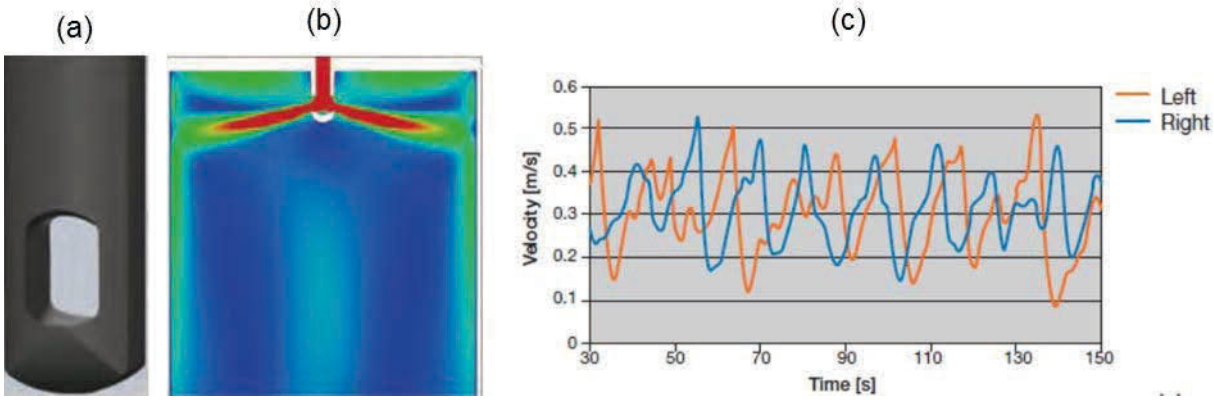

Figure 15. Sketch of the standard 2 port SEN made by RHI and a snapshot of the velocity distribution and the history of the submeniscus velocity for the standard design.[24]

In order to decrease the surface velocity, a modification was implemented at the port area of a standard SEN design as shown in Figure 15 (a). The modified SEN (Figure 16 (a)) comprises a groove in the SEN port bottom. This groove has a remarkable effect on the behaviour of the jet, leading to a far stable mold flow (Figure 16 (b) and (c)). This measure is recommended for a high throughput to keep the meniscus level stable.[24]

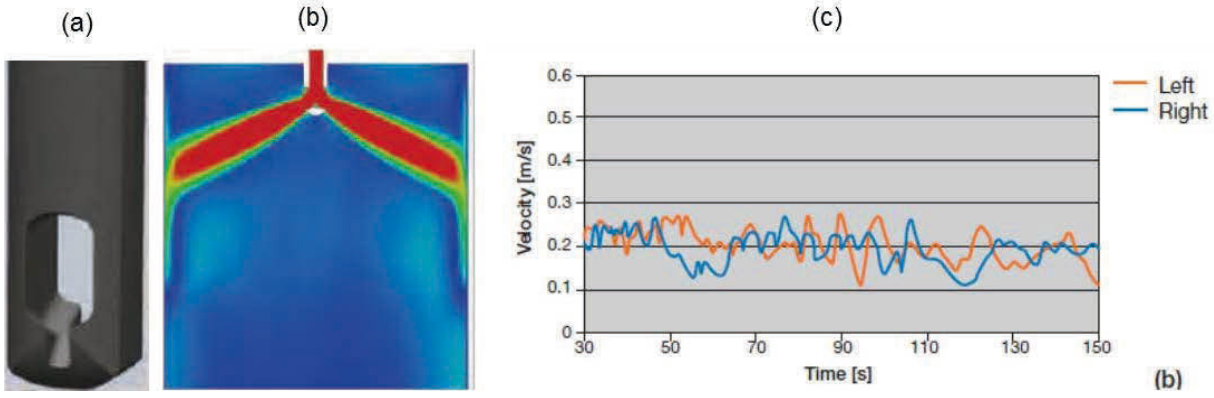

Figure 16. Sketch of the modified 2 port SEN made by RHI and a snapshot of the velocity distribution and the history of the submeniscus velocity for the modified design.[24]

Another modification of the standard 2 Port SEN design was investigated by Yuichi Tsukaguchi et al. (Figure 17). The generation of swirling flow in a submerged entry nozzle is a fundamental way to stabilize flow in a continuous casting mold. The swirling-flow submerged entry nozzle can improve the surface quality of slabs and steel coils and increase the casting speed by increasing flow stability in the mold.[28]

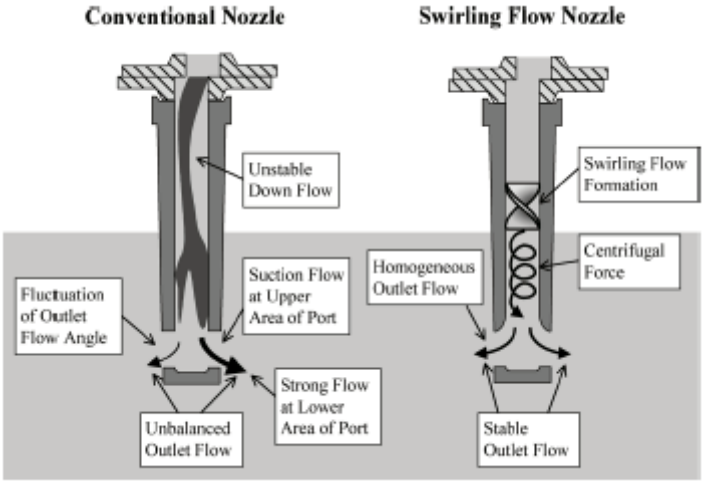

Figure 17. Schematic view of flow formation in nozzle.[28]

A third modification was investigated by Brunnmayer et al. Previous simulation work described a stabilisation effect of an additional hole with non-satisfying single roll flow at enormous wave heights. An improvement of the side port flow condition could be attained by eliminating the recirculation zone near these ports (Figure 18).[29]

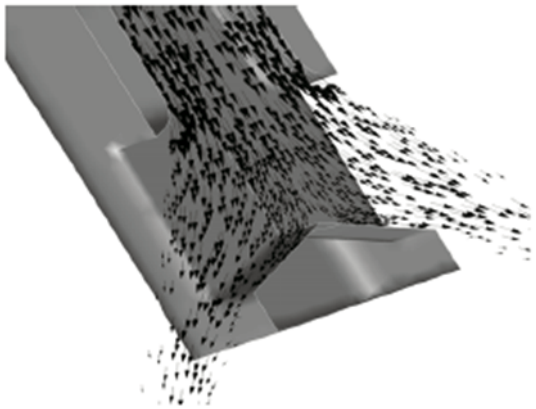

Figure 18. Optimized bifurcated SEN.[30]

Contours of velocity magnitudes and temperature (Figure 19 (a) and (b)) show a quasi-steady side port jet moving towards the narrow side of the mold and generating double roll flow pattern with a large upper recirculation.[29]

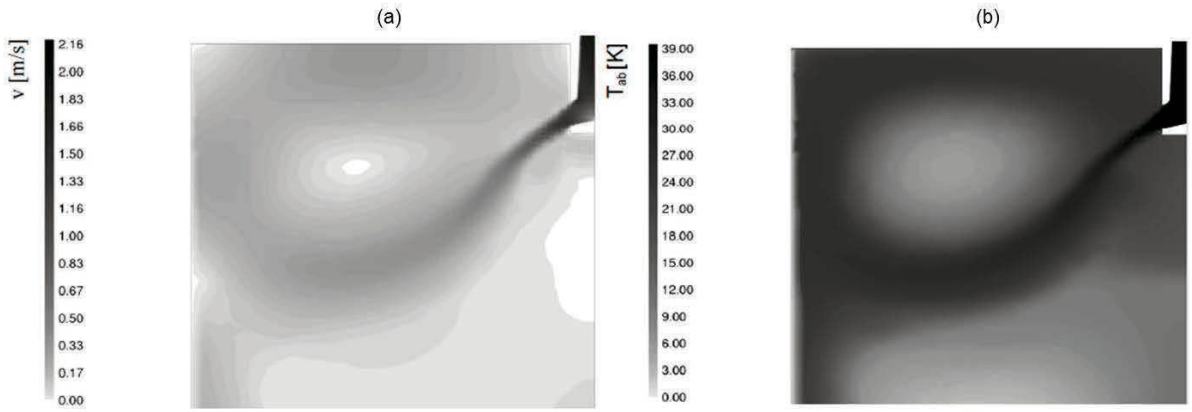

Figure 19. Velocity and temperature contours of the optimized SEN.[29]

A higher and more homogenous temperature distribution at the meniscus and a reduction of the wave heights to approximately a third compared to other 2- or 3- port SEN can be achieved. This seems to be good operation conditions for high quality slabs.[29]

1.2.1.2 2 – Port SEN Square Ports

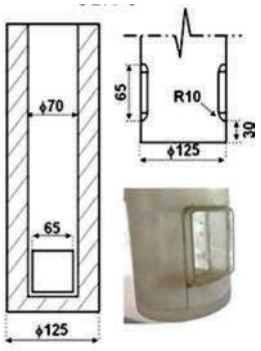

Figure 20. Geometry and size of a 2 - port SEN with square ports.[25]

By using the SEN with square ports at a shallow position (e.g.: 115 mm) the flow pattern can be described as single roll flow. The raveling effects using SEN with square ports are also more frequent compared to SEN with rectangular ports as is shown by the arrows in Figure 21 if it is used at deeper position (e.g.: 185 mm).[25]

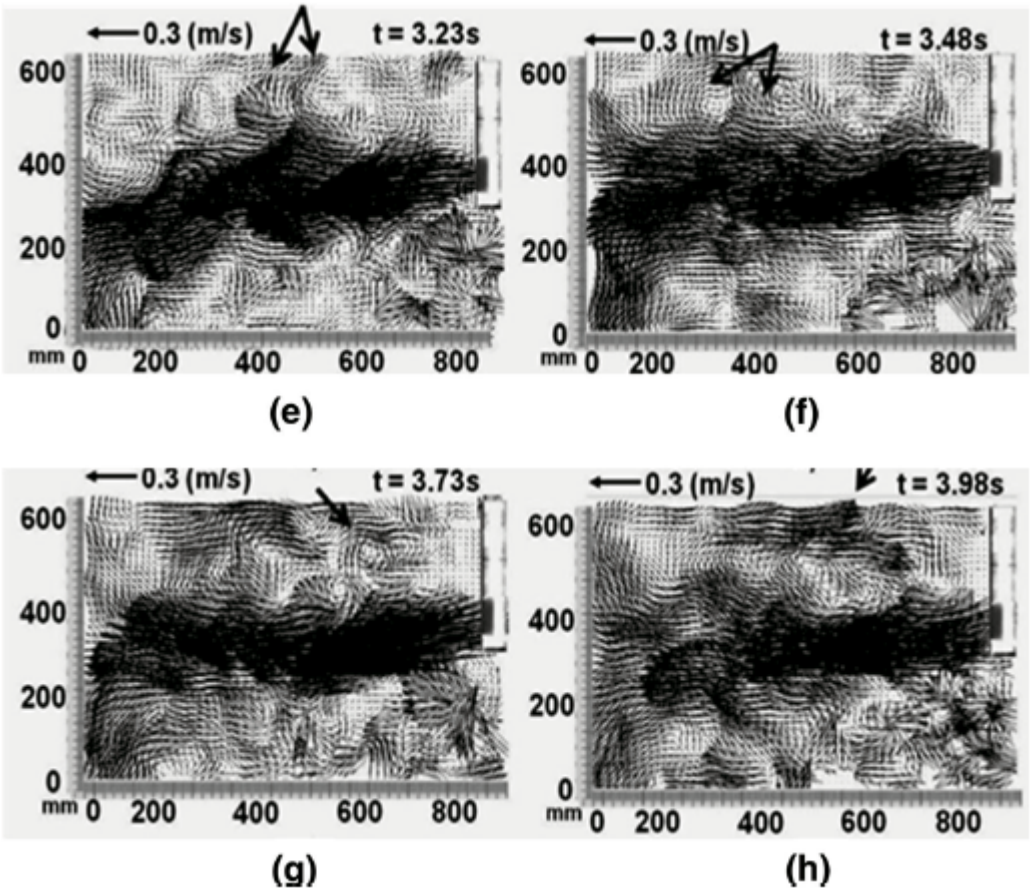

Figure 21. Velocity fields by using SEN with square ports.[25]

The SEN with rectangular ports yields larger meniscus velocities in the deep position than in the shallow position. SEN with square ports yields opposite effects. The discharging jets using either nozzle suffer effects of strong wandering and raveling effects with detached streams that enhance turbulence in the meniscus and submeniscus regions. When a detaching flow from the jet meets another originated by the impact with the mold, narrow wall turbulence is particularly intensified. These effects are more severe using SEN with rectangular ports. It is also shown that independent from immersion depth the SEN with square port show smaller velocity peaks. That is why SEN with square ports is recommended over SEN with rectangular ports for casting operations.[25]

1.2.1.3 2 – Port SEN Round Ports

It was found that rectangular port geometry works better than the typical cylindrical port.[30] SEN with round ports (Figure 22) generate more swirls and have a larger spread angle than rectangular ones having the same cross-section area.[25]

The delivered liquid presents less dispersion comparing to the SEN with cylindrical port designs which reduces the appearance of a backflow.[30]

Real C. did some numerical simulations with a bifurcated SEN with 2 round ports with a downwards angle of 15 degrees because this kind of SEN is in industry widespread. The black dots in Figure 22 indicate measuring points for the velocity inside the SEN. It was proved that using the LES (large eddy simulation) turbulence model it is possible to reproduce periodic behaviors observed in plant. It was observed that the periodic behaviour is a consequence of the dynamic interaction between the fluid at the SEN pool and the fluid immediately above it. Additionally, it was found that the characteristics of the periodic behavior depend at least on the casting speed.[26]

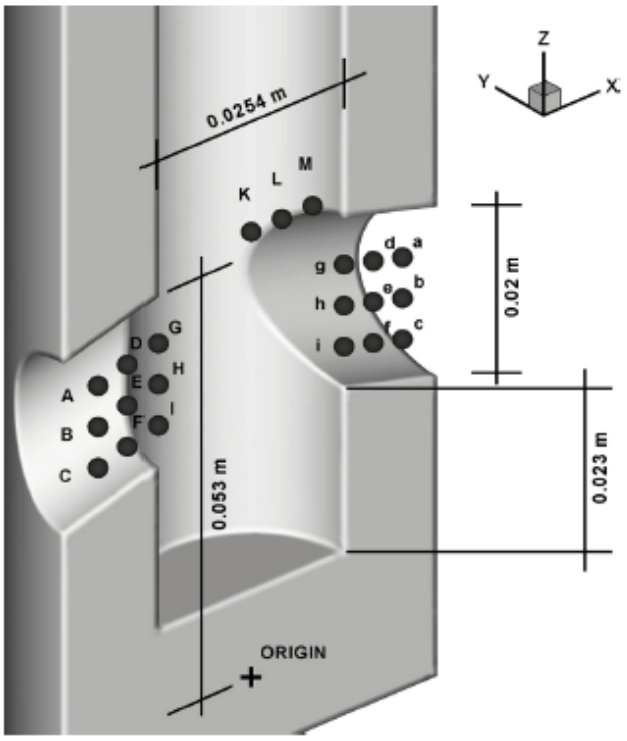

Figure 22. 2 Port SEN design with round ports and a recessed bottom.[26]

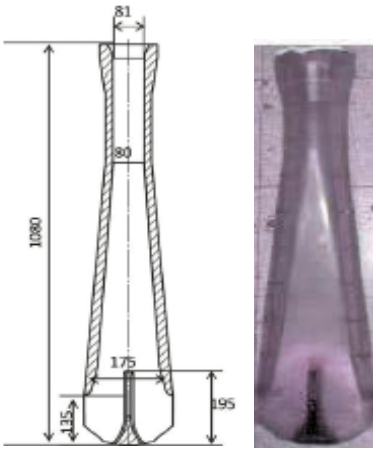

Figure 24. 2 - Port SEN Design 1.[17,18]

With the design shown in Figure 24 an upper flow without generating an active lower roll flow can be achieved and creates a stagnant large zone below the nozzle, which has a negative effect according to the casting operation (Figure 25). A change in immersion depth influences the flow pattern easily. The stagnant zone below the nozzle is decreasing. The shown results represent a casting speed of 7.5 m/min and two different immersion depths (220 mm and 350 mm).[17]

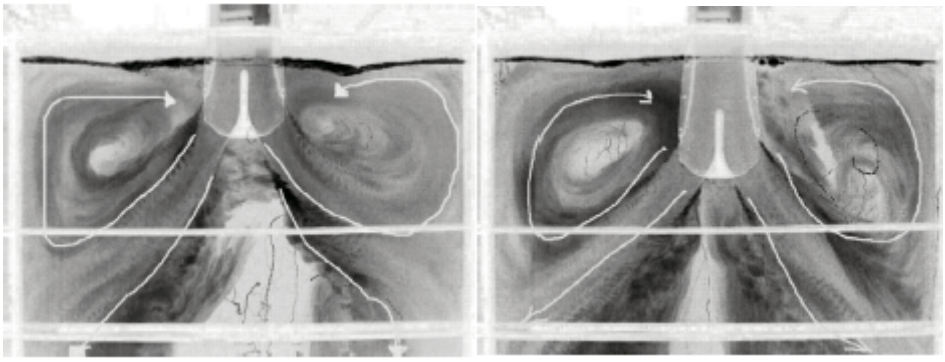

Figure 25. Flow pattern in the mold at immersion depth 220 mm and 350 mm at a casting speed of 7.5 m/min.[18]

The meniscus analysis shows heavy depressions at the positon of the funnel, including the formation of vortices (Figure 26 (a)). Figure 26 (b) shows the history of instantaneous velocity of the submeniscus velocity. The positon of the monitoring spot can be seen in Figure 27.

This positon was chosen because it is just the transition zone between the straight parallel wide molds and the funnel where the flow is more instable.[18]

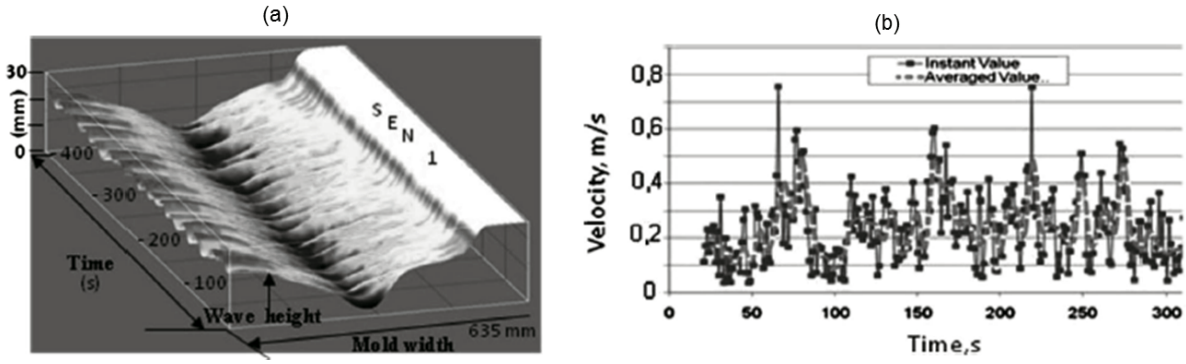

Figure 26. Wave fluctuation topography from water modelling at an immersion depth of 220 mm with analysis of the submeniscus velocity.[18]

This 2 – port SEN creates very high instantaneous velocities. This conveys a high probability for flux entrainment under these casting conditions.[18]

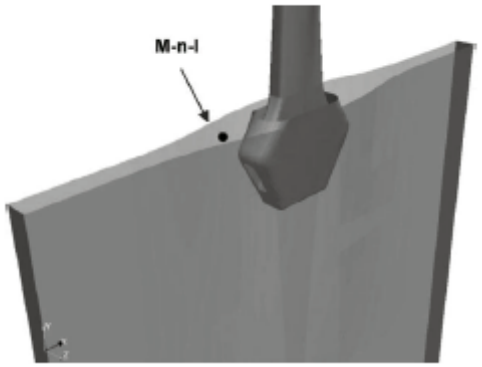

Figure 27. Position of the monitoring spot.[18]

1.2.1.5 2 – Port SEN Design 2

Compared to the nozzle design shown in Figure 24 similar results can be achieved with the 2 – Port SEN Design 2 (Figure 28).

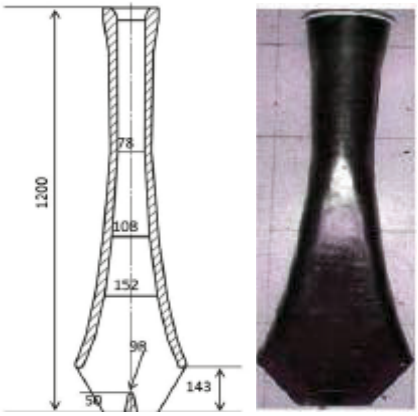

Figure 28. 2 - Port SEN Design 2. [17,18]

It also induces a strong single upper roll flow but without a stagnant zone below the nozzle bottom (Figure 29). The presence of severe meniscus depressions remains, thus indicating instability at the position of the funnel. By changing the immersion depth the flow pattern is changing complete. Stagnant zones exist in the corner of the mold due to non-symmetric mixing behaviour.[18]

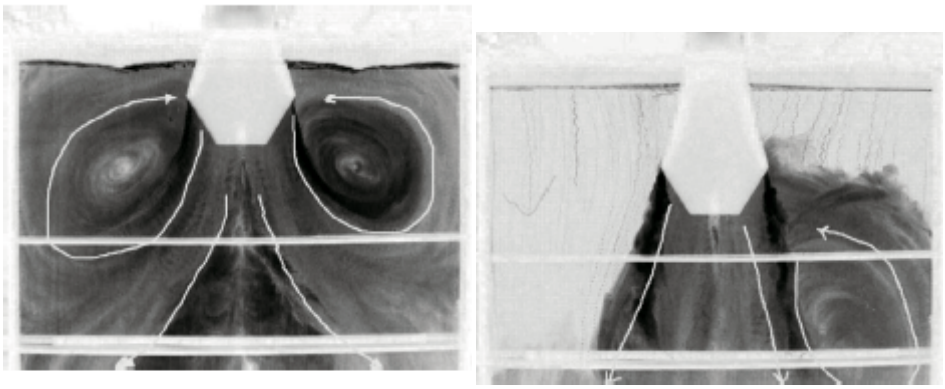

Figure 29. Flow pattern in the mold at immeriosn depth 220 mm and 350 mm at a casting speed of 7.5 m/min.[18]

The position of the monitoring spot can be seen in Figure 27. As Figure 30 shows similar results to the other 2 – port SEN with lower variations in velocity can be achieved.

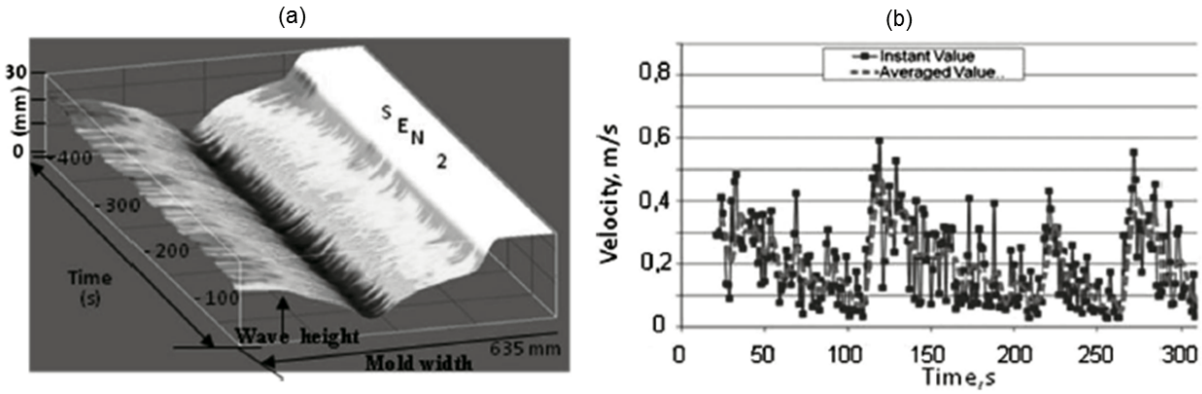

Figure 30.Wave fluctuation topography from water modelling at an immersion depth of 220 mm with analysis of the submeniscus velocity.[18]

1.2.2 4 - Port SEN

A four-port, funnel-shaped SEN produces shallower jet angles, lower peak velocities, and a greater effective area fraction, as compared with the standard bifurcated nozzle.[27]

1.2.2.1 4 - Port SEN Design 1

The 4 – port SEN shown in Figure 31 is designed to achieve turbulence control and meniscus stability by highly symmetric flow and a vortex free bath surface. This design is based on the theoretical aspects of boundary layer and aerodynamics principles applied to steel flow through the SEN.[17]

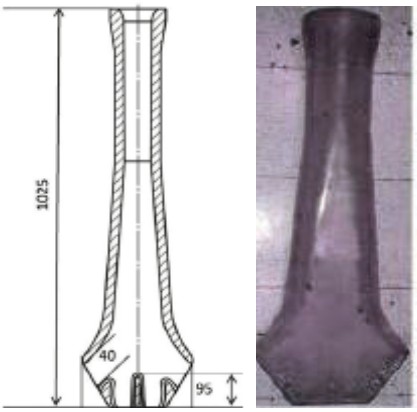

Figure 31. 4 Port SEN. [17,18]

In water model experiments done by Morales et al. can be seen that by using this 4 port SEN designs no stagnant zones and a double roll flow pattern can be achieved (Figure 32). This flow pattern is independent from the immersion depth. This 4 - port SEN maintains a stable meniscus without the formation of strong vortices or depressions.[17,18]

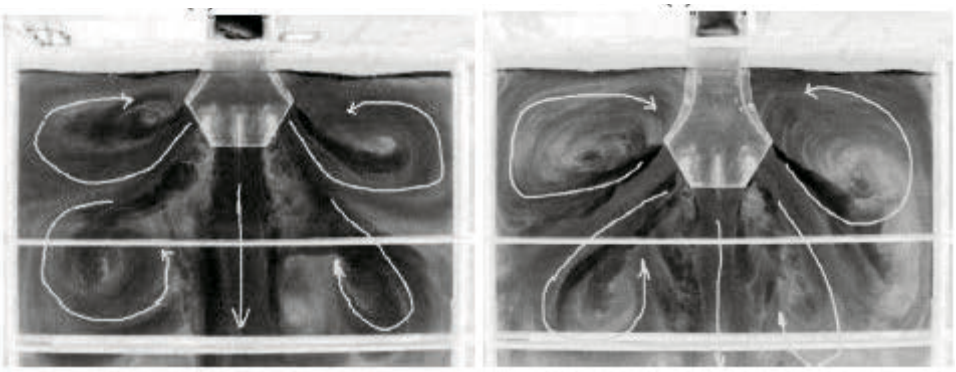

Figure 32. Average flow pattern at different immersion depth.[18]

This 4 – port design shows more stable meniscus Figure 33 (a) and creates compared to the two 2 – port SEN lower and constant velocities (Figure 33 (b)).[18] This results in stable bath topography.

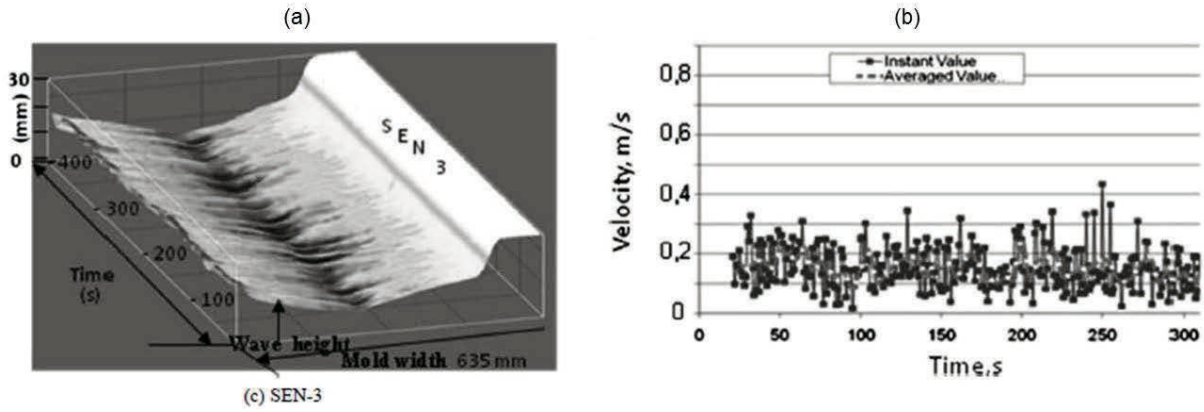

Figure 33.Wave fluctuation topography from water modelling at a immersion depth of 220 mm with analysis of the submeniscus velocity.[18]

1.2.2.2 4 - Port SEN Design 2

Simulations work with the 4 Port SEN design (Figure 34) was done by M.H. Zarea in cooperation with Saba Steel Iran.[31]

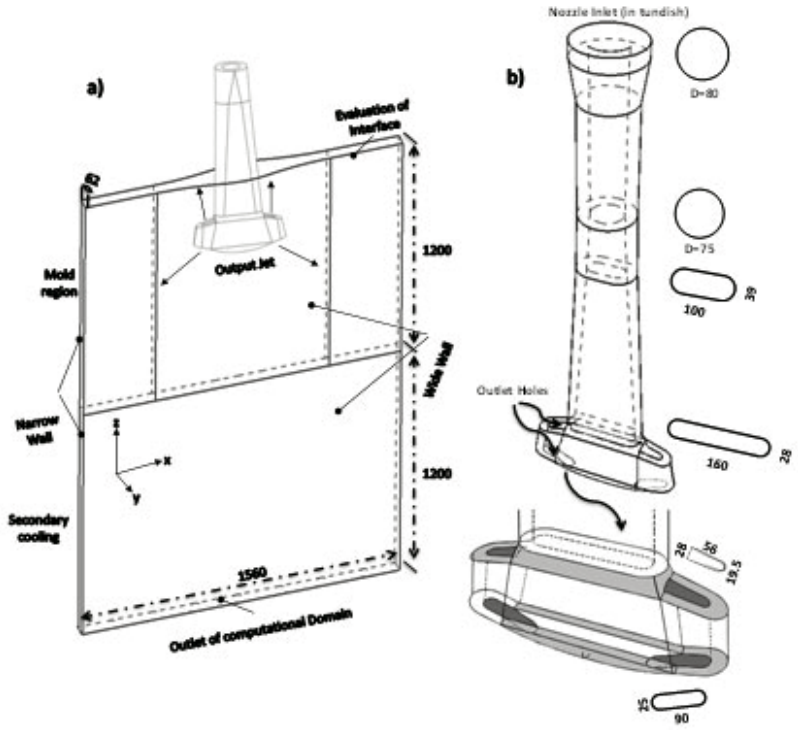

Figure 34. 4 - Port SEN designed by Saba steel company.[32]

In Figure 35 a 3D flow field at a casting speed of 3.4 m/min and an immersion depth of 300 mm can be seen. Based on the simulations about 14-17% of the input melt goes out from the upper ports which is preventing solidification of the steel on the top surface especially at the peripheral parts of the nozzles and moving part of the impurities to the free surface.[31]

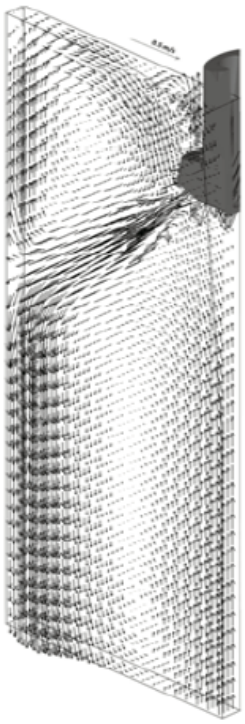

Figure 35. 3D liquid flow field pattern.[29]

The top recirculation zone is formed by the steel that reaches the narrow wall of the mold and then flows towards the steel/slag interface. The outlet flow from the lower port of nozzles touches the mold walls while it still intends to go down the mold and creates the lower recirculation zone.[31]

The results of the heat distribution of the liquid in the mold can be seen in Figure 36. The flow from the lower holes hits to the thin walls and forms lower and upper rings. In the centre of the mold the liquid temperature is lower because of low fluid flow velocity and lower super heat dissipation in this region. The melt flow at the top surface of the mold has enough super heat for avoiding freezing.[31]

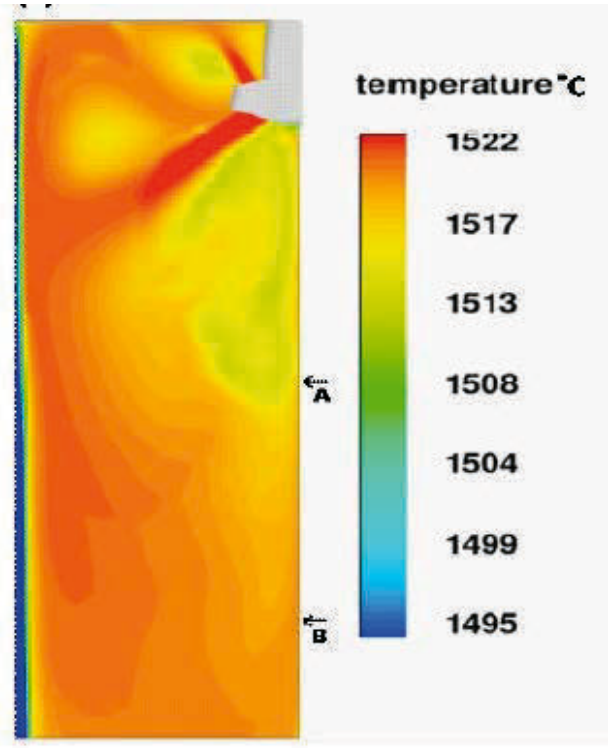

Figure 36. Heat distribution inside the mold (casting speed 3.5 m/min, immersion depth 300 mm).[31]

1.2.3 5 – Port SEN

Experiments and analysis with a 5 Port SEN design (Figure 37) was performed by Young Jin Jeon et al.[29]

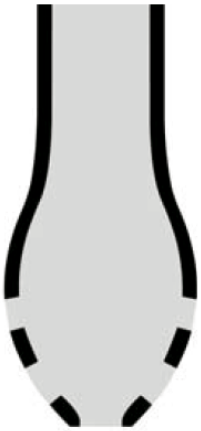

Figure 37. Sketch of a 5 Port SEN.[33]

For this investigation a casting speed of 6.17 m/min and the maximum flow rate U = 50 m³/h are selected. High flow rates generate recirculation flows with high velocity gradients. In Figure 38 the velocity distribution of three different flow rates can be seen. This 5 – port nozzle shows a complex flow pattern because of the five exits. The flow pattern seems to be similar independent from the flow rates. The lower vortex flow may be generated by the periodic meniscus flows. The vortex pairs appear between the SEN and the funnel and are generated by the crush and the rolling of the cross-flow. The formation of these vortices is affected by the meniscus velocity as well as the velocity in the vicinity of the meniscus. As the number of recirculation regions increases, the quantity of the flow that influences the meniscus is reduced. As a result, the inner and meniscus flows are stabilized.[33]

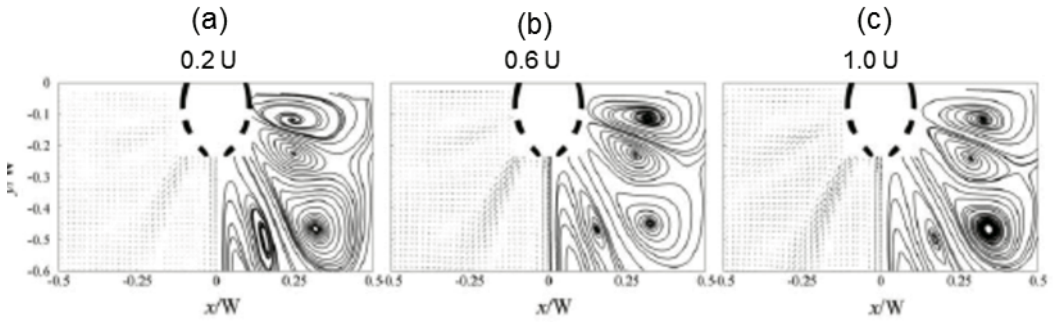

Figure 38. Mean velocity vectors and streamlines.[33]

Only a few publications have validated their mathematical simulations with experimental measurements of speed and flow pattern/behaviour in the mold and unfortunately this situation leaves the unanswered question: what characteristics of a SEN should be considered as the right ones for a specific task. As mentioned before there are many factors which influences the flow pattern and behaviour and that is why further studies have to be done for a better understanding of the whole process inside the mold. The latest development of the 4 – port and 5 – port SEN show good results during the casting process in thin slab castings to achieve goals like higher casting speed, good mixing behaviour, sufficient heat distribution and a stable meniscus topography.

(SEN) can be moved to any position to simulate any immersion depth (E) of the SEN. (see Figure 39). The immersion depth is defined from the meniscus to the upper edge of the port. The scale of the model is 1:2 to real size of thin slab casting.

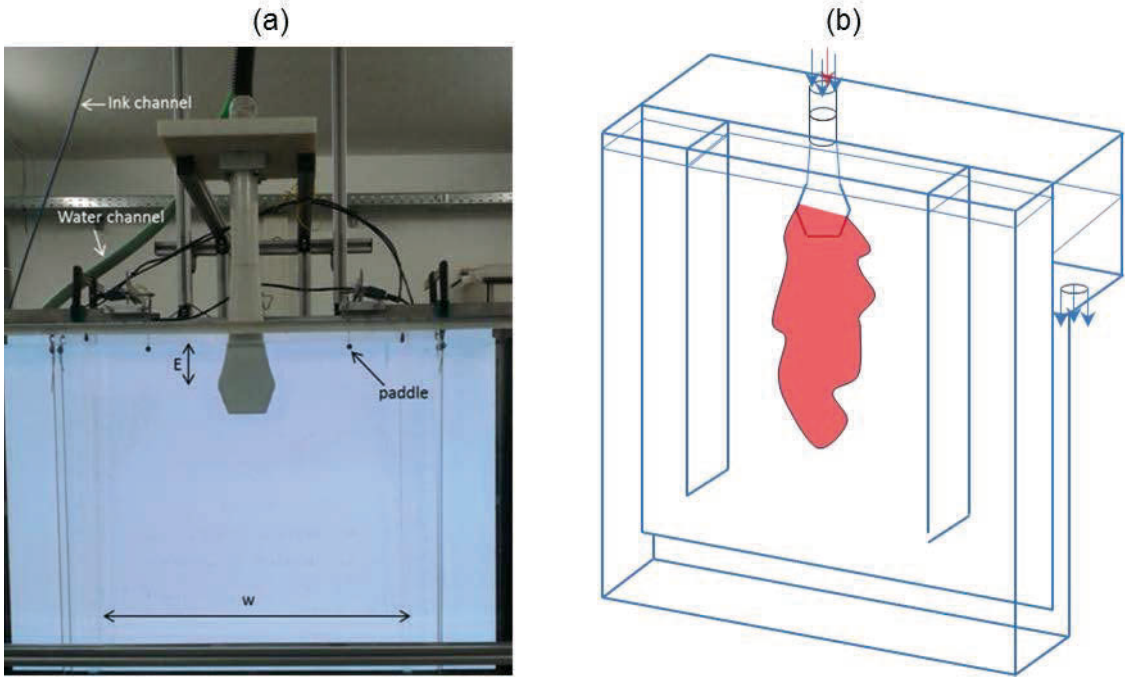

Figure 39. (a) water model set up (b) water model sketch.

Different UFM - single port SEN designs were produced by a 3D – printer at the RHI which should produce the flow pattern of a multi-port SEN design. The designs of the SEN with 6 mm gap and 18 mm can be seen in Figure 40.

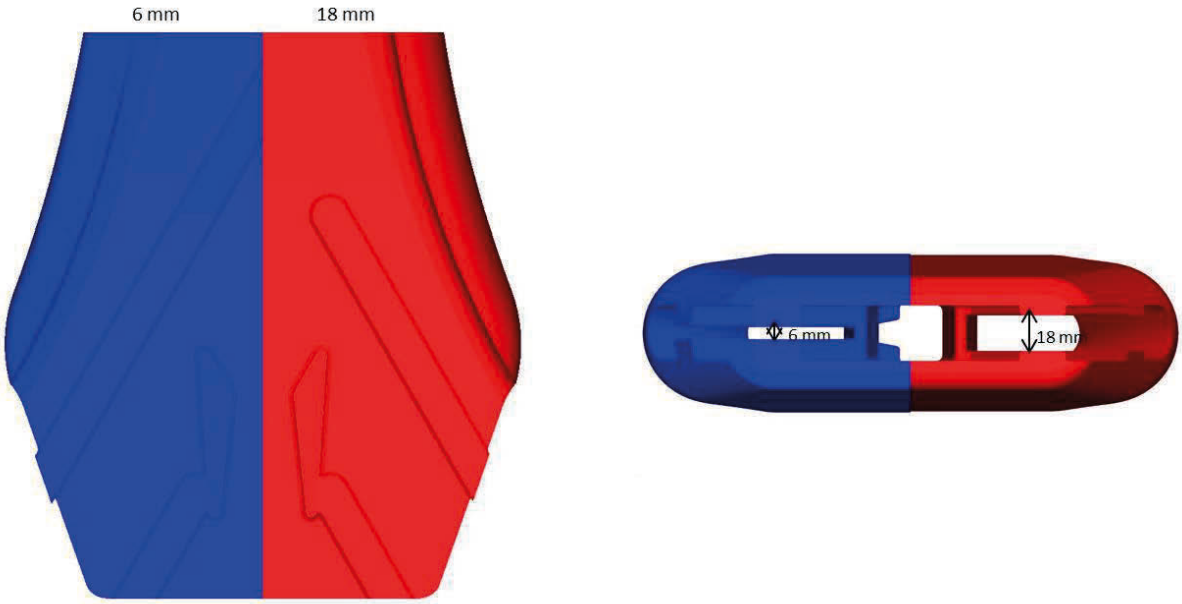

Figure 40. The UFM - single port SEN design with 6 mm (blue) and 18 mm (red) gap.

The water flow rate can be controlled automatically or by hand. To keep the water level constant there is an outlet on the back of the apparatus.

A separate dye or ink channel which is connected to the water channel is also present. The dye injection gives a good representation of the mixing behaviour. The experimental team of the RHI decided to use dye to make the jet flow visible instead of using particles. By using particles a few problems occur. First of all it is difficult to find a material which has almost the same density as water because if the particles are lighter than water the particles are trying to flow upwards or decrease the jet velocity. By using heavier particles the opposite effect appears. Another disadvantage of using small spherical particles is getting a sufficient amount of the particles into the channel to make the jet visible for a qualitative analysis possible. Using dye injection is the easiest way to make the jet and the flow pattern during the experiment visible.

The paddles on the left and right sight of the SEN which are positioned about 10 mm under the water surface measure the submeniscus velocity of the flow. This velocity is measured for duration of 30 min with a time step of 0.1 seconds. This is done to have enough data to analyse the submeniscus velocity and to be sure that the flow is stable before starting dye injection.

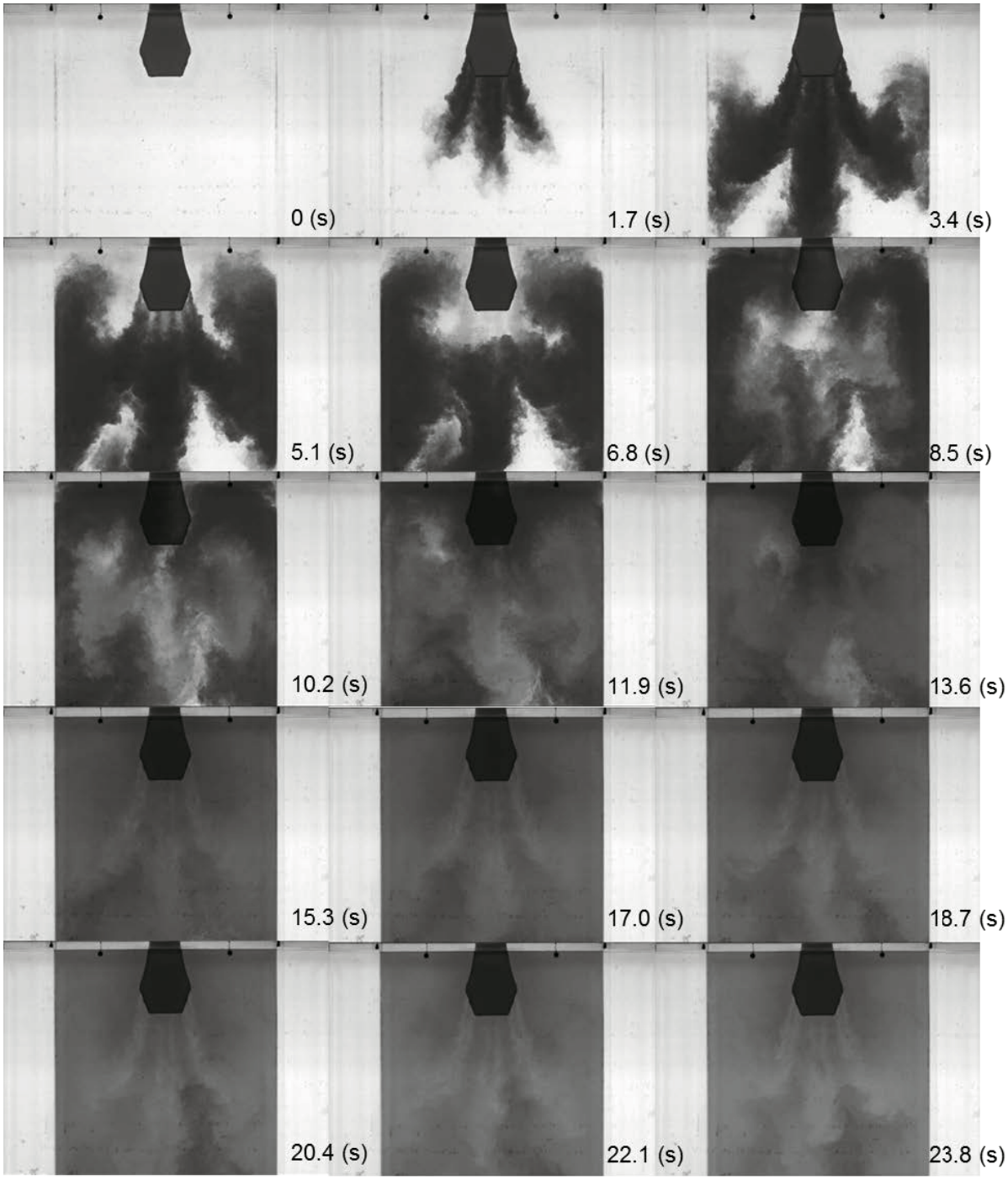

Figure 41. Example of flow pattern in the mold of case 1 (Table 1) with the SEN gap 12 mm. These snapshots are taken in a constant time interval of 1.7 (s).

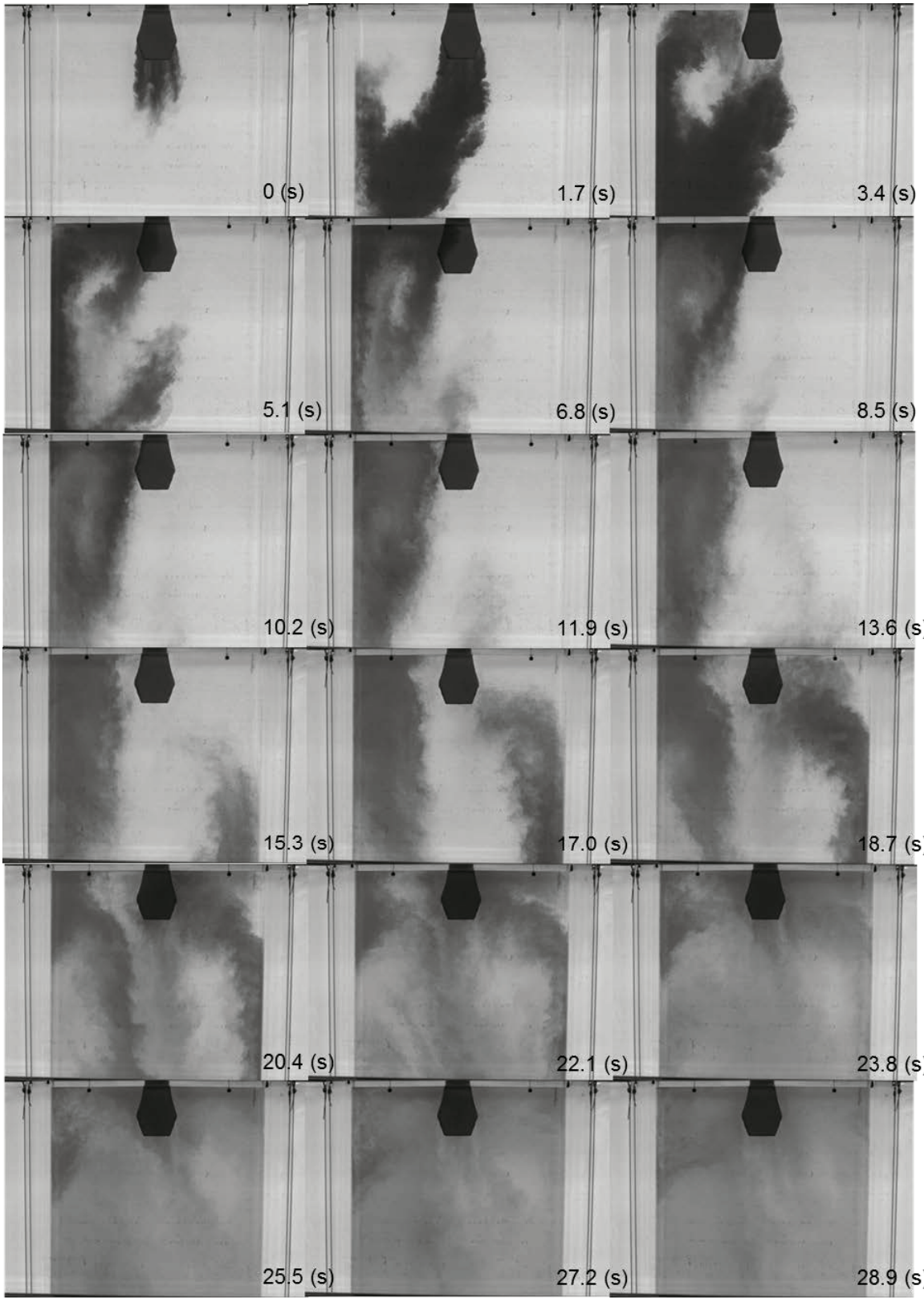

Figure 42. Example of the flow pattern in the mold of case 2c (Table 1) with the SEN gap 18 mm. These snapshots are taken in a constant time interval of 1.7 (s).

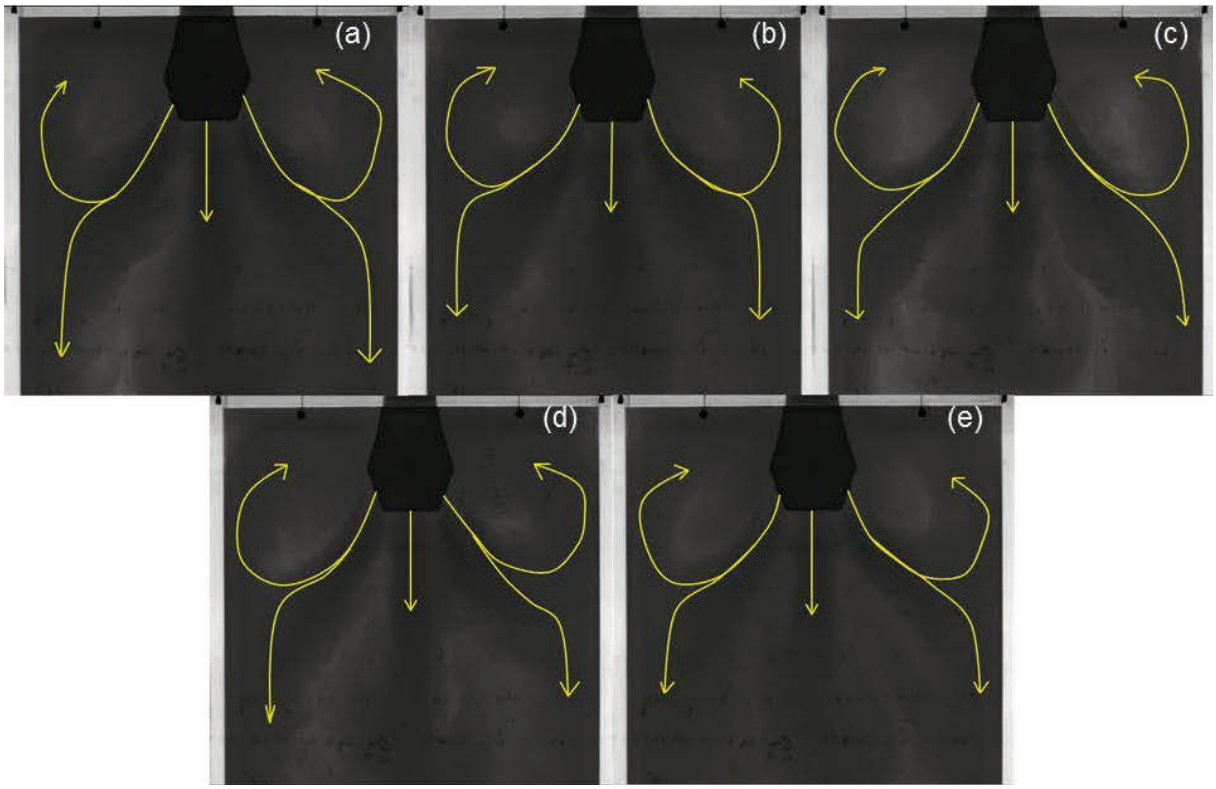

Figure 43. Results of case 1 for the SEN gap size 6 mm (a) – (e) (Run 1-5).

Insignificant differences may be seen in the size or shape of the vortexes on the left and right side. During the experiment the water was lead to every section in the mold which is also one aim during the casting process in the plant.

3.1.2 Case 1 SEN Gap Size 8 mm:

In Figure 44 all five runs of case 1 for the SEN gap size of 8 mm can be seen. The flow pattern is stable. There is a vortex development on the top of the mold. The dye is transported to ground. Slightly differences can be seen in the shape and size of the upstreaming vortexes on the left and right side of the SEN. The size and shape of the upper vortexes influences also the jets which stream in the direction of the wall and downwards. That is the reason why small differences in the flow pattern can be seen.

The metallurgical function of this SEN design to transport new material in all sections of the mold is fulfilled

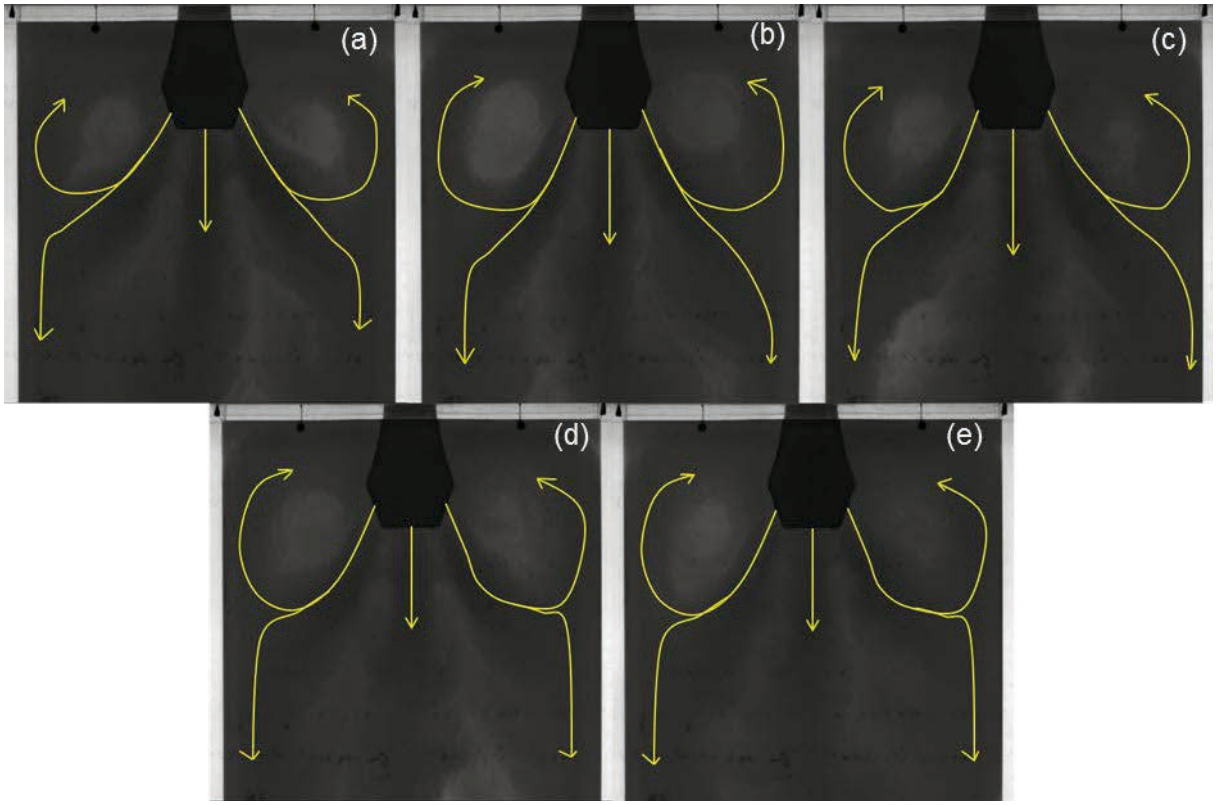

Figure 44. Results of case 1 for the SEN gap size 8 mm (a) – (e) (Run 1-5).

3.1.3 Case 1 SEN Gap Size 10 mm:

In Figure 45 all five runs of case 1 for the SEN gap size of 10 mm can be seen. This scenario describes a stable flow situation. As seen in the trials before there are small differences in the size and shape of the jets and vortexes. In Figure 45 (e), the fifth run, it is evident that during the experiment less dye was transported to the upper left corner than to the right one. In that case the down streaming jet starts oscillating compare to the different runs. A reason for the change of direction of the down streaming jet can be caused by the backflow from the bottom of the mold.

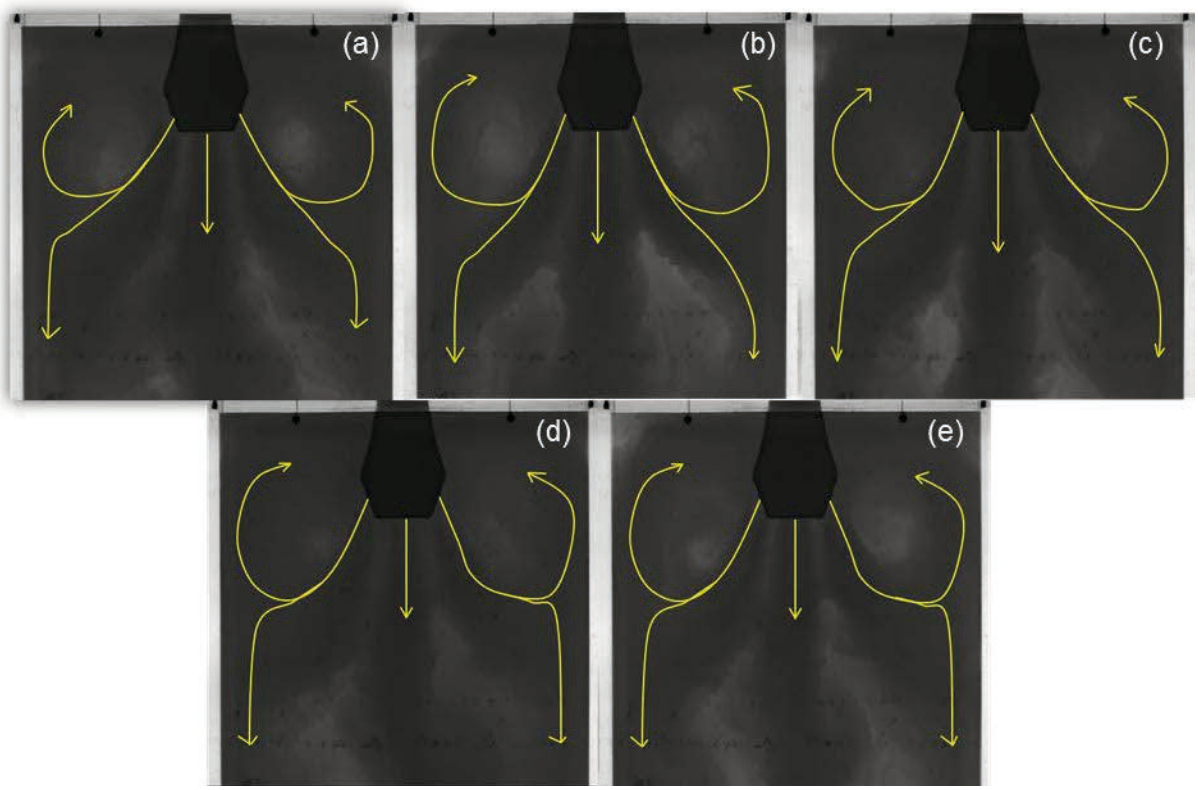

Figure 45. Results of case 1 for the SEN gap size 10 mm (a) – (e) (Run 1-5).

3.1.4 Case 1 SEN Gap Size 12 mm:

In Figure 46 the results of all 5 runs of the case 1 for the SEN with the 12 mm gap can be seen. The results shows similar flow pattern compared to the previous ones. The dye is transported to all sections of the mold. Some differences in the shape and size of the vortexes and jets between the several runs can be seen.

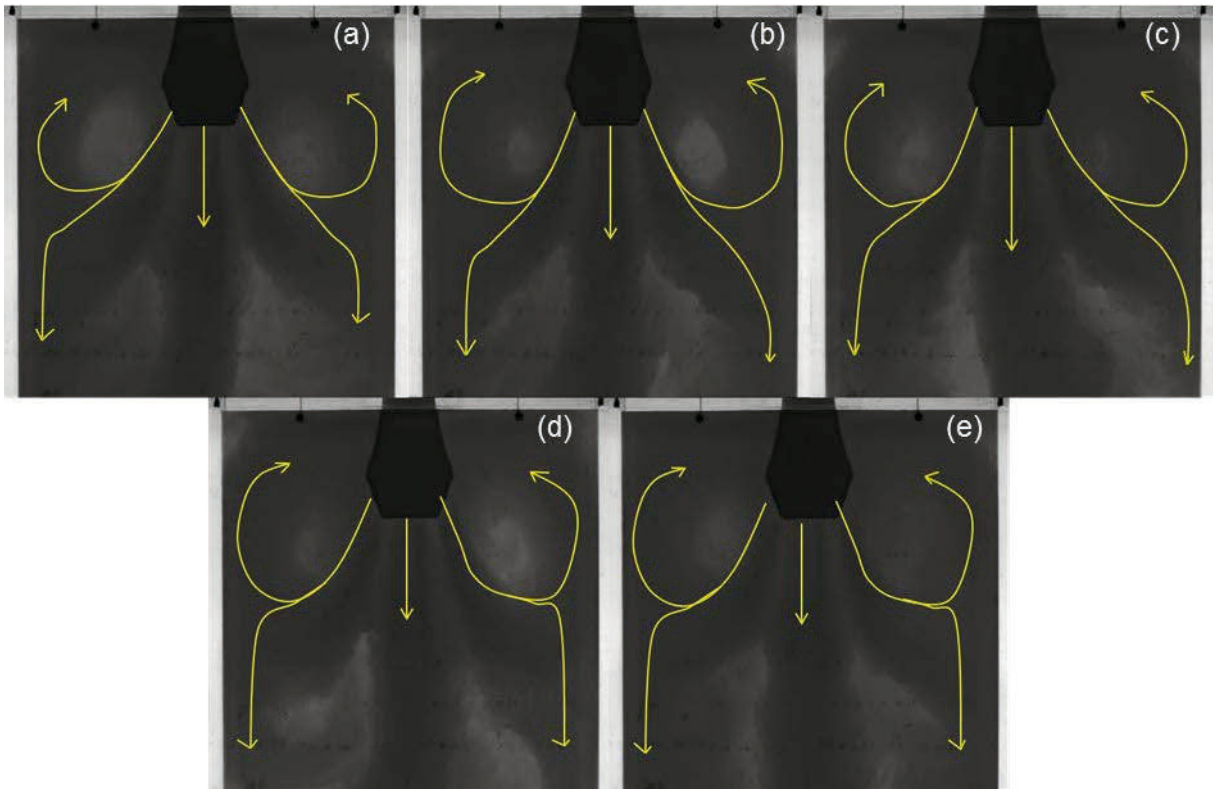

Figure 46. Results of case 1 for the SEN gap size 12 mm (a) – (e) (Run 1-5).

3.1.5 Case 2c SEN Gap Size 6 mm:

Case 2 is divided into three different parts/settings. The mold design and the SEN gap (18 mm) are always the same. The casting speed was varied. The different casting speeds are 2 m/min (Case 2a), 2.4 m/min (Case 2b) and 3.4 m/min (Case 2c). Case 2c is also done with all other SEN gap sizes. For case 2c a new SEN model with 15 mm gap size was produced.

Case 2c is defined by a mold width of 1400 mm times 112.5 mm and a casting speed of 3.4 m/min. In that case the SEN with the gaps of 6, 8, 10, 12, 15 and 18 mm are used. Every trial was is repeated five times.

In Figure 47 all five runs for case 2c with the same settings can be seen. The flow pattern in all five runs is same over the whole recording time of 30 seconds. In every image the jet which goes straight downwards can be recognized. Also the development of the vortex on the left and right top corner is clearly seen. From both side ports a current which flows diagonal downwards can be observed. In every part of the observed area dye is transported.

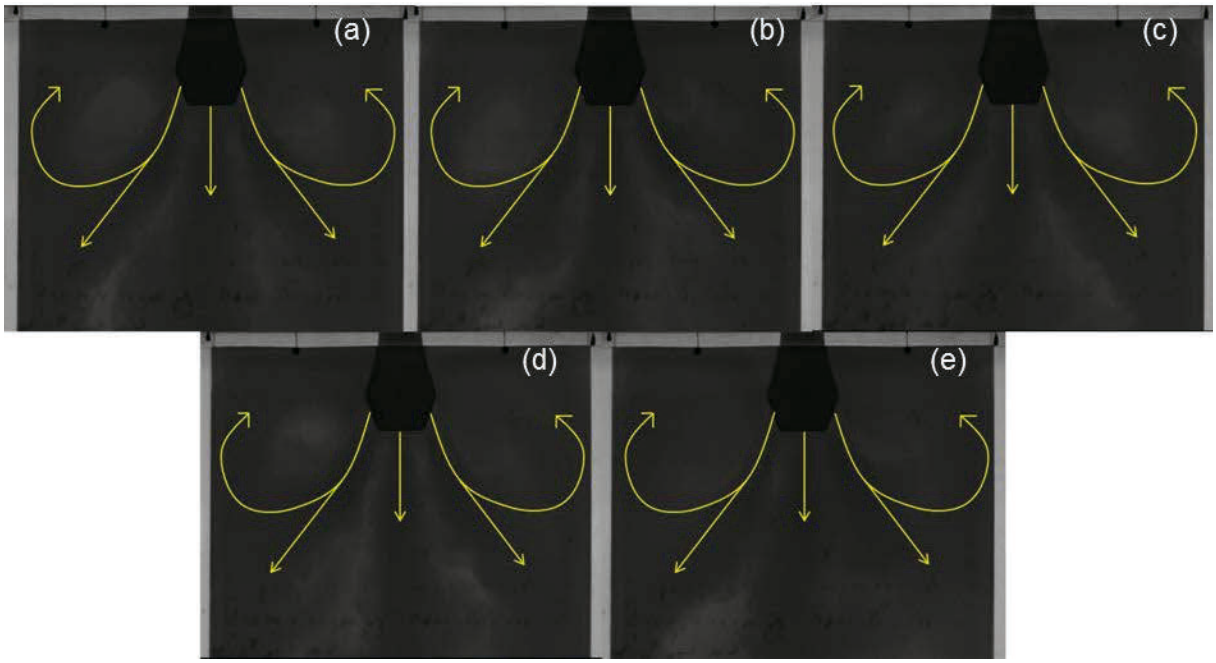

Figure 47. Results of case 2c for the SEN gap size 6 mm (a) – (e) (Run 1-5).

3.1.6 Case 2c SEN Gap Size 8 mm:

The results of case 2c for the SEN with the 8mm gap are similar to the results of gap size of 6 mm (Figure 47). In all 5 runs the flow pattern is same over the whole recording time. The side ports on the left and right side are creating a vortex at the top corner. Also currents out coming from the side ports which flow diagonal downwards are present. The beam which goes straight downwards is also clearly seen on all five images.

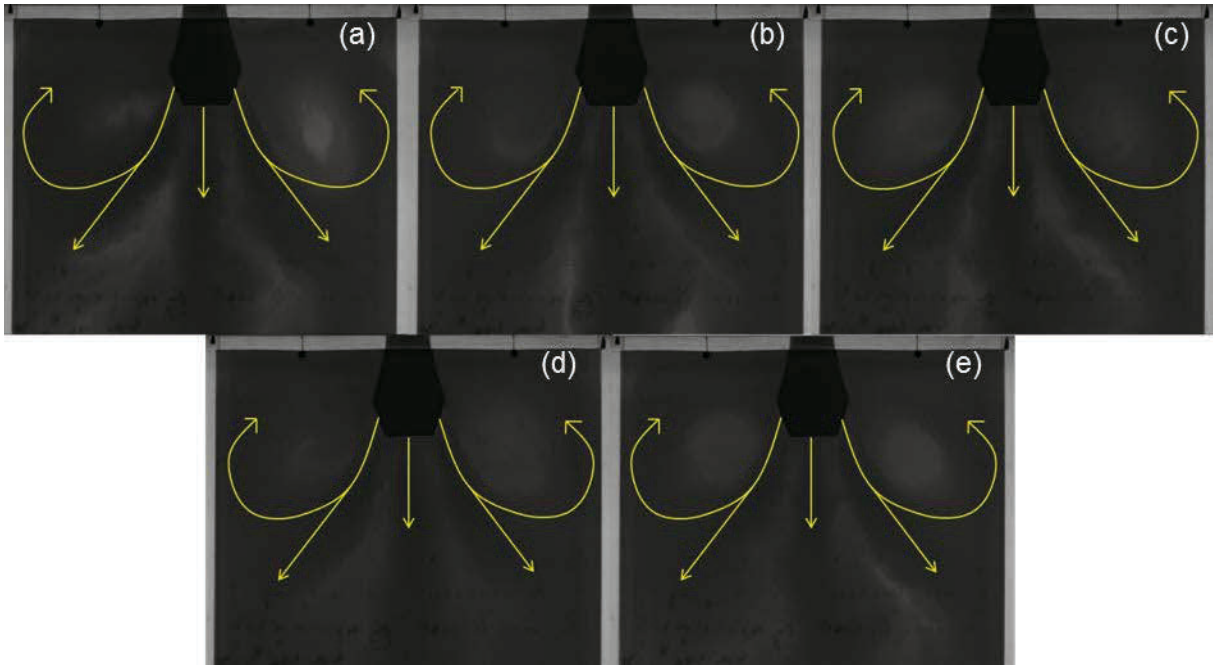

Figure 48. Results of case 2c for the SEN gap size 8 mm (a) – (e) (Run 1-5).

3.1.7 Case 3 SEN Gap Size 6 mm:

Case 3 is defined by a 1700 * 112.5 mm mold with a casting speed of 2 m/min. The SEN gaps used are 6, 8, 10, 12 and 18 mm. As in the other cases every trial was repeated five times to get a good overview of the flow pattern.

In Figure 49 all five runs with the same settings can be seen. There is no change in flow direction or behaviour observed. In all five runs a vortex creation on the left and right side with in the mold can be seen. In the first run (Figure 49 (a)) no dye is transported to the right corner in the bottom of the mold. In all five runs a current which goes straight down can be clearly seen.

Compared to the other results with the stable flow there are huge differences. In that cases there are just three instead of five single jets. In the first image no dye is transported to the right corner in the bottom which is not wished for the real plant. The size of the right vortex in the last image is a little bit different compared to the other four.

The creating of three currents instead of five, lead to a degradation of the mass and heat transport during the casting process.

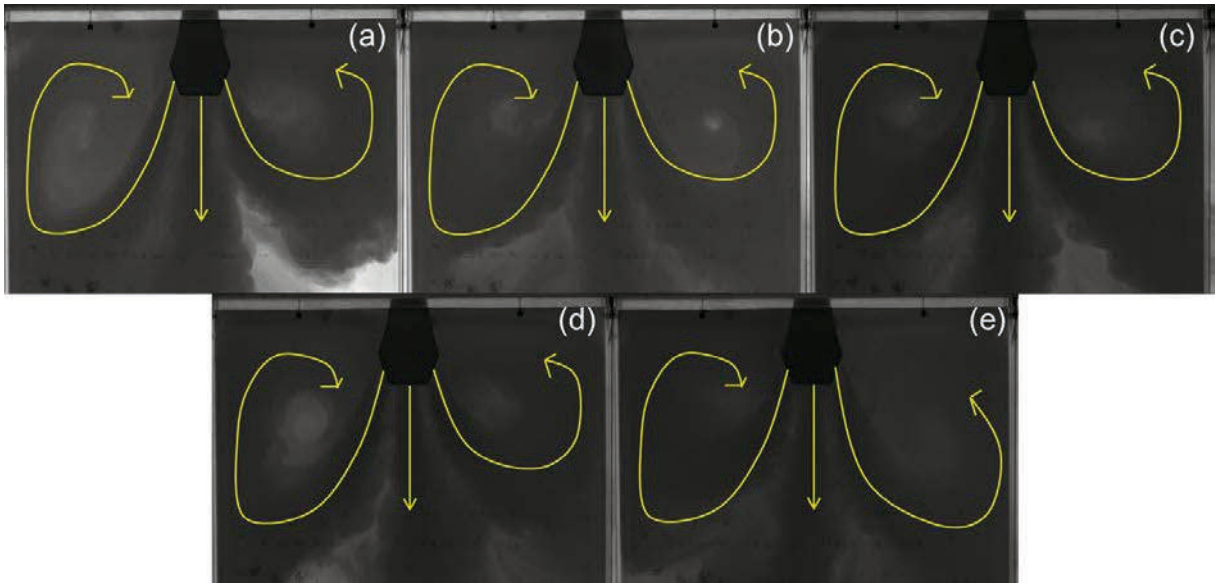

Figure 49. Results of case 3 for the SEN gap size 6 mm (a) – (e) (Run 1-5).

Stable flow pattern is one of the aims of the production of thin slab castings. It is important for constant mass and temperature distribution.

3.2 Transient Flow

Transient flow pattern is characterised by not repeating the exact same flow schemes during all five runs for the same settings.

3.2.1 Case 2c SEN Gap Size 10 mm:

The results of case 2c for the gap size of 10 mm can be seen in Figure 50. In the first four images the results are quite the same. Two vortexes are created and a single jet is going downwards. The vortices distinguish in size and shape. That is why there are lighter areas at the corners of the images because there is not as much dye being transported to these areas. In Figure 50 (d) dye is transported to the bottom because the vortices develop in a deeper section as in the Figure 50 (a)-(c). In Figure 50 (e), the fifth run, differences to the other four runs can be recognized. There are two upstreaming vortices, one going straight

downwards and two streaming diagonal to both mold walls. In that case the dye transport is more constant than in the other four runs.

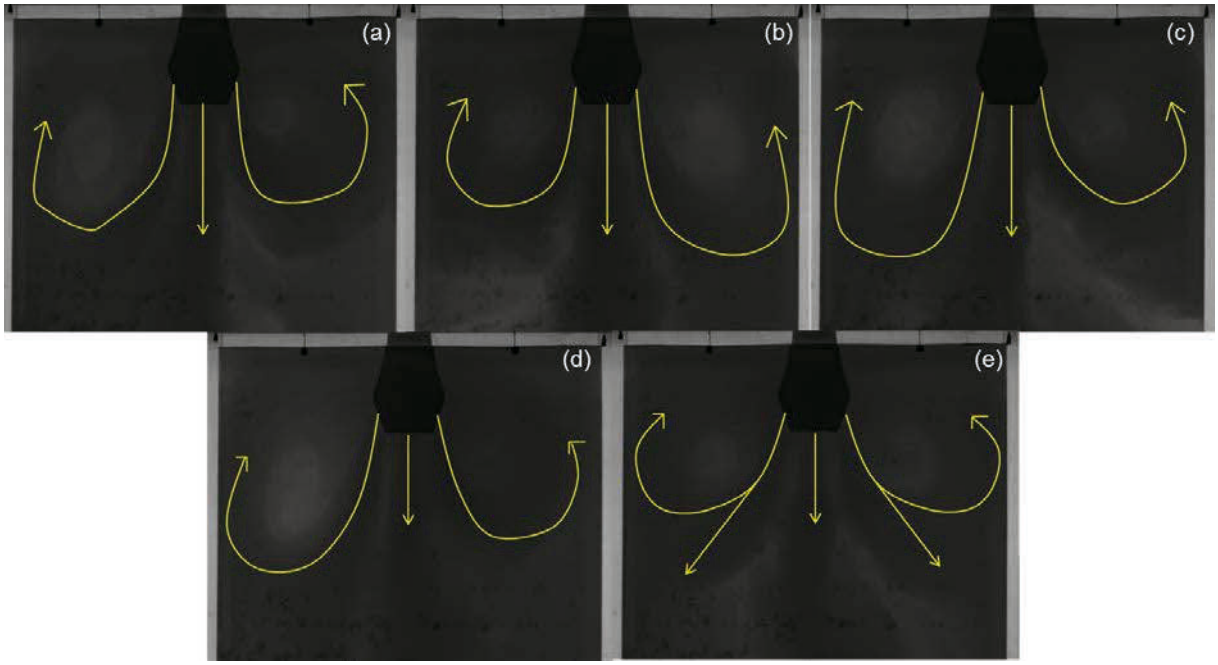

Figure 50. Results of case 2c for the SEN gap size 10 mm (a) – (e) (Run 1-5).

3.2.2 Case 3 SEN Gap Size 8 mm:

In Figure 51 (a) – (d) the first four runs can be seen. The flow pattern doesn't change during the recording time. In Figure 51 (a) two vortexes can be seen. The jet which flows straight downwards is present. There are some lighter sections which correspond to less dye concentration. In real plant casting this would be a huge disadvantage for producing slabs.

In the second run (Figure 51 (b)) the flow pattern is different to the first one. On the left side a vortex is seen which transports the dye to the left section at the top. The vortex on the right is larger than the left one. Also the jet which flows straight downwards is present. This flow behaviour is not preferable for real casting situations.

The third run (Figure 51 (c)) is also different compared to the previous runs. A straight downwards jet and a vortex on the right side can be observed. A backflow stream is upcoming from the left.

The fourth run shows just one beam which flows to the right side Figure 51 (d). One huge vortex is developed during the whole recording time. At the left side of the mold no dye is transported. In real thin slab casting processes this would be very dangerous because this can lead to an abort of the casting process.

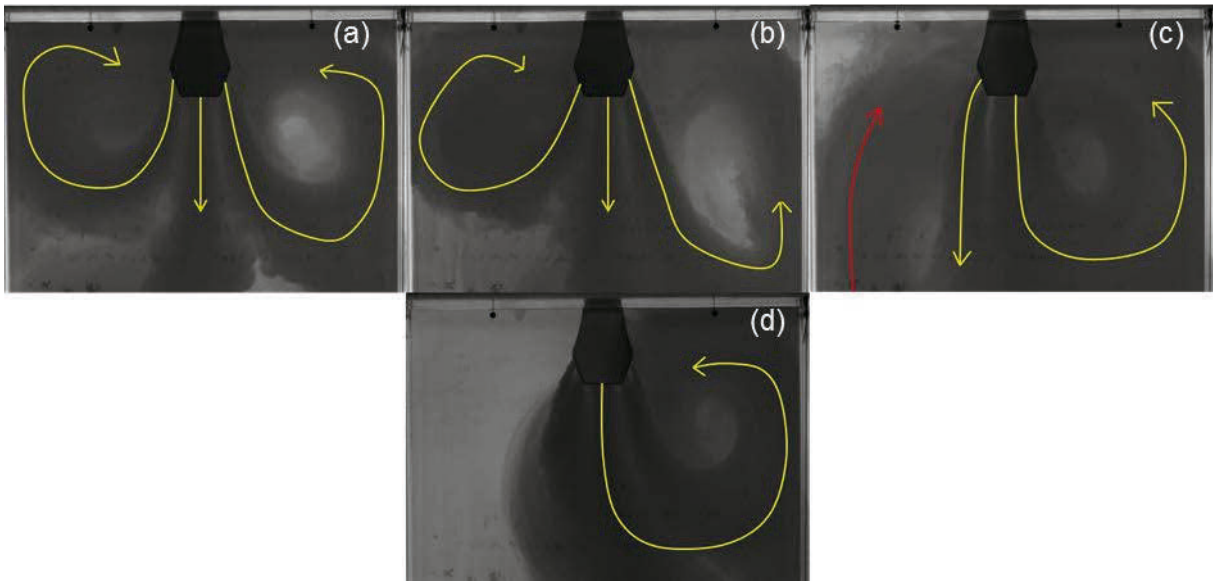

Figure 51. Results of case 3 for the SEN gap size 8 mm (a) – (d) (Run 1-4).

In the fifth run with of case 3 with the SEN gap size of 8 mm a change of the flow pattern can be observed. In Figure 52 (a) the first 21.25 seconds of this run can be seen. It looks like one beam is present which flows straight down and creates a vortex at the left side of the mold. At the right side a very strong backflow can be observed which reaches the surface and streams from the right to the left side. In Figure 52 (b) the last 10 seconds of recording time are shown. One jet is creating a vortex at the right side of the mold. At the left side there is a backflow upstreaming.

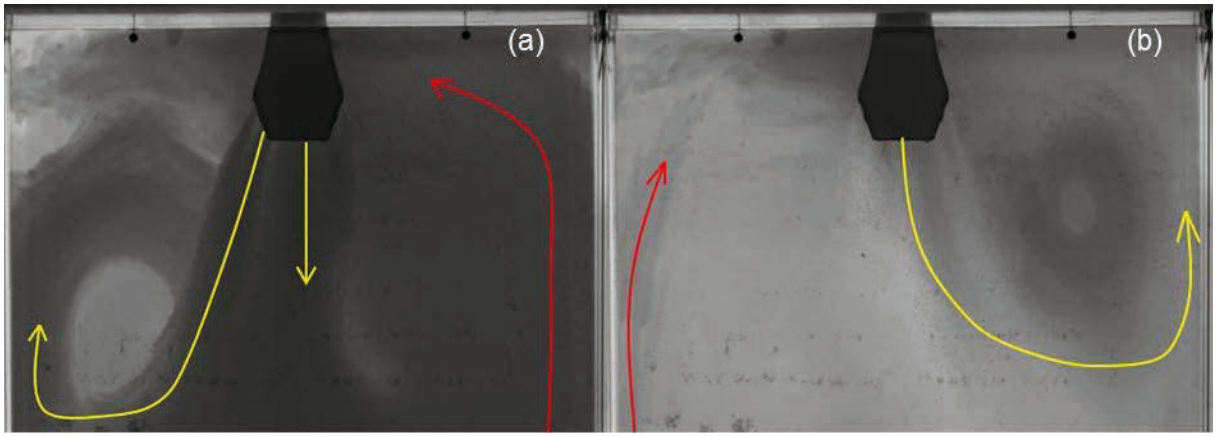

Figure 52. Results of case 3 of SEN for the gap size 8 mm (a) – (b) (Run5).

3.2.3 Case 3 SEN Gap Size 10 mm:

In Figure 53 (a) the first 21.06 seconds can be seen. A large vortex is created on the left side. The dye is transported to the left side because of the backflow at the right section. During the last 10.19 seconds one down streaming jet is present. In that last stage of the trial at both side of the wall a backflow is present (Figure 53 (b)).

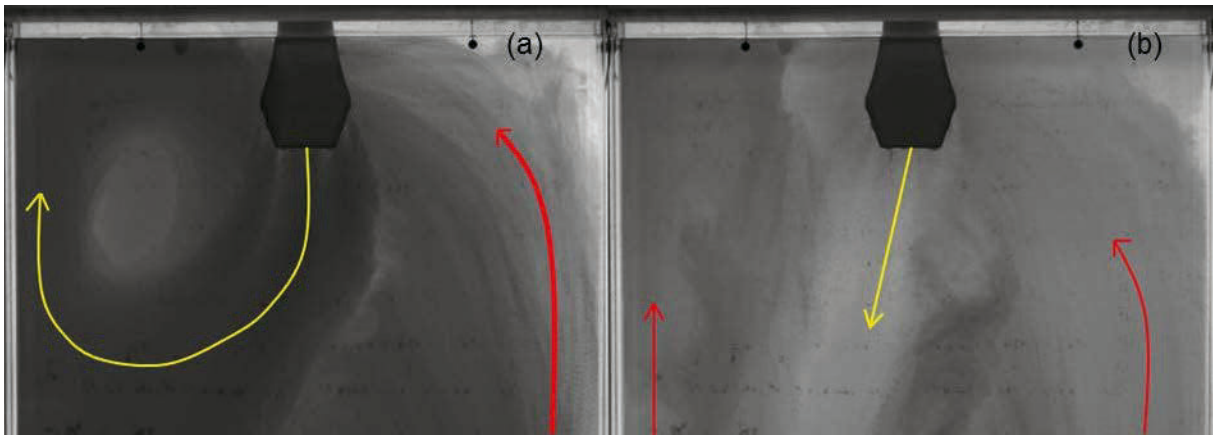

Figure 53. Results of case 3 for the SEN gap size 10 mm (a) – (b) (Run1).

In Figure 54(a) the first 16.25 seconds are seen. The jet is streaming straight downwards and a strong backflow on the right section is present. At the left section there is also an upstreaming backflow visible In Figure 54 (b) the jet changes its direction to the right section.

The backflows on both sides of the walls are still present for the last 15 seconds. It is recognizable that on the top left corner almost no dye was transported during the recording time.

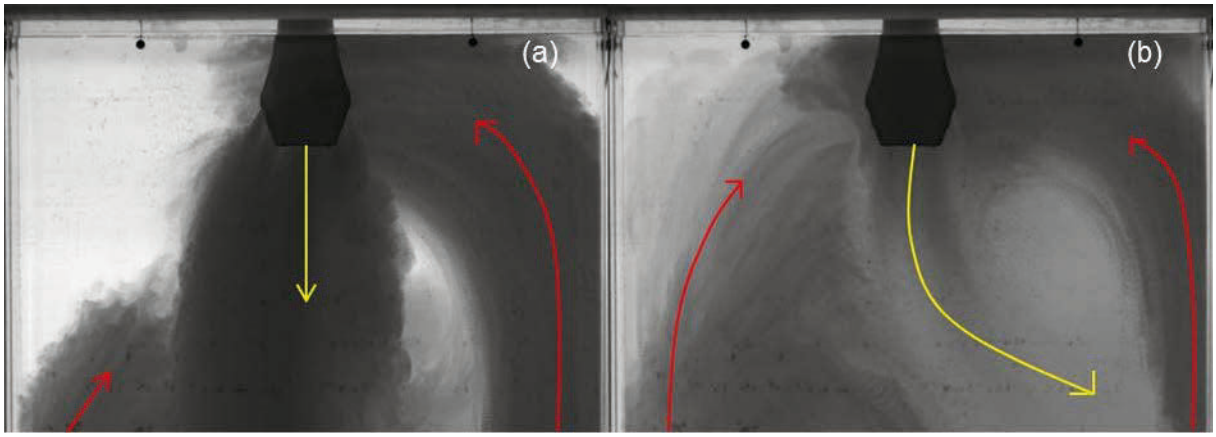

Figure 54. Results of case 3 for the SEN gap size 10 mm (a) – (b) (Run2).

In Figure 55 (a-c) the last three runs of case 3 for the SEN gap 10 mm can be seen. In Figure 55 (a)-(b) the two vortices at the left and right section can be seen. A beam which flows straight downwards is present at both runs. In the fourth run (Figure 55 (b)) it is observed that at the lower section at the left side almost no dye is transported.

During the fifth run (Figure 55 (c)) a beam which goes straight downwards and to the right can be seen. That is the reason for an upcoming backflow which creates a vortex at this section. At the upper part of the left section a vortex is present. At the lower left section less dye is transported.

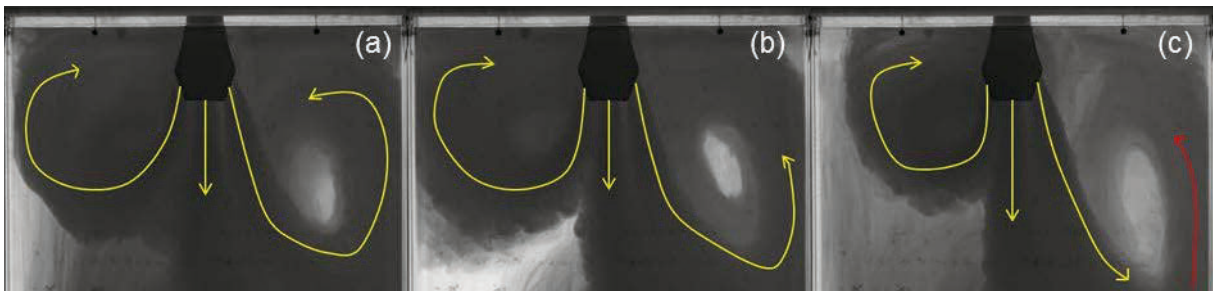

Figure 55. Results of case 3 for the SEN gap size 10 mm (a) Run3, (b) Run4, (c) Run5.

Transient flow can be very risky for the process of thin slab casting. There is a possibility of breakdown of the production because of this flow behaviour inside the mold. The heat and mass transportation is not constant which can lead to freezing inside the mold.

3.3 Unstable Flow

Unstable flow behaviour is characterised by an unpredictable flow pattern during the runs with same settings. Industries are interested in the cases with unstable flow, because the casting casting speed, i.e. mass flow rate, is much higher than other cases with a stable flow.

3.3.1 Case 1 SEN Gap Size 18 mm:

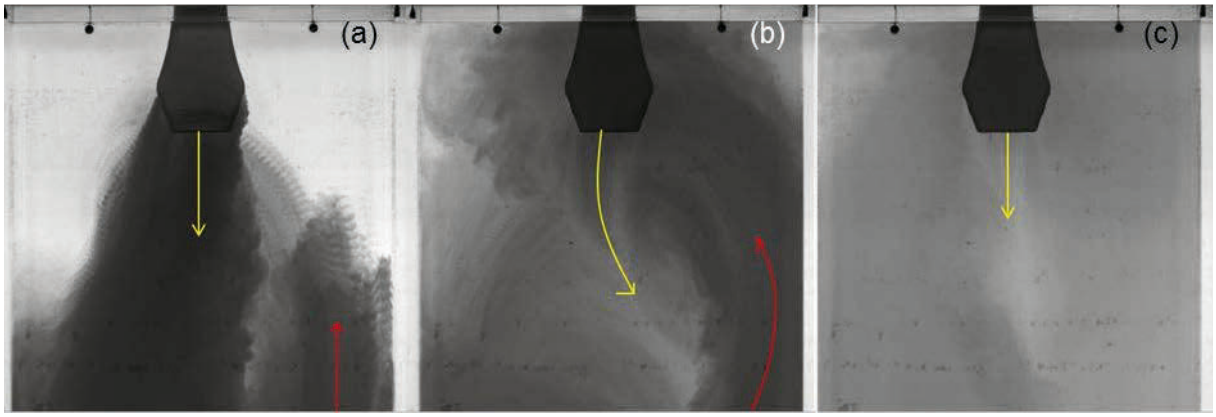

Figure 56. Results of case 1 for the SEN gap size18 mm (a) time interval 10.73 (s), (b) time interval 14.8 (s), (c) time interval 7.47 (s) (Run 1).

Using the SEN with 18 mm gap huge differences appear. In Figure 56 (a) one huge current which goes straight downwards can be seen. This lasts for 10.73 seconds. There is no separation in different jets as seen by the other cases before. At the right section of the mold a backflow from the bottom part of the mold can be recognized. A change of flow direction to the right side can be seen (Figure 56 (b)). The backflow reaches the surface. After a time interval of 14.8 seconds the beam flows straight downwards again Figure 56 (c).

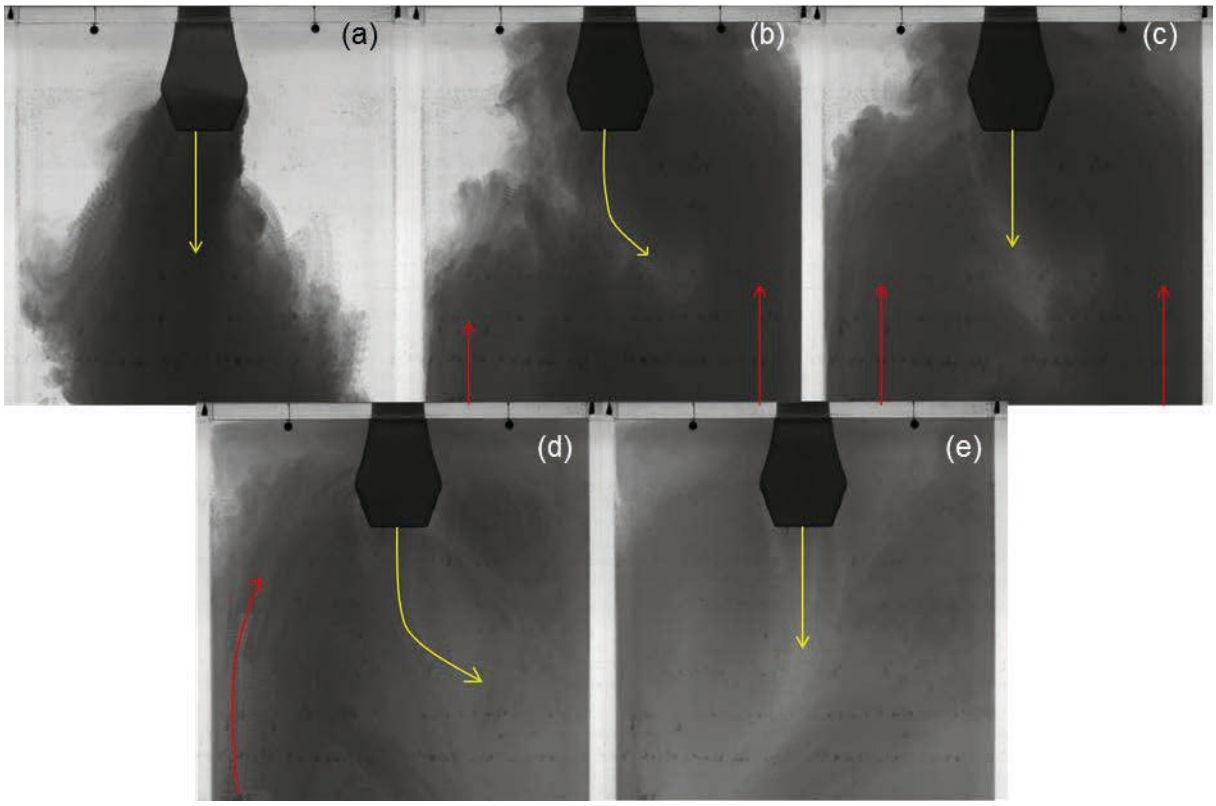

Figure 57. Results of case 1 for the SEN gap size 18 mm (a) time interval 6.66 (s), (b) timer interval 0.73 (s), (c) time interval 11.87 (s), (d) time interval 10.6 (s), (e) time interval 3.14 (s) (Run2).

The second run of the SEN with 18 mm shows differences in the flow pattern compared to the first run. A single jet goes downwards for 6.66 seconds which can be seen in Figure 57 (a). In Figure 57 (b) a short change in direction (0.73 seconds) to the right can be observed. Backflows at the right and left section at the mold walls are present. The next change of flow direction can be seen in Figure 57 (c) This flow pattern has a duration of 11.87 seconds. There the backflow on both sides of the mold walls is still present. Another change in direction can be seen in Figure 57 (d). Backflow of the water is just at the left section of the mold wall visible. This can be observed for another 10.6 seconds. A last change of flow direction can be seen in Figure 57 (e). At the end of recording time the current goes straight downwards.

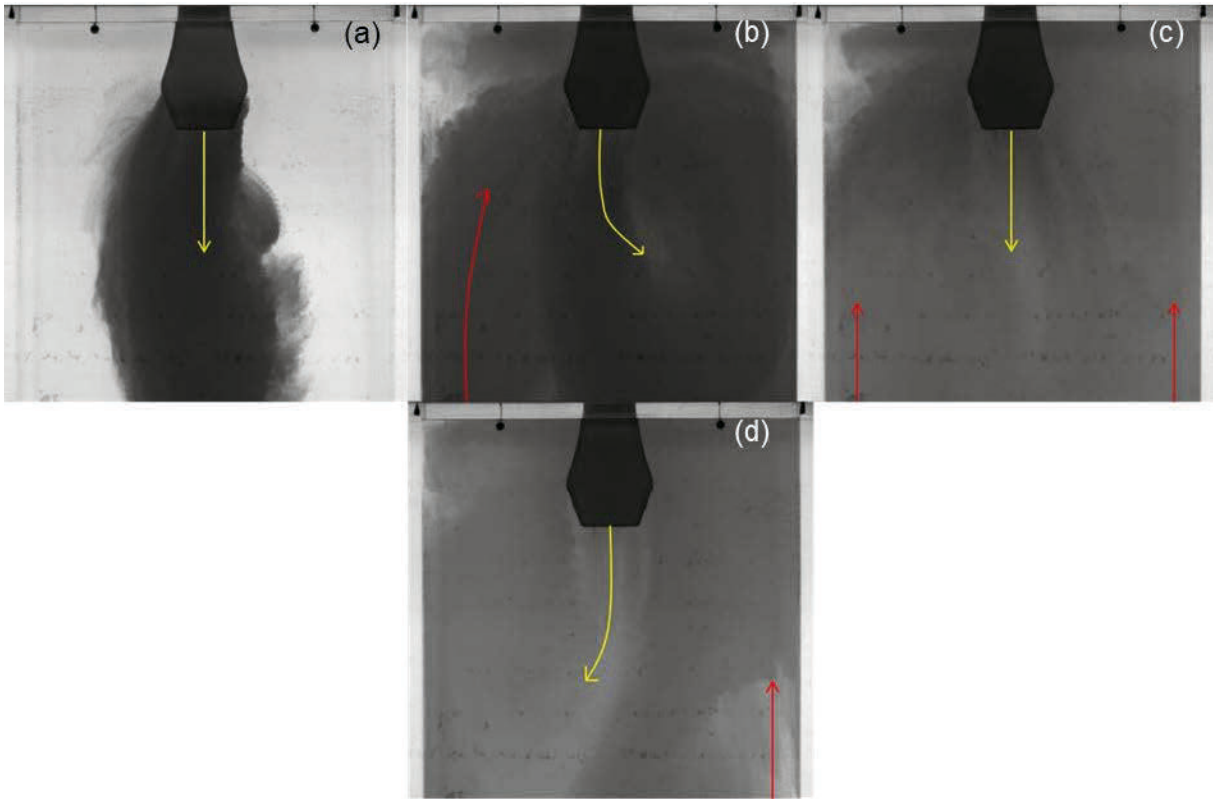

Figure 58. Results of case 1 for the SEN gap size 18 mm (a) time interval 5.6 (s), (b) time interval 16.67 (s), (c) time interval 8.2 (s), (d) time interval 2.6 (s) (Run3)

The third run of case 1 for the SEN gap size 18 mm also shows instability in flow behaviour. The first recorded jet is going straight downwards for 5.6 seconds (Figure 58 (a)). The next direction of the current is to the right and from the left bottom a huge amount of dye is coming back upwards. This flow behaviour takes place for about 16.67 seconds (Figure 58 (b)). The next 8.2 seconds the jet streams straight downwards again and backflow at both sections of the mold wall is streaming upwards (Figure 58 (c)). The last 2.6 seconds the single jet flows to the left section of the mold which is may caused by the backflow at the right section (Figure 58 (d)).

The beginning of the fourth run starts with a single jet to right section of the mold section. The backflow comes up from the left side of the wall. This takes 15.6 seconds and can be seen in Figure 59 (a). In Figure 59 (b) a change in direction can be observed. Also the backflow keeps coming up from the left section and is creating a small vortex. It can be seen that there is almost no dye transported to the top left corner of the mold. A small amount of backflow is coming up from the right corner at the bottom of the recording window. After 9.67

seconds the jet changes its direction to the right side. Figure 59 (c) summarizes the last 7.93 seconds of recording time. A backflow at the right corner is still present (Figure 59(c)).

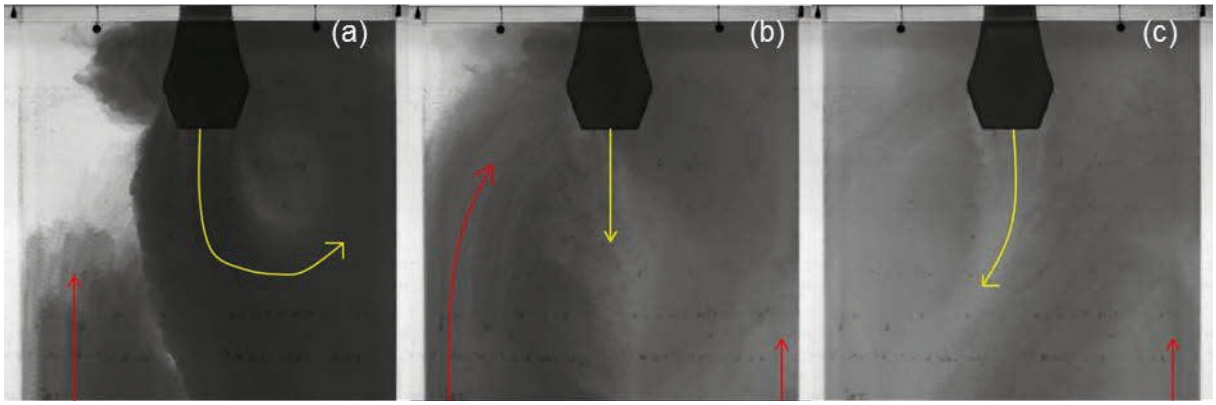

Figure 59. Results of case 1 for the SEN gap size 18 mm (a) time interval 15.6 (s), time interval 9.67 (s), (c) time interval 7.93 (s) (Run4)

The fifth run of case 1 for the SEN gap 18 mm starts with a left flow of the jet. A vortex creation at the right top corner can be seen in Figure 60 (a). This is recorded for 9.6 seconds. In Figure 60 (b) a change to a straight downwards flow can be seen. Also a strong backflow at both sides of the mold wall is present. This lasts for 4.4 seconds. It is clearly to see that until that time no dye is transported to the left top corner. There are also some sections at the right top corner with less dye concentration compared to others. In Figure 60 (c) a change of flow direction to the left side can be seen. The backflow is still present and visible. This is recorded for 15.2 seconds. In Figure 60 (d) the jet flows straight downwards again. The backflow is coming up from the right section of the wall.

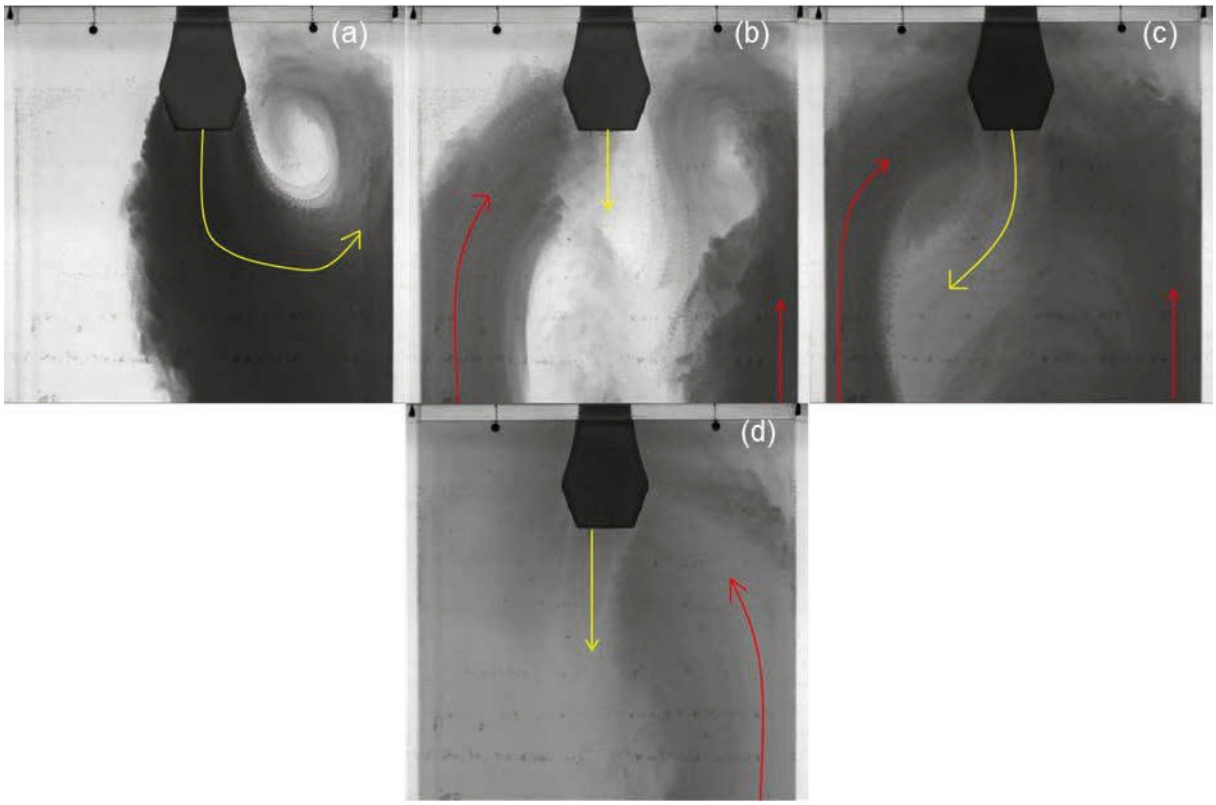

Figure 60. Results of case 1 for the SEN gap size 18 mm (a) time interval 9.6 (s), time interval 4.4 (s), time interval 15.2 (s), (d) time interval 3.8 (s) (Run5).

3.3.2 Case 2a SEN Gap Size 18 mm:

The first run for case 2a for SEN gap size 18 mm shows stable flow behaviour. One single vortex at the left section can be seen. From the right bottom a straight upcoming backflow is present. No dye is transported to the top right corner (see Figure 61).

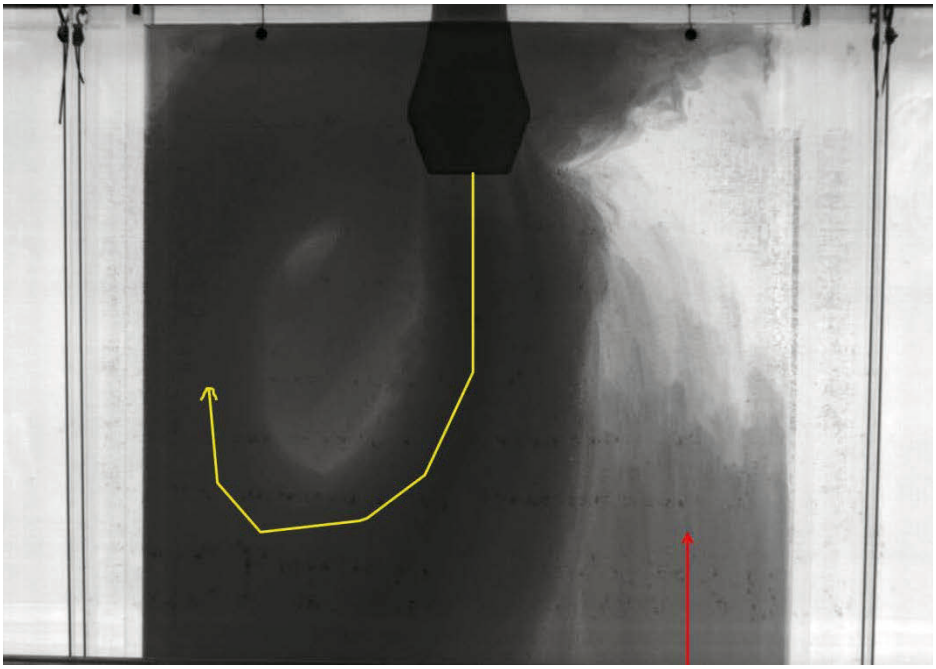

Figure 61. Results of case 2a for the SEN gap size 18 mm (Run1).

The second run shows huge differences in the flow pattern compared to the first one (Figure 61). In the beginning the beam flows to the right section of the mold and also a backflow from the bottom at the left side of the mold is seen (Figure 62 (a)). After 16.1 seconds the jet changes its direction to straight downwards and the backflow is still present. This happens for about 7.1 seconds. For the last seconds of recording time the down streaming jet is dividing into two jets. The backflow on the left side of the wall is still present (Figure 62 (c)).

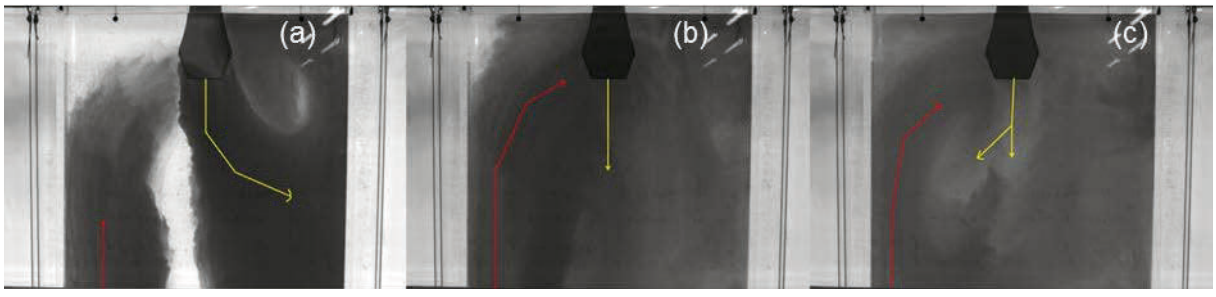

Figure 62. Results of case 2a for the SEN gap size 18 mm (a) time interval 16.1 (s), (b) time interval 7.1 (s), (c) time interval 9.8 (s) (Run2).

The jet at the third run creates a vortex at the left section of the mold. This flow pattern is visible for 21.27 seconds. During that time no dye is transported to the right section of the mold. Afterwards the jet changes the direction to straight downwards (Figure 63 (b)). In Figure 63 (b) the backflow at the right side of the wall is clearly to see.

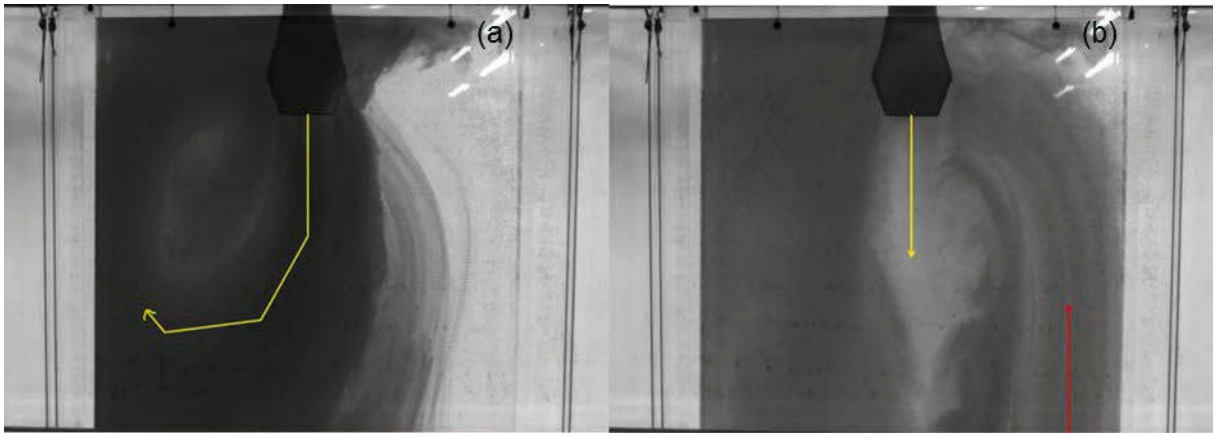

Figure 63. Results of case 2a for the SEN gap size 18 mm (a) time interval 21.27 (s), (b) time interval 11.73 (s) (Run3)

The fourth run starts with a large vortex development at the right section of the mold. At the left wall side of the mold a backflow is coming up (Figure 64 (a)). After 21.4 seconds the directions changes to straight downwards for 3.93 seconds (Figure 64 (b)). In the end the jet flows to the left side for 7.67 seconds (Figure 64 (c)). An upcoming backflow from the left side is also visible.

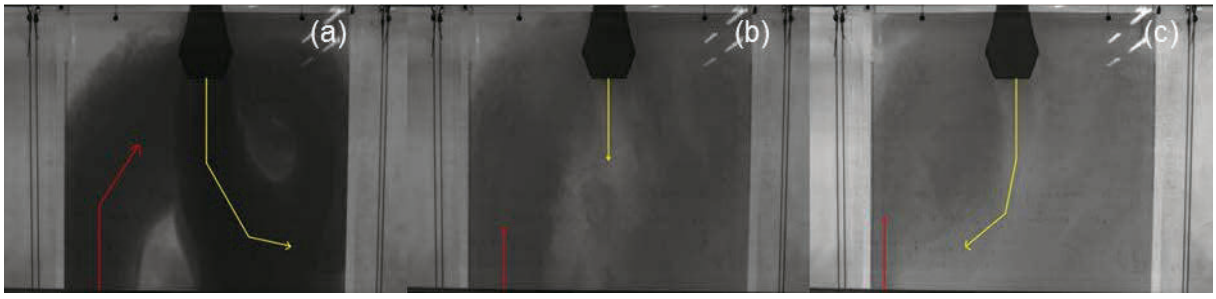

Figure 64. Results of case 2a for the SEN gap size 18 mm (a) time interval 21.4 (s), (b) time interval 3.93 (s), (c) time interval 7.67 (s) (Run4)

The fifth run of case 2a for the SEN gap size 18 mm starts with a creation of a huge vortex at the left section of the mold. This flow pattern is present for 10.13 seconds (Figure 65 (a)). Afterwards the jet changes to a straight downward flow for 9.73 seconds. An upcoming backflow is also present and producing a vortex which flows straight into the down streaming jet (Figure 65 (b)). This can be the reason why the jet changes its flow direction to the right section of the mold for the last 13.13 seconds (Figure 65 (c)).

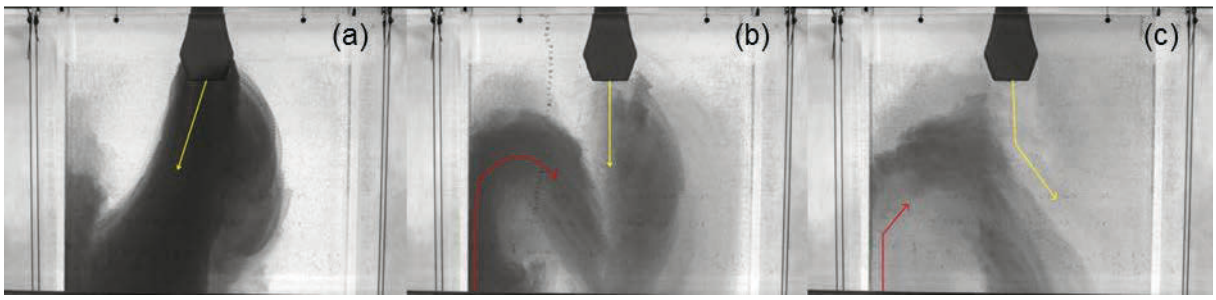

Figure 65. Results of case 2a for the SEN gap size 18 mm (Run5).

3.3.3 Case 2b SEN Gap Size 18 mm:

The first run with the settings of case 2b for the SEN gap size 18 mm starts with a straight down streaming flow. At both mold wall sides a backflow is coming up. The backflow at the left side is faster than at the right side. The backflow on the left side reaches the meniscus level and circulate to the right area of the apparatus. This takes place within 17 seconds (Figure 66 (a)). Afterwards the jet changes its direction to the left side for 13.27 seconds (Figure 66 (b)). The backflow at the right section of the mold still exists. For the last 2.73 seconds the jet changes its direction to straight downwards again. The whole area gets lighter because the dye solutes and distributes in the fresh incoming water (Figure 66 (c)).

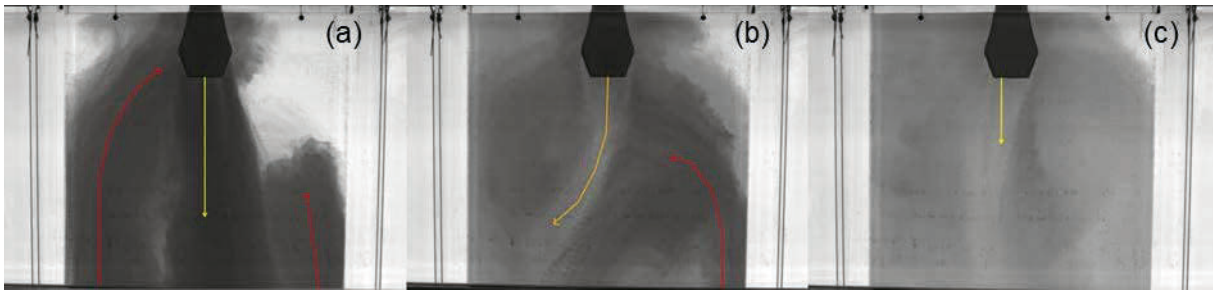

Figure 66. Results of case 2b for the SEN gap size 18 mm (a) time interval 17 (s), (b) time interval 13.27 (s9, (c) time interval 2.73 (s) (Run1).

The second run starts with a huge vortex development at the right section of the mold. This flow pattern takes 15.2 seconds (Figure 67 (a)). Afterwards the jet changes its flow direction to straight downwards for 15.47 seconds. Also a backflow on the left side can be seen (Figure 67 (b)). The last 2.3 seconds the jet flows to the left section of the mold. A backflow at the left and right mold wall can be observed (Figure 67 (c)).

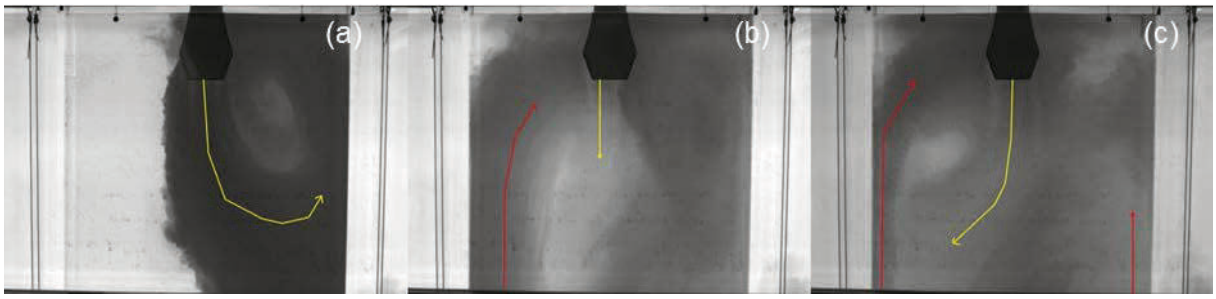

Figure 67. Results of case 2b for the SEN gap 18 mm (a) time interval 15.2 (s), (b) time interval 15.47 (s), (c) time interval 2.3 (s) (Run2)

The third run of case 2b for the SEN gap 18 mm starts with a left sided jet. This flow behaviour is present for 10.2 seconds. During that time no dye is transported to the left section of the mold (Figure 68 (a)). The next 5.73 seconds the jet flows straight downwards and at the right mold wall a strong backflow is streaming up. The last 17.07 seconds the jet changes its direction to right section of the mold. At the left side of the mold a backflow is coming up (Figure 68 (c)).

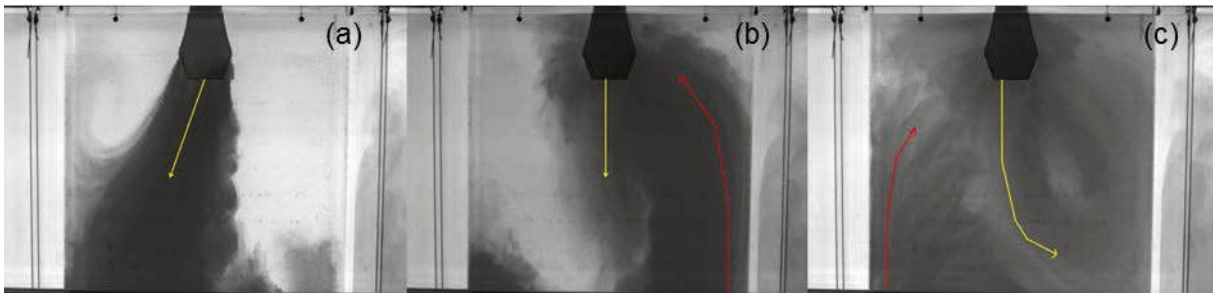

Figure 68. Results of case 2b for the SEN gap 18 mm (a) time interval 10.2 (s), (b) time interval 5.73 (s), (c) time interval 17.07 (s) (Run3).

The fourth run of case 2b for the 18 mm SEN gap size starts with a left flow of the jet. This flow pattern is present for 10.13 seconds (Figure 69(a)). At the right corner a backflow straight coming up from the bottom part of the mold can be seen. The next 2.06 seconds the jet goes straight downwards and the backflow is proceeding (Figure 69 (b)). The last 20.8 of recording time a jet flows to the right section of the mold. Also a new backflow at the left bottom corner of the mold is present (Figure 69 (c)).

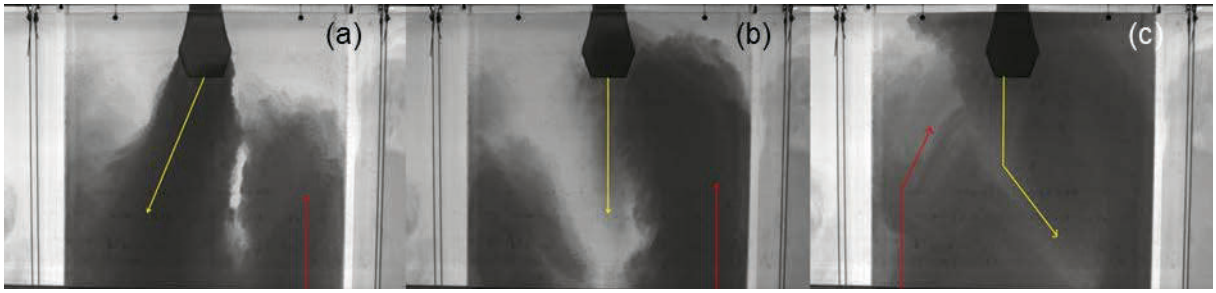

Figure 69. Results of case 2b for the SEN gap 18 mm (a) time interval 10.13 (s), (b) time interval 2.06 (s), (c) time interval 20.8 (s) (Run4).

The fifth run with the same setting starts with a left flow of the jet which is creating a huge vortex at the top of the left section of the mold (Figure 70 (a)). After 18.07 seconds the jet changes its direction to straight downwards for the next 5.27 seconds (Figure 70 (b)). For the last 9.67 seconds the out coming flow goes to the right side of the mold. At the left wall a backflow from the bottom part can be seen (Figure 70 (c)).

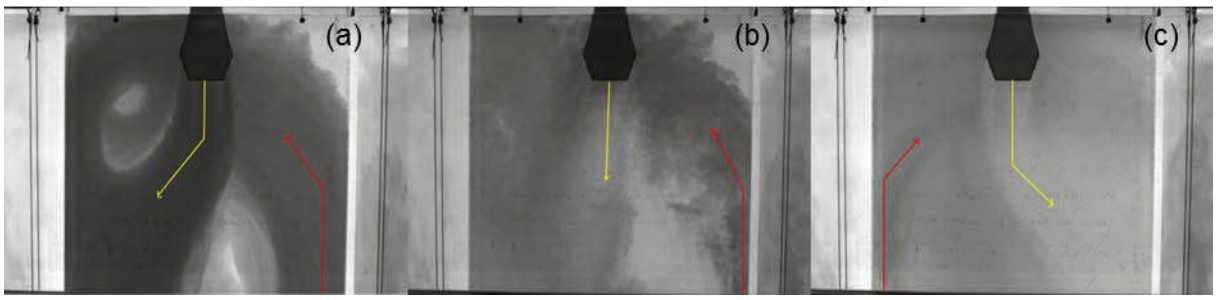

Figure 70. Results of case 2b for the SEN gap 18 mm (a) time interval 18.07 (s), (b) time interval 5.27 (s), (c) time interval 9.67 (s) (Run5).

3.3.4 Case 2c SEN Gap Size 12 mm:

The first run of case 2c with the SEN gap size 12 mm can be seen in Figure 71. Figure 71 (a) represents the first 6.6 seconds of this run. A large vortex development at the right section of the mold can be seen. A strong backflow at the left section can be seen as well. Figure 71 (b) the next 10 seconds can be seen. The jet flows straight downwards and at both side of the mold walls a backflow is present. For the next 2.75 seconds the jet changes its direction to the left section of the mold. A large vortex develops. The backflow is present at the right mold side at that stage of the trial (Figure 71 (c)). The last 9 seconds of this run can be seen in Figure 71 (d). The jet flows straight downwards again and the backflow at the right section of the mold is still present.

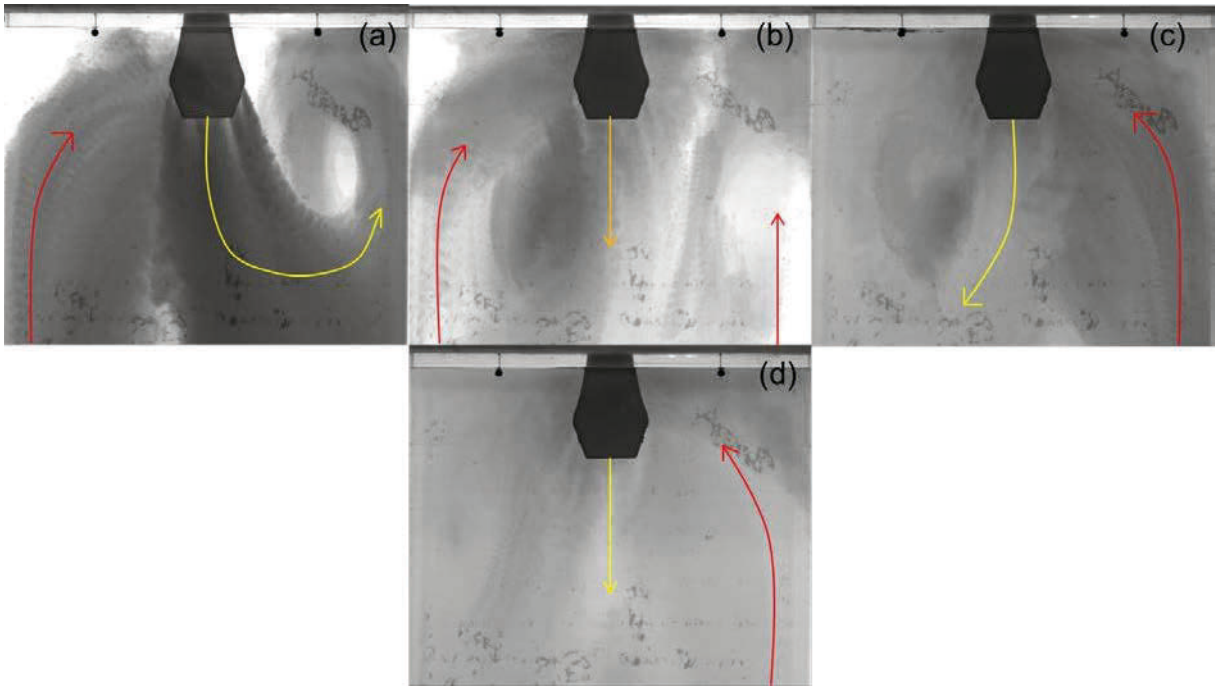

Figure 71. Results of case 2c for the SEN gap size 12 mm(a) time interval 6.6 (s), (b) time interval 10.0 (s), (c) time interval 2.75 (s), (d) time interval 9.0 (s) (Run1).

In Figure 72 (a) the first 18.4 seconds of the second run can be seen. The jet flows to the left section of the mold and creates a large vortex. At the right section of the mold a backflow is coming up from the bottom part of the mold. The jet changes its direction to straight downwards for 1.56 seconds (Figure 72 (b)). The backflow at the right section of the mold is still present. It can be seen that no dye is transported to top right corner until that time. The

last 11.25 seconds the jet changes its direction to the right section of the mold. At that period the backflow is at the left section (Figure 72 (c)).

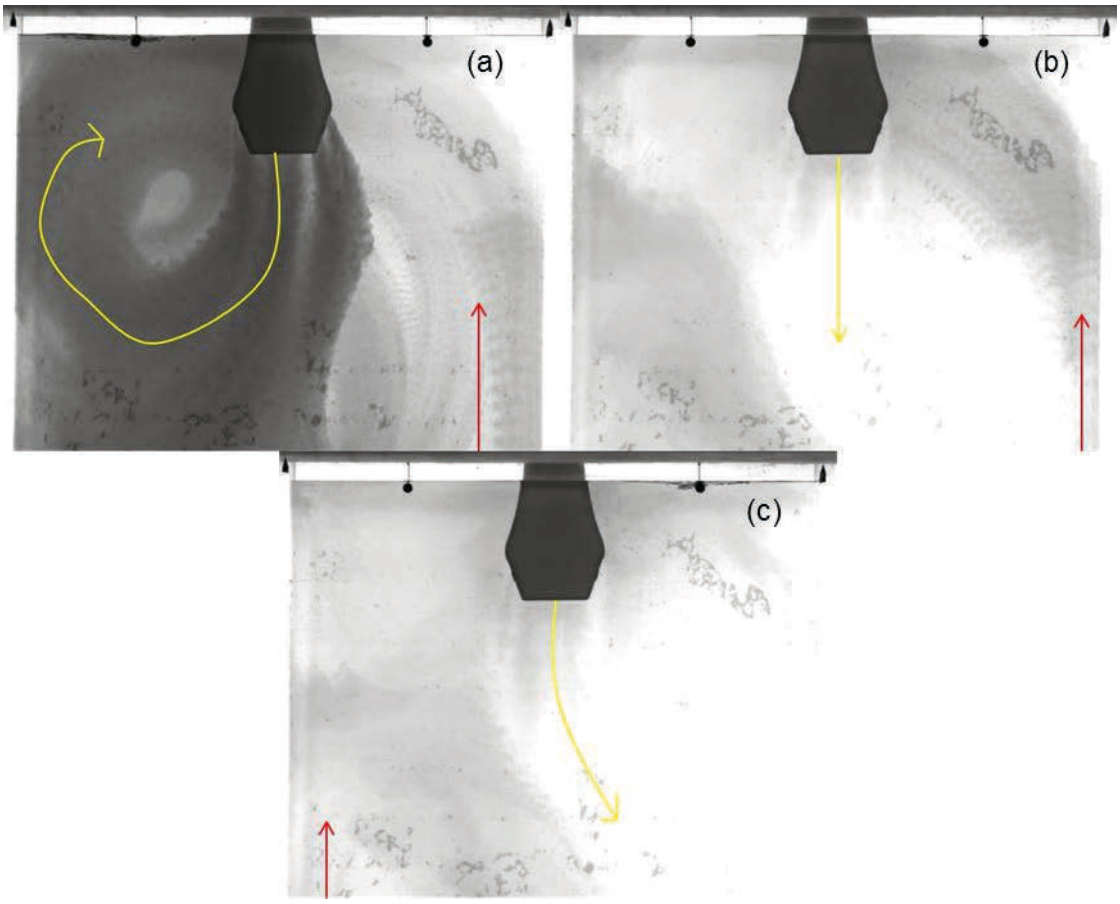

Figure 72. Results of case 2c for the SEN gap size 12 mm (a) time interval 18.4 (s), (b) time interval 1.56 (s), (c) time interval 11.25 (s) (Run2).

The first 9.38 seconds of the third run can be seen in Figure 73 (a). A jet creating a vortex at the left section of the mold can be seen. The jet changes its direction to straight downwards for the next 6.25 seconds (Figure 73 (b)). An upcoming backflow can be observed at both sides. The jet flows to the right section of the mold for the last 15.63 seconds. The backflow is present at the right section of the mold (Figure 73 (c)).

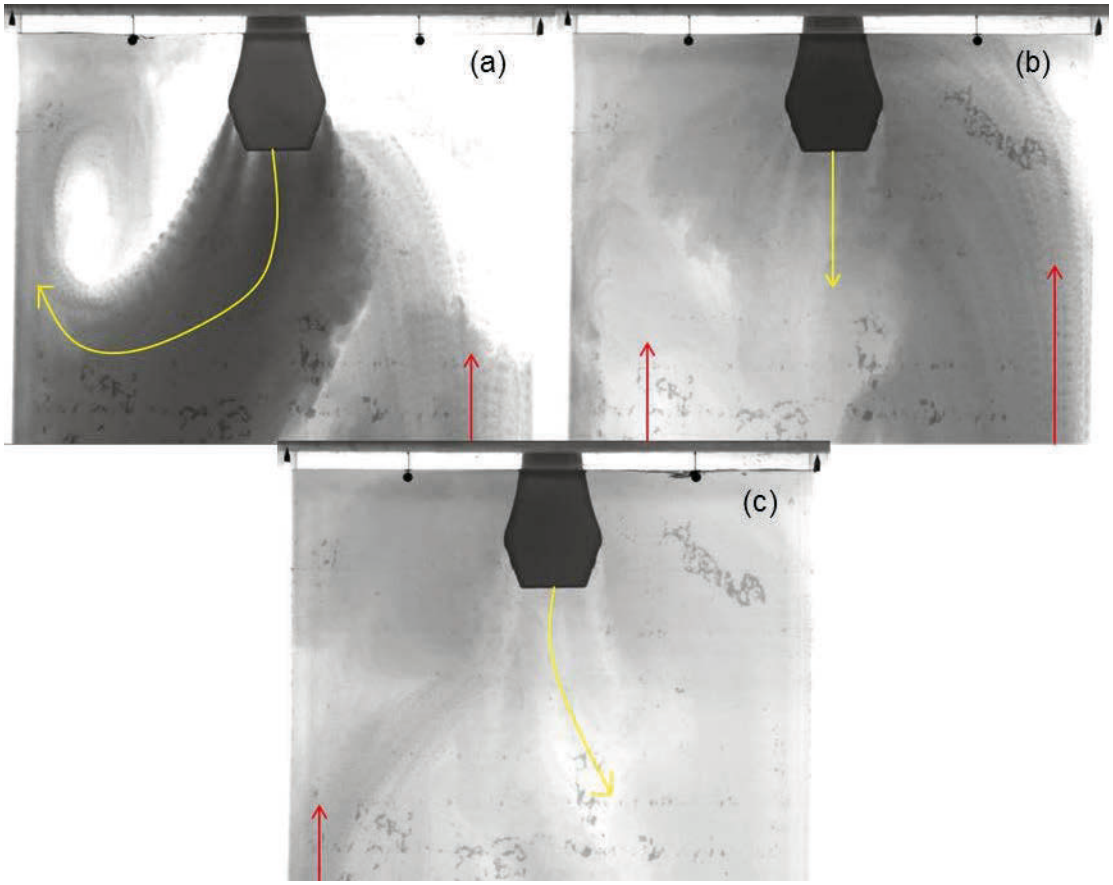

Figure 73. Results of case 2c for the SEN gap size 12 mm (a) time interval 9.38 (s), (b) time interval 6.25 (s), (c) time interval 15.63 (s) (Run3).

The first 5.8 seconds of the fourth run of case 2c with SEN gap size 12 mm can be seen in Figure 74 (a). The jet is down streaming to the lower area of the mold spreads out to the left section of the mold. During the next 2.3 seconds the jet flows in two directions (Figure 74 (b)). One flows to the left section and the other one straight downwards. An upcoming backflow at the right section of the mold can be observed. Afterward the jet flows to right section. During that time (15.25 seconds) a backflows at both sides is present (Figure 74 (c)). During the last 7.99 second the jet goes straight downwards again. A backflow at the right section of the mold can be observed Figure 74 (d).

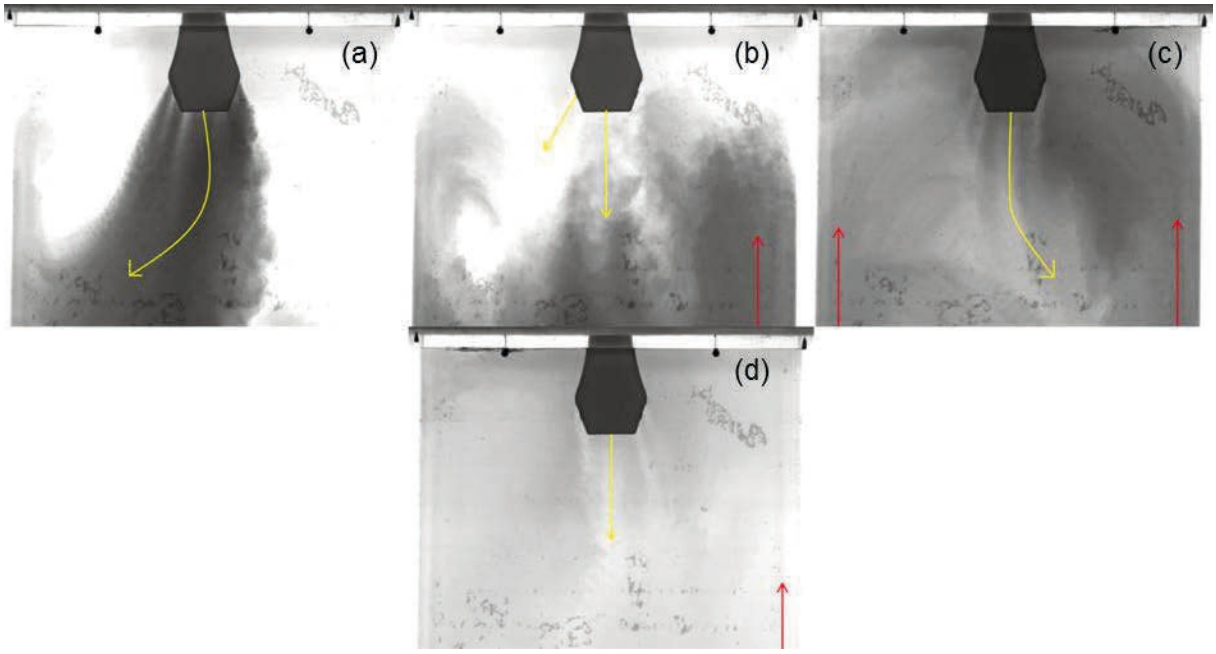

Figure 74. Results of case 3c for the SEN gap size 12 mm (a) time interval 5.8, (b) time interval 2.3 (s), (c) time interval 15.25 (s), (d) time interval 7.94 (s) (Run4).

The fifth run of case 2c for the SEN gap size 12 mm results in a stable flow pattern (Figure 75). A single jet during the whole recording time can be observed. The jet flows to the left section of the mold and creates a large vortex. A backflow is streaming up from the right bottom part of the mold. During the whole recording time no dye was transported at the right upper part of the mold.

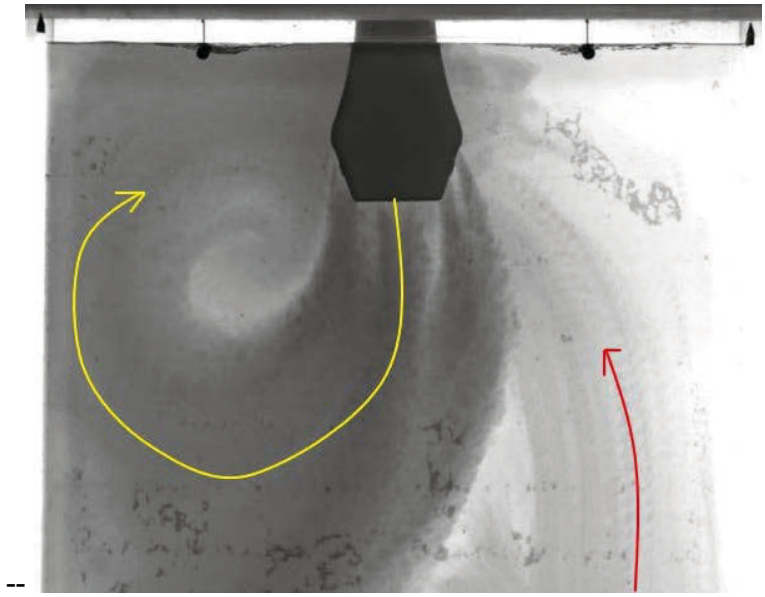

Figure 75. Results of case 2c for the SEN gap size 12 mm (Run5).

3.3.5 Case 2c SEN Gap Size 15 mm:

The first run of case 2c for the SEN gap size 15 mm starts with a single jet which flows straight downwards but its tip tend to the right section of the mold (Figure 76 (a)). A backflow from the left section from the bottom is streaming up. This period takes 12.2 seconds afterwards the jets changes to straight downwards flow. At both sides of the wall a backflow is present (Figure 76 (b). The last 2.43 seconds the jet flows to the left section of the wall where the backflow is still present (Figure 76 (c)).

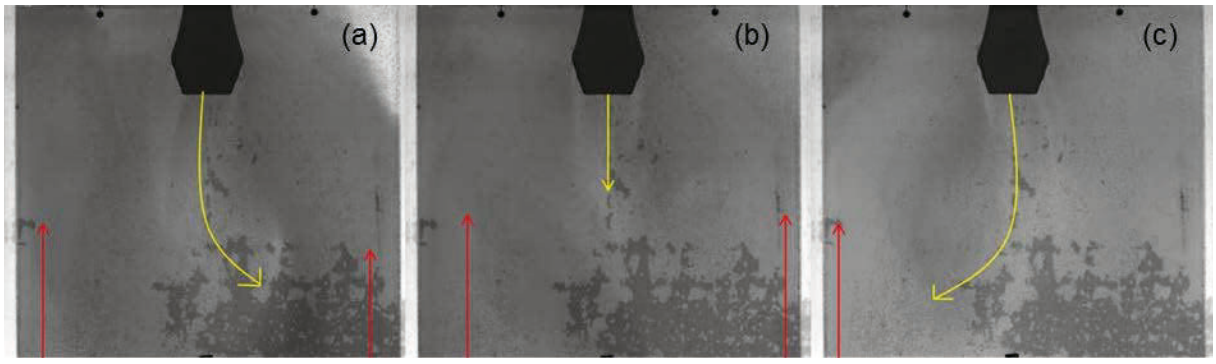

Figure 76. Results of case 2c for the SEN gap size 15 mm (a) time interval 12.2 (s), (b) time interval 18.37 (s), (c) time interval 2.43 (s) (Run1)

The first 9.28 seconds of the second run of case 2c for the SEN gap size 15 mm starts with a left streaming jet (Figure 77 (a)). A backflow is coming up from the left bottom part of the mold. The next 6.15 second the current flows straight downwards. The backflow on the left side can still be observed (Figure 77 (b)). The last 15.63 seconds the jet changes its direction to the left section of the mold. The backflow at the left section is still present (Figure 77 (c)).

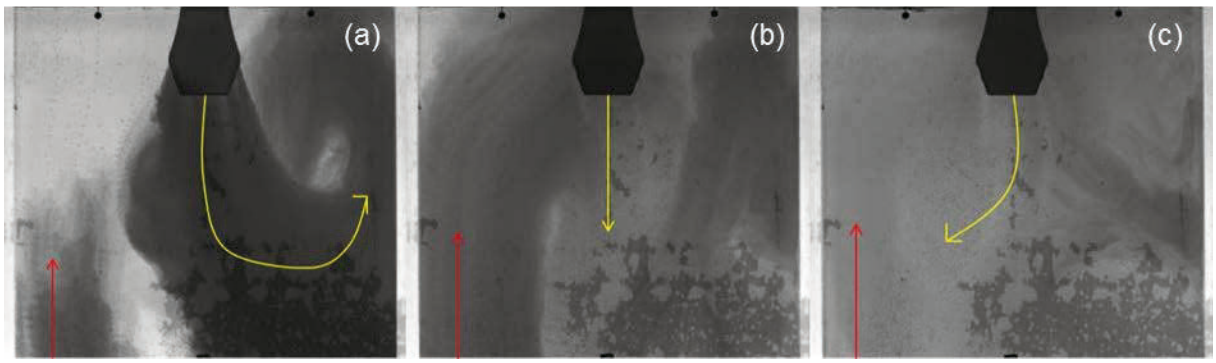

Figure 77. Results of case 2c for the SEN gap size 15 mm (a) time interval 9.28 (s), (b) time interval 6.15 (s), (c) time interval 15.63 (s) (Run2)

In Figure 78 (a) a vortex development at the right section of the mold is seen. A backflow is streaming up at the left side of the wall. This takes about 15.63 seconds. The jet changes its direction from flowing to the right side to straight downwards. The backflow at the left side is still present which can be seen in Figure 78 (b). This takes 5 seconds until the jet changes its direction again. For the last 10.63 seconds the jet flows to the left section of the mold. The backflow at the left section still can be observed. The last stage can be seen in Figure 78 (c).

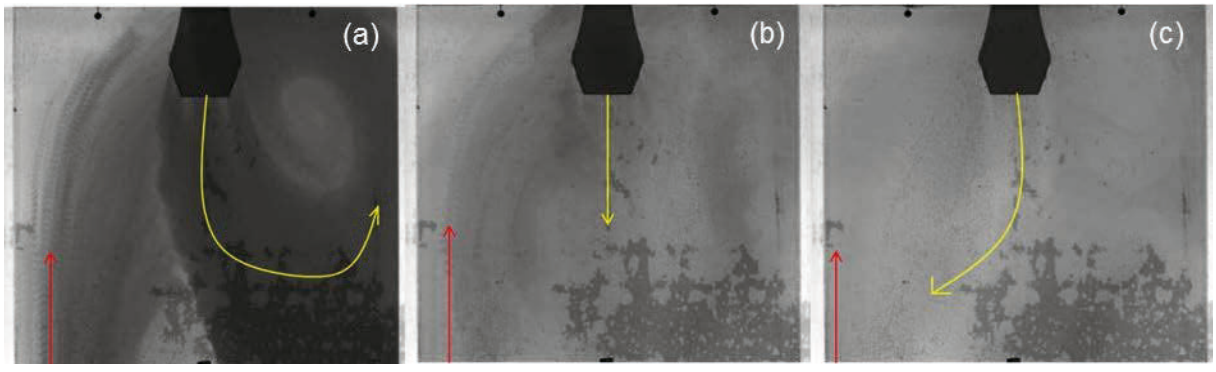

Figure 78. Results of case 2c for the SEN gap size 15 mm (a) time interval 15.63 (s), (b) time interval 5 (s), (c) time interval 10.63 (s) (Run3).

The fourth run of case 2c for the SEN gap size 15 mm can be seen in Figure 79. In Figure 79(a) a vortex development at the right section of the mold is seen. A backflow is streaming up at the left side of the mold. This flow pattern is visible for 12.5 seconds. In Figure 79 (b) a change in direction of the flow can be observed. The jet flows straight downwards and the backflow at the left side of the mold is still present. After a period of 8.13 seconds the flow pattern is changing again. In Figure 79 (c) the jet flows to the left section of the mold. A backflow is streaming upwards at the right mold wall. This is visible for 11.88 seconds.

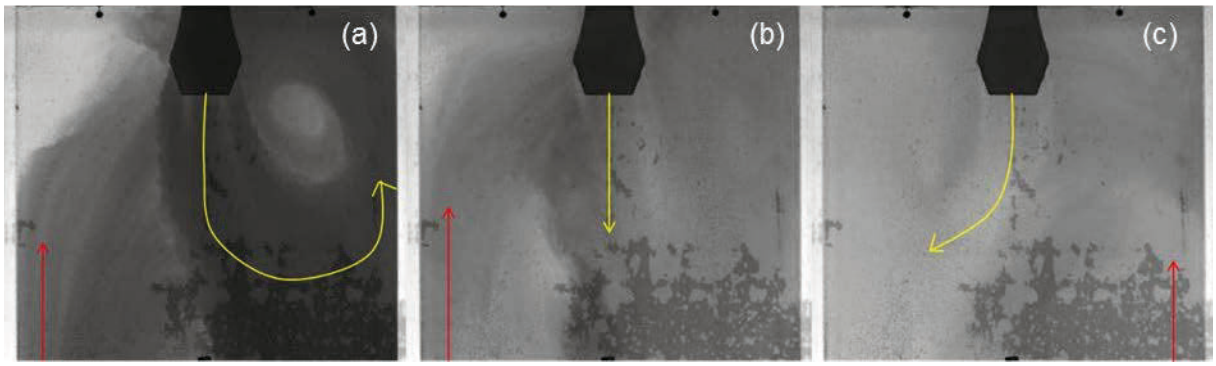

Figure 79. Results of case 2c for the SEN gap size 15 mm(a) time interval 12.5 (s), (b) time interval 8.13 (s), (c) time interval 11.88 (s) (Run4).

In Figure 80 the fifth run of case 2c for the SEN gap size 15mm can be seen. The jet flows to the left section of the mold and creates a vortex. A backflow at the right side of the mold is also present. This flow pattern is visible for 13.75 seconds and can be seen in Figure 80 (a). After 5.63 seconds the flow direction changes to straight downwards which can be seen in Figure 80 (b). A backflow at the left section of the mold can be observed. In Figure 80 (c) the jet changes its direction to the right section of the mold. The backflow at the left side of the mold is still present. This lasts for 11.88 seconds.

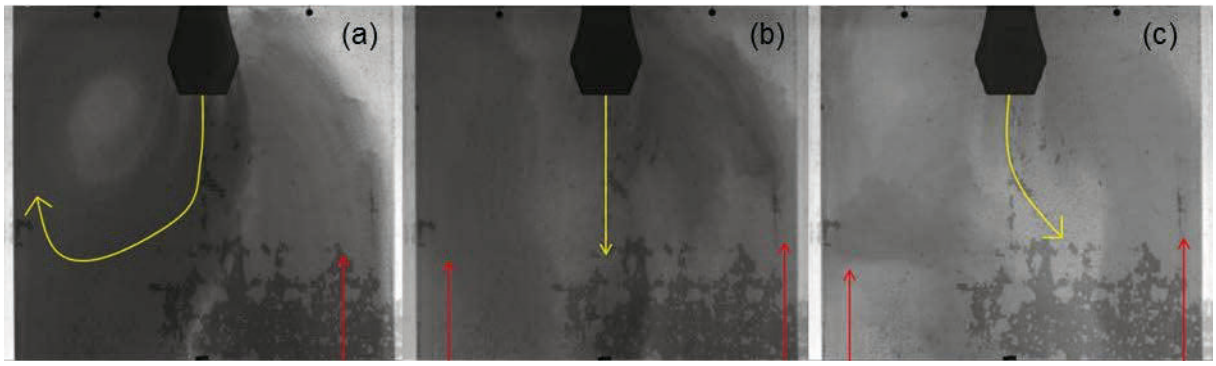

Figure 80. Results of case 2c for the SEN gap size 15 mm (a) time interval 13.75 (s), (b) time interval 5.63 (s), (c) time interval 11.88 (s) (Run5).

3.3.6 Case 2c SEN Gap Size 18 mm:

In Figure 81 results of the first run of case 2c for the SEN gap size 18 mm is seen. That case has the highest mass flow rate because of the SEN gap size of 18 mm and the casting speed of 3.4 m/min. Figure 81 (a) represents the first 15.33 seconds of this run. The jet flows to the left section of the mold and creates a vortex. During that time no dye is transported to the right section of the mold. In Figure 81 (b) the jet changes its direction to straight downwards and a backflow can be seen. The backflow creates a vortex which reaches the SEN and reaches the meniscus. This flow pattern is present for 11.47 seconds. The last 6.2 seconds of this run can be seen in Figure 81 (c). The jet flows to the right section of the mold. From the left bottom part of the mold a backflow is streaming upwards which influences the direction of the jet.

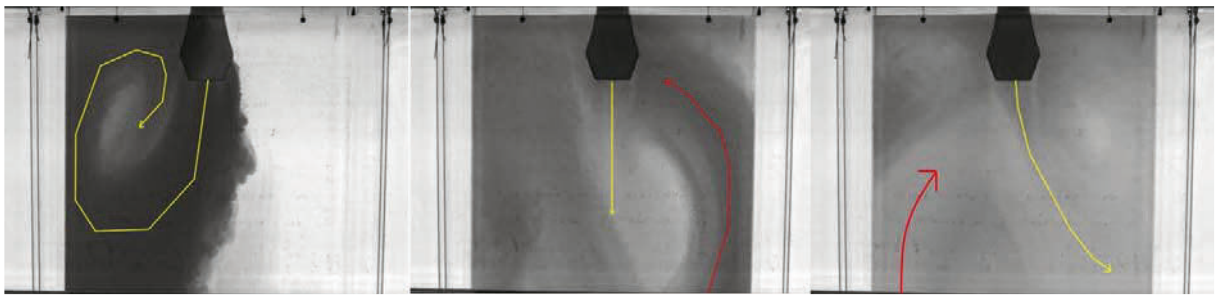

Figure 81. Results of case 2c for the SEN gap size 18 mm (a) time interval 15.33 (s), (b) time interval 11.47 (s), (c) time interval 6.2 (s) (Run1).

The jet of the second run flows slightly to the left section of the mold for 6.33 seconds (Figure 82 (a)). Afterwards the beam changes to a straight downwards flow which also generates a backflow at the left and right side of the jet (Figure 82 (b)). This flow pattern is present for 3.93 seconds. In Figure 82 (c) the beam changes its direction to the right which may is caused by the backflow streaming up from the bottom part of the mold. This flow behaviour is visible for 15.6 seconds. Another flow pattern can be seen for 5.2 seconds (Figure 82 (d). The jet flows straight downwards and causes also a backflow streaming up from the bottom of the mold. The last 1.93 seconds the direction is changing again to left section of the mold (Figure 82 (e)).

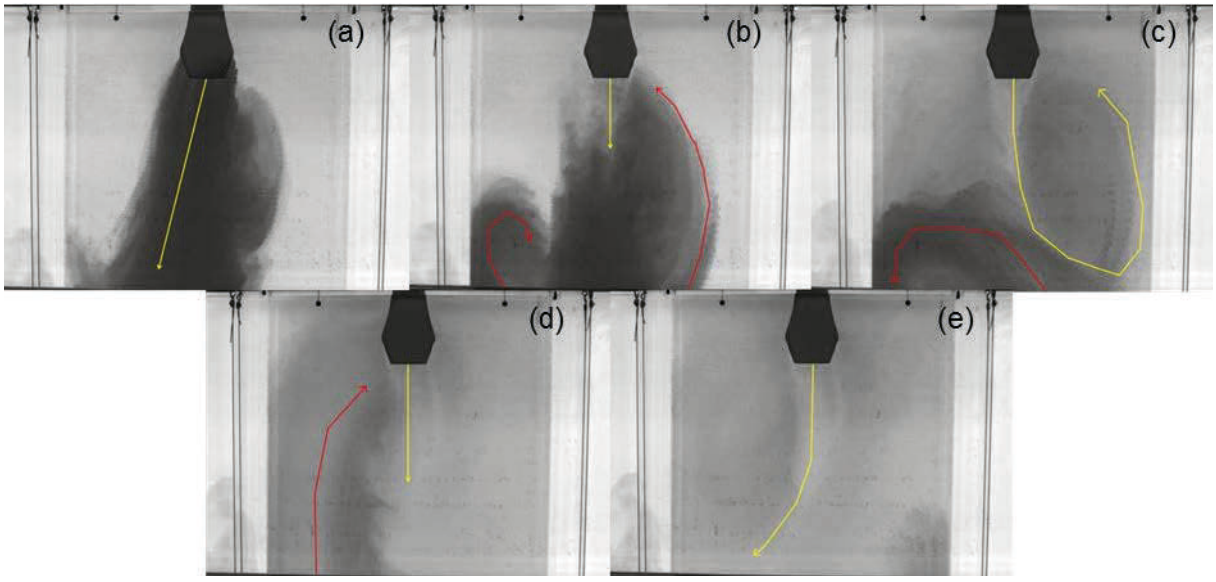

Figure 82. Results of case 2c for the SEN gap size 18 mm (a) time interval 6.33 (s), (b) time interval 3.93 (s), (c) time interval 15.6 (s), (d) time interval 5.2 (s), € time interval 1.93 (s) (Run2).

The third run of case 2c for the SEN gap size 18 mm can be seen in Figure 83. The jet flows to the right section of the mold. A backflow is streaming up from the right bottom part of the mold. This flow pattern can be seen for 10.93 seconds (Figure 83 (a)). Afterwards the jet is streaming straight downwards for 4.46 seconds (Figure 83 (b)). A backflow at both sides at the mold walls can be seen. The backflow from the left bottom part influences the jet and that is why the jet changes its direction to the right section of the mold (Figure 83 (c)). This flow

behaviour is present for 14.33 seconds. The last recording 3.27 seconds the jet flows straight downwards (Figure 83 (d)).

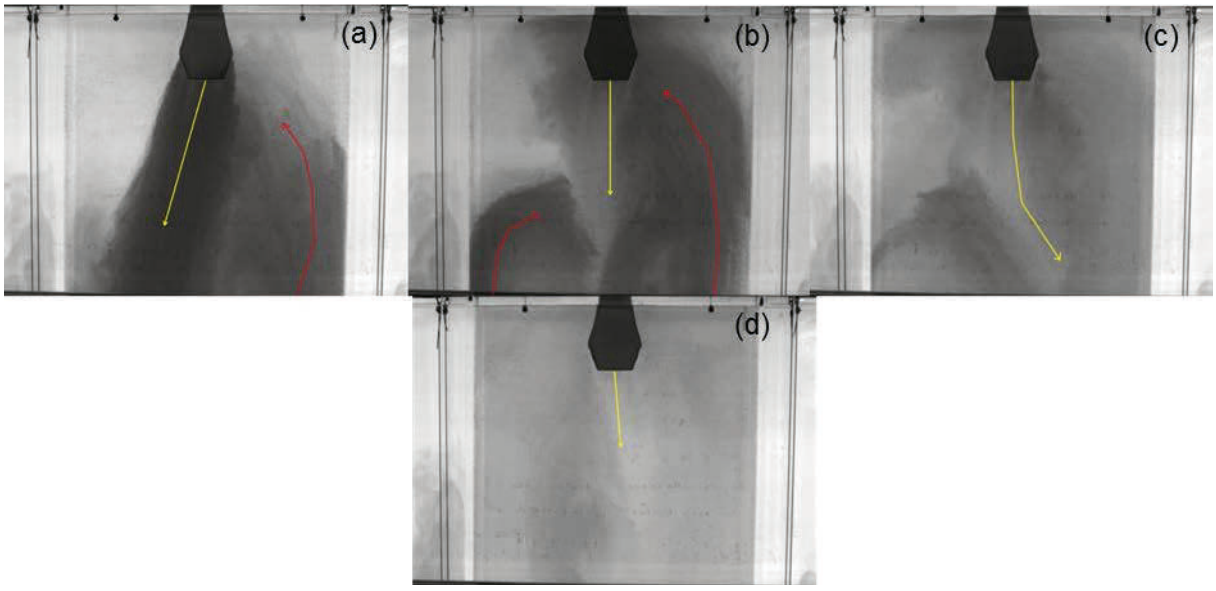

Figure 83. Results of case 2c for the SEN gap size 18 mm (a) time interval 10.93 (s), (b) time interval 4.46 (s), (c) time interval 14.33 (s), (d) time interval 3.27 (s) (Run3).

The fourth run of case 3c for the SEN gap 18 mm can be seen in Figure 84. The jet flows to the right section of the mold and creates a vortex. This flow behaviour is visible for 10.87 seconds (Figure 84 (a)). Afterwards the jet flows straight downwards again and from the left bottom of the mold a backflow is streaming upwards. This flow pattern is present for 6.87 seconds (Figure 84 (b)). The last 15.27 seconds the beam changes its direction again. The right upstreaming backflow influences the jet. That is the reason why the jet changes its flow direction to the left section of the mold (Figure 84 (c)).

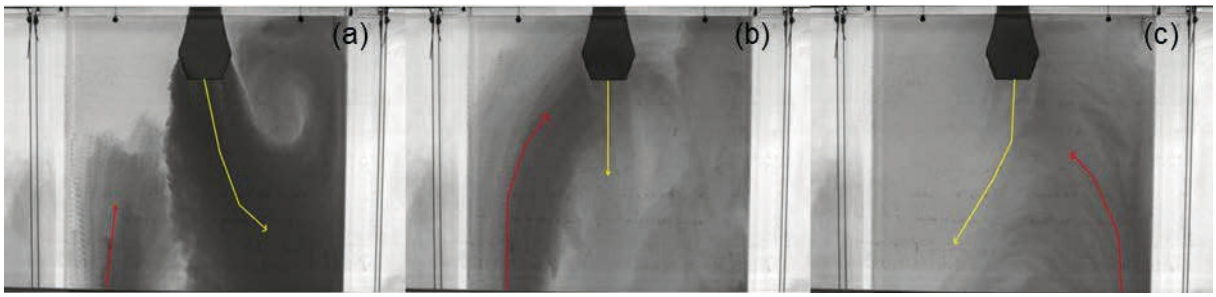

Figure 84. Results of case 2c for the SEN gap size 18 mm (a) time interval 10.87 (s), (b) time interval 6.87 (s), (c) time interval 15.27 (s) (Run4).

The fifth run with the same setting can be seen in Figure 85. The jet flows for 15.8 seconds to the left section of the mold (Figure 85 (a)). At the left mold wall a vortex is developed. Also a backflow from the right bottom part of the mold is streaming up. Afterward the jet flows straight downwards for another 2.2 seconds. The backflow from the right bottom part of the mold is still present (Figure 85 (b)). The jet flows to the right section of the mold for the last 15 seconds of recording time. At this period no significant backflow can be seen Figure 85 (c).

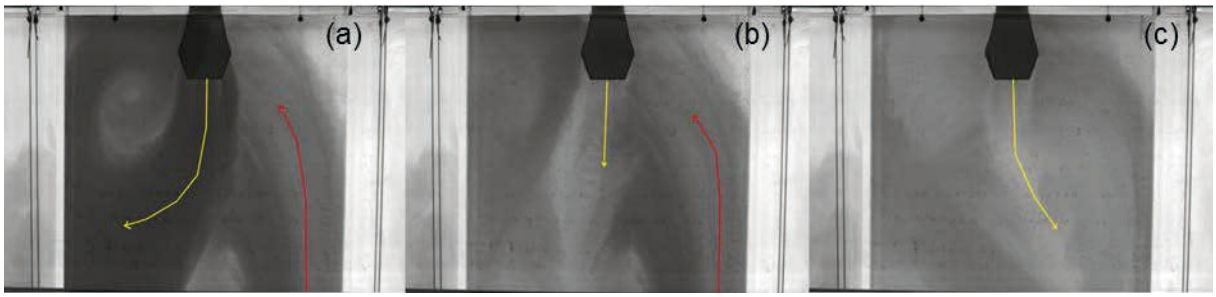

Figure 85. Results of case 2c for the SEN gap size 18 mm (a) time interval 15.8 (s), (b) time interval 2.2 (s), (c) time interval 15.0 (s) (Run5).

3.3.7 Case 3 SEN Gap Size 12 mm:

In Figure 86 the results of case 2 for the SEN gap size 12 mm can be seen. The jet flows to the right section of the mold as seen in Figure 86 (a). The development of the vortex at the right mold wall is influenced by the backflow and the jet. Another backflow at the left mold

wall is also present. This period takes 20.63 seconds until it changes its direction to straight downwards for the last 10.63 seconds. The two backflows at both mold walls are still present at this period (Figure 86 (b)).

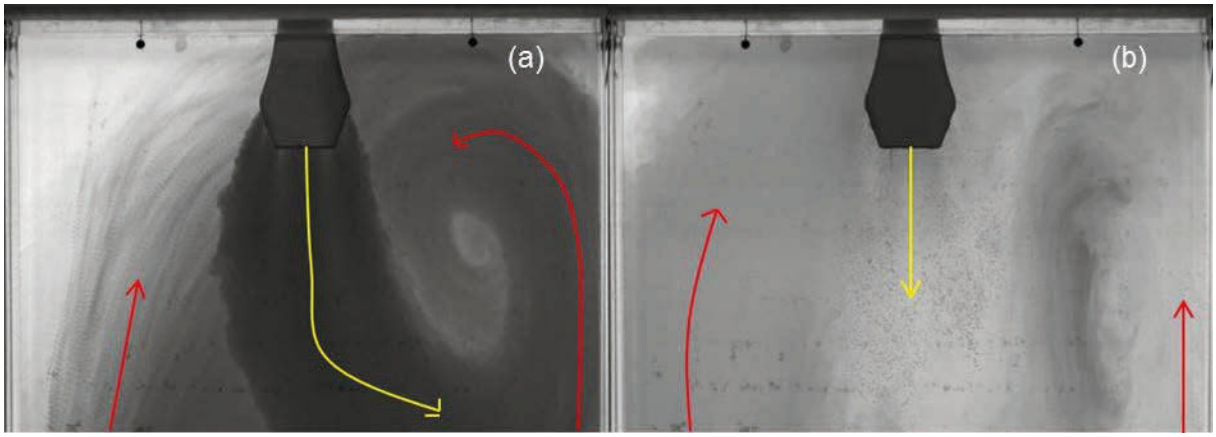

Figure 86. Results of case 3 for the SEN gap size 12 mm ((a) time interval 20.63 (s), (b) time interval 10.63 (s) (Run1).

The second run starts the same way as the first run with the same settings. The jet flows to the right section of the mold. At this area a vortex is created. A backflow is streaming up from the bottom part of the mold (Figure 87 (a)). This flow pattern can be observed for 15 seconds. Figure 87 (b) represents the last 16.25 seconds of recording time. During that period two backflows are present. At the whole recording time no dye was transported to the top left corner.

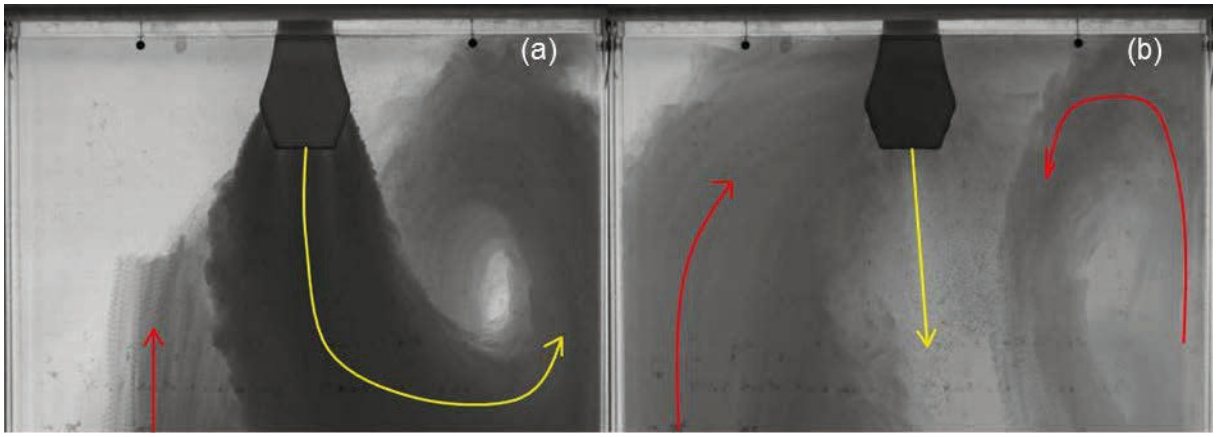

Figure 87. Results of case 3 for the SEN gap size 12 mm (a) time interval 15.0 (s), (b) time interval 16.25 (s) (Run2).

In Figure 88 the results of the third run of case 3 for the SEN gap size 12 mm can be seen. The jet flows to the left section of the mold and creates a large vortex. Almost the whole left area is mixed with the dye (Figure 88 (a)). At the right section of the mold a backflow is coming up. This flow pattern is present for 21.45 seconds. After that time the jet changes its flow direction to straight downwards. A backflow at the right side of the mold is still present and at the top right corner the concentration of dye is very low. The last period takes 10 seconds (Figure 88 (b)).

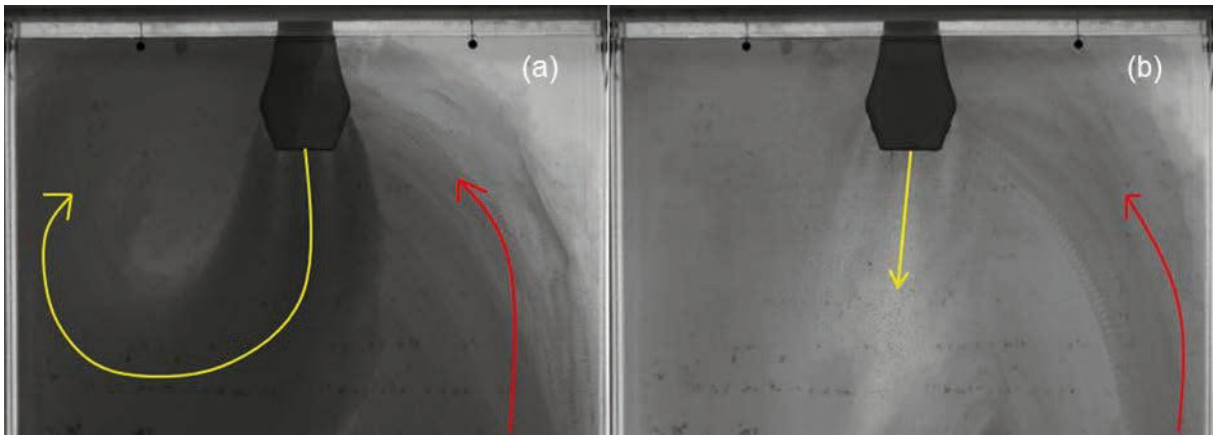

Figure 88. Results of case 3 for the SEN gap size 12 mm (a) time interval 21.45 (s), (b) time interval 10.0 (s) (Run3).

At the beginning of the fourth run a jet flowing to the right section of the mold can be seen (Figure 89 (a)). A backflow from the right bottom part of the mold is streaming up This flow

period takes 12 seconds. Afterwards the jet is streaming straight downwards. Backflows at both sides at the mold walls are visible. This flow pattern is seen 19.25 seconds (Figure 89 (b)).

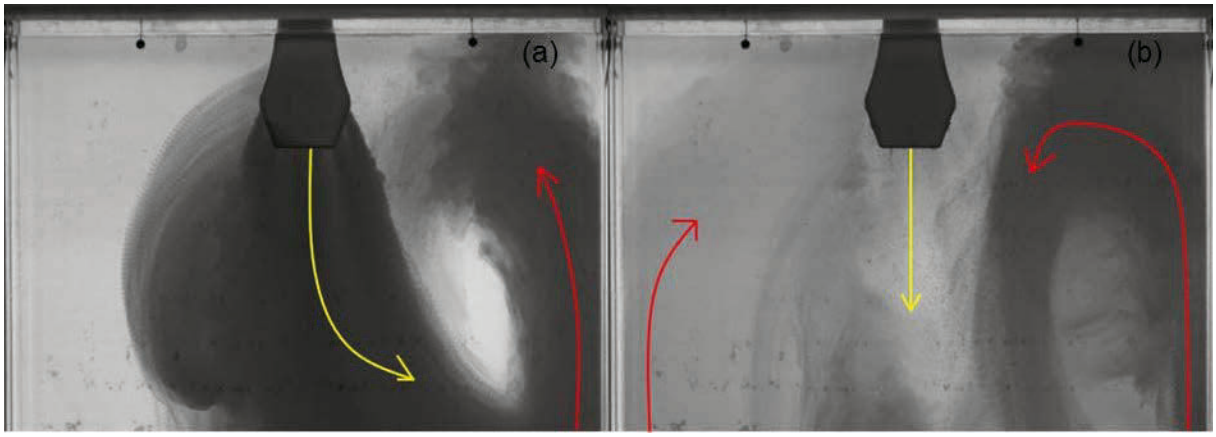

Figure 89. Results of case 3 for the SEN gap size 12 mm (a) time interval 12.0 (s), (b) time interval 19.25 (s) (Run4).

The fifth run of case 3 for the SEN gap size 12 mm shows compared to the other runs differences in the flow pattern. The flow behaviour is stable during the whole recording time (Figure 90). The jet flows to the right section of the mold and creates a vortex. At the left side of the mold a backflow is streaming up from the bottom part of the mold. No dye is transported to the top left corner of the mold.

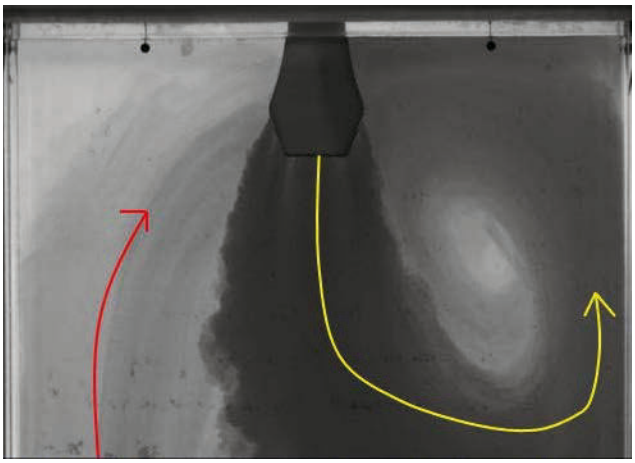

Figure 90. Results of case 3 for the SEN gap size 12 mm (Run5).

3.3.8 Case 3 SEN Gap Size 18 mm:

The first run of case 3 for the SEN gap size 18 mm can be seen in Figure 91. The jet streams straight downwards. A backflow from the right bottom part of the mold is coming up (Figure 91 (a)). At the left side of the jet some dye is recognizable which may come from some backflow at this section of the mold. This flow pattern is visible for 19.44 seconds. Afterwards the jet changes its direction to the left section of the mold (Figure 91 (b)). At the right area of the mold the backflow spread out further. During the whole recording time no dye is transported to the right top corner.

Figure 91. Results of case 3 for the SEN gap size 18 mm (a) time interval 19.44 (s), (b) time interval 13.56 (s) (Run1).

The second with the same setting starts with a straight downward flow which takes 10.19 seconds and can be seen in Figure 92 (a). The backflow is coming up from the left bottom part of the mold.

In Figure 92 (b) the change of the flow direction to the left section of the mold can be seen. It last for 21.06 seconds. Backflows at both sides of the walls are recognizable. During recording time no backflow is transported to the right corner of the mold.

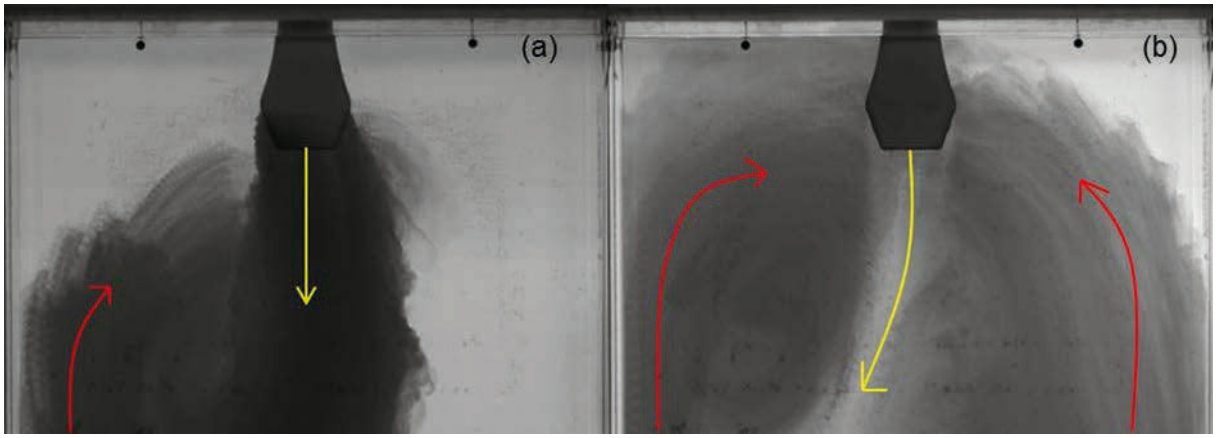

Figure 92. Results of case 3 for the SEN gap size 18 mm (a) time interval 10.19 (s), (b) time interval 21.06 (s) (Run2).

The results of run 3 of case 3 for the SEN gap size 18 mm show stable flow behaviour of the jet. A backflow at the right section of the mold is built by the down streaming jet and the upstreaming backflow at the right side at the mold wall. A backflow at the left section of the mold is also present and can be seen in Figure 93. After recording time it is recognizable that the dye was not transported to the whole area of the mold.

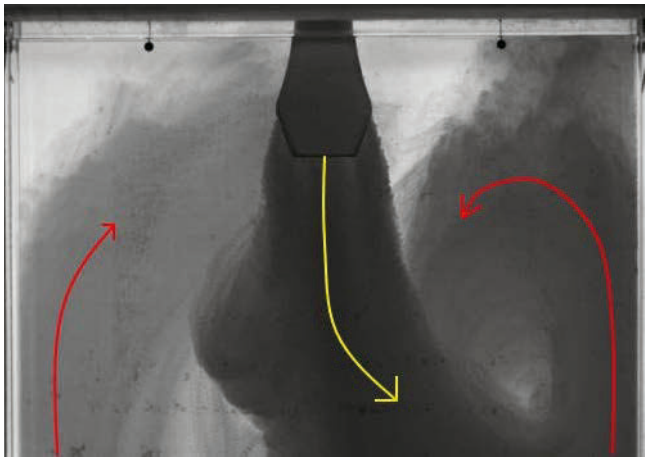

Figure 93. Results of case 3 for the SEN gap size 18 mm (Run3).

The jet of the fourth run streams to the right section of the mold. Also a backflow is streaming up at this area. This flow pattern is present for 9.56 seconds and shown in Figure 94 (a). During that period no dye is transported to the left section of the mold.

The jet flows straight downwards for the last 21.69 seconds of recording time (Figure 94 (b)). Backflow at the left and at the right mold walls appears. Almost no dye is transported to the top left corner during the whole recording time.

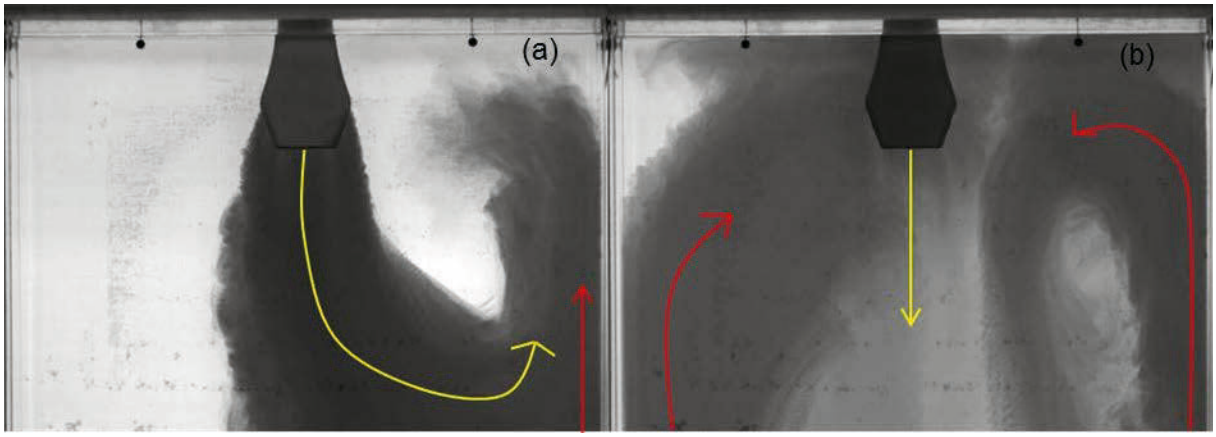

Figure 94. Results of case 3 for the SEN gap size 18 mm (a) time interval 9.56 (s), (b) time interval 21.69 (s) (Run4).

Figure 95 represents the last run of case 3 for the SEN gap size 18 mm. The flow pattern is stable during recording time. The jet streams straight downwards. Backflow at the right and the left sections of the mold are visible. During recording time no dye was transported to the top left corner of the mold.

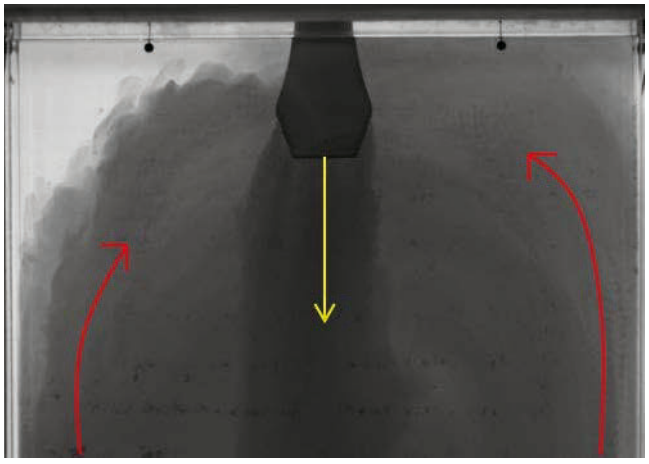

Figure 95. Results of case 3 for the SEN gap size 18 mm (Run5)

Unstable flow should be avoided during the process in real plants. Because of this flow pattern at only one section of the mold new melt, water is transported, which can lead to an undercooled zone inside the mold because of inappropriate heat/ mass transportation. Also the quality of the finished products cannot be guarantee at a certain level.

3.4 Comparison of the Submeniscus Velocity

The submeniscus velocity is measured for all cases and SEN gap sizes. The measurement was done before dye injection. Two paddles underneath the surface were fixed at the left and right sight of the SEN (Figure 96).

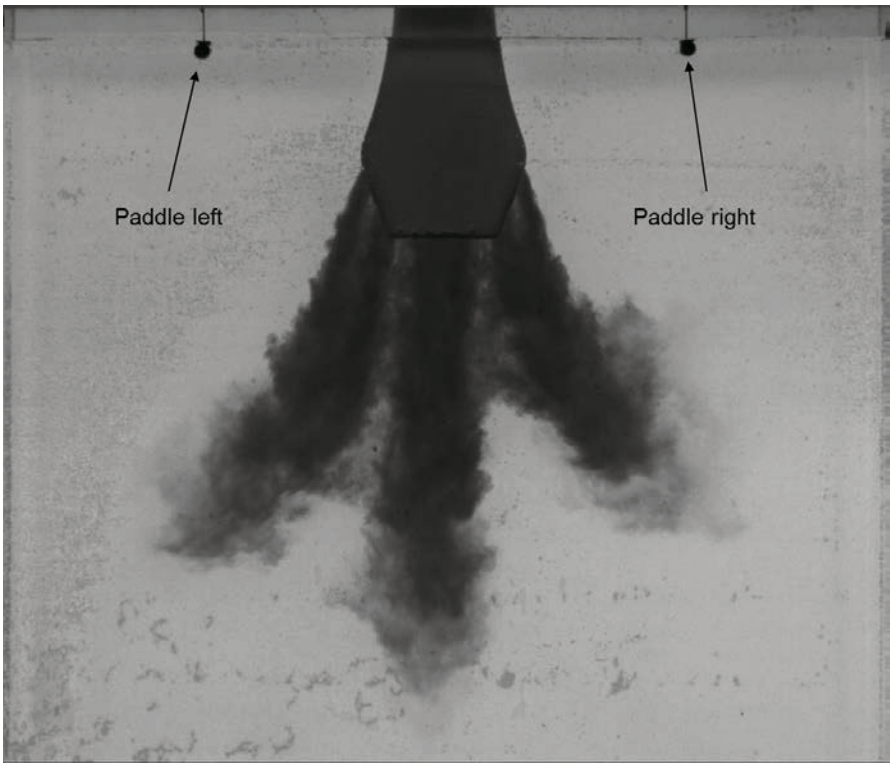

Figure 96. Schematic of submeniscus velocoty measurement.

The paddles measure the velocity for 30 minutes with a time step of 0.1 seconds. The software used is programed by RHI. The collected data are copied to Microsoft Excel.

High meniscus velocities indicate high wave fluctuations, which increase the probability of slag entrapments. A very low submeniscus velocity can be explained for example by a single down streaming jet which does not create an upstreaming vortex.

First step was to transform all data into absolute values and to calculate the average of the data of the left and right paddles by using equation 3 and 4.

$$u_{avg}^{L,R} = \frac{\Sigma |u_i|}{n} \tag{3}$$

$$u_{avg} = \frac{u_{avg}^{L} + u_{avg}^{R}}{2} \tag{4}$$

3.4.1 Case 1:

In Figure 97 the average of the measured velocities of the left and right paddles of case 1 for all gap sizes can be seen. It is recognizable that there is a difference in velocities between the left and the right section of the mold. Except by using the SEN with the gap size of 8 mm. For that case the submeniscus velocity seems to be equal.

An obviously significant decreasing of the submeniscus velocity by using the SEN with the 18 mm gap can be seen.

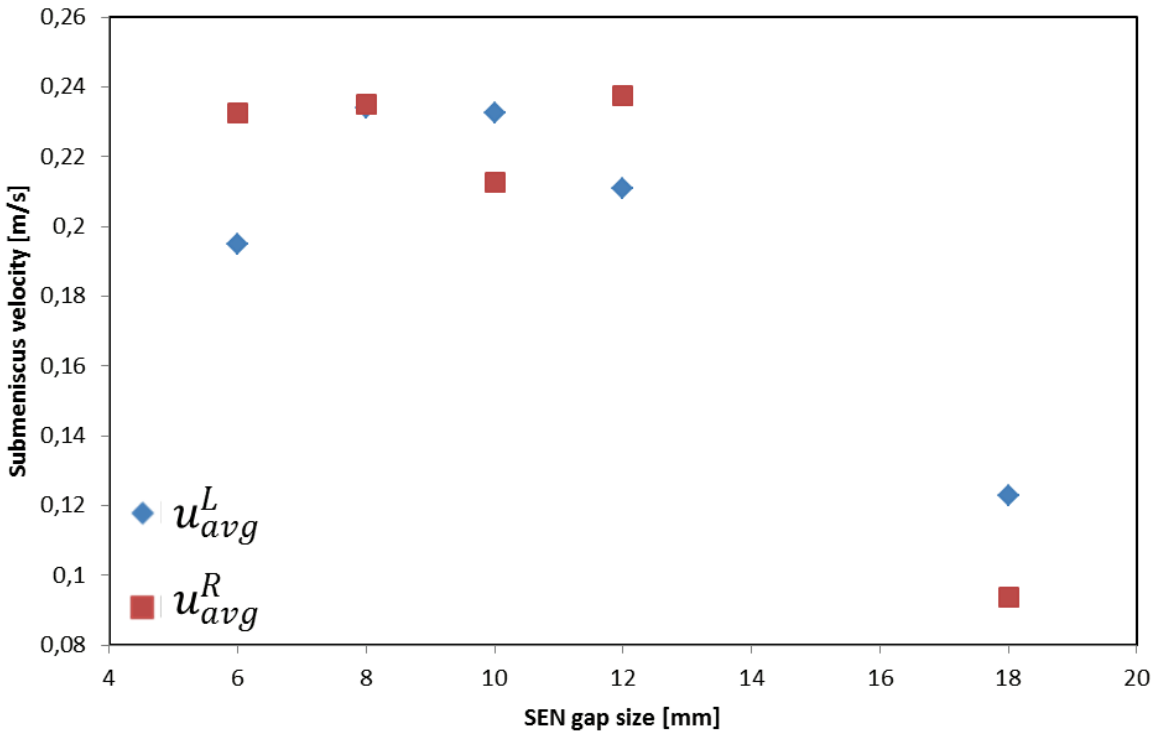

Figure 97. Average submeniscus velocity of case 1.

In Figure 98 the total average of the velocities for all gap sizes of case 1 is seen. In this diagram it is clearly seen that by using the SEN with 18mm gap size the submeniscus velocity is decreased by almost 50%.

For SEN gap sizes 6 to 12 stable flow is achieved which industry is trying to obtain during production. Unstable flow is not reliable for the production process.

The flow pattern for the SEN gap sizes 12, 15 and 18 mm are unstable. For these gap sizes the velocities are lower compared to the other ones. Otherwise the measured velocities are very similar for the left and right paddles.

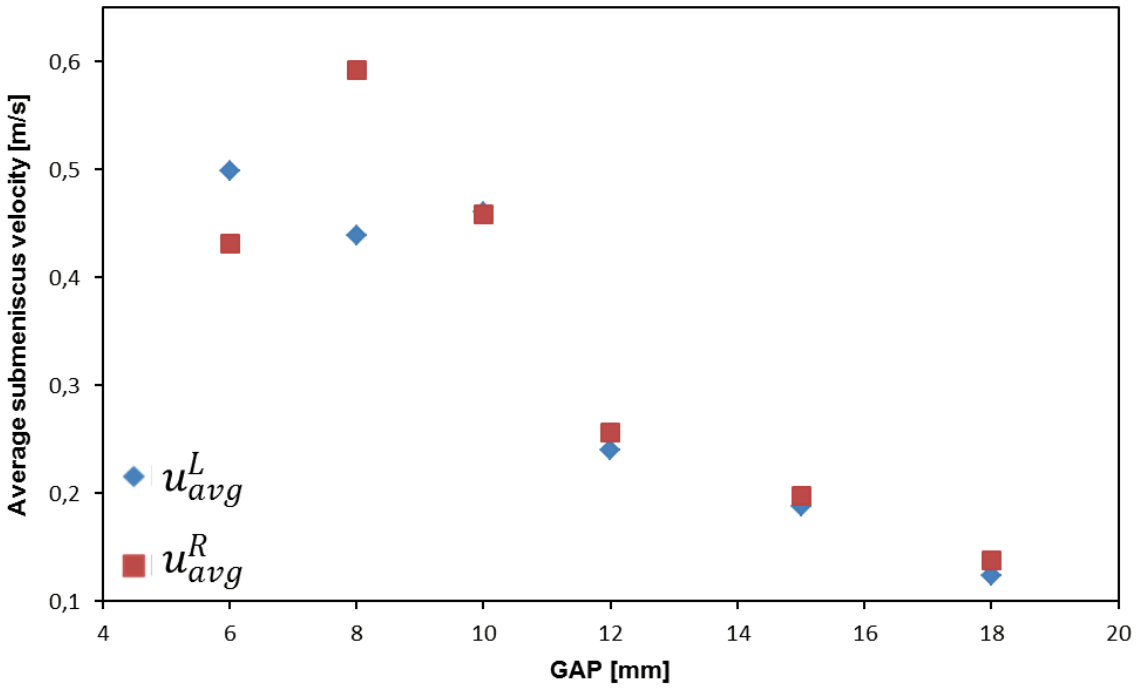

Figure 99. Average submeniscus velocity of case 2c.

In Figure 100 the total average submeniscus velocities can be seen. As described before the submeniscus velocities are decreasing by increasing the gap sizes. The velocities for the SEN gap size 6 and 10 are almost at the same level. The highest value can be seen for the SEN gap size of 8 mm. It seems that the velocities for the SEN gap 12 decreases linear to the velocity for the SEN gap size 18 mm.

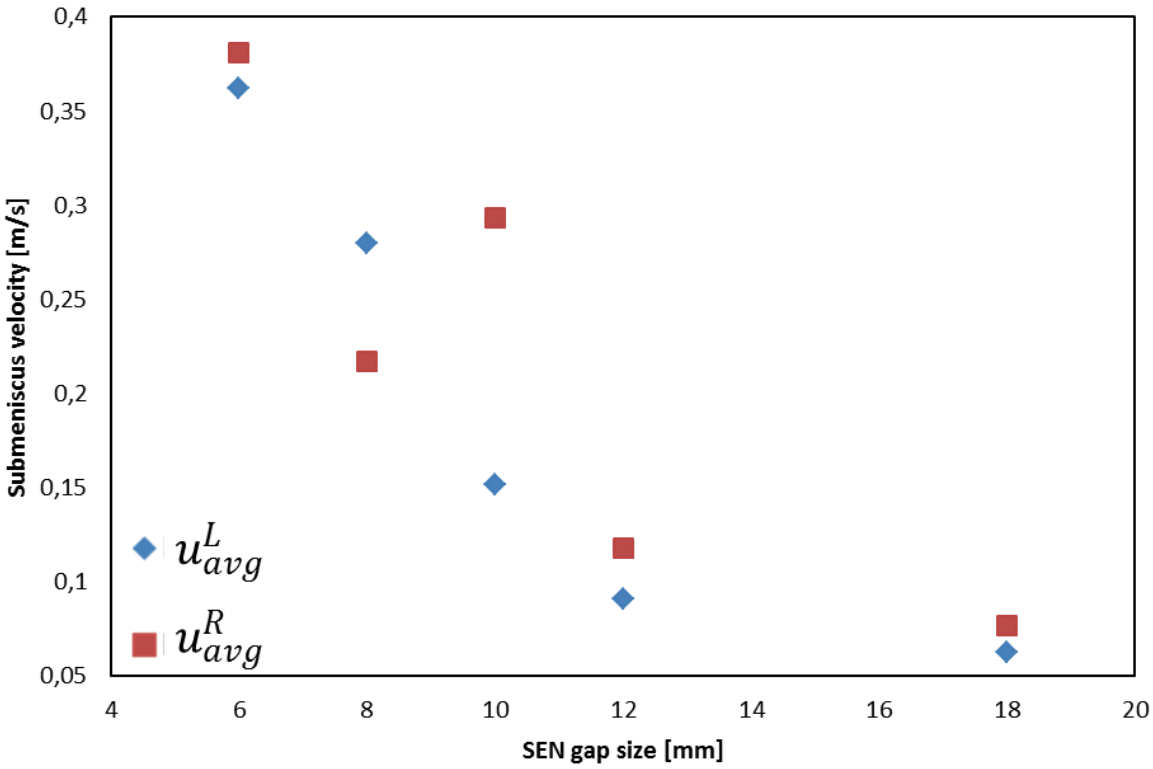

Figure 101. Average submeniscus velocity of case 3.

In Figure 102 the total average of the submeniscus velocity can be seen. Compared to the other cases the velocities decreases faster by using SEN with larger gaps. The highest value is measured for the SEN gap size 6 mm and the lowest for SEN gap size 18 mm. The flow pattern for 6 mm is stable and transient for the SEN gap sizes 8 and 10 mm. Unstable flow behaviour can be recognized for the gap size 12 and 18 mm.

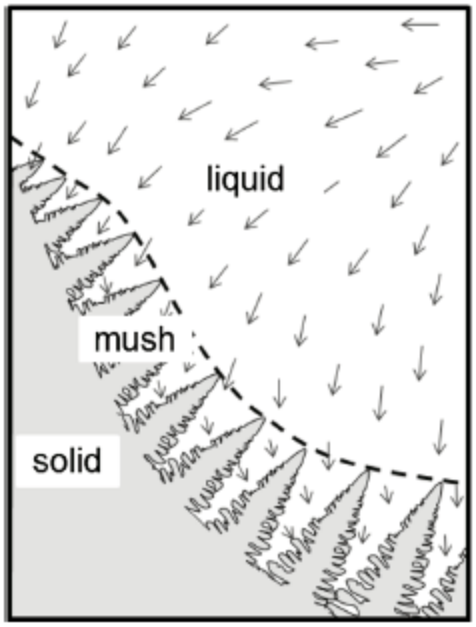

Figure 103. Schematic of the solidifying mushy zone. [34]

This model was later extended by including the turbulence model and applied to study the solidification and formation of macrosegregation under the influence of forced convection. [34]

The motion of the solid shell was assumed to be parallel and the moving velocity is constant everywhere and equal to the casting velocity by conventional continuous casting. These assumptions do not apply to TSC, where the strand shell is subject to continuous deformation due to the funnel type mold. Despite the same consideration of the experimentally determined heat flux, the use of the funnel – type mold must be treated properly, because it guides the motion of the solid shell of the strand and influences the melt flow inside the strand. [34]

4.1 Simulation Model

For simulating solidification and turbulence flow an enthalpy – based mixture solidification model has to be applied, done by Vakrushev A.[34] This mixture combines a liquid and solid phase. They are quantified by their volume fractions, f_l and f_s and $f_f + f_s = 1$.The morphology of the solid phase is usually dendritic but in that case the dendritic solid phase is

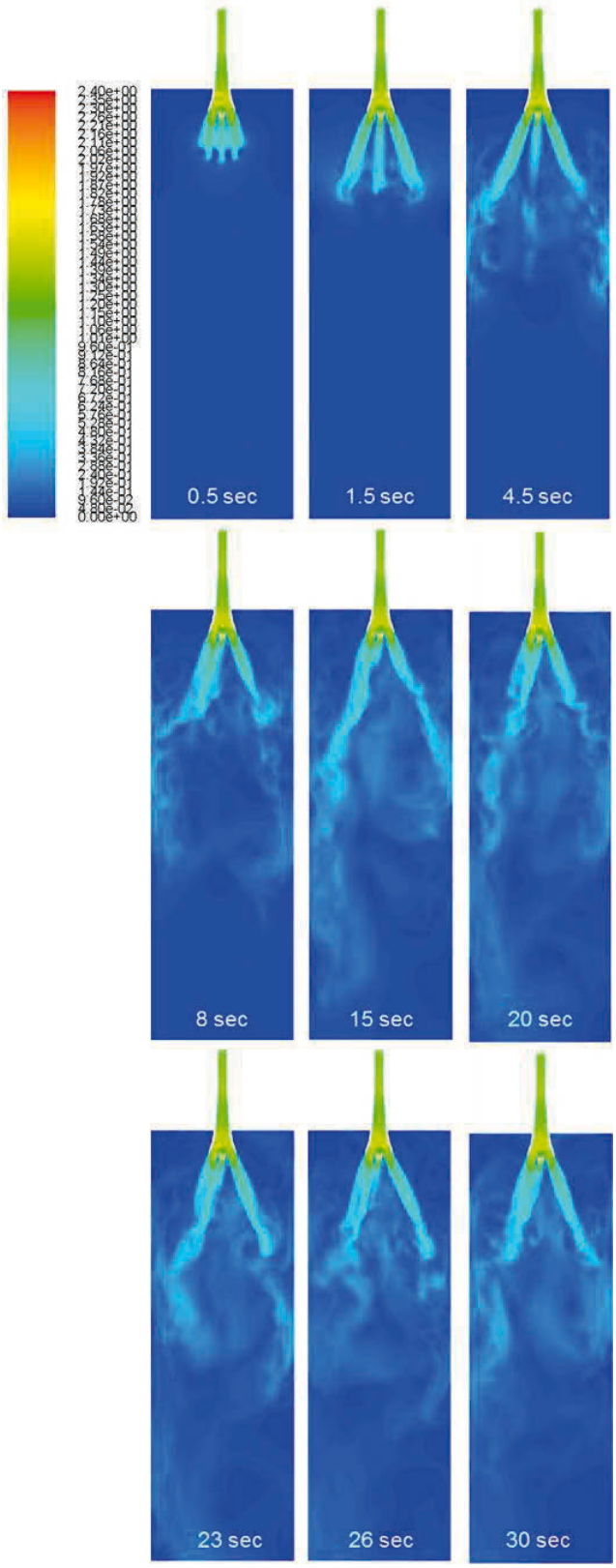

Figure 106. Evolution of the flow with simulated with 0.7 million node points (casting speed 3.4 m/min).

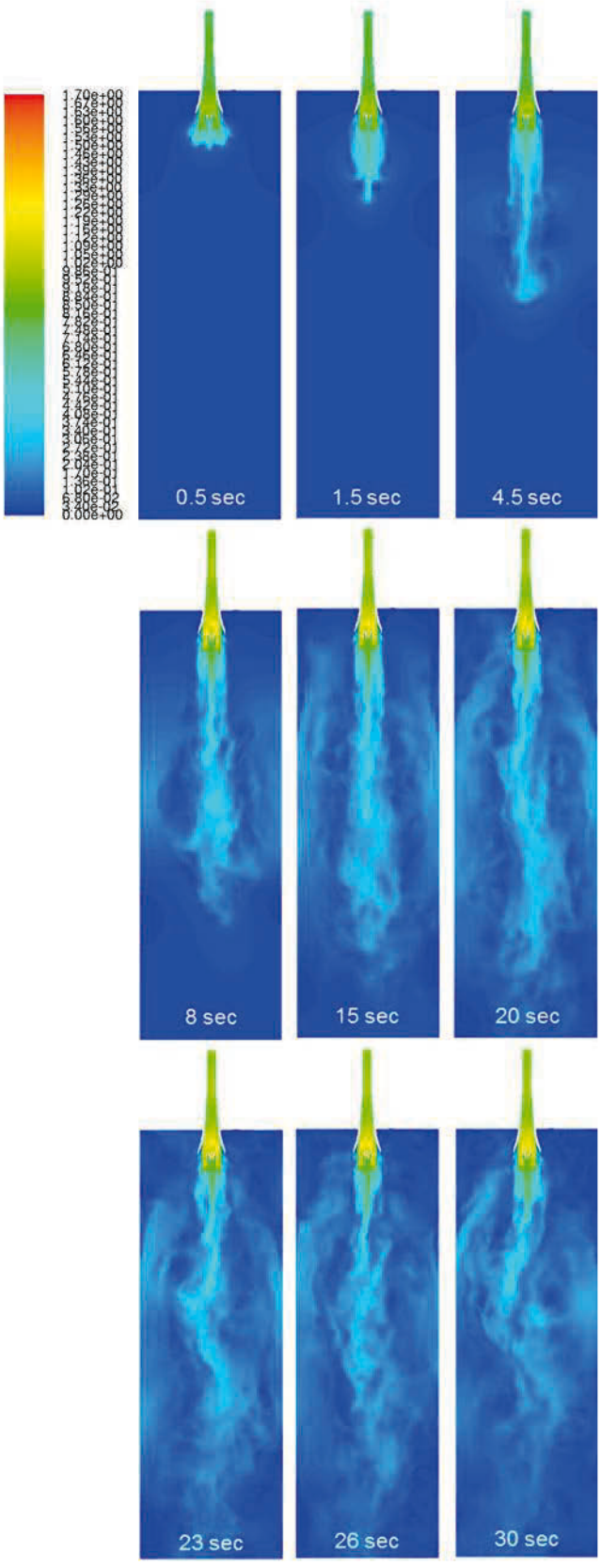

Figure 107. Evolution of the flow with simulated with 1.8 million nodes (casting speed 2.4 m/min).

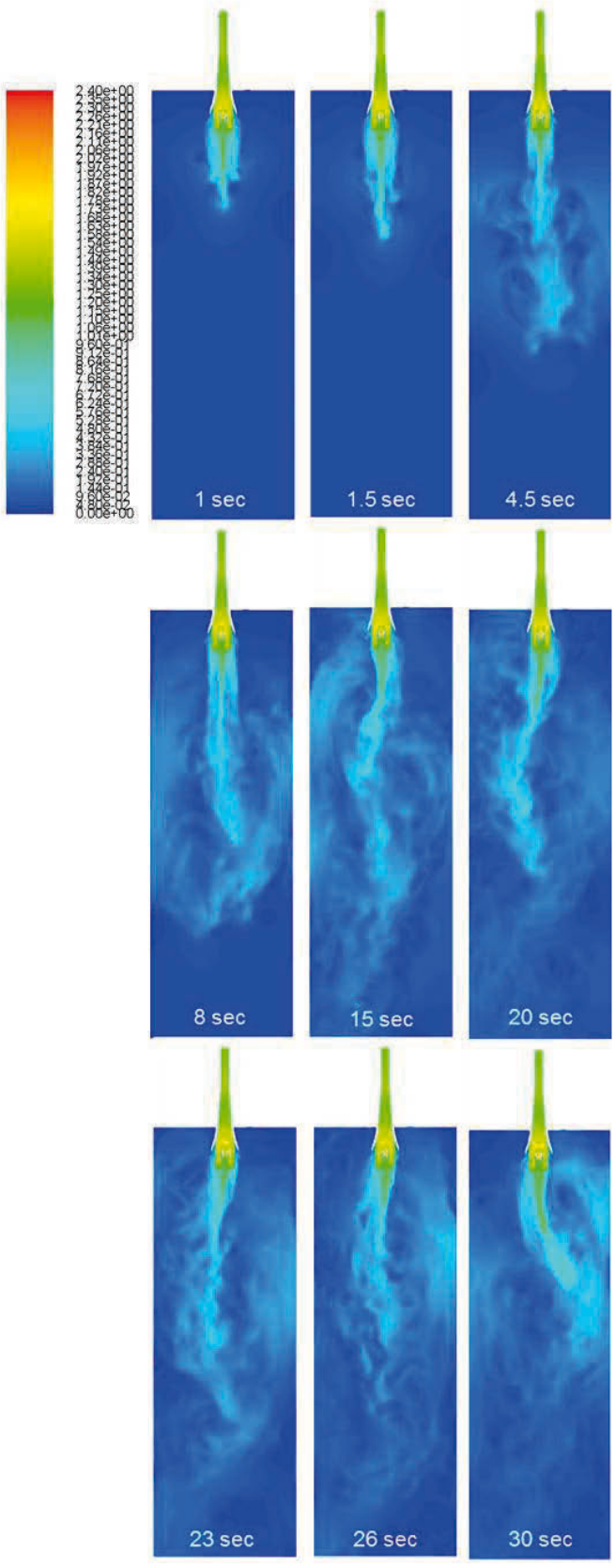

Figure 108. Evolution of the flow with simulated with 1.8 million nodes (casting speed 3.4 m/min).

4.4 Comparison with Experiment

To make a comparison between the results of water model experiment and the simulation a unify time scale has to be fixed. The moment of the dye injection is the starting point because before injection it is impossible to make any flow pattern at the water model experiment visible.

4.5 0.7 Million Node Points with 3.4 m/min Casting Speed

At the beginning of the experiment and simulation the results seems to be very similar. In Figure 109 (a) the out streaming dye is visible. Figure 109 (b) represents the results of the simulation at the same moment. At this moment it seems to be that one down streaming jet will be developed.

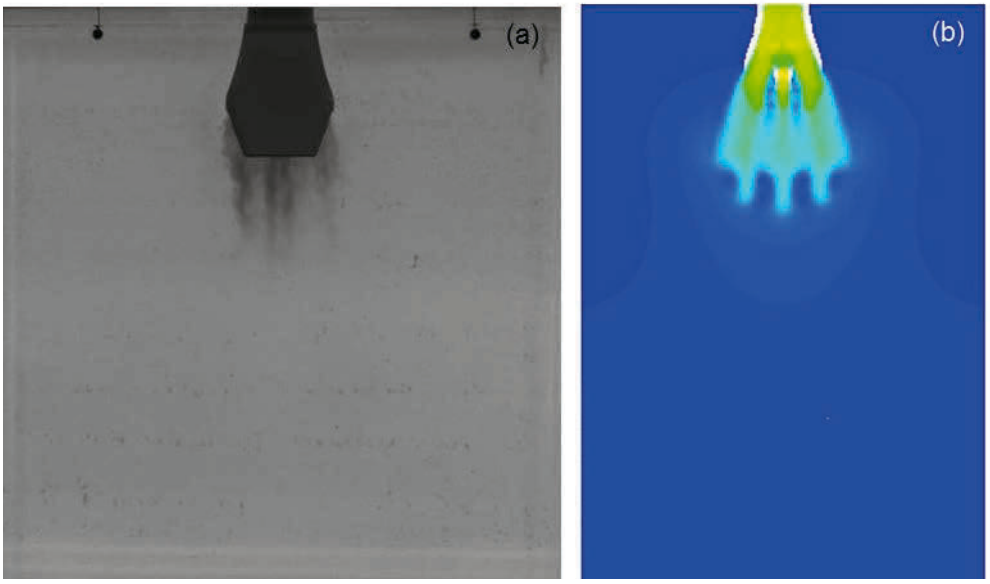

Figure 109. Comparison of experiment (case 2c) and simulation after 0.5 seconds of dye injection.

The results after 3 seconds can be seen in Figure 110. In Figure 110 (a) the down streaming single jet of the water model experiment can be seen. It is recognisable that the jet flows to the left section of the mold and is creating a vortex. The backflow reaches the meniscus level. Figure 110 (b) represents the results of the simulation. The differences in results are obvious. Compared to the results of the water model experiments are in the

simulation results three jets present at this time point. The right jet reaches deeper section of the mold at the left one. Vortices are built at the end of all three jets and create a backflow.

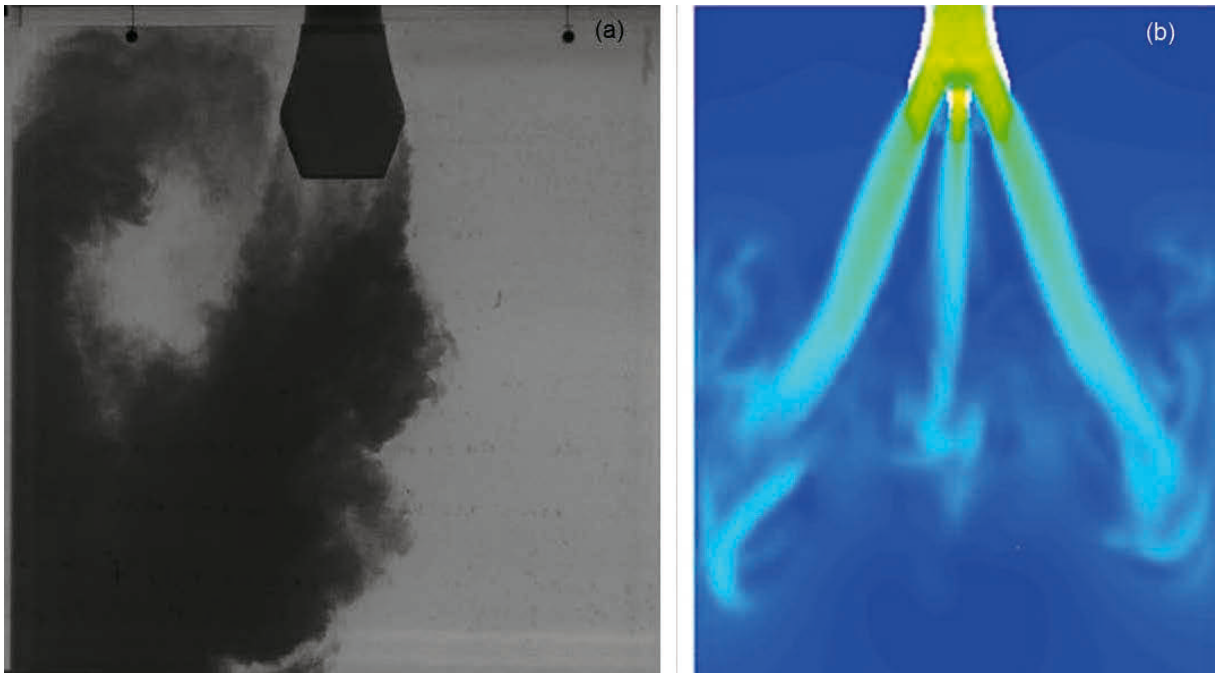

Figure 110. Comparison of experiment (case 2c) and simulation after 3 seconds of dye injection.

Figure 111 summarizes the results after 15 seconds of dye injection. The results of the water model experiment Figure 111 (a) demonstrate a single straight down streaming jet. Backflows at the left and right mold walls are present. The backflow at the left section of the mold wall reaches the meniscus level while the right one seems to flow in direction of the SEN.

The simulation result Figure 111 (b) shows that just 2 jets are present. The middle jet gets connected with the jet which stream out of the two left ports. Backflows are at both mold walls present.

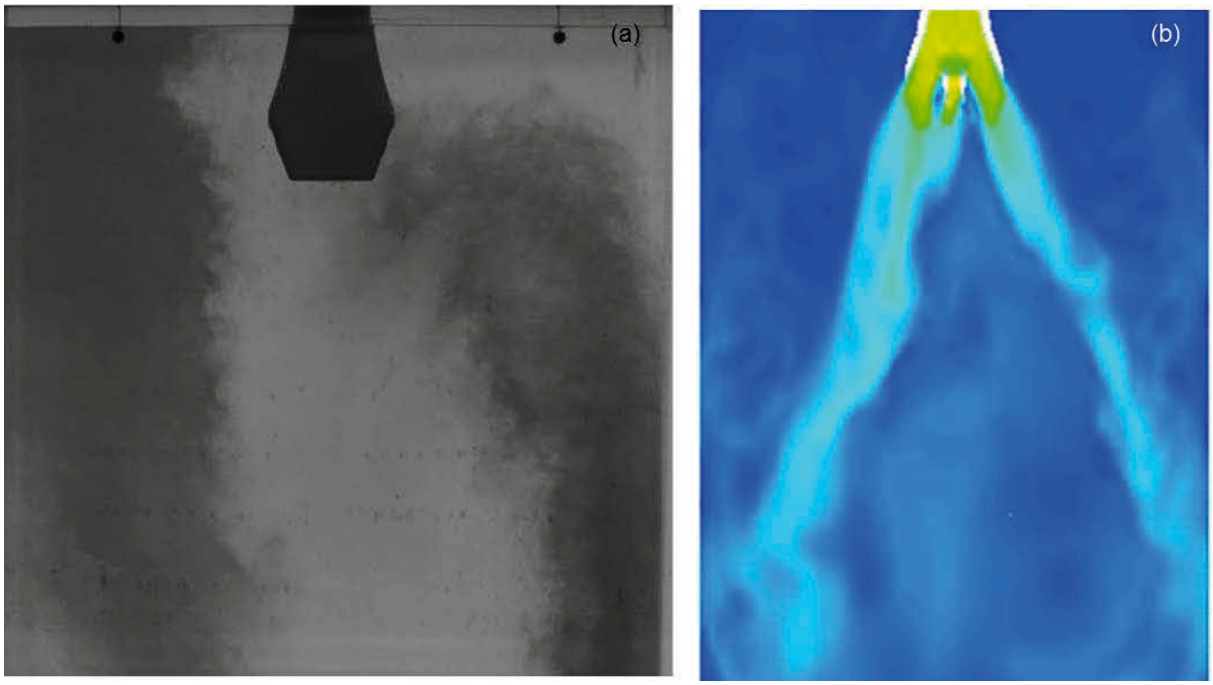

Figure 111. Comparison of experiment (case 2c) and simulation after 15 seconds of dye injection.

Figure 112 represent the results of water model experiment and the simulation after 25 seconds of dye injection, which is almost the end of recording time of the experiment. The photograph of the water model still shows a single jet flow pattern and backflows at the left and right side of the walls (Figure 112(a)).

The result of the simulation still shows two out coming jets (Figure 112 (b)). The middle jet is still connected with the jet out coming of the left ports. The areas below the jet seems to be very turbulent and backflows and vortices are developed. At that moment no flow reaches the top left corner of the mold.

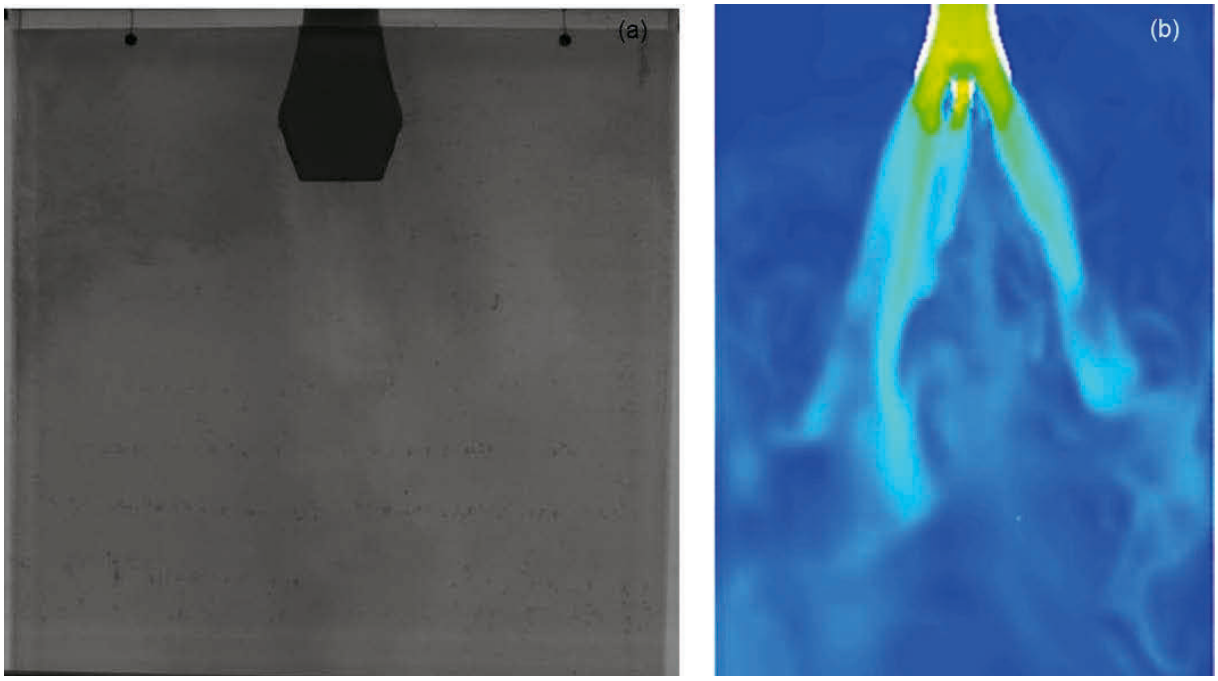

Figure 112. Comparison of experiment (case 2c) and simulation after 25 seconds of dye injection.

The results of the simulation with 0.7 million node points deliver different results compared to the experiment. It leads to the conclusion that the enmeshment has to be refined. The results from the simulation are not usable to make a qualitative statement of the flow behaviour.

4.6 1.8 Million Node Points with Casting Speed 2.4 m/min

In that case the enmeshment is finer and the casting speed is reduced to 2.4 m/s. The number of nodes increases from 0.7 to 1.8 million.

In the early stage the results look quite similar (Figure 113). In that period it seems that one straight down streaming jet will develop.

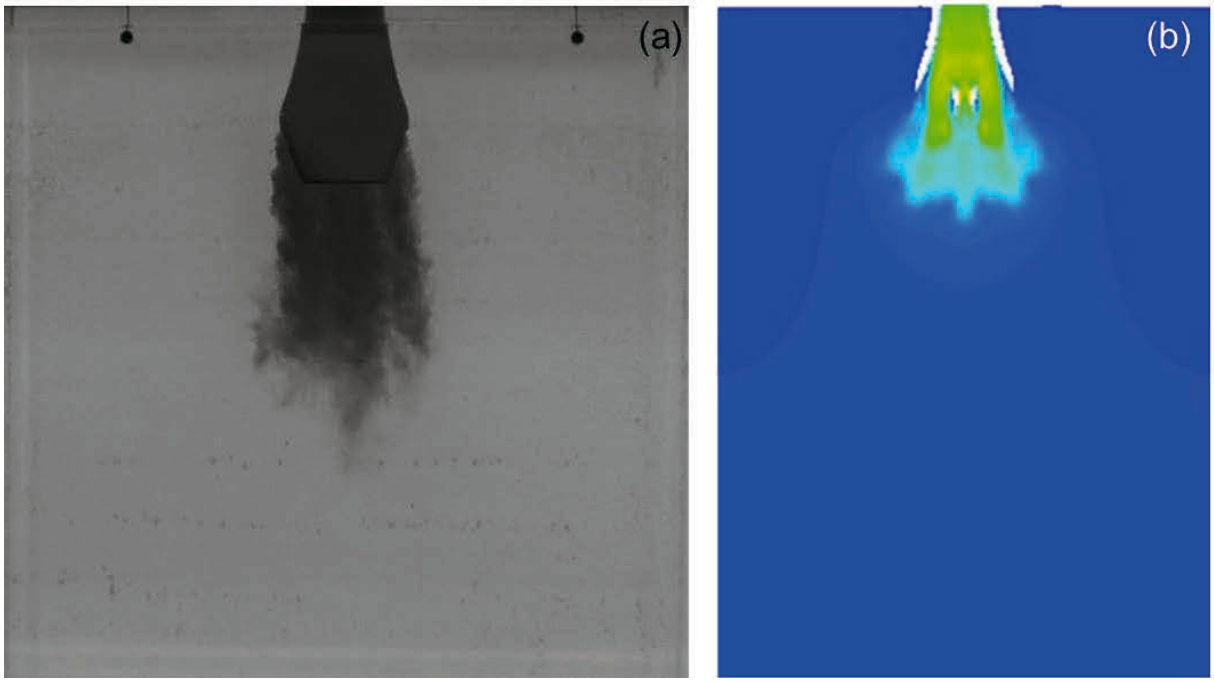

Figure 113. Comparison of experiment (case 2b) and simulation after 0.5 seconds of dye injection.

Figure 114 represents the results for the dye injection after 3 seconds. In the results of the water model experiment Figure 114 (a) and the simulation Figure 114 (b) one down streaming jet is visible. At that moment no backflow or vortices are created.

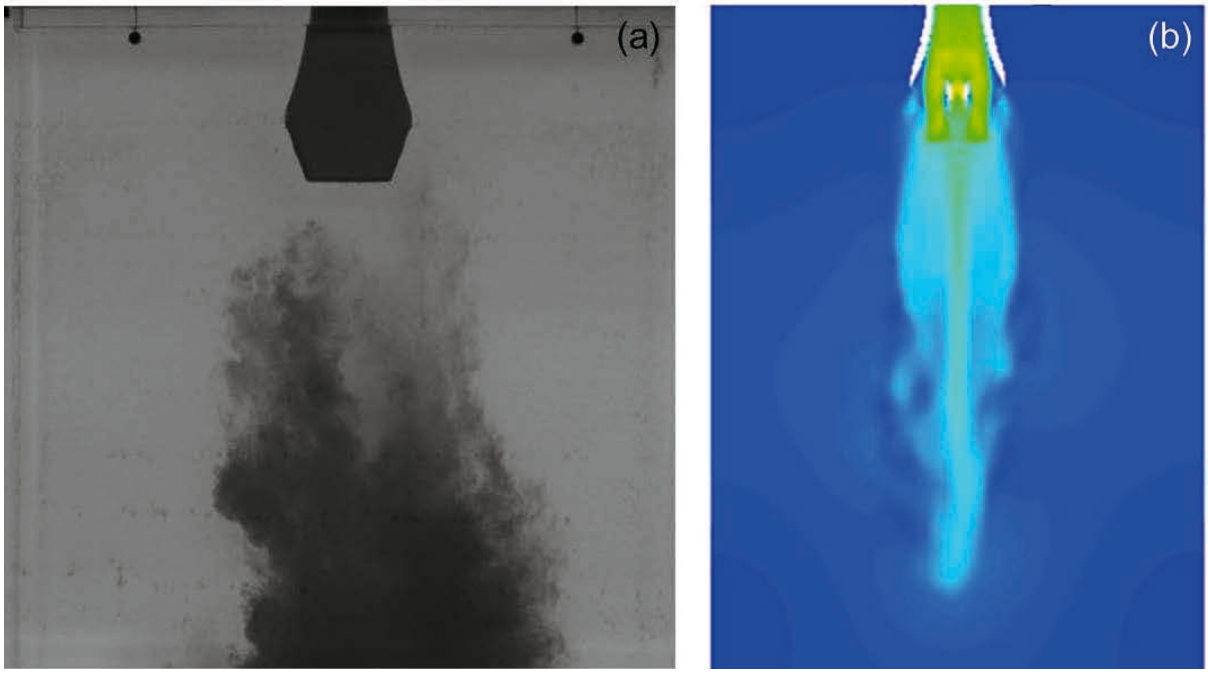

Figure 114. Comparison of experiment (case 2b) and simulation after 3 seconds of dye injection.

Differences are recognizable at 13 seconds after dye injection (Figure 115). The flow pattern of the water model experiment shows a jet which flows to the left section of the mold (Figure 115 (a)). A backflow from the right bottom part of the mold is streaming up and may influence the jet. At the left side of the mold a backflow from a previous period is still present.

The simulation result still shows a straight down streaming jet (Figure 115 (b)). Backflows are present at both sides of the mold walls. Small vortices are created at almost the whole section.

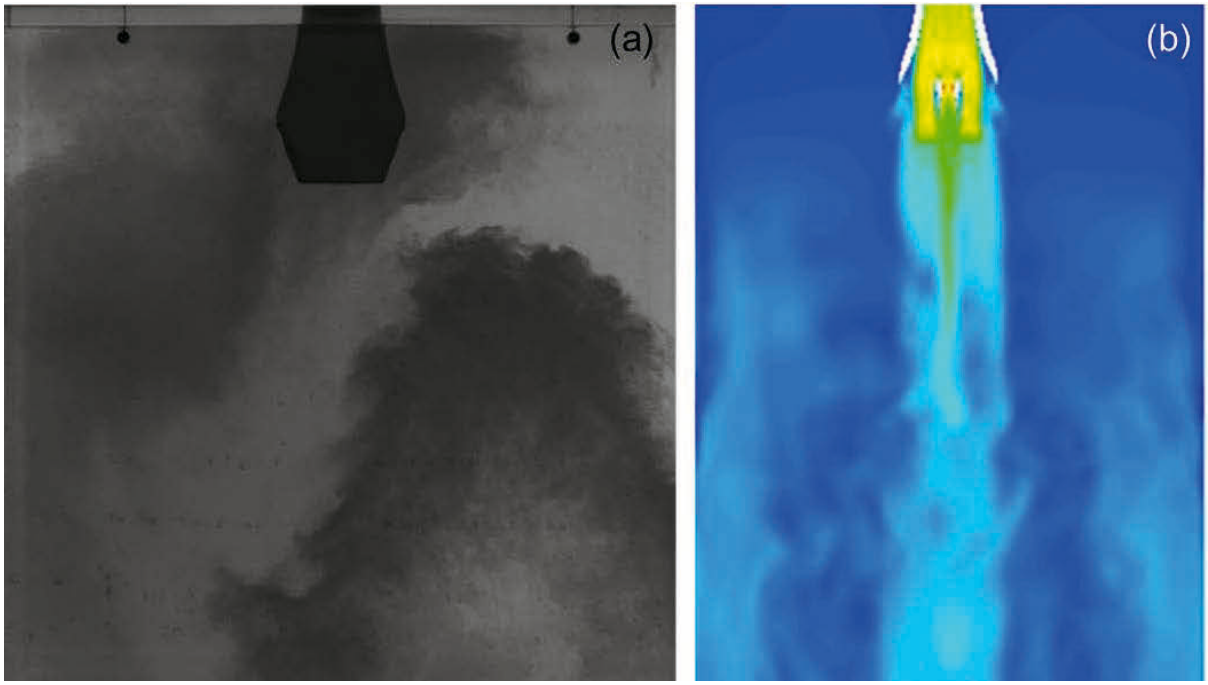

Figure 115. Comparison of experiment (case 2b) and simulation after 13 seconds of dye injection.

The results at the end of the recording time are quite similar again (Figure 116). The jet in the experiment has the same direction as the beam in the simulation result. Both are going straight downwards and the backflows which can be seen reaches the surface. The jets at both figures are sinuous. The backflow in the water model experiment is stronger at the left section of the mold. The same situation is found in the results of the simulation.

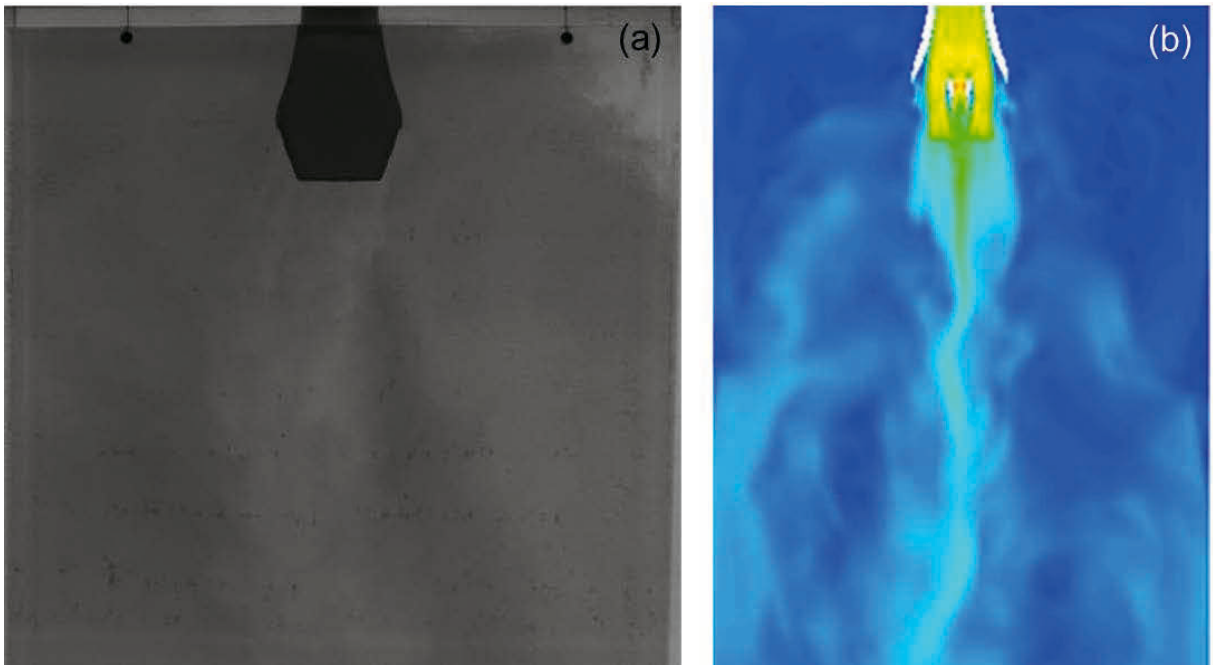

Figure 116. Comparison of experiment (case 2b) and simulation after 25 seconds of dye injection.

The results of the water model experiment and simulation are similar and comparable. The enmeshment is sufficient to deliver qualitative results.

4.7 1.8 Million Node Points Casting Speed 3.4 m/min

The enmeshment is the same as in the simulation case described in chapter 4.6. The casting speed is increased from 2.4 to 3.4 m/min. In Figure 117 the first second after dye injection can be seen. Both results show one single jet which goes straight downwards.

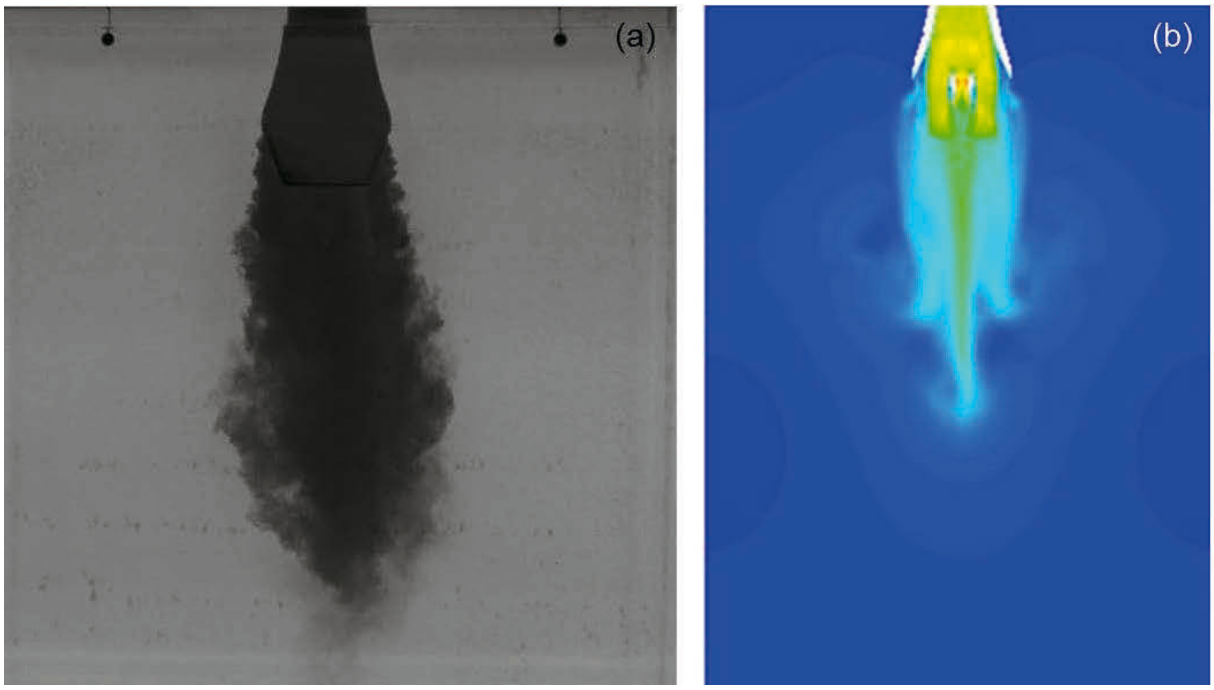

Figure 117. Comparison of experiment (case 2c) and simulation after 1 seconds of dye injection.

Figure 118 represents the results of dye injection after 5 seconds. The result of the water model experiment shows a single straight down streaming jet. At the bottom part creation of backflow and vortices can be seen (Figure 118 (a)). The simulation result for the same point shows similar results (Figure 118 (b)). One single down streaming jet is recognizable and in the middle of the visible mold small vortices are developing.

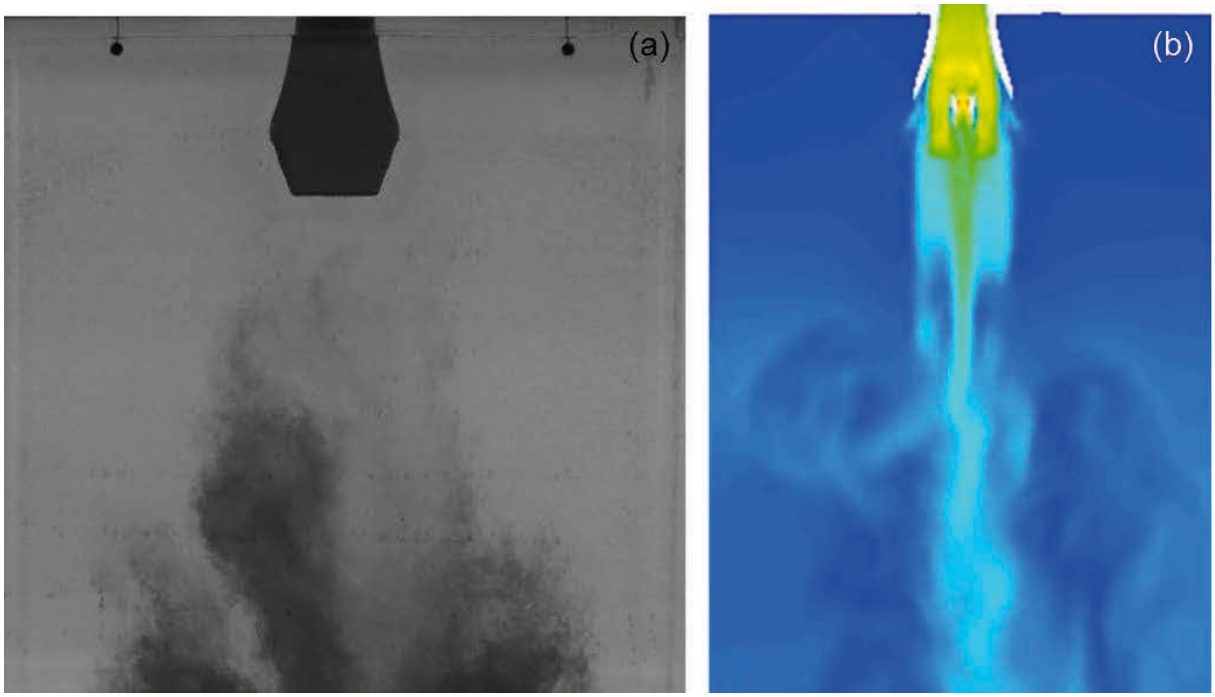

Figure 118. Comparison of experiment (case 2c) and simulation after 5 seconds of dye injection.

The flow pattern after 15 seconds of dye injection can be seen in Figure 119. It is recognizable that the result of the water model experiment and the simulation are quite similar. Figure 119 (a) shows a single jet which streams to the left section of the mold and creates a large vortex and backflow. At the right section of the mold a backflow is also present. At the right top corner less dye is transported until that moment.

In Figure 119 (b) the result of the simulation can be seen. As mentioned before the flow pattern is similar to the water experiment. A single jet is visible which tend to flow to the left section of the mold. A vortex and backflow is visible at the left section of the mold. A smaller vortex can be seen at the lower right section. Also the top right corner is less influenced by the flow behaviour inside the mold.

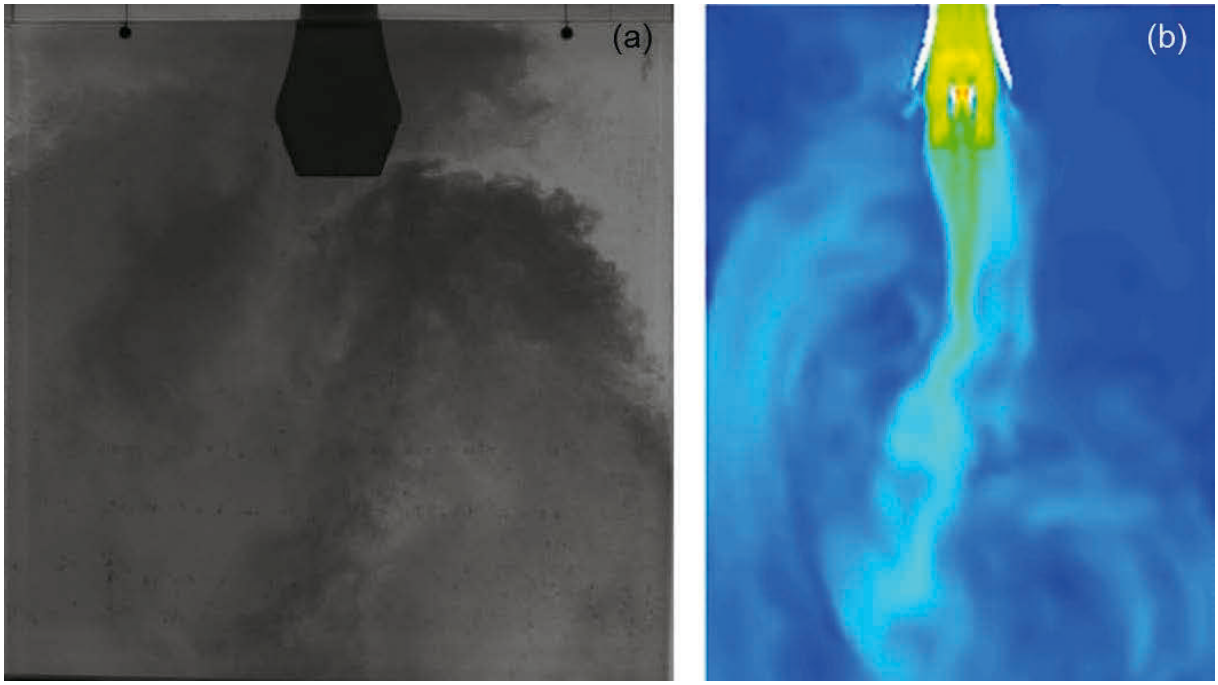

Figure 119. Comparison of experiment (case 2c) and simulation after 15 seconds of dye injection.

Figure 120 illustrate the results of dye injection after 20 seconds. The results are quite similar as at the previous time points.

The experiment shows that the jet streams straight downwards but tends to go to the left section of the mold (Figure 120 (a)). A reason therefore may be the backflow at the right side of the mold which streams up to the region of the SEN and influences the jet.

The result of the simulation also shows a single down streaming jet (Figure 120 (b)). It is recognizable that a part of the jet creates a vortex at the left section of the mold. The backflow at the right section seems to be less turbulent than the backflow at the left section.

The result of the water model experiment shows that no dye was transported to the top right corner: The simulation also shows that this part of the mold is less influenced by the flow behaviour inside the mold.

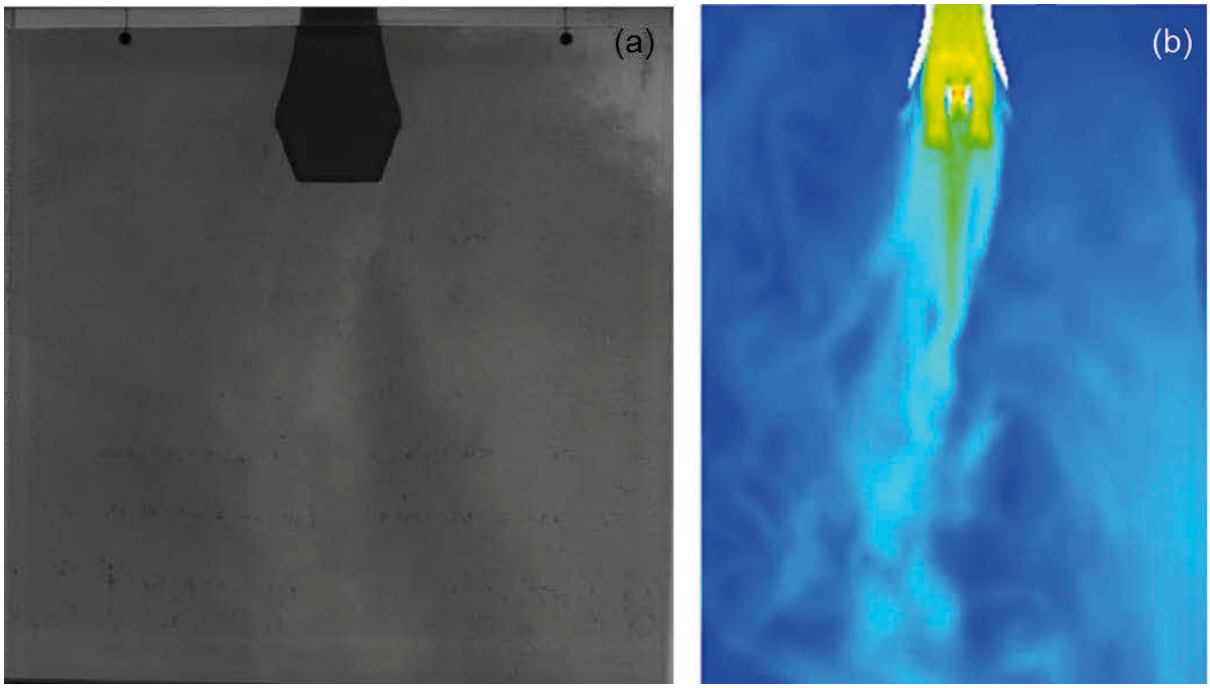

Figure 120. Comparison of experiment (case 2c) and simulation after 20 seconds of dye injection.

The comparison of the water model experiment and the simulation leads to the conclusion that both results are comparable if sufficient mesh refinement is done. As seen in chapter 4.5 the results of the simulation with 0.7 million nodes is completely different as the results of the water model experiment with the same setting.

There are advantages if the results of the experiments and simulation can be compared. More information of the process or flow behaviour can be carried out by simulation. This can lead to an improvement of the product or process.